GENERATION AND CHARACTERIZATION OF LASER INDUCED PLASMA FROM A FEW SOLID TARGETS

G. PADMAJA

THESIS SUBMITTED
IN PARTIAL FULFILMENT OF THE REQUIREMENTS
FOR THE DEGREE OF
DOCTOR OF PHILOSOPHY

DEPARTMENT OF PHYSICS
COCHIN UNIVERSITY OF SCIENCE & TECHNOLOGY
COCHIN - 682 022

1993

CERTIFICATE

Certified that the thesis entitled "GENERATION AND CHARACTERIZATION OF LASER INDUCED PLASMA FROM A FEW SOLID TARGETS" is the report of the original work carried out by Ms. G PADMAJA in the Department of Physics, Cochin University of Science & Technology, Cochin 682 022, under my guidance and supervision, and that no part thereof has been included in any other thesis submitted previously for the award of any degree.

Cochin - 682 022,
November 23, 1993

Dr. C P Girijavallabhan,
(Supervising Teacher)
Professor, Department of Physics
Cochin University of Science &
Technology, Cochin 682 022

DECLARATION

Certified that the work presented in this thesis entitled "GENERATION AND CHARACTERIZATION OF LASER INDUCED PLASMA FROM A FEW SOLID TARGETS" is based on the original work carried out by me in the Department of Physics, Cochin University of Science & Technology, Cochin 682 022, under the guidance and supervision of Dr. C P Girijavallabhan, Professor, Department of Physics, Cochin University of Science & Technology, Cochin 682 022, and that no part thereof has been included in any other thesis submitted previously for the award of any degree.

Cochin 682 022,
November 23, 1993
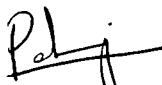
G PADMAJA

PREFACE

Plasma created by intense radiation from a focussed laser source was first observed with the advent of `gaint pulse' Q-switched Ruby lasers by Maker *et al* in 1960. When the laser pulses of moderate power are focussed on an opaque surface they can produce high heating rates and very high temperatures. At lower laser energies heating without phase change occurs, whereas with higher intensity pulses, ionization occurs which leads to the plasma formation. Spectroscopic studies of optical emission of a laser induced plasma is the most effective method for characterizing both the laser target interaction and the resulting plasma. The generation of the plasma from a solid target by irradiating it with laser pulse is an interesting problem from the point of view of not only the plasma physics but also of the practical application of it to spectrochemical analysis. Plasma produced by this method is important for several applications as in the surface microanalysis, fabrication of materials, deposition of thin film, ion source for beam lines and in controlled fusion devices, in addition to it use as tool for plasma diagnostics.

The work presented in this thesis concerns with the experimental studies on the plasma produced with moderately high power lasers. The characterization of laser induced plasma from different solid target materials like metals (Aluminium and Copper), polymers (Polytetrafluoroethylene), graphite and high T_c superconductors ($YBa_2Cu_3O_7$ & $GdBa_2Cu_3O_7$) using pulsed Q-switched Nd:YAG laser has been carried out. Here the spectroscopic as well as time resolved analysis of the plasma obtained from the above materials is reported. The spectroscopic study of laser induced plasma is a very convenient method to identify the neutral, ionic and oxide species in the plasma. Identification of these species is important in understanding the complicated ablation and deposition processes. In order to understand the detailed aspects of laser beam interaction with the target

I

material and recombination processes following the laser ablation, the time resolved studies of the spectral emission from the plasma offer the most logical approach.

The present thesis is organized into nine chapters. A brief description of the contents of each chapter is given below.

The chapter I is divided into two sections A & B. Section A includes, general introduction and the basic theory underlying the processes of interactions of laser beam with materials which leads to the formation of plasma. In the second section different techniques used in the diagnostics of laser induced plasma and their applications are described.

A brief overview of the some of the important previous work in the field of laser induced plasma is attempted in the chapter II. The emphasis is given to the characterization of the plasma rather than its applications.

The chapter III outlines the general experimental methods followed in this study. Details of the experimental set up used for the measurement of spectroscopic as well as time resolved analysis are discussed separately. The various subsystems like plasma chamber, spectrograph, monochromator, microdensitometer, boxcar averager and storage oscilloscope used for the above measurements and their specific features are also discussed.

Chapter IV presents the spatial and temporal analysis of laser induced plasma from polymer sample Teflon (Polytetrafluoroethylene). Detailed study of the spatially resolved emission spectra corresponding to different regions in the plasma at various distance from the target shows distinctly different characteristics. The emission line due to higher ionization states of carbon (CI,CII, CIII and CIV) are clearly seen in the core and mid region of the plasma. Molecular bands of C_2 (swan bands) and CN are predominant in the spectrum of extended region of the plasma. From the relative intensities of the above bands the vibrational temperatures of these species are calculated and their variation with laser energy are also

obtained. From the time resolved analysis of the different species in the plasma and from the variation of the time delay as well as decay time of emission at different regions of the plasma, several interesting conclusions related to the structure and composition of the plasma have been obtained.

As in the case of Teflon target, the spatial variation of the spectroscopic features and time resolved analysis of plasma obtained from the carbon (graphite) plasma are described in chapter V. The plasma emission spectrum shows somewhat similar characteristics as that obtained from the Teflon plasma. The plasma emission spectrum in the central core region of the plasma is found to be dominated by the higher ionized state of carbon lines (up to CV), while the spectrum in the extended region is dominated by the molecular bands of C_2 and CN molecules. From the time delays measured for different species in the plasma the expansion velocities of the various species are calculated and their variation with respect to laser energy is also obtained. From the relative intensities of the molecular bands, the vibrational temperature of the above molecules are obtained and these are found to be in good agreement with each other.

The results obtained from the analysis on the characteristics of plasma from high T_c superconductors are presented in the chapter VI. Most of the earlier spectroscopic studies do not clearly reveal the presence of Cu and CuO. But here, the characteristics spectral emissions from GdO, YO, BaO, CuO along with the emission lines of ions and neutral atoms from these samples are clearly observed. The time resolved spectroscopic studies on these species have also been done. Important parameters such as electron temperature and velocity of the ionic species are evaluated from the ion probe technique.

The spatially resolved plasma emission spectra of metal targets (Aluminium and Copper) are discussed in the chapter VII. The plasma emission spectrum at various regions of the plasma shows distinct characteristics. The spectrum of Aluminium plasma in the outer region of the plasma plume is dominated by AlO bands

with $\Delta v = +2, +1, 0, -1,$ and -2 due to the transitions from the $B^2\Sigma \dashrightarrow X^2\Sigma$. The vibrational temperature of these bands are calculated and their variation with laser energy is discussed. From the Langmuir probe studies of the Aluminium plasma the parameters such as probe characteristics, plasma temperature, and the velocity of positive as well as negative ions are calculated.

An experimental set up for the preparation of the thin films by the laser ablation technique is described in the chapter VIII. As a preliminary study, metal films (Aluminium and Copper) have been prepared by this technique and the optical transmission characteristics of the films thus obtained in relation to different parameters such as laser energy, number of pulses, substrate temperature and the distance between the target and the substrate are investigated. In order to obtain a better and uniform film a modified substrate heater has been used and the design details of this set up have been discussed in this chapter.

Chapter IX gives general conclusions obtained from the present investigations which have been carried out by the author during the past five years in the laser division, at the department of physics, Cochin University of Science & Technology.

Part of the investigations have been published in the form of following papers.

1. Spectral features of laser induced plasma from Y-Ba-Cu-O and Gd-Ba-Cu-O high T_c superconductors
   G PADMAJA, *A V Ravi Kumar, V Vidyalal, P Radhakrishnan, V P N Nampoori and C P G Vallabhan,* Pramana, 32, L693, (1989).

2. Time evolution of laser induced plasma from Gd-Ba-Cu-O high T_c superconductors
   G PADMAJA, *A V Ravi Kumar, V Vidyalal, P Radhkrishnan, V P N Nampoori and C P G Vallabhan,* J.Phys.D: (Appl Phys), 22, 1558, (1989).

3. Detection of oxide species in the laser ablated plasma of high T_c superconducting sample

G PADMAJA, *A V Ravi Kumar, V Vidyalal, P Radhkrishnan, V P N Nampoori and C P G Vallabhan*, Proc. IEEE National Seminar on lasers in Engineering and Medicine (IEEE-LASEM-89), page 124-126, (1989).

4. Characteristics of laser induced plasma from high T_c superconductors

G PADMAJA, *A V Ravi Kumar, V Vidyalal, P Radhkrishnan, V P N Nampoori and C P G Vallabhan*, Bull. Mat.Sci., 14, 545, (1991).

5. Evaluation of laser ablation threshold in polymer samples using pulsed photoacoustic technique

A V Ravi Kumar, G PADMAJA, *P Radhakrishnan, V P N Nampoori and C P G Vallabhan*, Pramana-J.of Physics, 37, 345, (1991).

6. Determination of laser damage threshold using pulsed photoacoustics

A V Ravi Kumar, G PADMAJA, *P Radhakrishnan, V P N Nampoori and C P G Vallabhan*, J.Acoust.Soc.Ind., 18, (1991).

7. Pulsed photoacoustic technique for the measurement of laser damage threshold in bulk polymers

A V Ravi Kumar, G PADMAJA, *P Radhakrishnan,V P N Nampoori and C P G Vallabhan, In the book* 'Photoacoustics and Photothermal Phenomena III', Edited by Dane Bicanic, Springer-Verlag (Heidelberg), (in press), (1992).

8. Spatial and Temporal studies of laser induced plasma from a polymer

G PADMAJA, *A V Ravi Kumar, P Radhkrishnan, V P N Nampoori and C P G Vallabhan*, J.Phys.D: (Appl Phys), 25,35(1993).

CONTENTS

CHAPTER 3   EXPERIMENTAL SET UP FOR LASER PLASMA STUDIES

CHAPTER 4   LASER INDUCED PLASMA FROM POLYMER SAMPLE

CHAPTER I

INTRODUCTION TO LASER INDUCED PLASMA

ABSTRACT

This chapter is divided into two parts. *Part A includes, general introduction and the basic theory underlying the processes of interaction of laser beam with materials which lead to the plasma formation.* *Part B presents the different techniques used in the laser plasma diagnostics.*

THE FOURTH STATE OF MATTER - PLASMA : AN OVERVIEW

1.1. GENERAL INTRODUCTION, HISTORY

Matter manifests itself generally in three distinct states *viz*, solid, liquid and gaseous. In recent years, however more and more attention has been directed to the properties of matter in a fourth and unique state, which is called plasma. In solid bodies, atoms and molecules are arranged usually in a regular order and are constrained to a rigid order. In liquid states, they can move, but their freedom of movement is limited. In a gas, molecules and atoms move freely. But in the case of plasma, the electrons are liberated from the atoms and acquire complete freedom of motion. With the loss of some of their electrons, atoms and molecule acquire a positive electric charge, and they are then called ions. Thus a plasma is a gas consisting of positively and negatively charged particles in such proportions that the total charge is equal to zero. Freely moving electrons can transport electric current and thus, plasma is a conducting gas.

In a plasma, the electrons are separated from atoms or molecules by forces produced by the fast motion of hot particles, the action of light or an electrical discharge. The special properties of plasmas give some scope for technological applications both as electrical conductors as well as a possible high temperature medium. In electrical applications, plasma has an advantage over metals in the sense that it is about a million times lighter. The electrons within the atom perform a harmonic dance whereas in a plasma they exist without any order, like the molecules in a gas. It is an important property of plasmas that their motion can be ordered. The particles can be forced to move in a regular fashion. The agency that forces the free electrons to submit to rigid discipline is the magnetic field. Unlike atoms or in a solids, electrons and nuclei move collectively in

cohesive groups. The motion of plasma particles is constrained in a magnetic field. In a hot plasma, the particles pass each other quickly without much interference. Such a plasma offers virtually no resistance to electric currents since its conductivity is very high. In a cold plasma with low conductivity on the other hand, interactions between particles due to collisions allow the magnetic field to leak through the plasma. In a `cold` plasma, the temperature will be of the order of electron volts, where as in a `hot` plasma, the temperature is of the order of a few hundred electron volts. If the plasma particles do not hit the walls they must move in a regular manner within the magnetic trap. But due to some instabilities, the ions and electrons move around in all directions and strike the walls and thus waste their energies. Plasma in a magnetic field is capable of a large variety of modes of oscillations, with emissions from x-rays to radio-waves. Random oscillations which we call noise have also been observed. Plasma resonators and wave guides can be constructed which can force the plasma to oscillate at predetermined frequencies.

Plasma can be considered as a dielectric medium whose dielectric constant is a function of frequency, wavenumber and direction of propagation. A plasma can be thought of as any collection of charged particles sufficiently dense that space-charge effects can result in strongly coherent behaviour. The charged particles in a plasma interact with each other in a coherent way by long range forces. The electric field due to a point charge decreases only as a inverse square of distances, whereas at a given density, the total number of charges increases as cube of linear dimension. Thus it is possible for an electric field, an assembly of charged particles to add together in a coherent way. This feature give rise to collective modes of plasma behaviour which do not exist in ordinary gases, where molecules interact with short range force. Plasma physics is thus a many body problem.

Consider two parallel plane conducting surfaces which are

separated by a distance 2x and are held at the same potential ϕ_0. Let the space between these surfaces be occupied by a uniform number density n of particles carrying an identical charge q each. The potential at the middle plane is $\phi_m = \phi_0 + 2\pi n q^2 x^2$ so that energy required to transfer a particle from the surface to the mid plane is q $(\phi_m - \phi_0) = 2\pi n q^2 x^2$. The particles have thermal motion characterized by a temperature T. The collective motion effects then dominate over the particle's random behaviour if the above energy is larger than the one dimensional mean energy of the particles random motion, 1/2 kT ie, if

$$ x \; > \; \left[\frac{kT}{4\pi q^2 n} \right]^{1/2} \; = \; \lambda_D \qquad\qquad ..(1.1) $$

The quantity λ_D is the most fundamental unit length in plasma physics. As it appeared in the theory of electrolytes developed by P Debye, it has been given by the name Debye length. It is then obvious that an ionized gas can be called a plasma only if its dimensions L are much larger than Debye length.

$$ L \; \gg \; \lambda_D \qquad\qquad\qquad (1.2) $$

when q = e, the electron charge,

$$ \lambda_D \; = \; 740 \left(\frac{kT}{n} \right)^{1/2} \qquad\qquad (1.3) $$

where kT is the energy of random motion in eV, n is the electron number per cm^3 and λ_D is independent of particle mass. The Debye length can also be expressed in the following manner,

$$ \lambda_D \; = \; \left[\frac{kT_c}{8\pi N_o^2 e} \right]^{1/2} \qquad\qquad (1.4) $$

where N_o, T_c and e are the equilibrium concentration, temperature and charge of electrons and k is the Boltzmann

Constant.

When charges of both signs were present in the plasma, these are strongly attracted to each other and are forced to intermix intimately. This tendency grow towards neutrality is particularly striking in all ionized gases which are satisfied by the condition (equation 1. 2) in which the charged particles do not deviate drastically from statistical equilibrium. In all such cases the difference in potential energy of particles at different points in the space charge field can at most be of the order of the mean random energy. In a plasma, the electrons and ions are constrained to move without separating appreciably and they are bound to each other collectively by space charge forces.

If there are large number of charged particles in the Debye sphere, N_D and if the plasma description is to be statistically meaningful, we must require that,

$$N_D = \frac{4\pi n}{3} (\lambda_D)^3 \qquad (1.5)$$

The above equation can be written in terms of the mean kinetic and inter particle potential energy as,

$$\frac{\langle K.E. \rangle}{\langle P.E. \rangle} \approx \left[\frac{kT}{q^2 n^{1/3}} \right] = 4\pi \lambda_D^2 \, n^{2/3} = (36\pi)^{1/3} (N_D)^{2/3} \gg 1 \qquad (1.6)$$

If the ionized gas is not to recombine, then we must have K.E. > P.E. Introducing the critical distance $r_c = q^2/kT$, ie, the distance at which the potential energy equals to kinetic energy and the simple Rutherford scattering path $\lambda_c = (4\pi r^2 n)^{-1}$, then the Debye length is given by,

$$\lambda_D = \lambda_c \, r_c \qquad (1.7)$$

So generally, a gaseous plasma will have,

$$r_c \ll n^{-1/3} \ll \lambda_D \ll \lambda_c \qquad (1.8)$$

So that

$$\Lambda = \lambda_D/r_c = \lambda_c/\lambda_D \qquad (1.9)$$

5

Which is a dimensionless parameter describing the statistical quality of the plasma.

we can construct a fundamental frequency,

$$\omega_p = \nu/\lambda_D \tag{1.10}$$

$$\omega_p = \left[\frac{4\pi n q^2}{m}\right]^{1/2} \tag{1.11}$$

This the so called plasma frequency. This quantity is the characteristics oscillation rate for electrostatic disturbances in the plasma [1]. In the laboratory plasmas, this frequency usually lies in the microwave region. The plasma frequency is of such fundamental importance that the plasma density is frequently described by the quantity ω_p rather than n itself.

In order to convert a gas in to a plasma state it is necessary to remove at least some of the electrons from the atoms, thus converting these atoms into ions. This detachment of electrons from atoms is called ionization. In a dense plasma, ionization occurs through electron collisions, whereas in a rarefied plasma, ionization occurs by the action of radiation (UV to X-ray). Ionization can also be accomplished by atom-atom as well as atom-ion collisions, but considerable energies are then necessary. The inverse process to ionization is called recombination, which is essentially the combining of ions and electrons to form neutral atoms or molecules. Of the various elementary processes in plasma physics, the charge exchange is one of the most important processes. In this case, an ion colliding with an atom acquires electrons from the atom so that the ion becomes an atom and the atom an ion. In a dense, partially ionized plasma, an atom can capture an extra electron and be converted into a negative ion.

1.2. DIFFERENT TYPES OF PLASMA

In nature and in the laboratory, ionization can be produced by various methods. The most important of these are,

1. ionization by heat
2. ionization by radiation
3 ionization by electric discharge

Based on the method of ionization, plasma can be divided into the following different types [2].

1.2.1. NATURAL PLASMA

All naturally occurring plasmas are produced by heating. All substances become ionized if they are heated to sufficiently high temperatures. This process is called thermal ionization. It is necessary that the temperature be close to that corresponding to the energy of the most weakly bound electrons, *ie*, the lowest ionization energy of the atom or molecule. The most weakly bound electrons are in the case of alkali metals and the most firmly bound electrons are in the case of inert gases. In order to obtain a fully ionized plasma by thermal means, it is necessary for the temperature to reach several tens of thousand degrees. Stars consist entirely of thermal plasma. Weakly ionized plasmas with high densities and relatively low temperatures can be obtained thermally through the use of easily ionizable additive. The electrical conductivity of the plasma enhances with the presence of the alkali-metal additive. Ionization by radiation becomes significant in a very tenuous gases, where any significant density collisions between particles are not much important than the action of radiation. This means that ionization is important in astrophysics, the UV radiation from hot stars causes ionization in the surrounding gaseous vapours and interstellar gas. The radiation of sun gives rise to ionization in the outer layers of earth's atmosphere. Attempts to use radiation ionization in technology have not been very successful because typical densities are such that inverse processes of recombination of electrons with ions proceeds very rapidly and leads to condition of equilibrium.

In nature, plasma produced by electric discharge is in lightning. In technology, typical examples of gas discharge

plasmas are electric sparks, electric arcs, gaseous flash lamps
and other gas discharge devices.

1.2.2. ELECTRODE PLASMA

Ionization in a discharge tube provided with electrodes
(cathode and anode) depends on the production of avalanche.   In
order to produce avalanche it is necessary that the electric field
to the gas be large enough to so that energy imparted to the
electrons in their mean free paths is sufficient to knock out at
least one electron from an atom on impact.   These secondary
events are sufficient even if there is only a small number of free
electrons since they can liberate new electrons after being
accelerated by the field.   In this way electron multiplication
proceeds in a geometrical progression.   The electrodes establish
an electric field in the plasma.   The charge separation caused by
this field produces polarization of the plasma.   In order to have
stationary current flow through the plasma the space charge that
arises in the plasma must be compensated by electrons that come
from external sources.

Since the negative electrons are much more mobile than that of
the positive ions, in the presence of applied field, they move to
the positive electrodes (anode) and the plasma columns between the
the electrodes become positively charged.   In order for the
current flow to occur under these conditions, it is necessary that
negative electrode inject electrons into the plasma.   The
injection of electrons by a solid body is called emission.
Special means for exciting cathode emission must be employed in
order to obtain a discharge at low voltage.   It is possible to
shine light with a sufficiently short wavelength on the electrode
for knocking electrons out of it (photoelectric effect), or
cathode can be heated to a high temperature (thermal emission).
Such a discharge maintained by external means is called a
nonself-sustaining discharge.   If the voltage between the
electrodes is high enough, then the cathode can emit electrons

without any external agency. This type of discharge is called self-sustaining discharge.

There are a variety of emission mechanisms. In a dense gas, at very high voltages the cathode is simply heated by ions that strike its surface. In this case the emission is thermal, as in the nonself-sustaining discharge with a hot cathode. Such a discharge are called arcs (electric arcs). In rarefied gas at moderate voltages, various forms of cold or glow discharges are possible. Here cathode emits electrons by a mechanism called field emission. The electric field near the cathode surface extract electrons directly from the metals. An additional role can be played by secondary electron emission. If the emission is unlimited, the plasma polarization can be completely cancelled by the electron current from the cathode. In a self-sustained discharge this emission is not unlimited so that the plasma column far away from the cathode retains a positive charge. It is called the positive column. The application of voltage primarily affects the region near the cathode, where it facilitates electron emission. This region is called the cathode fall.

1.2.3. INDUCTIVELY COUPLED PLASMA (ICP)

In a direct current (dc) arc or in an inductively coupled plasma (ICP), the energy is absorbed through ohmic heating produced by the low frequency or direct current flowing in the plasma. The electrical conductivity of an ideal plasma is given by,

$$\sigma = \frac{ne^2}{m}\left[\frac{\nu - i\omega}{\nu^2 + \omega^2}\right] \qquad (1.12)$$

Where n is the electron density, e the electronic charge, m the mass of electron, ω the radiant frequency of the applied electric field, ν the effective collision frequency for electrons and i the square root of -1. In the inductively coupled plasma the currents are induced into the plasma from alternating currents

9

flowing in the surrounding solenoidal coil. The arc is sustained within a container that determines the plasma diameter, where as the length of the plasma is determined by the length of the solenoid.

The inductively coupled plasma operates at frequencies well below the plasma frequency

$$\omega_p = (ne^2/m\varepsilon_o)^{1/2} \qquad (1.13)$$

where ε_o is the permitivity of free space. In this frequency range, the electromagnetic field does not propagate as a wave within the plasma, but is attenuated as an evanescent wave over distances of the order of skin depth,

$$\sigma = \frac{c}{\left[\omega_p - \omega^2\right]^{1/2}} \qquad (1.14)$$

Where c is the speed of the light. Thus plasma is sustained by energy absorbed within a small layer near its outer surface that produces a rather flat temperature profile within the plasma and limits the maximum temperature that can be obtained.

1.2.4. LASER INDUCED PLASMA (LIP)

Plasma generated by radiation from focussed laser beams were first observed with the advent of "giant pulse" Q-switched ruby lasers by Maker et al [3]. A laser pulse focussed on an opaque surface can produce high heating rates and high temperatures. At low laser energies heating without change of phase occurs. With higher intensity pulses, ionization occurs which lead to the plasma formation. The optical emission from a laser induced plasma (LIP) is useful in characterizing both the laser target interaction and the resulting plasma [4]. Plasma produced by a focussed laser beam on a solid surface evolves in two phases. During the first phase, a plasma is initiated at the surface and in the surrounding medium. If the surrounding medium is air, the

10

plasma grows rapidly generating either a laser supported detonation wave [5] or a laser supported combustion wave [6], which absorbs the incident laser radiation and influences the coupling of incident laser energy to the surface. The nature of interaction depends on the incident laser irradiance and several possible regimes have been identified [7]. The second phase of the plasma evolution occurs after the laser pulse is over, when the plasma begins to expand and cool.

Several parameters of lasers like wavelength, pulse width, pulse rate and irradiance will effect the ablation process. Most frequently used lasers for plasma production are solid state lasers like the ruby (695 nm), Nd:YAG or Nd:Glass (1064 nm) and gas lasers like CO_2 (10.6 μm), nitrogen (337 nm) and excimer lasers ($\approx$ 300 nm) and dye lasers (220 nm-740 nm). Results suggest that among these lasers, those having shorter wavelength produce more ablated material [3]. The dependence of wavelength on the absorption coefficient is given by,

$$K = \frac{4\pi\mu}{\lambda}$$ (1.15)

where K is the surface absorption coefficient, λ the wavelength and μ the solid state absorption index [4]. When the repetition rate of the laser increases, greater amount of material is ablated which reduces the sample inhomogeneities and the effect of laser energy variation between the pulses. When the laser irradiance is greater than 10^9 W/cm^2, and the pulse width > 100 nsec, the laser vapourization of the material takes place. Figure (1.1) shows the dependence of the laser absorption as a function of wavelength and irradiance. The wavelength of the laser often controls the mode of evapouration. Long wavelength lasers usually induce a thermal evapouration process, in which the evapourated materials exhibit well defined translation and internal temperatures in equilibrium with local surface temperatures [5]. Operation of the lasers at short wavelengths initiates processes that are non-thermal in nature. The
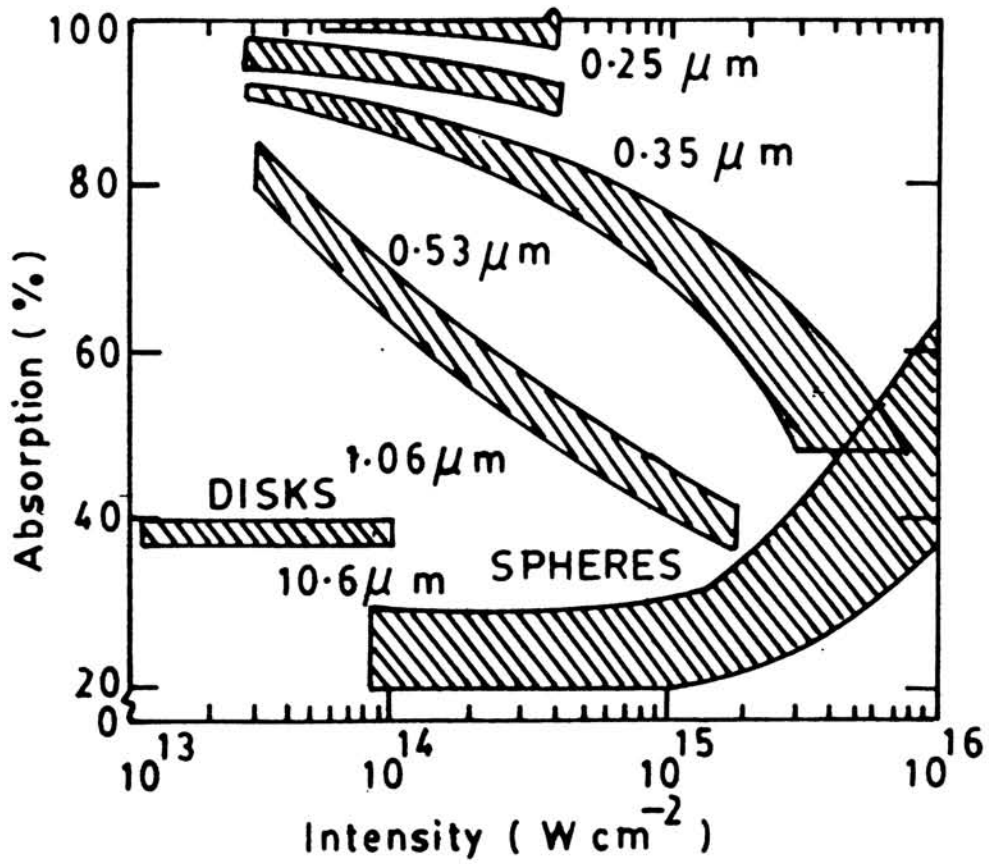
Fig.1.1. The dependence of the laser absorption as a function of wavelength and irradiance.
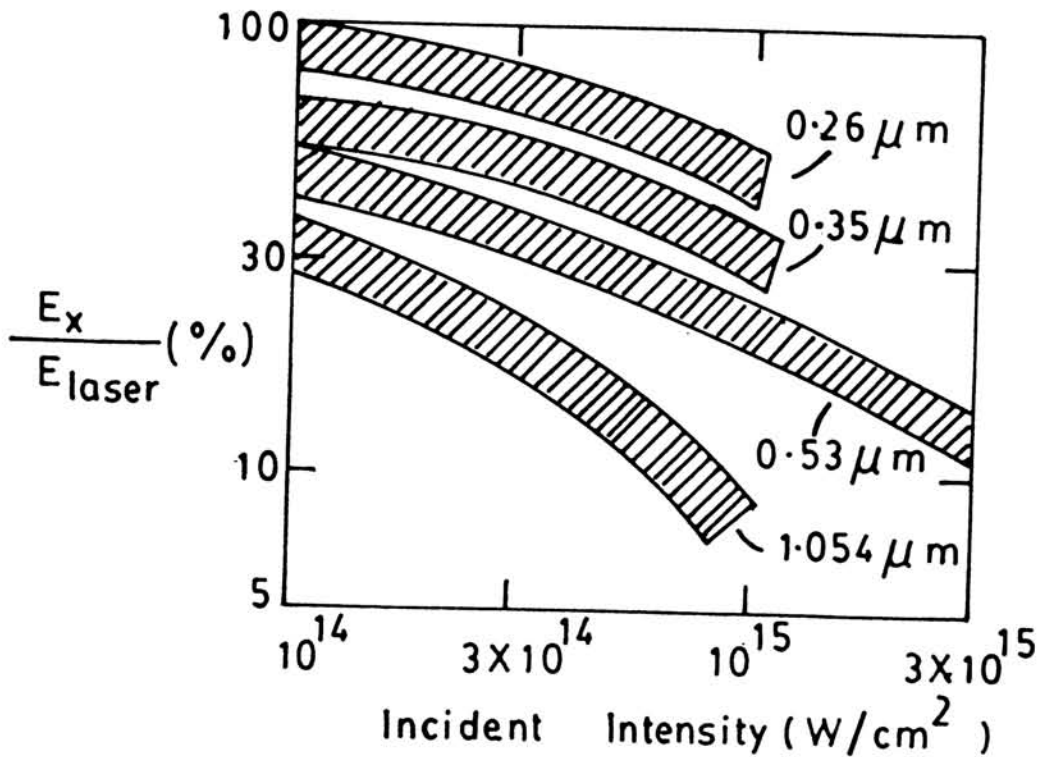
Fig.1.2. X–Ray conversion efficiency at different wavelength of the laser

comparison of the laser interaction with the solid targets at different wavelengths show that short wavelengths are favourable for energy penetration in the solid because there will be large ablation rate at short wave lengths. The absorption also increases at short wavelengths. So short wavelength lasers are mainly used for fusion experiments.

High power lasers are now widely used as energy sources to change the thermodynamic state of matter over wide range of temperatures. The advantage of laser source over the other conventional sources like electric discharges is its high speed of introducing a quantity of energy at desired time into matter at the selected location. Therefore lasers are used in experimental investigations such as plasma physics, thermonuclear physics, isotope separation, thermophysics, spectroscopy, surgery and industry. Melting, evapouration and ionization of matter by lasers has many practical applications.

The temporal coherence of the laser, which is related to monochromaticity of the laser has got application in spectroscopy and in optical fiber communications. The property of spatial coherence which is related with directionality of the laser is useful for focussing the laser in to a very small volume $\approx 1 ~\mu m$, which produces very high energy density at the solid surface. The force due to electric field of lasers is comparable with the electric field that prevails inside the atoms resulting in the nonlinear response of the medium, whereas force due to electric field of conventional source is very weak compared to inter atomic fields and this leads only to a linear response of the medium.

The advent of laser has produced a light source of high enough power that considerable heating effects may be generated when the light is absorbed. Some of these phenomena have aroused considerable interest in effects which involve a change of phase of the absorbing material and the luminous plume of vapourized material blasted from a metallic surface [8,9]. However in most cases surface heating without phase change is of interest, as in studies of thermionic emission produced by the laser radiation

[10]. In treating the changes of phase, it will appear that different approaches should be invoked for ordinary laser beams and Q-switched beams. For ordinary lasers, vapourization appears to be described by conventional processes of boiling. But the vapourization produced by Q-switched lasers, depends on the thermal properties of the absorber and the parameters of the laser pulse [11]. At higher laser power densities, the surface temperature of the metal rapidly rises to its vapourization temperature. For example in the case of at a power density of $\approx$ 10^9 W/cm^2, the vapourization temperature of any metal will be reached in less than 1 nsec. At this point the input energy begins to supply the latent heat of vapourization to a thin layer of material at the surface.

In the case of laser induced plasma, different regimes are identified when the laser irradiance is between 10^{13}-10^{16} W/cm^2, which are applicable for laser fusion studies. When the laser irradiance is < 10^{12} W/cm^2 low temperature plasmas are obtained, which have got applications in material processing, chemical analysis and also for producing plasma recombination lasers. X-ray emission from LIP is not only of considerable interest for inertial-confinement fusion application, but is also of importance to a number of other applications. The increased absorption and the reduced electron generation observed with short wavelength laser radiation have also led to increased conversion efficiency of laser light to X-rays at short wavelength laser-matter interaction. It was shown that the efficiency of conversion of the absorbed laser light to soft X-rays should vary as λ_L^{-2} [12]. At shorter wavelengths, the increased conversion efficiency is due to the higher level of collisional absorption and the high coronal electron density. Figure (1.2) shows the X-ray conversion efficiency at different wavelength of the laser. The physical reason for the increased conversion at low intensities is that under these conditions, the plasma can radiate the energy fast enough to maintain a relatively cool coronal absorption region with a long scale length absorption and emission region. At high

laser intensities radiational process cannot cool the plasma fast enough and consequently, much of the energy is lost in the low density plasma blowing off the target and in energy transport to the denser region of the target.

1.3. LASER BEAM INTERACTION WITH MATERIALS

ABSORPTION OF LASER LIGHT

Laser light, in order to cause any lasting effect on a material, must first be absorbed. This absorption turns out to be the most critical step in laser processing of materials. This process can be considered as a secondary source of energy inside the material. It is this secondary source, rather than the laser beam which determines as to what happens to the irradiated material.

1.3.1. FUNDAMENTAL OPTICAL PROPERTIES

PLANE WAVE PROPOGATION

The simplest form of light is a monochromatic, linearly polarized plane wave. The electric field associated with the laser beam propagating in a homogeneous and non-absorbing medium can be represented as,

$$E = E_o \exp\left[i\left(\frac{2\pi z}{\lambda} - \omega t\right)\right] \qquad (1.16)$$

where, z is coordinate along the direction of propagation, ω the angular frequency and λ the wavelength of radiation is given by,

$$\lambda = \frac{2\pi}{\omega} \frac{c}{\eta} \qquad (1.17)$$

c is the speed of the light and η the refractive index of the material. The electric and magnetic fields are related by,

$$H_o = E_o \eta_1 \varepsilon_o c \qquad (1.18)$$

where, ε_o is the dielectric constant in vacuum. The force exerted by the electromagnetic wave on an electron is given by,

$$f = - e \left[E + \left(\frac{\eta_1}{c} \right) \left[V \times H \right] \right] \qquad (1.19)$$

The contribution due to magnetic field is smaller than that due to the electric field by a factor $\approx V/c$, where, V is the electron velocity.

The energy flux per unit area is termed as irradiance and is given by,

$$I = |E \times H| = \eta_1 \varepsilon_o c E_o^2 \qquad (1.20)$$

where I corresponds to a photon of energy $\hbar\omega/2\pi$. The irradiance is maximum near the optical axis and falls of laterally. The lateral distribution of a cylindrically symmetric Gaussian beam can be represented as,

$$I(r) = I_o \exp\left(-\frac{r}{w}\right)^2 \qquad (1.21)$$

I_o is the irradiance on the axis (r=0) and w is the beam radius. This applies to a laser operating in its fundamental resonator mode (TEM$_{oo}$). The wave front of a freely propagating Gaussian beam can always be taken as close to planar. In a first approximation, where the diffraction effects are ignored, this holds for a focussed beam in the vicinity of the focal spot [13]. The total power of the beam is given as,

$$P = \pi w^2 I_o \qquad (1.22)$$

In an absorbing media, the real refractive index η_1 must be replaced by a complex index $\eta = \eta_1 + i\eta_2$. The electric field propagating over a distance z now decreases by a factor exp $(\omega\eta_2 z/c)$, indicating that some of the light is absorbed. The

absorption coefficient for the irradiance I is given by,

$$\alpha = - \left[\frac{1}{I}\right] \left[\frac{dI}{dz}\right] = \frac{2\omega}{c} \eta_2 = \frac{4\pi}{\lambda} \eta_2 \qquad (1.23)$$

where the inverse of α is the absorption length. The reflectance and absorption coefficients determine the amount of beam power absorbed within the material. The power density deposited at a depth z by a perpendicularly incident beam of irradiance I is given by,

$$J_a(z) = I(1-R) \; \alpha \; \left[1-\exp\left[-\int_0^z \alpha(z')dz'\right]\right] \qquad (1.24)$$

This expression represents the secondary source and the integral in the exponential function is the optical thickness of the material between 0 and z. In opaque materials ($z \gg 1/\alpha$), the fraction of the energy absorbed is determined by 1-R, the absorbance of the material.

1.3.2. MACROSCOPIC MATERIAL PROPERTIES

A relation between the refractive index and the properties of the medium of propagation is given by the Maxwell's equations so that,

The wave equation can be written as,

$$\nabla^2 \overline{E} = \left[\frac{\varepsilon}{c^2}\right] \frac{\partial^2 \overline{E}}{\partial t^2} + \left[\frac{\sigma}{\varepsilon_o c^2}\right] \frac{\partial \overline{E}}{\partial t} \qquad (1.25)$$

The complex refractive index can be written as,

$$\eta^2 = \varepsilon + \frac{i\sigma}{\varepsilon_o \omega} \equiv \varepsilon = \varepsilon_1 + i\varepsilon_2 \qquad (1.26)$$

ε is the complex dielectric function, which is the generalized response function of the material to weak electromagnetic

radiation. It depends on the frequency of light in a manner determined by the microscopic structure of the material.

(a). NON-METALS

Insulators and semiconductors in the absence of excitations have only bound electrons and are basically transparent, except in the vicinity of the resonance region. The dielectric function is the ratio of the total field (wave plus polarization) to the field of the wave alone. In quantum mechanics, a resonance corresponds to the transition of an electron between two states, the energy difference ΔE of which determines the resonance frequency $\omega = \Delta E/h$. For a non-metal with N_e bound electrons, showing one single resonance, the dielectric function is given by.

$$\varepsilon = 1 + (N_e e / m_e \varepsilon_o)f_{osc} \frac{(\omega^2-\omega_o^2 + i\Gamma\omega)}{[(\omega^2 -\omega_o^2)^2 -\Gamma^2 \omega^2]} \qquad (1.27)$$

Here f_{osc}, the oscillator strength, is a measure of probability of transition, while the damping constant Γ describes the width of resonance that arises from the finite width of the initial and final electron states. The optical effects using as a consequence of a resonance are shown in the figure (1.3). A peak in the absorption coefficient due to resonance is invariably accompanied by a peak in the reflectance. The most important resonance arises from the transitions of valence - band electrons to the conduction band (interband transitions). To induce an interband transition, the incident photon must have an energy at least equal to the band gap energy E_g. The free carriers (electrons and holes) created in pairs in interband transitions can, if present in sufficient numbers, influence the optical response of the material. Insulators have band gaps corresponding to the light frequencies in the vacuum ultraviolet and carrier excitations in the sun light illumination is small. Semiconductors on the other hand, have band gaps in the visible or IR part of the spectrum. Free carriers (optically or thermally
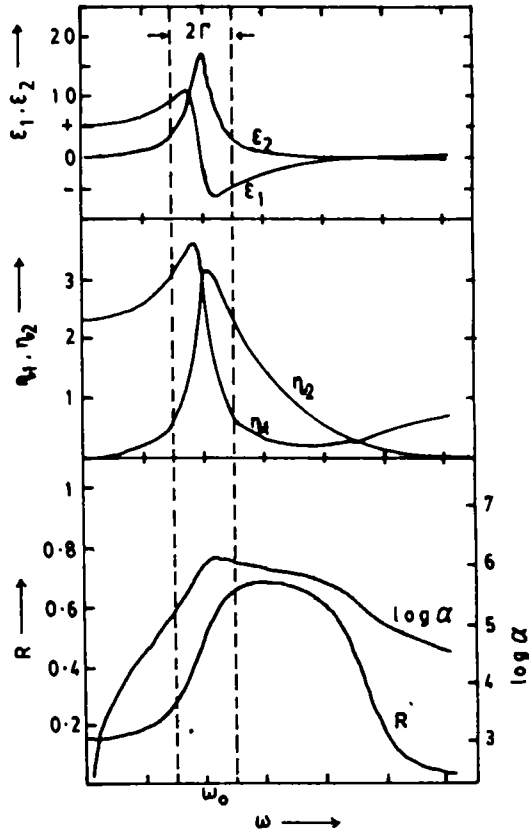
Fig.1.3   Frequency dependence of the dielectric function, the
refractive index, the fresnel reflectance and absorption
coefficient for a medium with a single resonance at ωo
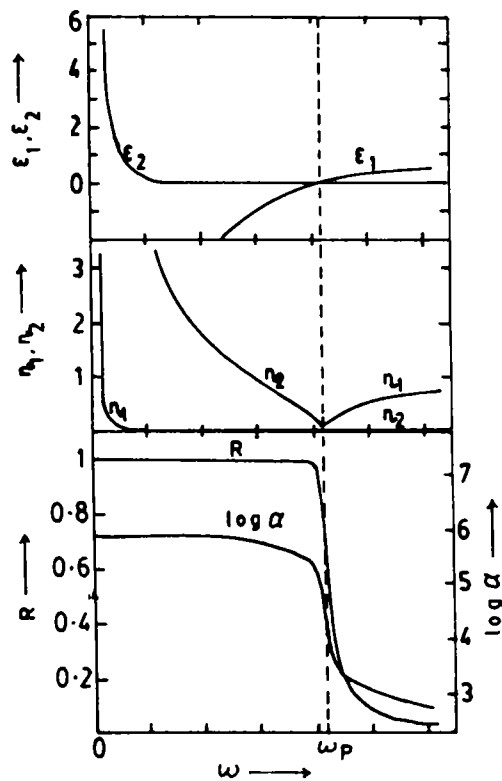
Fig.1.4   Frequency dependence of the dielectric function, the
refractive index, the fresnel reflectance and absorption
coefficient for a free electron metal

generated) contribute measurably to the metal like reflectance of many semiconductors in the visible region.

Most non-metals show in addition to electronic transitions, resonant coupling to high frequency optical phonons located in the NIR region of the spectrum. Phonon coupling can be described by resonance terms, but with masses and damping constants characteristics of the lattice vibrations rather than electronic vibrations. The absorption of the material increases as the photon energy approaches the band gap.

In the case of an inhomogeneous non-metals the optical absorption is modified by light scattering at the grain boundaries or inclusions. This results in strong absorption even in the case of materials which are intrinsically transparent (ceramics). This effect can be due to multiplication of the light path inside the material caused by the large number of scattering events.

(b) METALS

The optical response of a metal is dominated by the conduction electrons. Since the electron gas is degenerate, only electrons in the states close to the Fermi level referred to as "free electrons", contribute to the optical properties. There is no resonance frequency for a free electron, and its only interaction with the lattice is by collisions. The dielectric function of the free-electron metal can be obtained from (equ 1.27) by formally replacing the damping constant Γ by the inverse collision time $1/\tau_e$ and setting the resonance frequency equal to zero and f_{osc} equal to 1. So the resulting expression will be,

$$\varepsilon = 1 + \omega_p^2 \left[-\tau_e^2 + i\tau_e/\omega \right] \left[1 + \omega^2 \tau_e^2 \right] \qquad (1.28)$$

Where, $\omega_p = \left[\dfrac{N_e e^2}{m_e \varepsilon_o} \right]^{1/2} \qquad (1.29)$

18

ω_p is the electron plasma frequency. At $\omega = \omega_p$ (which is in the vacuum UV for most metals), both ε_1 and η_1 vanish. The variation of ε and associated quantities with light frequency is shown in the figure (1.4). The plasma frequency is seen to separate into regimes of rather different optical properties. ie, large R and α for $\omega < \omega_p$ and small R and α for $\omega > \omega_p$.

The optical properties of a free-electron metal for $\omega < \omega_p$ are related to the DC conductivity σ_o through the Drude expression [14],

$$\sigma_o = \frac{N_e e^2 \tau_e}{m_e} = \omega_p^2 \varepsilon_o \tau_e \qquad (1.30)$$

useful approximate expressions for the optical parameters can be obtained. For the range $\omega \ll 1/\tau_e$ (far IR region), equation 1.30 gives

$$\varepsilon_1 \simeq - \frac{\sigma_o \tau_e}{\varepsilon_o} \qquad (1.31)$$

and

$$\varepsilon_1 \simeq \frac{\sigma_o}{\varepsilon_o \omega} \qquad (1.32)$$

from which it follows that

$$\eta_1 = \eta_2 = \left[\frac{\sigma_o}{2\varepsilon_o \omega} \right]^{1/2} \qquad (1.33)$$

$$1-R = \left[\frac{8\varepsilon_o \omega}{\sigma_o} \right]^{1/2} \qquad (1.34)$$

$$\alpha = \left[\frac{2\omega\sigma_o}{\varepsilon_o c^2} \right]^{1/2} \qquad (1.35)$$

For the range $1/\tau_e \ll \omega < \omega_p$ (NIR and visible regions in the case of most metals), so that,

$$\eta_1 = \frac{\omega_p}{2\omega^2\tau_e} = 0 \qquad\qquad (1.36)$$

and $\qquad \eta_2 = \omega_p/\omega \qquad\qquad\qquad\qquad\qquad (1.37)$

which gives,

$$1 - R = \frac{2}{\omega_p\tau_e} = \frac{2\varepsilon_o\omega_p}{\sigma_o} \qquad\qquad (1.38)$$

and $\qquad \alpha = 2\omega_p/c \qquad\qquad\qquad\qquad\qquad (1.39)$

The optical properties predicted in the (fig.1.4) corresponds to bulk materials. Metal surfaces show lower reflectances than the bulk due to contamination (adsorbates, oxide layers etc.) or macroscopic defects. Deviation from bulk behaviour may also arise from the intrinsic surface effects such as plasmon excitation or diffuse electron scattering particularly in thin films. The optical behaviour becomes dominated by the surface effects when the dimension of the metal becomes of the order of the absorption length, such as in extremely thin evapourated films or in aggregate structures consisting of small insulated metallic particles [1.15].

1.3.3. MODIFIED OPTICAL PROPERTIES

When the low intensity light is incident on the material, the states of the atom or the electrons are not perturbed. But powerful laser irradiation can alter the optical properties of many materials so that coupling is then not characterized by a static dielectric function but it becomes a dynamical processes.

All laser -induced changes in the optical properties of the material can be described by the one of the three following mechanism, which are in the sequence of irradiance.

(1) Heat production and resulting changes in the density or electronic characteristics of the material. Prominent

20

effects include thermal self-focussing in transparent media as well as thermal run-away phenomena in semiconductors and metals.

(2) Optical generation of free carriers by interband transitions or impact ionization in semiconductors and insulators. As a result, the absorption coefficient increases dramatically, possibly causing explosive material damage.

(3) Non-linear distortion of electron orbits or whole molecule by the electric field of an intense beam. A host of non-linear optical phenomena, including self-focussing and multiphoton absorption are due to field effects.

Apart from these 'intrinsic effects', beam-solid coupling also tends to be affected by the laser induced changes in the shape of the material usually in connection with melting or vapourization.

1.3.3.1. SELF-FOCUSSING

NON-LINEAR EFFECTS IN LIP : SELF FOCUSSING PHENOMENON

The self-focussing occurs when the refractive index of a medium varies with laser irradiance. Extensive reviews on this topic have been made by several authors [16,17,18]. The intensity of the laser beam near the axis is large compared to that of the away from the axis, an irradiance dependent refractive index has an effect somewhat similar to a lens placed in the laser beam path. As illustrated in the figure (1. 5), this is converging if the refractive index η_1 increases with laser irradiance and the phase velocity decreases towards the beam axis causing the plane wave front to become concave and eventually to collapse. The lens is diverging if the η_1 decreases as a function of irradiance. This self-defocussing is inconsequential as far as energy deposition is concerned, but self-focussing increases the effective irradiance and reinforces other irradiance dependent phenomena. The variation in refractive index can itself be thermal or field

induced.

The temperature dependence of refractive index can be taken as consisting of two parts

$$d\eta_1/dT = (\delta\eta_1/\delta T)\rho + (\delta\eta_1/\delta\rho) d\rho/dT \qquad (1.40)$$

This first term accounts for the temperature dependence of electronic or molecular polarizability due to shifts in the absorption bands. Thus in materials with band-gap energies in the ultraviolet region that decreases with temperature, this term tends to be positive in the visible spectrum. The second term connected to thermal expansion is usually negative since $\delta\eta_1/\delta\rho >$ 0 and $d\rho/dT < 0$. So the first term favours the self-focussing and the second tends to oppose it. These two contributions will have different relaxation times and there may be transient self-focussing for short pulses even if the steady state value of $d\eta_1/dT$ is negative.

Electric field induced self-focussing, unlike its thermal counterpart is a high irradiance effect relevant only for powerful nano or picosecond pulses. The root of the field induced changes in the refractive index is the anharmonicity of all interparticle potentials. The intensity dependent refractive index can be written as

$$\eta_1 = \eta_1^{(o)} + \gamma I \qquad (1.41)$$

where $\eta_1^{(o)}$ is the linear refractive index and $\gamma = \varepsilon^{(2)}/2c\varepsilon_o\varepsilon^{(o)}$
In the case of transparent medium with $\gamma > 0$, the effect of self focussing on a Guassian beam can be described in terms of field induced thin lens with a focal length that depends on irradiance [17],

$$Z_{nl} = w \left[2\eta_1/\gamma I\right]^{1/2} \qquad (1.42)$$

The lens exactly balances diffraction if $Z_{nl} = Z_0$. This holds, independently of the incident beam radius, if the power is equal to the threshold value,

$$P_{tr} = \lambda^2 / 2\pi\gamma\eta_1 \qquad\qquad (1.43)$$

With the availability of high power laser beam a large number of interesting non linear phenomena have been studied both theoretically and experimentally. Here we will consider a particular phenomenon viz, the self-focussing of powerful laser beams in dielectrics. This phenomenon is due to the dependence of the complex dielectric constant, ε_{eff} on the intensity of the propagating wave.

Consider a beam propagating in a non-linear medium. As the beam gets focussed due to non-linearity, the intensity increases causing further enhancement of nonlinearity and hence the extent of non-linear focussing.

In regions near the focus the present theory based on the WKB approximation is indeed not expected to be valid on account of high light intensities in these regions and also the occurrence of optical break down in the conversion of the state of the material into the plasma state. It is observed that light is finally focussed in filaments of diameter 3 to 5 μm [19]. An electrostriction mechanism for filamentary track formation in transparent optical glass has been reported by Kerr E L [20].

The nonlinearity on the refractive index of a dielectric material arises due to the nonlinear relationship between the displacement vector D and the electric vector E. The two main mechanism for this nonlinearity are

(1) Electrostriction :- This the force which a non-uniform electric field exerts on a material medium (solids). The material tends to be drawn into the high field region. The electromotive force proportional to the gradient of the square of the electric field ie, the gradient of intensity. This force affects the density of the material, which in turn modifies the dielectric constant.

(2) Kerr Effect :- If molecules of a liquid have anisotropic-polarizability tensor, an intense light wave will tend to orient the allotropically polarized molecules such that the
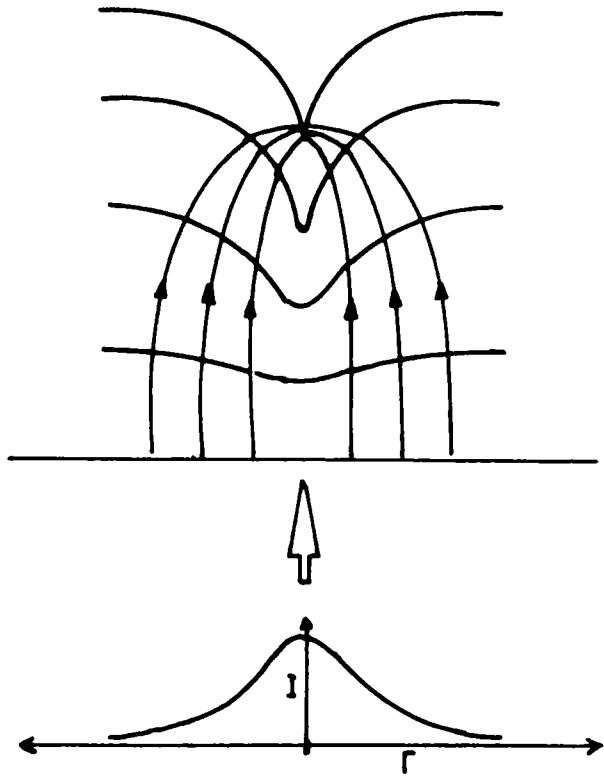
Fig 1.5. Geometrical rays and phase fronts of a gaussian beam undergoing self-focussing in a medium in which local refractive index increases as a function of irradiance.

(a) Desorption
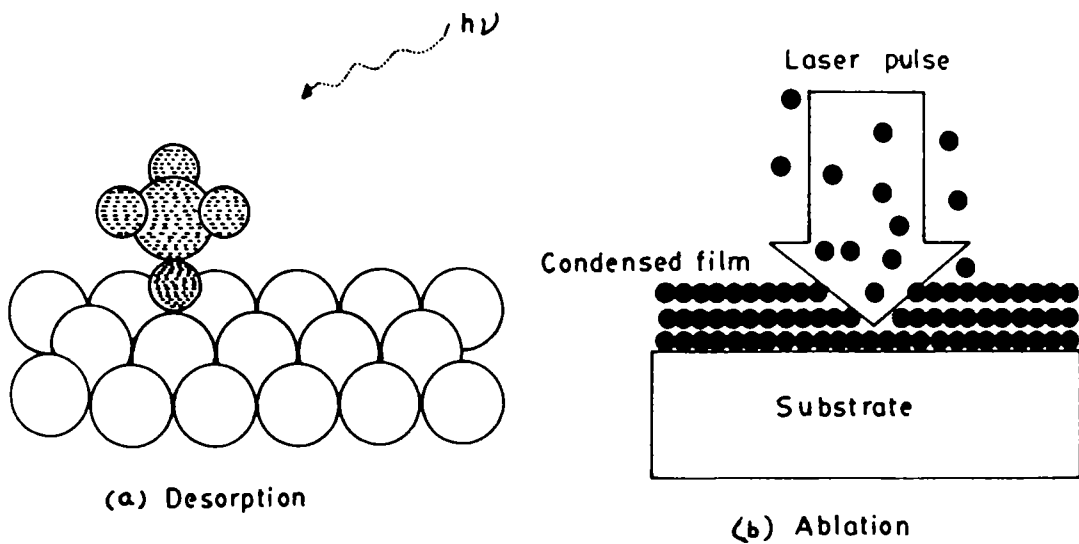
(b) Ablation

Fig.1.6 Schematic representation of (a) desorption of an isolated molecule by an absorption of a photon (b) localized multilayer ablation by a single laser pulse

direction of maximum polarizability is along the direction of the electric vector. This changes the dielectric constant of the medium.

In the case of absorbing medium, an intense light beam, with a radial distribution of intensity causes a radial gradient of temperature and hence the dielectric constant. This leads to the focussing and defocussing of the laser beam depending on the nature of variation of dielectric constant with temperature. If $d\varepsilon/dT > 0$, self focussing occurs, whereas if $d\varepsilon/dT < 0$, defocussing of the beam occurs.

1.3.3.2. FREE-CARRIER EFFECTS

Free carrier generation is the most important self-induced coupling effect in non-metals. In order to consider the impact of free carriers, on the optical properties of a non-metal, the simplest approach is the total material polarization and hence to take the dielectric function as a sum of lattice and the carrier contributions.

In semiconductors, holes tend to be mobile and contribute significantly to absorption. Since electrons and holes come in equal numbers, it is convenient to treat them together and the total absorption coefficient can be written as,

$$\alpha = \alpha_o + N_{eh}\, \Sigma_{eh} \qquad\qquad (1.44)$$

α_o is the lattice absorption coefficient, $N_{eh} = N_e = N_h$ is the density of the carrier pairs and Σ_{eh} is the absorption cross section of a carrier pair which is defined as,

$$\Sigma_{eh} = \left[\frac{e^2}{\varepsilon_o \eta_1 c \omega^2}\right] \left\{ \left[\frac{1}{m^*_e \tau_e}\right] + \left[\frac{1}{m^*_h \tau_h}\right] \right\} \qquad (1.45)$$

where m^*_x and τ_x , (x = electron/hole) are the effective masses and collision times of the electron and holes respectively [21]. Σ_{eh} varies with λ^2, making free carrier absorption relevant for

24

infrared beams.

1.3.4. DESORPTION AND ABLATION

Pulsed laser induced desorption offers ways of studying the dynamics of surface processes. The monochromaticity of the laser radiation allows a selective excitation of defined states and in ideal cases it may be possible to confine energy to the substrate, adsorbate or multilayer film covering the substrate.

Desorption is the processes by which mono or submono layer amounts of molecules leave the substrate surface, whereas in the ablation processes many layers leave the condensed system irrespective of the forces holding the condensed phase together (Vander Waals or exchange forces) and irrespective of the energy of the photons of the laser pulse (UV or IR photons).   Figure (1.6(a) and (b)) give the schematic representation of the desorption processes and ablation.

(A). RESONANT IR AND UV EXCITATION

Transitions between vibrational levels of isolated molecules are usually described by simple models such as the harmonic oscillator or the anharmonic oscillator.   In order to explain the behaviour of polyatomic molecules under high power laser irradiation, the two ladder three region model has been introduced [22,23].   This models assume that the first few photons are absorbed in one vibrational mode in high order multiphoton processes defining region 1.   At higher levels of excitation, rapid intermolecular energy exchange will occur with other vibrational modes.   Optical pumping in this second region, called the "quasicontinuum", is stepwise and incoherent.   At even higher energies in region three, the possibility of dissociation exists.

In the region 1, a mode selective laser excitation is possible, which is destroyed by the efficient intermolecular energy transfer in the quasicontinuum.   So IR multiphoton dissociation is

molecule selective, but not bond selective under collision-free conditions.

In a condensed phase polyatomic molecules due to intermolecular energy exchange, it is difficult to accumulate 20 or 30 IR photons in one molecule and to achieve multiphoton dissociation. So there is no selective coupling between an excited vibrational mode and adsorption potential, as indicated in the figure (1.7), leading to nonstastical desorption. On the otherhand it has been suggested that the surface phonons may communicate well with the low frequency mode of the adsorption potential but a bottleneck exists for the flow of energy into the chemical bonds of the desorbed molecule [24]. This effect would also allow a non statistical behaviour in the case of energy flow from the substrate to the adsorbed molecules.

Figure (1.8) shows the three examples of the laser induced photon dissociation processes. The first one is the coupling with a repulsive upper state possessing no energy minimum, the second one shows a transition to an upper bound state with slightly larger internuclear distance, leading to dissociation by internal conversion and the third case illustrate the direct dissociation into electronically excited products by excitation of bound state with energy excess of the dissociation energy.

(B). ENERGY CONSIDERATIONS

One may make a comparison of photon energy with the corresponding binding energies in the molecular system in order to see whether the quantum processes is energetically possible at a considered wavelength. In the case of molecular system, weak Vander Waals bonds and /or chemical bonds hold the condensed phase together. Typical Vander Waals energies are in the 0.3 eV range and therefore an IR photon may have enough energy for single photon processes. With UV photons, on the otherhand not only the Vander Waals bonds but also chemical bonds can be broken from the energetic point of view. In this case the quantum yield
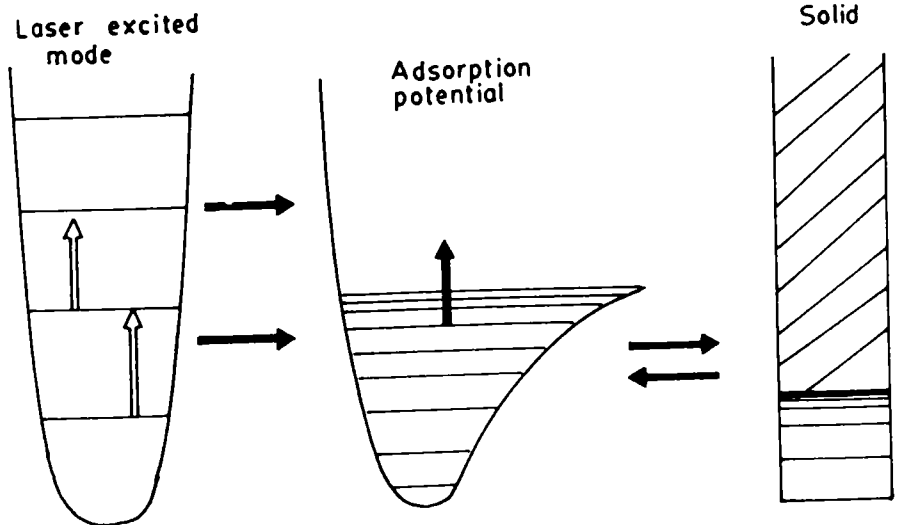
Fig.1.7. Energy situation for IR excitation considering the vibrational levels of the excited vibrational mode, the adsorption potential and the phonons in the solid

(a)

(b)

(c)
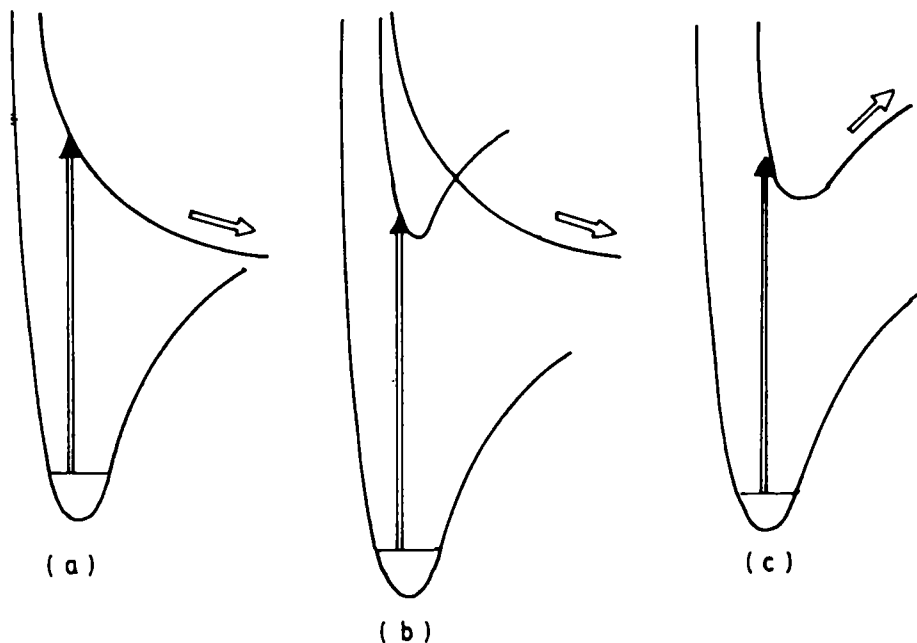
Fig 1.8. Energy situation for UV excitation considering (a) direct dissociation to ground state products by excitation of UV repulsive state (b) upper state excitation followed by the internal conversion and (c) direct dissociation in to electronically excited products

represent the fraction of the absorbed photons leading to photolysis and this fraction essentially heats the sample and finally breaks the Vander Waals bonds. In the latter case, quantum yields greater than one may be observed whereas in a chemically bonded network, the quantum yields are considerably lower. Figure (1.9) shows the comparison of the energy for typical IR and UV photons with the interaction energy of a chemical bond and a Vander Waal bond.

1.3.5. PHASE TRANSITION AND SHAPE EFFECTS

Powerful laser beams not only affect the intrinsic properties of the material, but also the shape of an irradiated material. This influences solid-beam coupling in various ways. Shape effects are related to melting and evapouration.

1.3.5.1. EVAPOURATION AND PLASMA EFFECTS

The vapours formed by the intense irradiation can play important role in beam -solid coupling, particularly for IR beams. The level of irradiance at which the evapouration takes place ranges from 10^3 W/cm^2 to the highest irradiance 10^{15} W/cm^2 or more. It is clear that many physically distinct regimes are found in this enormous range.

At relatively moderate irradiance (below 10^6 W/cm^2), the vapour is tenuous and essentially transparent, but with increasing irradiance it tends to become supersaturated as it evolves from the surface. The vapour cloud is a medium of refractive index different from its surroundings and hence distorts the incident wavefront.

Between 10^7 and 10^{10} W/cm^2, depending on the wavelength, vapour becomes partially ionized and absorbs substantial fraction of the laser energy. The black body radiation emitted by the vapour plasma tends to be absorbed by the solid more efficiently than the laser radiation particularly for IR lasers. If the plasma stays
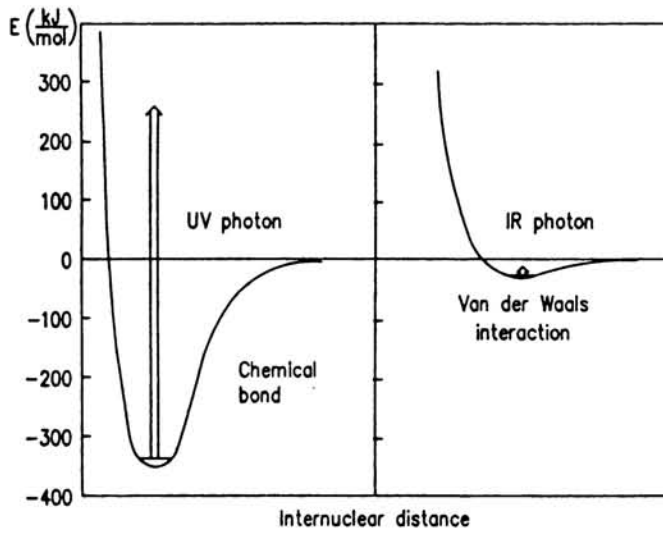
Fig 1.9. Comparison of the energy of a typical IR and UV photons
with the interaction energy of a chemical bond and a
Vander Waals bond
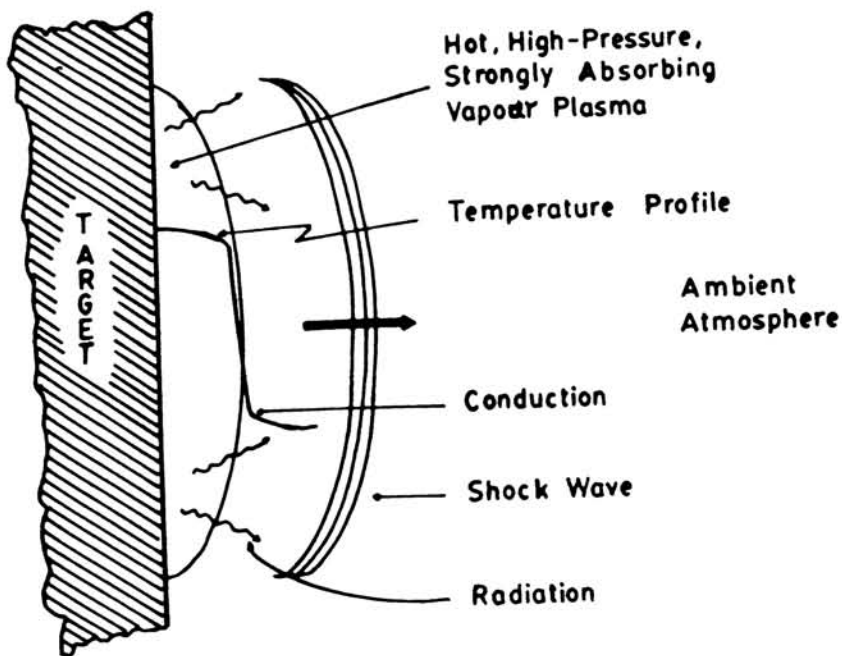
Fig.1.10 Features of interaction between the vapour plasma and
the ambient gas

close to the surface, it may actually enhance the fraction of beam energy absorbed in the solid. At irradiance somewhat higher than those producing ionization of the hot vapour, ionization may occur in the ambient gas due to optical breakdown. The breakdown plasma typically propagates as a supersonic absorption wave against the incident beam and shields the material completely. This effect seriously limits the energy deliverable by the IR beams to targets at atmospheric pressure.

At still higher irradiance (above 10^9-10^{10} W/cm^2), plasma owing to its high temperature, becomes transparent and light is again transmitted to the dense surface. The ablation pressure drives a shock wave into the material which may alter its optical properties. Finally at the highest irradiance any sharp boundary between the condensed material and the plasma disappears. Light is absorbed at the surface where the electron density makes the plasma frequency equal to the laser frequency. Additional absorption and reduced reflectance arise in the plasma from turbulent collective motion of electrons.

1.4. CREATION AND FEATURES OF A PROPAGATING PLASMA

The interaction of the hot vapour plasma with the surrounding atmosphere in the two ways is explained in the figure ((1.10)), (1) the expansion of the high pressure vapour drives a shock wave into the atmosphere and (2) energy is transferred to the atmosphere by a combination of thermal conduction radiative transfer and heating by the shock wave. The relative importance of these processes in determining subsequent plasma evolution depends on irradiance size of the vapour plasma bubbles, large vapour composition ambient gas composition and pressure, and laser wavelength. At low irradiance, conduction dominates the early stages of plasma development in the surrounding gas, the vapour plasma is too thin spatially and optically to transport energy efficiently by radiation. At high irradiance, shock heating dominates.

28

In the initial stages, the absorption wave is characterized by high temperature and also by high pressure caused by the shock wave driven of the target surface during the initiation process. The subsequent evaluation of the plasma follows three major paths depending on irradiance, spot size and ambient gas conditions. The radiative transfer surface pressure, plasma velocity and plasma temperature are strongly influence by the nature of the plasma.

The three major types of laser absorption wave are

(1) Laser-supported combustion (LSC) waves

(2) Laser-supported detonation (LSD) waves

(3) Laser-supported radiation (LSR) waves

The main difference between the waves arise from the different mechanisms used to propagate the absorbing front into the cool transparent atmosphere. The characteristics difference which distinguish the above three waves are velocity, pressure and the effect of radial expansion on the subsequent plasma evolution.

The general configuration of the absorption wave is described in the figure (1.11). This will illustrate the zones that must be considered to describe the class of the waves and their development with respect to the time. The zones are the precursor shock, absorption region and plasma left behind the propagation region. The shock and the absorption wave are propagating away from the larger surface, whereas the plasma behind the wave is expanding radially. The range of irradiance at which the absorption wave propagate with subsonic velocity with respect to the gas (ambient atmosphere or vapour) is called LSCW. At low irradiance, LSCW are produced, which consists of a precursor shock that is separated from the absorption zone and the plasma (figure.1.11). With further increasing irradiance the temperature, pressure and velocity of the absorption wave increases. At the same time wave becomes more absorbing and consumes larger fraction of beam flux. Compression rather than heat conduction becomes the dominating propagation mechanisms. The velocity in this region is supersonic with respect to the gas
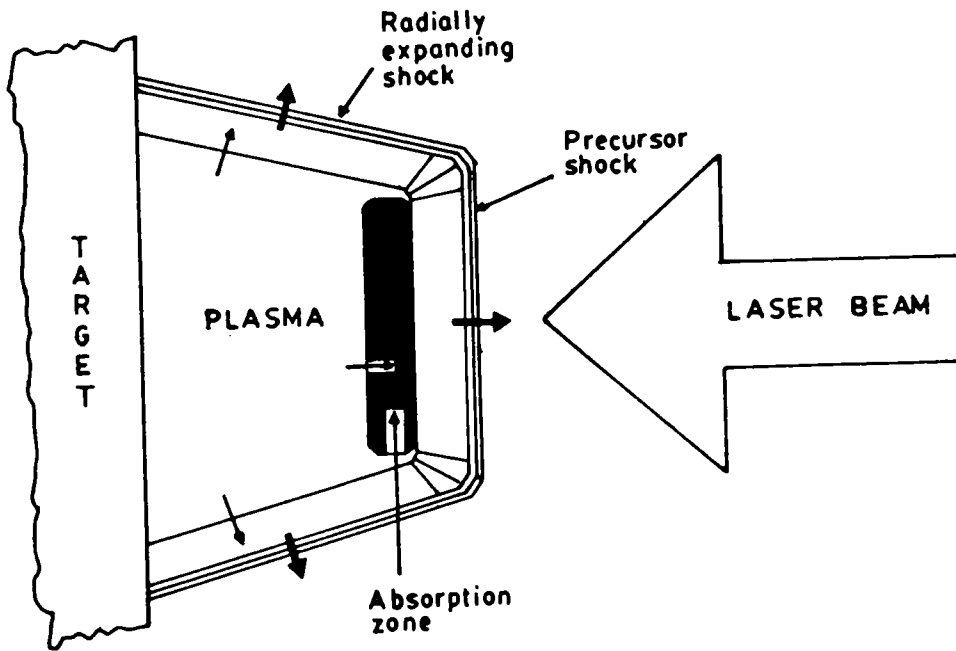
Fig.1.11 Features of propagating laser supported plasma created above the target
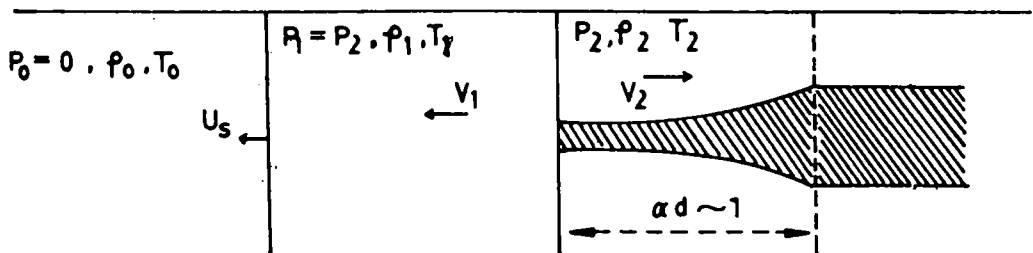
Fig.1.12 Three-zone model of irradiated material in a self regulating plasma regime.

ahead of the wave and hence the wave is a shock wave, which is called LSDW. At sufficiently high irradiance, the plasma radiation is so hot that prior to the arrival of the shock wave, the ambient gas is heated to the temperatures where the laser absorption begins and the absorption wave formed in this condition is called LSRW.

1.5. PHENOMENA AT VERY HIGH IRRADIANCE

Here the light flux exceeding from 10^9 W/cm^2 or 10^{10} W/cm^2, where the plasma produced are dense and hot enough to achieve thermonuclear fusion. The practical application of the use of the plasma as pulsed sources of X rays or fast ions. In the low irradiance region, the optical density of the gaseous plasma increases with irradiance. But in the case of high irradiance the plasma is fully ionized and the above processes are reversed since the degree of ionization cannot be further increased. The temperature at which this processes happen to be depend on the atomic number of the material. In the case of lightest metal which are of interest in laser fusion and where the full ionization can be achieved.

In this irradiance regime even non-metals can be considered as strongly absorbing, because the breakdown will occur within a fraction of pulse duration. At highest irradiance (10^{15} W/cm^2 or more), ionization occurs by multiphoton absorption. The specific energy acquired by the material exceeds the heat of evapouration and even the dense phase can be treated as ideal gas. But a strong non-equilibrium exist between the electrons and ions will prevail when such pulse lasts.

Consider a dense and strongly absorbing material, in the first few tens of nanometer, the energy at a rate of 10^{20} W/cm^2 is liberated. Part of this energy is converted into direct kinetic energy by thermal expansion of the heated layer. In a regime of characteristic nanosecond (Q-switched) pulses, which is dominated by the expansion and ablation of material and a second

regime, characteristic of psec (mode locked laser) pulses, in which heat conduction dominates, as the hydrodynamic motion.

The thermal pressure of the heated layer, orders of magnitude greater is sufficient to cause significant compression to the underlying target material. If we consider different zones Figure (1.12), the undisturbed solid (denoted with subscript o), the compressed layer (subscript 1) and the vapour (subscript 2). Various models have been considered which differ mainly in the treatment of light absorption in the region1 1 and 2. A model appropriate for intermediate fluxes (between some 10^9 and 10^{14} W/cm^2 for light targets) is based on the idea proposed by [25], of a self regulating plasma.

PART B

PLASMA DIAGNOSTICS

1.6. LASER PLASMA DIAGNOSTICS

1.6.1. INTRODUCTION

The interaction of intense laser light with matter has been an active topic in the fields of atomic and plasma physics for more than two decades. During this period, an amazingly rich diversity of plasma conditions have been investigated. As an indication of interesting range of parameters, the following conditions have been encountered, *viz.*, (1) electron temperatures (T_e) from 10 eV to many keV, (2) Scale lengths $(T_e/\Delta T_e)$, as short as few microns, (3) Self generated magnetic fields of more than megagauss orders, (4) Particles accelerated to energies as high as megavolt/amu (5) Imploded compressed densities of $>$ 30 g/cm^{-3} (while keeping $T_e \approx 1$ KeV) (6) Ionization stages as high as those of helium-like krypton.

In discussing the diagnostics of laser plasmas, it is very useful to consider the spatial structure involved. This structure is illustrated in figure (1.13 & 1.14), starting from the absorption and scattering of incident laser energy and proceeding through the transport of this energy to denser regions and the resulting ablation pressure which can be used to drive implosions. The structures indicated in the above mentioned figures and their characteristic parameters (temperature, density, gradient, scale lengths *etc*) are evolving in time scale varying from tens of picoseconds to many nanoseconds. The basic progression of interaction (from absorption through compression) is however preserved. In recent years, it was revealed that there exists a strong dependence of absorption and scattering processes on the laser wavelength [26,27]. In the case of laser

32
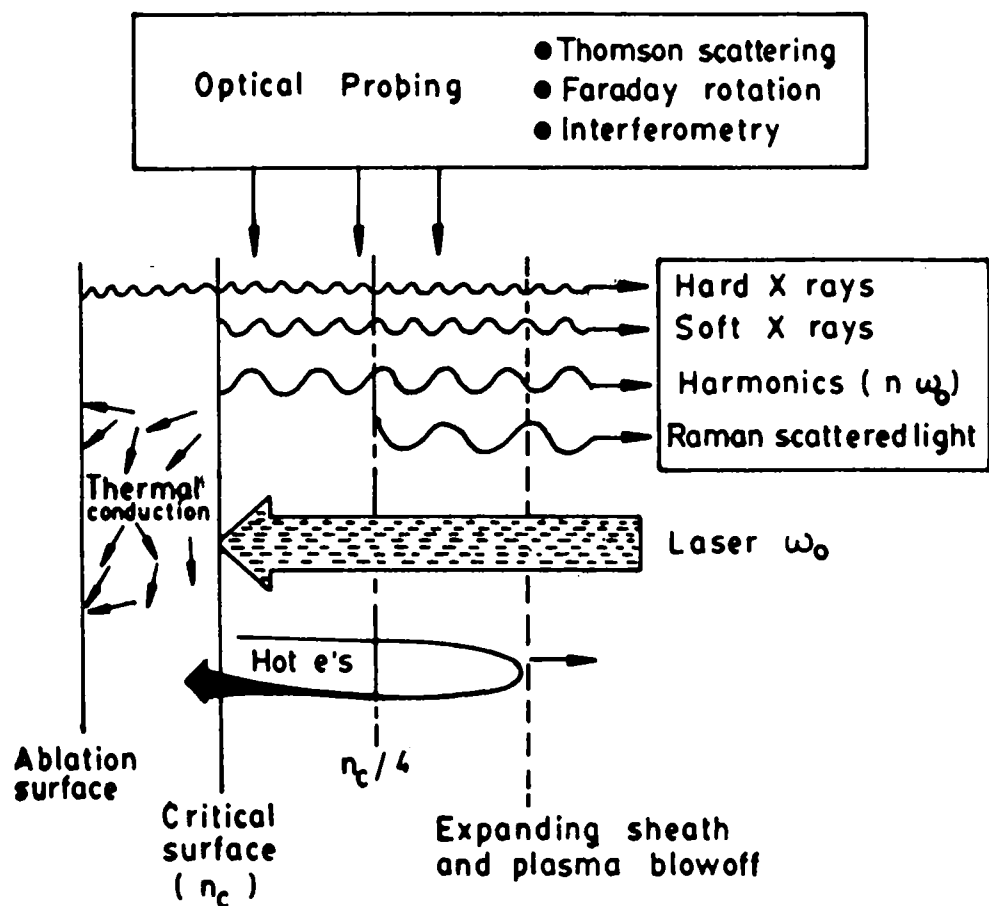
Fig.1.13   Laser plasma interaction-absorption/transport process
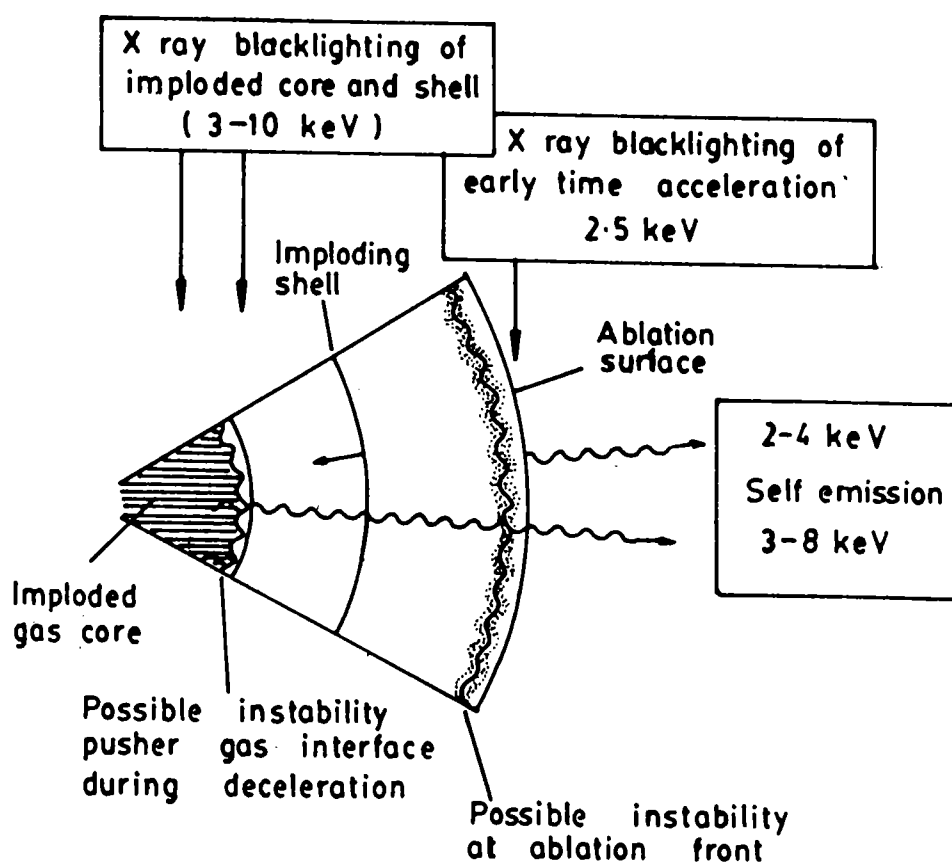
Fig.1.14.   Laser plasma interaction-acceleration/implosion process

fusion applications, short-wavelength laser interaction studies are mainly considered. The density and temperature profile are shown in figure (1.15). It was seen that the density and temperature gradients become much less steep as the irradiance is reduced.

With reference to the figure (1.15), laser light is often absorbed by the collisional processes of inverse bremsstrahlung up to a region near critical surface (where the plasma frequency $\approx$ Laser frequency), where it is reflected and absorbed by the parametric processes. From the critical surface towards the laser, scattered harmonic light offer a rich source of information on both local absorption processes and local plasma conditions.

Table 1.1   Critical densities of some important lasers

Laser	Wave length (μm)	$n_c(cm^{-3})$
CO_2	10.6	10^{19}
Nd glass (ω_o)	1.06	10^{21}
Nd glass ($3\omega_o$)	0.35	9.0×10^{21}
KrF	0.25	1.6×10^{22}

In spanning the range of irradiance from about 10^{12} to 10^{16} W/cm^2, the background T_e varies from few hundred eV to several keV. The critical (electron) density for a given laser wavelength is given by $n_c \approx 10^{21}/\lambda^2$ cm^3 (λ is in microns). The above mentioned trend towards short wavelength lasers thus implies the investigation of plasma processes at a higher density where collisional effects will be emphasized. The critical densities of some common laser wavelengths are shown in Table (1.1).
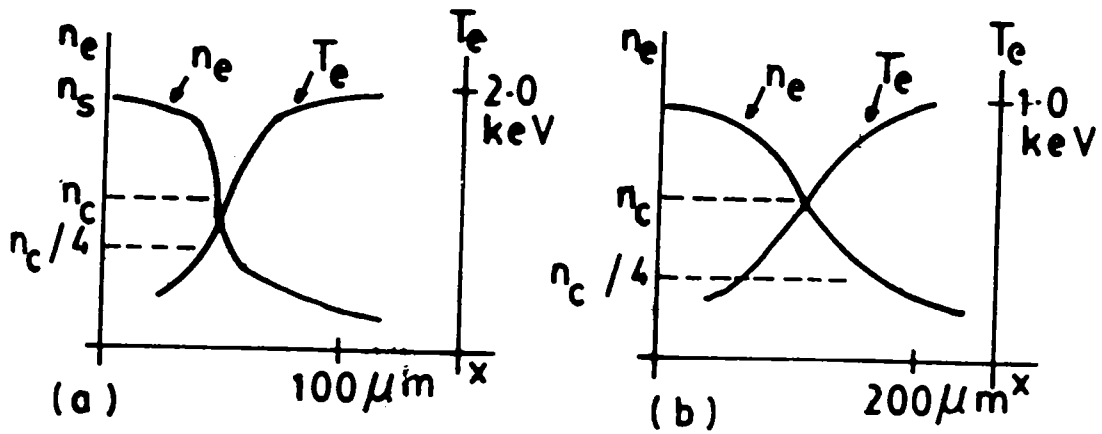
Fig.1.15. Typical density and temperature profiles for (a) high and (b)low intensity irradiation. n_c is the critical density and n_s is solid density
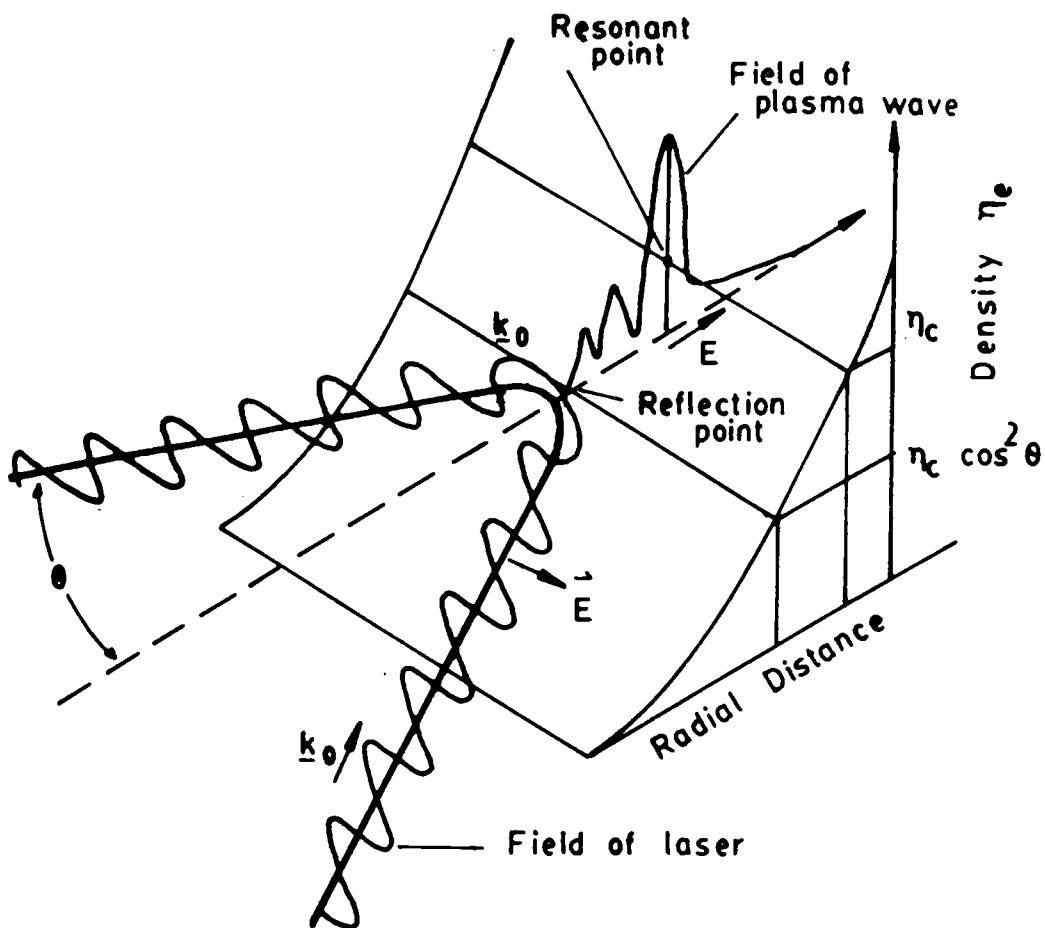
Fig.1.16. Schematic of resonant absorption processes for P-polarized light

1.6.2. INTRODUCTION TO OPTICAL DIAGNOSTICS.

Optical plasma diagnostic techniques can be separated into two main categories. (1) Those involving the analysis of the emission spectrum from the plasma and (2) Those analyzing the changes undergone by the radiation introduced into the plasma in the form of a probe beam.

In a laser-produced plasma, we have two main contribution to the emitted spectrum. One contribution consists of the emission from the self-luminous plasma itself, ie, the continuum and line radiation. The analysis of this radiation has been an important diagnostic tool in laser plasma physics. However, for laser plasmas in the range 100 eV to 1000 eV (in the case of laser fusion studies), most of the emission will lie in the spectral region ranging from the vacuum UV to X-ray region. In application such as chemical analysis, temperatures are usually below 100 eV. In such studies the ion and continuum emission is in the optical and ultraviolet regions. A second contribution to the radiation emitted from the plasma is the emission associated with the scattering of the incident laser light by different modes in the plasma. This emission occurs through parametric processes and the generation of harmonics as well as fractional harmonics of the incident laser light.

Another optical diagnostic technique is to use a separate laser beam as a probe beam. Information about the plasma can be obtained from the changes in the optical properties of the probe beam. One example for this is interferometry by which the electron density, spatial distribution and gradients are commonly derived by measuring the change in the phase front of the probe beam.

(A). PLASMA DIAGNOSTICS BY SCATTERED LIGHT

(I). PARAMETRIC INSTABILITIES

Intense laser light can excite a collection of instabilities in

the under-dense plasma [28]. From the point of view of plasma diagnostics, there are two areas of interest related to parametric instabilities, one of which is the study of the parametric instabilities themselves. The mostly used diagnostic for the study of parametric instabilities in laser plasma has been the scattering of an electromagnetic wave (the laser radiation itself) from one of the longitudinal waves resulting from the decay. Typical examples are scattered light associated with instabilities such as SRS (Stimulated Raman Scattering) and stimulated Brillouin scattering (SBS) [29]. Another example is the $3\omega_o/2$ emission [30] resulting from the scattering of laser electromagnetic wave from plasma waves produced by the decay of the laser light into two plasma waves [31].

A second area of interest in the parametric instabilities is the use of the scattered light as a diagnostic of the plasma itself. This is an important diagnostic tool to characterize the temporal evolution of the plasmas.

(II).HARMONIC EMISSION

When laser light is incident on a target, the reflected light is found to contain the second harmonic component of the incident laser light [32] and also higher harmonics [33,34]. Harmonic generation in laser plasmas is very closely related to the process known as resonant absorption. The measured efficiency of harmonic production and the polarizations of the harmonic wave can provide insight into the general properties of the plasma. Two aspects of the plasma response are possible contributors to the production of harmonics *ie*, (1) steep density gradient arising from the radiation pressure and (2) self-focussing originating from the intensity modulation of the laser beam.

In resonant absorption, laser light incident on a plasma density gradient at an oblique angle can excite resonant plasma oscillations near the critical density region as shown in figure (1.16). At the turning point, the electric field of the laser

light is parallel to the electron density gradient.   Electrons
oscillating under this field will be moving into the region of
higher and lower electron density, and thus harmonic components
will be superimposed on their oscillations and also similarly on
the electromagnetic wave they radiate.   The number of harmonics
will be a function of the intensity of the laser light and the
steepness of the electron density gradient.

(B). OPTICAL PROBING OF LASER PLASMAS

(I). BASICS OF OPTICAL PROBING

Optical probing of plasma is an important and mature area of
plasma physics.   Optical interferometry has been used for
measuring electron density.   In recent times, Thomson scattering
has been one of the most important diagnostics to characterize the
density and temperature of electrons in Tokamak machines.

The application of optical probing to laser plasma is somewhat
difficult due to the relatively higher densities encountered in
the plasma.   Because the probe pulse is limited to electron
densities less than the critical density ($n_e < n_c$) at which
plasma frequency equals to laser frequency, a laser probe with a
short wavelength is required to propagate through the high
densities encountered in these plasmas so that the interaction
with the plasma will be weak and the plasma conditions will not be
disturbed.

(II). ELECTRON DENSITY MEASUREMENTS

Optical interferometry is a well established technique for
measuring the refractivity of plasmas by directly comparing the
phase of a wave front passing through the plasma with that of a
reference beam [35].   Interferometry can be used to determine the
electron density distribution because in highly ionized plasmas
the refractive index μ is related to free electron density.   The

36

refractive index in a plasma is given by

$$\mu(r) = \left[1 - \frac{n_e}{n_c} \left[1 \pm \frac{\omega_c}{\omega} \right]^{-1} \right]^{1/2} \qquad (1.46)$$

where ω is the frequency of the probe and ω_c is the electron cyclotron frequency.

In laser plasmas, the limited size of the plasma permits the use of single beam interferometer arrangement in which plasma is placed off axis, thus using half of the laser beam as the probe. This arrangement permits to use the other half of the beam as the reference. Folding the wave over itself or splitting the beam in to two and shifting one component allows for a compact and stable arrangement. Further improvement is to use the holographic interferometry [36] because of its reduced requirements on the quality of some of its optical components and improved spatial resolution. Because all phase information is recorded, the focussing of the interferometer is not important. One important consideration of utilizing interferometry for density distribution measurements in laser plasma is to have a probe pulse that is sufficiently short in time to freeze the motion of the plasma. Because the plasma density contours move outward with high velocity, the probing pulse length τ must be, to first approximation,

$$\tau < \frac{\text{required spatial resolution}}{\text{velocity of density contour}} \qquad (1.47)$$

For greater probe pulse durations, the interferometric fringes will smear and loose contrast, and eventually disappear. For electron density contour velocities of the order of $\approx 10^6$ cm/sec and spatial resolution of $\approx 1\mu m$ and probe pulse duration ≈ 100 psec is required.

(III). MAGNETIC FIELD MEASUREMENTS

In the presence of strong anisotropy, the polarization vector of a probe beam can suffer a rotation and can be used as a diagnostics itself. If the anisotropy is produced by strong magnetic fields, the rotation of the electric field of the probing pulse (Faraday rotation) provides the basis for measuring these fields. The linear polarization is decomposed into two oppositely rotating circular polarizations. In a magnetized medium, one of these rotates in the direction of the electrons, with the other rotating in the opposite direction. The dispersion equation yields different phase velocities for these two wave components, resulting in a rotation of linear polarization. The polarization vector is rotated when a component of the propagation vector is aligned with the magnetic field vector. The rotation angle is given by,

$$\phi = 2.6 \times 10^{-25} \lambda^2 \, n_e(r)B(r)dr \qquad (1.48)$$

where ϕ is in radiance, λ is in μm and the magnetic field $B(r)$ is in gauss which is the component of the magnetic field in the direction of the propagation vector. Even for large magnetic fields (megagauss), the rotation ϕ is very small (a few degree).

The interest in magnetic field measurement in laser plasmas is based on theoretical and computational evidence of spontaneous magnetic fields at megagauss level, which may themselves be useful in applications. Spontaneous magnetic fields can be generated by the following possible mechanisms.

(1) the flux of the charged particles emitted from the plasma.

(2) the electron temperature gradient having a component perpendicular to density gradient

(3) charge separation during plasma expansion and

(4) momentum deposition by the laser beam

(IV). THOMSON SCATTERING

A laser beam incident on a medium can be scattered by the inhomogeneities in the medium. In a plasma, such scattering is mainly due to electron density fluctuations. Every charged particles in the plasma is capable of scattering light, but because the scattering cross section is inversely proportional to the square of the particle mass, the contribution from ions is negligible compared with that from the electrons. The spectrum of the electron density fluctuation in the plasma is impressed on the scattered light, thus providing information about the collective as well as non collective motion (velocity distribution) of electrons. These features make Thomson scattering a powerful diagnostic, providing direct information about these two aspect of electron fluctuations. Although only the electron scattering is detectable, the motion of the ion modifies the electron fluctuations. Thus information about the ion motion is also obtained. Scattering from a collection of charged particle occurs only if there are spatial fluctuations in the electron density. Conservation of momentum tells that the wave number of the density fluctuation must satisfy the condition $k = (k_s - k_i)$, where k_i and k_s are the wave numbers of incident and scattered beams respectively. The magnitude k is given by

$$k = \frac{4\pi}{\lambda} \sin\frac{\theta}{2} \qquad (1.49)$$

where θ is the angle between k_s and k_i. The vector k is fixed by selecting a laser wavelength and a scattering angle. The quantity k^{-1} is the scale length for scattering and represent the length on which the plasma fluctuations are viewed. Fixing the k vector selects the spatial fourier component of electron density distribution and the frequency spectrum that will be observed. Some fourier components correspond to the resonant modes in the plasma, appearing as peak in the frequency spectrum. Since the plasma resonance can exist only for modes with wavelengths larger than Debye length λ_D, the kind of scattering spectrum that will be

observed can be characterized by comparing the k^{-1} and λ_D. If $k^{-1} \ll \lambda_D$, the movement of the individual of the electron will be observed. If $k^{-1} \gg \lambda_D$, collective motion of the electrons/ions will be observed. A convenient parameter α can be defined to characterize the different scattered spectra which is given by,

$$\alpha = \frac{1}{k\lambda_D} \qquad (1.50)$$

1.7. MASS SPECTROSCOPY AND TIME OF FLIGHT ANALYSIS TECHNIQUES

(A). MASS SPECTROSCOPY

Laser vapourization is rapidly gaining popularity as a method of sample introduction is mass spectroscopy [37,38]. Pulsed lasers are typically used in this experiments, and sample vapourization and ionization take place in one of the two modes. In one case relatively high intensity pulses, I > 100 MW/cm^2 are used to simultaneously vapourize, ionize and in some cases fragment the sample of interest [39]. This type of instrumentation is often referred to as a laser microprobe or laser ionization mass spectrometer [40]. In the second case relatively gentle irradiation I < 10 MW/cm^2 is used to vapourize intact or largely intact molecules. In this type instrumentation, ionization and fragmentation occur by a secondary process, typically electrons impact [41], chemical ionization [39] or photo ionization by a second laser [42], subsequent to vapourization.

The common characteristics of both methods are, (1) No background is introduced due to the bulk heating of the sample (2) Spatial resolution can be very good, limited only by diffraction of the incident beam (typically ≈ 1 μm in diameter) and at high flux, cratering of the surface (typically ≈ 10 μm) occurs. This capability can be important for small samples and samples containing inhomogeneously distributed components. (3) Little

sample preparation is needed. (4) Sensitivity is excellent and detection limit frequently falls in the femtogram to attagram or sub-parts-per-billion range. (5) The possibility exists for absolute measurements without recourse to standard samples. A variety of laser sources have been used in the laser evapouration mass spectrometry in which pulsed lasers are mainly used. Irradiation of the sample may occur either from the back side or from the front side. In the case of post ionization, pulsed dye lasers are commonly used. Tuning capability allows the use of resonant intermediate state in a multistep ionization processes, thus increasing both the probability of ionization for most atoms and molecules and the selectivity of ionization which is used in the analysis of complex mixtures. With the use of resonant intermediate state the ionization can be saturated within the laser focal volume. The mass spectrometry has been used with multichannel detection in time of flight (TOF) techniques and also in fourier transform spectrometers.

(b). TIME OF FLIGHT TECHNIQUES

The time-of-flight (TOF) technique has attracted increasing interest recently in the study of pulsed laser ablation. Two different types of instrument are used in the TOF mass spectrometry as shown in (figure 1.17(a) and 1.17(b)). The first type of instrument consists of two lasers, one for ejection of neutrals and partial ionization and a second one for post ionization in the gas phase to increase the number of ions. These ions are accelerated into and separated in an ion drift tube and detected with a channel plate detector. The advantage of this method lies in the registration of the whole mass spectrum of the different species ejected by a single laser pulse. This instrument is mainly used in laser mass spectrometry specially for organic compounds.

The second TOF method is also based on pulsed laser ablation of neutrals. After a certain flight distance, the neutrals are

41

Fig.1.17   Time of filght technique

Fig.1.18.   Langmuir probe circuit

ionized by electron bombardment in the ionizer of a quadrupole mass spectrometer. An ion produced with high abundance is selected for time resolved detection in the quadrupole mass spectrometer. This technique allows the accurate registration of TOF distributions for selected mass.

The TOF method using a quadrupole mass spectrometer enables accurate determination of transilational energies of molecules ejected by IR or UV laser pulses. The neutral particles ejected from the surface are ionized with relatively low efficiency by electron impact. The ionized particles are extracted by ion optics into the quadrupole mass filter for mass selection and time resolved detection. The drift time of the ions in the analyzer depends on the ionizer potential and is approximately proportional to the square root of the mass. After the subtraction of the delay time, the TOF distribution can be transferred into a velocity distribution. The velocity and translational energy of a particle can be calculated from its mass, the flight time and flight distance.

An indigenous method of attaining perfect focussing also makes the use of ions moving in a plane perpendicular to a magnetic field. All such ions which originate at a point will pass through this point after completion of circular paths in the field, whatever their mass, direction or speed. But, while the time taken by an ion to complete each circular orbit will also independent of its direction and speed of injection, it will depend on the mass according to the equation

$$t = 2\pi m/He$$ (1.51)

Thus mass may be resolved by observing their times of flight for complete revolution in a magnetic field.

Another type of mass spectrometer is that in which the time-of-flight of the ions is measured between the source and the collector in the absence of a magnetic field, so that the ions flow a linear path. These employ measurement of the drift time

of a pulse of ions of known energy down a long evacuated tube. The time interval between the arrival of masses m_1 and m_2 at the collector is proportional to $(m_1)^{1/2}-(m_2)^{1/2}$ and the spectrum may be displayed by amplifying the pulses and applying to oscilloscope whose time base is triggered by the original pulse.

1.8. FUNDAMENTAL ANALYSIS OF SOLID BY LIP

1.8.1. PHENOMENOLOGY OF LASER HEATING OF CONDENSED PHASE TARGET

The introduction of high power laser beam with a condensed phase target leads to a wide range of linear phenomena [43,44]. This is of particular interest in the context of the elemental composition analysis of condensed specimens in the formation of plasma plume that grows out of the surface when the incident laser irradiance exceeds a certain threshold value [45].

The intensity profile of a typical Q-Switched laser pulse has an approximately trapezoidal shape in time. The slope of the laser intensity rise in the leading edge is of the utmost importance in attaining a plasma plume that in both representative of the condensed-phase specimen in its elemental composition and robust in its emission characteristics for quantitative spectroscopy. The leading edge must meet two requirements in that it must be able to heat the target at a rate (1) fast enough to remove the surface layers at a speed equal to or greater than that of the thermal conduction front moving into the bulk and (2) slow enough to allow continued evapouration without triggering runaway absorption by the plasma plume prematurely. When the plasma is near its peak density and temperature the laser plasma interaction enters into a nonlinear regime. One of the measurable consequence is the generation of the second harmonic of the incident laser beam [46].

When the plasma at different distance from the target is recorded, the emission spectrum near to the target displays a continuum character right at the onset of the plasma, indicating

an extremely rapid heating. But the line emission character is quiet pronounced. The luminosity in the region at further distance from the target is due to fast ions and neutrals moving ballistically away from the plasma core near the target surface. After a short period corresponding to the time delay between the fast ion front and shock front arrival, intense emission lines emerge. These are due to shock heating of the ambient gas and residuals from the earlier expansion of the fast ions and neutrals from the plasma of the target elements. Finally, the expanding plasma core with a full display of a rich emission line spectrum is observed. The variation of emission line spectrum from one region of the plasma to another is due to variations in the plasma temperature. The observed temporal and spatial change of the plasma, when analyzed by quantitative spectroscopy, give rich information regarding the formation and evolution of the LIP processes.

1.8.2. QUANTITATIVE SPECTROSCOPY

Determination of the elemental composition of a condensed phase target by means of LIP requires the measurement of the intensities of the spectral lines that are characteristics of the individual species present in the plasma. The intensities must then be related to the number densities of the species present in the plasma and these relationships turn out to be dependent on the temperature of the plasma.

The plasma of depth D is in a state of thermodynamic equilibrium at temperature T. The specific intensity at frequency f of an emission line is defined as the energy emitted from the plasma per unit time, unit surface area, unit solid angle and unit frequency. The change in the specific intensity $I(f)$ is given by the equation of radiative transfer [47],

$$\frac{dI(f)}{dx} = K(f) \cdot \left[B(f,T) - I(f) \right]$$

(1.52)

where x is the coordinate axis perpendicular to the surface area of the plasma and B(f,T) is the Planck's black body function. The absorption coefficient of the plasma K(f) is given by,

$$K(f) = hf_o \, P(f) \, n_i B_{ij} \left[1 - \exp(-hf_o/kT)\right]$$ (1.53)

h is the Planck's constant, n_i the number density of the species in the lower of the two energy levels between which the radiative transition for the emission takes place and k the Boltzmann constant. P(f) is the line profile function of the emission line whose central frequency is f_o, which is normalized.

When Equ.1.52 is integrated with respect to x, between the two confining planes of the plasma separated by D so that,

$$I(f) = 1 - \exp\left[-K(f)D\right] \, B(f,T)$$ (1.54)

The product K(f)D is the optical thickness of the plasma. In the limit K(f)D is increasing infinitely, the specific intensity is given by the black body function, thus reducing the plasma to a blackbody surface radiator at temperature T. So the specific intensity I(f) remains constant throughout the plasma describing the state of a blackbody in which both the particles and photons exist in a state of complete thermodynamic equilibrium.

The integrated intensity of an emission line with center frequency f_o as given by,

$$I = \int_{f_o-\infty}^{f_o+\infty} I(f) \, df$$

so that,

$$I = B(f_o,T) \int_{f_o-\infty}^{f_o+\infty} \left[1 - \exp\left[-K(f)D\right]\right] df$$ (1.55)

This integrated intensity grows with the concentration of the species in the plasma through the number density n_i of the species populating the lower energy designated by i, as contained in the expression of $K(f)D$, which is a strong function of temperature and is given by the Boltzmann distribution,

$$n_i = \frac{n_o g_i \exp(-E_i/kT)}{Q}$$ (1.56)

Here, n_o is the total number density of the species in the same state of ionization and E_i is the energy of the ith level as measured in reference to the ground state level of the species in the same state of ionization. The single particle cannonical partition function Q for the electronic degrees of freedom of the species in a particular state of ionization is given by,

$$Q = \sum_s g_s \exp(-E_s/kT)$$ (1.57)

The sum is over all allowed electronic levels.

The concentration dependence of the integrated intensity is generally non-linear because the optical depth of the plasma decreases with increasing concentration [48]. When the plasma is optically thin, the integrated intensity grows linearly with the number density. In this limit, the integral of equ.1.55 can be expanded in a Taylor series so that,

$$I = \frac{hf_o D A_{ji} g_j n_o \exp(-E_j/kT)}{Q}$$

(1.58)

Where the normalization of the profile function is used together with the expression for Planck's blackbody function.

Calculation of the intensity vs concentration relation requires the value of line profile function, which is in general given by a convolution integral of two or more line profile functions corresponding to the line broadening mechanisms within the plasma

46

[48]. For plasmas that are modestly optically thick and therefore conveniently suitable for quantitative spectroscopy, the degrees of ionization of constituent species are small and the line broadening by Stark effect is modest. Then the line profile function can be represented by the Viogot function,

$$P(f) = \frac{\Delta f_L}{\pi^{2/3} (\Delta f_D)^2} \int_{-\infty}^{+\infty} \frac{\exp(-q^2)\, dq}{(\Delta f_L \, \Delta f^2)_D + [(f - f_0)_D \Delta f - q^2]}$$

(1.59)

Here Δf_L is the half width at half intensity of the Lorentzian profile representing the collisional broadening mechanism. Also Δf_D is the half width intensity of Guassian profile function arising from Doppler broadening. Once the line profile function is given in some form (equation 1.53) can be used to determine the functional dependence of the integrated intensity on the number density of the species of interest. When the optical thickness of the plasma increases, then the relation between the intensity and density becomes non-linear. Another factor that affects the optical thickness is the magnitude of the Einstein coefficient A_{ij}. The larger of this value, more readily the intensity and density relation becomes non-linear.

It has been shown that the integrated intensity of an emission line of an elemental species can be expressed in terms of atomic and thermodynamic properties, including species concentration given that the plasma is in a state of thermodynamic equilibrium. When the intensity is measured and all other properties are known, the number density of the species can be determined. The accuracy of such measurement depends on the extend to which the plasma is optically thin and also on the information about the

47

plasma properties obtained by other measurements.

1.8.3. INTENSITY MEASUREMENTS AND ELEMENTAL ANALYSIS

The integrated intensity of an emission line can be measured by a number of means. The simplest and quite accurate method is to set the entrance slit of the spectrograph wide enough so that its width on the image plane is wider than the width of the emission line. The image plane slit width is given by the product of geometrical width of the slit on the image plane and the linear dispersion of the spectrograph. The resultant intensity at the line center is the integrated intensity. Such integrated intensities of the emission lines for the plasma can be measured by any one of several type of detectors, such as PMT, photo diodes and spectroscopic film. For films the signals will be in the form of blackening as quantified by the neutral density of the exposed area. In the case of photoelectric detectors, the resulting signals may be handled as photoelectric current or by a photon-counting scheme. Integrated intensity can be obtained once the detector sensitivity is established, either by direct calibration with a radiation standard or by compiling all of the intrinsic properties of the detector's data chart elements. The external optics must also be analyzed in regard to the light gathering solid angle, reflective, absorptive and scattering losses and the definition of the plasma volume contributing to the intensity. The efficiency of the spectrograph also enters into the analysis. Another effective approach is to calibrate the entire detection system as a function of wavelength with a calibrated radiation standard source placed at the plasma source.

The plasma temperature can be measured by line intensities to varying degree of accuracy depending on the optical thickness of the plasma. In the optically thin limit, the intensity ratio of the pair of emission lines of one atomic species in a given state of ionization can be written from equation (1.55) as,

$$\frac{I_1}{I_2} = \frac{(f_0 A_{ji} g_j)_1 \exp - (E_{1j} - E_{2j})/kT}{(f_0 A_{ji} g_j)_2} \tag{1.60}$$

This equation is used for the measurement of temperature. In general, the relative transition probabilities are much more accurately known than the absolute values for the measurement of temperature.

The above measurement must be repeated several times with different pairs of emission lines from the same atomic species as well as with those of other species present in the plasma. From the distribution of the resultant temperature values, a determination can be made of the degree to which the plasma has established a state of local thermodynamic equilibrium. In general, a state of thermodynamic equilibrium exists when the collision time in the plasma is small compared with the characteristics time over which the state of plasma changes significantly [49]. For LIP, the characteristic time ranges from few nanoseconds in the leading edge part of the laser pulse to a few tens of micro seconds in the post pulse plasma after glow.

Once plasma temperature is established, and the optically thin segment of the laser plasma is identified, elemental composition analysis may be carried out using the integrated line intensities. Consider two emission lines, one from an atomic species 'a' and the other from 'b'. Then the intensity ratio is obtained from the (1.60) so that,

$$\frac{I_a}{I_b} = \frac{(f_0 A_{ji} g_j)_a Q_b N_a \exp - (E_{aj} - E_{bj})/kT}{(f_0 A_{ji} g_j)_b Q_a N_b} \tag{1.61}$$

This can be used to measure the relative elemental abundance of the element a in relationship to b. It follows that for multi-element specimens it is desirable to choose the most abundant species as a reference for the determination of the all other elemental abundance, thus providing the basis for establishing the percentage of concentration of the elemental species in the

49

specimen.

Optically thick plasmas are more complex to interpret for elemental composition analysis than those in optically thin limit but the basic approach is same.

1.8.4. LANGMUIR ION PROBE FOR PLASMA CHARACTERISTICS

One of the fundamental techniques for measuring the properties of plasma is the use of electric probes. This technique was developed by Langmuir as early as 1924 and is called the method of Langmuir probes. Basically an electric probe is a small metallic electrode, usually a wire inserted into a plasma. The probe is attached to a dc power supply capable of biasing it at various voltages positive and negative relative to the plasma and the current collected by the probe then provides information about the conditions in the plasma. Using this langmuir probe we can obtain the plasma parameters such as density, electron temperature and the velocity of positive as well as negative ions.

Compared to other plasma diagnostic techniques like spectroscopic or microwave propagation, which give information averaged over a large volume of plasma, in the the probe method local measurements can be done.

A simple probe circuit is shown in the figure (1.18). Experimentally the electric probes are simple devices, consisting merely of an insulated wire used with a d.c power supply and an ammeter or an oscilloscope. The physical process can be described by langmuir probe characteristics which is a plot of negative or electron current against probe voltage V_p and is given in figure (1.19).

At the point V_s, the probe is at the same potential as the plasma. There are no electric field at this point and the charged particles migrate to the probe because of their thermal velocities. When the probe voltage is made positive relative to the plasma, electrons are accelerated towards the probe. Near the probe surface there is therefore an excess of negative charge

50
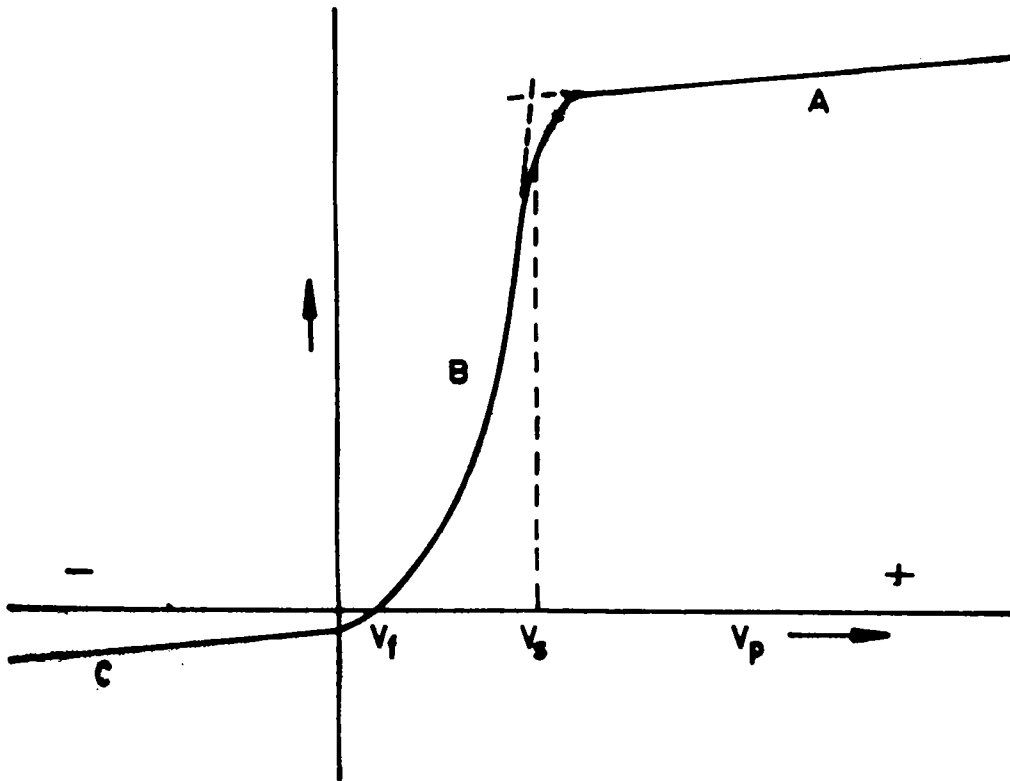
Fig.1.19. Langmuir probe characteristics

which builds up until the total charge is equal to the positive charge on the probe. This layer of charge called sheath which is relatively constant as the probe voltage is increased so that we have the fairly flat portion A of the probe characteristics. This is called the region of saturation electron current.

When the probe potential is made negative relative to Vs, probe begins to repel electrons and accelerate ions. The electron current decreases in region B which we call the transition region or retarding field region of the characteristics. Finally at the point V_f called the floating potential, the probe is sufficiently negative to repel all electrons except a flux equal to flux of ions, and therefore draws no net current.

At large negative values of Vp, almost all electrons are repelled and we have ion sheath and saturation ion current (region C). This is similar to region A, but there are two points of asymmetry between saturation ion and saturation electron collection aside from the obvious one of the mass difference, which causes the disparity in the absolute magnitude of the currents. This is due to the fact that the ion and electron temperatures are usually unequal and it turns outs that sheath formation is considerably different when the colder species is collected than when the hotter species is collected.

It is possible to place a probe in a plasma in such a way that the plasma is not greatly disturbed by the probe, then we can obtain from the probe characteristics information regarding the local plasma density n, electron temperature T_e and space potential V_s and also the magnitude of the saturation electron current is a measure of $n(kT_e)^{1/2}$ from which n can be obtained [50].

The electron temperature can be determined with respect to the volt-amphere characteristics in the region in which the probe has a negative potential relative to the plasma. So the probe repels the electrons and the surface of the probe can only be reached by those electrons in the Boltzmann distribution which have energies sufficient to overcome the potential difference $(V-V_o)$ where V is

the probe potential and V_0 is the plasma potential such that,

$$\text{Log } i = \frac{e}{kT_e} V + \text{Const.} \tag{1.62}$$

By plotting the probe current i as a function of the potential V on a logarithmic scale, we obtain a straight line. The slope of this line can be used for the determination of the electron temperature T_e.

The plasma electron velocity is given by,

$$V_e = \left[\frac{8 \, k \, T_e}{\pi \, n_e} \right]^{1/2} \tag{1.63}$$

For the positive ions in the plasma, velocity is given by

$$V_+ = \left[\frac{8 \, k \, T_e}{\pi \, n_+} \right]^{1/2} \tag{1.64}$$

Where n_e and n_+ are the mass of electrons and positive ions respectively.

1.8.5. VIBRATIONAL TEMPERATURE ANALYSIS OF MOLECULAR BANDS

The intensity distribution in a band can be used for determining the temperature of the source of emission or absorption. The temperature obtained by this way are effective (rotational or vibrational) temperatures. They represent the true temperature only if either the excitation is strictly thermal or is of such type that it does not affect the thermal distribution. The determination of vibrational temperature from the relative intensities of neighbouring bands with different upper vibrational levels seem to be most interesting method since it does not require very high resolution. The band spectroscopic methods for the determination of temperatures are naturally of particular importance when the usual methods cannot be used, *ie*, in the determination of the temperature of the electric arc

[51,52].

The plasma emission spectrum can be recorded photographically. The degree of the blackening in the film is proportional to the peak of the spectrum in a microdensitometer. The relative intensities of vibrational bands are usually obtained using a microdensitometer, by comparing the the peak of each bands with a calibration curve. The intensity distribution in the band can be used for determining the vibrational temperature' of the plasma emission source. This method is adopted in the present studies.

According to the vibrational sum rule for the intensities of different bands in a progression, the sums of band strengths of all bands with same upper or lower state are proportional to the number of molecules in the respective states [53].

$$\sum_{v''} \frac{I(v'v'')}{\nu^4} \quad \alpha \quad N_{v'} \tag{1.65}$$

and

$$\sum_{v'} \frac{I(v'v'')}{\nu^4} \quad \alpha \quad N_{v''} \tag{1.66}$$

Where $I(v'v'')$ is the emission intensity from the vibrational level v' of the upper electronic state to the different vibrational levels v'' of the lower electronic state and ν is the frequency in cm^{-1}. $N_{v'}$ and $N_{v''}$ are the number of molecules in the vibrational levels of upper and lower electronic state respectively.

In thermal equilibrium, the number density at various vibrational levels of the molecule in the excited state can be evaluated using the formula,

$$\log \sum_{v''} \frac{I(v'v'')}{\nu^4} = C_1 - \frac{G'(v')hc}{kT_{vib}} \tag{1.67}$$

Where C_1 is a constant, h is the Planck's constant, c the velocity of the light, k the Boltzmann constant and $G'(v')$ is the

term value corresponding to the excited state vibrational levels and T_{vib} is the vibrational temperature. Therefore by plotting the logarithms of the sums of band strengths measured in the various v" or v´ progressions against vibrational term values G(v), a straight line is obtained. While the intercept is of no significance, the slope is a direct measure of the vibrational temperature.

The advantage of using this method is that no information about the transition probabilities is necessary. It is better suited for molecular systems with radiative decay as the dominant relaxation processes. The disadvantage of this method is the necessity of measuring the intensities of all bands in the progressions used.

When the transition probabilities are known, the intensity ratio of two transitions (v´v") and (w´w") also reflects the vibrational temperature,

$$\frac{I(v´v")}{I(w´w")} = \frac{A(v´v")}{A(w´w")} \exp\left[-\frac{G(v´) - G(w)}{k_B \, T_{vib}}\right]$$ (1.68)

Where A(v´v") and A(w´w") are the Einstein spontaneous emission coefficients. Two upper level energy separations should be comparable to T_{vib}, but the wavelengths should be as close as possible so that we can optimize the error induced by using band head intensity instead of integrated band intensity [54]

The work presented in the following chapters of this thesis concerns with the experimental studies on the plasma produced with moderately high power lasers. The characterization of laser induced plasma from different solid target materials like metals (Aluminium and Copper), polymers (polytetrafluoroethylene), graphite and high T_c superconductors ($YBa_2Cu_3O_7$ & $GdBa_2Cu_3O_7$) using pulsed Q-switched Nd:YAG laser radiation was done. Here the spectroscopic as well as the time resolved analysis of the plasma obtained from the above materials is reported. The spectroscopic study of LIP is a very convenient method to identify the neutral, ionic and molecular species in the plasma.

Identification of these species is important in understanding the complicated ablation, transport and deposition processes. In order to understand the detailed aspects of laser beam interaction with the target material and the recombination processes following the laser ablation, the time resolved studies of the spectral emission from the plasma offer the most logical approach.

The metal film produced by such laser ablation technique can be used as optical filters. Pulsed laser ablation of high purity graphite is considered as one of the most effective methods for the deposition of diamond like carbon films, which is used in infrared applications. Over the past few years, the pulsed laser deposition has emerged as a viable method for *in situ* growth of superconducting oxide thin films. Formation of high T_c thin films is great interest for a variety of applications ranging from interconnections in integrated circuits to hybrid semiconductor/superconductor devices. This thesis also contains the details of the attempts made in this direction by the authors.

REFERENCES

[1] Kunkel W R," *Plasma Physics in theory and Application*", (New Yok, London, 1966)

[2] Frank -Kamentski D A. "*Plasma ,The fourth state of matter*", (Plenum press, New York, 1972)

[3] Maker P D, Terbune R W and Savage S M,*Quantum. Electron. :proc.3rd Intern.congress*, (New York , 1964)

[4] Ready J F, "*Effects of High power laser radiation*", Academic, New York, (1971)

[5] Razier Y P, *Sov.Phys.JETP Lett.*, 21, 1009, (1965)

[6] Razier Y P, *Sov.Phys.JETP Lett.*, 26, 302, (1970)

[7] Hughes T P, "*Plasma and laser light*", Wiley, New York, P.285, (1975)

[8] Ready J F, *Appl.Phys.Lett.*, 3, 11, (1963)

[9] Howe J A, *J.Chem.Phys.*, 39, 1362, (1963)

[10] Litchman D and Ready J F, *Phy.Rev.Lett.*, 10, 342, (1963)

[11] Ready J F, *J.Appl.Phys.*, 36, 462, (1965)

[12] Mead W C and Campbell K M., " *Laser interaction and related plasma phenomena*", (Plenum Press, 1987), Page - 7

[13] Kogelnik H, *Bell.Syst.Tech.J.*, 44, 455, (1965)

[14] Wooten F, "*Optical Properties of Solids*", (Academic Press, New York, 1972)

[15] Bohren C F and Huffman D R, "*Absorption and Scattering of light by small particles*", (Wiley, New York, 1983)

[16] Akhmanov S A, Hurbust M J and Duston D, *Sov.Phys.JETP.*, 23, 1025, (1966)

[17] Svelto O, " *Progress in optics* ", 12, 3, (1974)

[18] Shen Y R, *Rev.Mod.Phys.*, 48, 1, (1976)

[19] Kaw P, Schmidt G and Wil cox.T, *Phys Fluids*, 16, 1522, (1973)

[20] Kerr E.L, 1971, *Phys.Rev.A*, 4, 1195, (1971)

[21] Fan H Y, "*Semiconductors and Semimetals : III*", (Academic Press. New York, 1967) chapt. 9

[22] Ben-shaul A and Popovics C., "*Lasers and chemical change*", (Springer, Berlin, Heilberg, New York, 1981)

[23] Letokhov V S, "*Nonlinear laser chemistry*", (Springer, Berlin. Heilberg. New York. 1981)

[24] Zare R N and levine R D, *Chem.Phys.Lett.*, 136, 593, (1987)

[25] Krokhin O N, *Sov.Phys.Tech.Phys.*,9, 1024, (1965)

[26] Garban-Labaune C, Fabre C and Max E, *Phys.Fluids*, 28, 2580, (1985)

[27] Turner R.E and Drake R P, *Phys.Rev.Lett.* 54, 189, (1985)

[28] Drake R P and Young P E, *Phys.Fluids*, 17, 778, (1974)

[29] Forslund D.W, Kindel J.M and Lee K, *Phys.Fluids*, 18, 1017.(1975)

[30] Karttunen S.K, *Laser and Particle beams*, 3, 157, (1985)

[31] Goldman M.V , *Ann.Phys.* 38, 117, (1966).

[32] Bobin J L, Meyer B and Vitel Y , *Phys.Rev.Lett.*, 30, 594, (1973)

[33] Burnett N H, Baldis H A and Enright G D, *Appl.Phys.Lett.*, 31, 172, (1977)

[34] McLean E A and Ripin B L, *Appl.Phys.Lett.*, 31, 825, (1977)

[35] Jahoda F.C and Sawyer G.A, *plasma physics*, 9, partB, (Academic Press, New York,1971)

[36] Attwood D, *IEEE.J.QE.*, 14, 909, (1978)

[37] Houk R S, *Anal.Chem.*, 58, 97A, (1986)

[38] Houk R S ,"*Laser Ionization Techniques For Analytical Mass Spectrometry*", in 'Analytical Applications of Lasers ', Ed. Piepmeier E H, (Wiley-Interscience, New York, 1986)

[39] Cotter R J, *Anal.Chim.Acta*, 195, 45, (1987)

[40] Dennoyer R, Gricken R V, Adams F and Natusch D F S *Anal.Chem.*, 54, 26A, (1982)

[41] Land D P and Tai T L, *Anal Chem.*, 59. 2924. (1987)

[42] Nogar N S, Estler R C and Miller C M , *Anal.Chem.*, 57, 2441, (1985)

[43] Hora H, " *Laser plasmas and Nuclear energy*", (Plenum, New York, 1975)

[44] Hora H. " *Physics of Laser driven plasma*", (Wiley, New York, 1981)

[45] Caroll P K and Kennedy E T, *Contemp.Phys.*, 22, 61, (1981)

[46] Walters C T and Clauer A H, *Appl.Phys.Lett.*, 33, 713, (1978)

[47] Kim Y W and Sincerny P, "*Proceedings of the 17th International Conference on Phenomena in Ionized Gases*", (Budapest, 1985)

[48] Banfi G B and Gobbi O G, *Opt.Comm*, 44, 337, (1983)

[49] Chandrashekar S, "*Radiative Transfer*", (Dober Publications, New York, 1960)

[50] Griem H R, "*Spectral Line Broadening by Plasmas*", (Academic Press, New York, 1974)

[51] Griem H R, "Plasma Spectroscopy", (McGraw-Hill, New York, 1964)

[52] Huddlestone R H and Leonard S L, "Plasma Diagnostic Technique", (Academic Press, New York, 1966)

[53] Ornstein I. S and Brinkman H, Proc.Amst., 34, 33, (1931)

[54] Ibid., 34, 498, (1931)

[55] Herzberg G. "Molecular Spectra and Molecular Structure -I: Spectra of Diatomic Molecules", (Van Nostrand, New York, 1950)

[56] Danylewyeh L L and Nicholls R W, Poc.R.Soc.London A, 339, 213, (1974)

CHAPTER II

LASER INDUCED PLASMA

REVIEW OF PREVIOUS WORK

ABSTRACT

A brief overview of the some of the previous work in the field of laser induced plasma is presented in this chapter. The emphasis is given to the characterization of laser induced plasma rather than to its applications.

59

2.0. INTRODUCTION

In recent years lasers have been attracting increasing interest in surface science. Properties such as brightness (high photon flux), narrow band width (high monochromaticity) and short pulse length (picosecond pulse width or shorter) allow novel approaches to be made for the studies on the complicated processes occurring at the gas-solid interfaces.

Important applications of lasers in surface science include the static-selective investigation of the dynamics of the molecule-surface interactions, the study of surface properties using lasers as probes and the laser induced variation of the state of the surface. The latter category of the applications includes melting, desorption, ablation leading to the plasma formation, etching and deposition.

This chapter summarises recent developments in the investigations of laser induced plasma studies from different solid samples by high power IR and UV laser pulses. The information obtained by the optical emission studies and the characteristics features of the laser induced plasma processes are discussed in detail. The laser induced plasma processes in the UV and IR region are compared to gain insight into wavelength specific behaviour. Finally thin film deposition of the material by using LIP under various laser parameter conditions are also discussed.

The availability of the short pulse allows the realization of rapid heating rates not achievable by conventional methods. Using microseconds to nanoseconds laser pulses, heating rates of 10^8 - 10^{12} K/s have been achieved whereas heating rates as high as 10^{15} K/s have been reported in the case of femtosecond pulses [1]. These high heating rates should be compared with the traditional heating rates of about 10 K/s or less in thermal programmed desorption in order to appreciate new opportunities offered by the lasers in the study of the surface processes. The experimental findings that even large molecules can be desorbed intact with a

pulsed laser, whereas slower heating rates leads to effective fragmentation, are interpreted as the competition between the the rate of desorption and the rate of reaction [2-4]. This is based on the efficient energy exchange that occur between the surface bonds and the chemical bonds of physisorbed molecules when a laser beam is incident on an optically transparent or weakly absorbing substrate covered by the adsorbed species in a suitable wavelength region. With pulsed IR lasers, an efficient excitation of internal vibrational modes of molecules in the submonolayer, monolayer and multilayer coverage region is possible. Studies involving electronic excitation of the molecular adsorbate and films as well as molecular solids using UV and visible lasers have been made. For electronic excitation, excimer lasers are of increasing importance. The molecular systems which possess different binding energies (as in polymers), that the use of photons with varying energy (IR, UV) provides insight into the mechanism of laser induced desorption and ablation.

The development of pulsed lasers has stimulated research in the interaction of the laser light with matter. Most of the experiments which have been reported however, have used lasers in the visible and IR range. It is only recently that pulsed UV lasers have found use in the field of plasma production.

2.1. LANGMUIR PROBE TECHNIQUE

The langmuir probe theory was used to describe high density plasmas generated by excimer laser photoablation [5]. Both ion velocities and ion densities have been determined in addition to electron temperatures. High ion velocities indicate that substantial optical absorption must be occurring in the plasma directly. It is also possible that direct excitation of the electron may occur at 248 nm due to several close by electronic transitions [6]. So this diagnostic technique will provide valuable information about the laser produced metal vapours in

terns of their plasma characteristics.

There is a considerable interest in the processing of surfaces by laser pulses like, in the surface etching of semiconductor and in the laser etching of metals and ceramics which are used for the processing of electronic microcircuitary in integrated circuits [7].

2.2. LIP FROM METALS

When a metallic surface is illuminated by a laser beam several effects may operate and lead to electron extraction. These include (a) the surface photoelectric effect, (b) Volume photoelectric effect (c) thermionic emission (d) the field emission effects and (e) the plasma formation [8].

When a laser induced plasma is formed near a metallic surface irradiated by a powerful laser radiation, the mechanism of laser target interaction is dramatically changed. This enhanced action was obtained in experiments with pulsed CO_2 lasers, the near surface plasma being a non-linear transformer of laser energy to the metal target.

When a dense gas plasma is formed near the irradiated surface, its properties and subsequent evolution are fully determined by the laser intensity I and geometry of the irradiation and do not depend on the surface properties. When the target surface is involved as an initiator of the gas breakdown, it influences the threshold intensity which is required for the plasma formation. It was shown that [9] in the initial stage of the gas breakdown near the metallic surface, the material is overheated by the laser radiation, evapourates and serves as the initial micro-plasma sites.

The interactions of near infrared and mid infrared pulsed laser beams with metals have been studied extensively [10] because of its importance in micromachining, thin film deposition and lithography. The UV lasers are much more useful for such applications because of low UV reflectivity for most of the metals

and more energy coupling efficiency and high optical resolution offered by the short wavelength lasers [11-13]. It is also seen that neutral vapour removal regime could be maintained at a high irradiance level than for IR lasers because of the increased threshold for plasma generation.

The spatially and temporally resolved optical emission spectra of plasmas produced by the flash lamp pumped dye laser focussed on an aluminium target have been recorded and analyzed by Knudson et.al [14]. These spectra provide a map of electron density and temperature distribution in the plasma. Relative ion emission intensities provide electron temperature and stark broadened line widths provide electron densities. These quantities are reported as a function of the distance from the target surface and the laser intensity.

The results of the study of the delay in the production of plasma from the surface of metals and insulators were studied by Panchenko et.al [15]. They have determined how the plasma expansion velocity depends on the particular material and the composition and the pressure of the surrounding gas during the illumination of the metals with the laser beam at the wavelength of 308 nm.

2.3. LIP FROM POLYMERS

Laser induced ablation of polymers due to resonant absorption of laser radiation in the UV spectral range was pioneered by a Japaneese research group [16,17] and an American research group [18,19]. The clean and efficient photoablation of molecular materials provide potential applications in processing microelectronic devices and this accounts for the widespread use it has received. The various mechanistic aspects such as direct photochemical bond breaking and photothermal degradation have been discussed by several workers [20-22]. With respect to the mechanism involved, polymer ablation with pulsed CO_2 lasers is of great interest [23].

It is reported that excimer photoablation provides an efficient and technologically viable means for structuring organic polymer surfaces [24-27]. From this, it is concluded that there should be strong absorption in the wavelength of excimer laser and significant ablation occurs if the light intensity exceeds a threshold value (laser fluence of the order of 10-100 J/cm^2 for pulses of 15-20 nsec durations). In the case of weakly absorbing polymers like Teflon, highly intense short UV pulses can induce strong absorption [28,29]. There has been much research directed towards the preparation and characterization of plasma polymerized Teflon films. They are used as protective films on optics and other passive components used in corrosive environments like that in the cavity of an excimer laser, where the halogen gas environment tends to corrode the laser optics [30] inside the laser cavity. Over the years, it has been shown by many groups that interaction of pulsed UV laser radiation with polymer surface can lead to a precise removal of material in a geometry that is defined by the light beam [31]. The interaction of UV laser pulses with polymer molecules will lead to a multiphoton excitation to the upper electronic states resulting in ionization and decomposition by a variety of paths [32,33]. When the pulsed UV laser radiation falls on the surface of an organic polymer, the material at the surface is spontaneously etched away to a depth of 0.1 to several microns and the depth of etching can be controlled by controlling the number of pulses and fluence of the laser [34,35]. This was later confirmed by other groups working with different lasers and other polymer samples [36-39]. Optical emission spectroscopy has been used by several groups for the detection of transient species such as atoms and diatomic molecules (which are the source of light emission) formed by the secondary photolysis of the initially formed product [25]. This technique can be used as a fundamental method to probe the transient species such as C_2 and CN molecules in the laser ablation of several polymeric samples [24].

The spatially resolved spectroscopy and time resolved analysis

of the laser produced plasma from polyethylene was studied by Boland *et al* [40]. The spectroscopic analysis of the spatial resolution estimated the electron temperature as a function of distance from the target surface. The time resolved analysis, through the Saha-Boltzmann equation gives an estimate of the plasma electron temperature, electron density and velocity of carbon ions having charge I to VI. Srinivasan and co - workers have suggested that at 193 nm excimer laser wavelength, in the case of polymers, the mechanism of ablation is necessarily due to photochemical and bond breaking processes, whereas at longer wavelengths, thermal contributions may arise [35,41].

The spectroscopic study of the laser ablation from PMMA was made by Davis *et.al.*[42]. Their results are consistent with previous suggestions [34,43,35] that the ablation occurs as a result of direct bond scission by the energetic laser pulses.

2.4. LIP FROM GRAPHITE

Recently there has been growing interest in the plasma assisted techniques for diamond like carbon-film deposition [44]. Large areas of film of high optical quality and uniformity were grown in vacuum [45-48], and in gas mixtures containing hydrogen [49,50]. Optical diagnostics of excimer laser induced graphite plasma in ambient gas mixture of argon and hydrogen using direct emission spectra were made by Chen *et al* [51]. They found the occurrence of C_2 and CN bands in addition to the atomic and ionic lines in the plasma emission spectra. They obtained the vibration temperatures of the C_2 and CN radical as $\approx (1.22 \pm 4.8) \times 10^4 K$ and $(1.48 \pm 4.9) \times 10^4 K$ respectively, which are found to be in good agreement with each other but much higher than the graphite melting point. The laser interaction with the plasma plume is considered to be responsible for this.

Diamond has many physical properties which makes it attractive as an electrical material [52]. Diamond like film was produced from graphite target by using pulsed frequency doubled Nd:YAG

laser on a silicon substrate [53]. It was found that crystalline hexagonal, diamond-like films of sub-nanometer thickness grew epitaxially on the silicon surface. The mechanism for electron creation and acceleration in a laser produced plasma from a graphite surface was studied by Cronberg et al [54]. Graphite is an appropriate choice for such studies, because laser induced emission of clusters is believed to be a thermal process [55]. Electronic excitation and ionization should therefore be due to process in the plasma and not in the bulk. They showed that electrons in a laser induced plasma can be accelerated to energies in excess of 15 eV. The energy distribution of the electrons, which depends on the laser pulse energy was found to have a strong dependence on the chemical state of the emitted species.

2.5. LIP FROM HIGH T_c SUPERCONDUCTORS

Laser ablation is well suited for implementation into automated fabrication schemes for producing superconducting thin film devices [56]. Spectroscopic study of the laser ablation technique is useful because information can be obtained about deposition parameters such as laser power, plasma chamber pressure, substrate temperature etc. By controlling the above parameters high quality thin film will be obtained. Wayne A Weimer [57] studied emission spectra generated during the excimer laser ablation of high T_c superconductor $YBa_2Cu_3O_7$. Evapouration techniques using thermal sources produce only neutral metals in the gas phase and result in the oxygen defficient thin films [58]. It may be possible to enhance the formation of metal oxides within the plasma by producing ionic forms of the material during ablation.

The plasma emission spectra obtained by the Nd:YAG laser and by the excimer laser show that more excited atoms than ions were produced by the excimer lasers [59]. The ion/atom ratio should affect the chemistry of reaction between the various species and correspondingly the quality of the deposited films.

The ablation process is used for fundamental understanding of the processes and they relate the quality of the films. Analysis of the optical spectrum emitted from the plume has been used to identify the emitting species vapourized and ejected from the target [60-62]. Identification of these species is important in understanding the complicated ablation, transport and deposition processes.

An analysis of optical emission produced by laser ablation of YBaCuO target using wide range of laser wavelengths showed that 193 nm radiation produced mostly excited atomic species [60]. The production of mostly ionic species reported using the longer wavelength lasers may simply be the result of a smaller energy overshoot existing between the energy of several Nd:YAG photons and ionization potential of Y,Ba and Cu as compared to sum of smaller multiple of the higher energy excimer laser photons.

The formation of oxides in the plume is shown to be essential for the production of high quality superconducting thin films, indicating the value of optical spectroscopy as a diagnostic tool [63]. The time resolved measurements of optical emission shows that a strong prompt emission and other a slow delayed emissions peaking after a few microseconds. It is also observed that the overall optical emission begins after a 7 nsec delay after the start of the laser pulse indicating the time required for significant evapouration of the species from the surface. The prompt emission result from the laser excitation of the evapourated species. On the other hand the slow emission is most likely due to the electronic collisional excitation and is sensitive to oxygen pressure particularly in the case of oxide species.

It is reported that in comparative study of the high T_c thin films obtained using various lasers, the emphasis is on the optimization of the laser processes, the parameters which include wavelength, intensity and pules duration [60]. From their studies it is observed that (1) The CW Nd:YAG laser is better than the excimer laser and is much better than the pulsed Nd:YAG laser

(2) Of the same Nd:YAG laser the second harmonic is better than fundamental, which is due to the higher absorption coefficient

(3) Film deposited at lower temperatures will be better ($100°C - 450°C$). It was also found that in general, short wavelength lasers and short pulses and high repetition rate were advantageous for the formation of stochiometric films.

Among the different successful techniques already developed for the superconducting thin film deposition, including electron beam evapouration, sputtering and molecular beam evapouration, the pulsed laser ablation of superconducting targets appears to be one of the most promising because of its relative simplicity, high deposition rates and ability to control the deposition in terms of film thickness and composition. Moreover it has been shown that [63] the characteristics of high T_c films are strongly dependent on the oxygen partial pressures within the pulsed laser induced thin film deposition vessel.

From the time and spatially resolved spectroscopic studies of plasma emission from high T_c samples by using excimer laser ablation under different oxygen pressures it is seen that the emission intensities of almost all the detected lines and bands are significantly enhanced under oxygen atmosphere compared to vacuum conditions [64]. It has also been concluded that the ejection velocities of ablated products are very sensitive to oxygen pressures in the plasma chamber and that the velocities of the atomic species (neutral and ionic) remain constant from vacuum up to an oxygen pressure of $\approx 10^{-2}$ mbar and decreases rapidly beyond this, whereas the velocities of diatomic species seen to decrease regularly with the oxygen pressure.

The application of high T_c superconductors in microelectronics depends on to a large extent on the availability of the high quality for the superconducting thin films. Films with high transition temperatures have mostly been fabricated by the post annealing of deposited thin films. This processes have several drawbacks like high annealing temperature causing the reaction with the substrate, coarsening of the surface, contamination from

environment during the transfer to the furnace and distributed interface in further processing [64]. During the high T_c thin film growth, sufficient oxygenation has got several advantages like (1) lower substrate temperature and less interdiffusion, (2) smooth surface by a direct epitaxial growth of the final structure on a single crystal substrate and (3) suitable growth of an interface.

Girault *et al* [65] studied the KrF laser-induced plasma plume located above the target by time and spatially resolve spectroscopic measurements, under vacuum and oxygen pressure. A high resolution plasma emission spectrum from high T_c target were obtained and ejection velocities and decay constants of the ablated species were deduced from their temporal evolution. These parameters are of interest as they influence the deposition process and the hence the properties of the deposited film. From the time resolved studies, they concluded that the expansion velocity varies with species and its evolution processes with oxygen pressure, which is similar for all atomic (neutral and ionic) and molecular products. The velocities remain constant from vacuum up to a pressure of 10^{-2} to 10^{-1} mbar and decrease rapidly beyond this.

The pulsed laser ablation of laser materials is relatively simple to implement and can transfer fairly large amounts of materials to a collector substrates at large rates. The energy of the ejected species tend to appear in the translational rather than internal (electronic, vibrational and rotational) degrees of freedom [66-70]. For many materials, large molecules can be transferred to the substrate without decomposition so that the stochiometry of the target can be preserved in the deposited film [71]. Thin film of YBaCuO by 1.06 μm laser radiation from Nd:YAG laser from a non superconducting target in an oxygen atmosphere in room temperature substrate was studied by Lynds *et al* [72]. The approach of using 1.06 μm radiation instead of excimer radiation was suggested by past success in Nd:YAG laser ablation of oxides which produced stochiometric, large domain crystalline films.

Thus laser ablation of high T_c material may be important because the low energy photons is less likely to initiate the photochemistry leading to damage and decomposition. Further, all gaseous environments will be transparent to 1.06 μm radiation so that the target ablation in the presence of an oxidizing atmosphere is to incorporate the necessary oxygen in the deposited film.

Thin films of high T_c YBaCuO superconducting sample were prepared using Nd:YAG laser ablation by Misra *et al* [73]. They showed that when the repetition rate of the laser increases, the superconducting transition of the film obtained will be more sharp and also when the film is cooled faster after deposition.

2.6. PRESENT STATUS OF THE WORK

Most of the earlier workers in this field have used excimer lasers rather than IR lasers. Here with present work, 1060 nm radiation from Nd:YAG laser spatial and temporal analysis of the plasma characteristics were studied and several interesting results were obtained. Using polymer (PTFE) and graphite samples, spatial variation of vibrational temperature of C_2 and CN molecules with laser energy were calculated. In the case of high T_c materials, most of the earlier workers haven't identified the presence of oxide species whereas in this work the oxide species were detected along with the lines of neutral and ionic species. The time resolved analysis of all species were done and some important results regarding temporal dependence of the plasma evolution processes were obtained.

Eventhough the main application of laser ablation processes is in producing thin films, this work is mainly concerned with the studies on spectral as well as temporal/spatial analysis of plasma characteristics which will help to optimize different deposition parameters like laser energy, number of pulses, substrate temperature and the pressure of the ambient gas which affect the deposition conditions (plasma density and temperature). Since

all the above parameters affect the property of the thin film obtained using laser ablation technique, the information about the plasma conditions are extremely important and this has motivated the present series of investigations given in the succeeding chapters of this thesis.

REFERENCES

[1] Shank C V, Yen R and Hirlimann C, *Pays.Rev.Lett.*, 50, 454, (1983)

[2] Hall R B and DcSantolo A M, *Surf.Sci.*, 137, L533, (1984)

[3] Sherman M G , *Surf.Sci.*, 149, L25, (1985)

[4] Deckert A A and George S M, *Surf.Sci.*, 182, L215, (1987)

[5] Gutfeld R J and Dreyfus R W, *Appl.Phys.lett.*, 54, 1212, (1988)

[6] Meggers W F, Corliss C H and Scribner B F, *"Tables of Spectral line intensities Part I*, (US department of commerce printing office, Washington, DC, 1975)

[7] Chuang T J, *J.Vacuum.Sci.Technol B*, 21, 798, (1982)

[8] Logothetis E M and Hartmann P L, *Phys.Rev*, 187, 460, (1969)

[9] Walters C T and Barner R H, *J.Appl.Phys.*, 49, 2937, (1978)

[10] Von-allmon M, *"Laser beam interaction with materials"*, (Springer series in materials science, 1987)

[11] Woodroffe J A, Hsia J and Ballantyne A, *Appl.Phys.lett.*, 36, 14, (1980)

[12] Rosen D , *J.Proc.SPIE*, 476, 118, (1984)

[13] Andrew J K and Froster D, *Appl.Phys.lett.*, 43, 1076, (1983)

[14] Knudson J T, Green W B and Sutton D G, *J.Appl.Phys.*, 61, 4771, (1987)

[15] Panchenko A N and Tarasenko V F, *Sov.J.Plasma Phys.*, 14, 450, (1988)

[16] Kawamura Y, Toyoda K and Namba S, *LaserKenku*, 8, 941, (1981)

[17] Kawamura Y, Toyoda K and Namba S, *Appl.Phys.Lett.*, 40, 374, (1982)

[18] Srinivasan R and Mayne-Banton V, *Appl.Phys.Lett.*, 41, 576, (1982)

[19] Srionivasan R and Leigh W J, *J.,Am.Chem.Soc.*, 104, 6784, (1984)

[20] Srinivasan R, *"Laser processing and Diagnostics"*, (Springer, Berlin, Heildelberg 1984), Page-343

[21] Yeh J T C, *J.Vac.Sci.Technol A*, 4, 653, (1986)

[22] Srinivasan R , *Science*, 234, 559, (1986)

[23] Brannon J H and Lankard J R, *Appl.Phys.Lett.*, 48, 1226, (1986)

[24] Srinivasan R and Braren B, *Chem.Rev.*, 89, 1303, (1989)

[25] Yeh J T C, *J.Vac.Sci.Tech.A*, 4, 653, (1986)

[26] Lazare S and Granier V, *Laser.Chem.*, 10, 25, (1989)

[27] Brannon J H, *J.Vac.Sci.Tech.B*, 7, 1064, (1989)

[28] Kuper S and Stuke M, *Appl.Phys.Lett.*, 54, 4, (1989)

[29] Srinivasan R, Sutcliffe E and Braren B, *Appl.Phys.Lett.*, 51, 1285 (1987)

[30] *"Laser Focus"*, June (1992)

[31] Srinivasan R, *"Springer Series in chemical Physics"*, 39, 343, (1984)

[32] Zandeel L and Bernstein R B, *J.Chem.Phys.*, 70, 2574, (1979)

[33] Koplitz B D and McVey J, *J.Phys.Chem.*, 89, 4196, (1985)

[34] Srinivasan R and Leigh W J, *J.Am.Chem.Soc.*,104, 6784, (1982)

[35] Srinivasan R and Mayne-Banton V, *Appl.Phys.Lett.*, 41, 576, (1982)

[36] Deutsch T F and Geis M W, *J.Appl.Phys.*, 54, 7201, (1983)

[37] Geis M W, *J.Vac.Sci.Tech.B*, 1, 1178, (1983)

[38] Kawamura Y, Toyoda K and Namba S, *Appl.Phys.Lett.*, 40, 374, (1982)

[39] Andrew J E and Dyer P, *Appl.Phys.Lett.*, 43, 717, (1983)

[40] Boland B C, Irons F E and McWhirter R W P, *J.Phys.B*, 1, 1180, (1968)

[41] Jellinek H H G and Srinivasan R, *J.Phys.Chem.*, 88, 3048, (1984)

[42] Davis G M, Gower M C and Fotakis C, *Appl.Phys.A*, 36, 27, (1985)

[43] Srinivasan R, *J.Vac.Sci.Technol. B*, 1, 923, (1983)

[44] Feldman A and Holly S, *SPIE Proc.*, 1146, (1990)

[45] Demers R T and Harris D G, *SPIE Proc.*, 2948, (1991)

[46] Krishnaswamy A, Rengan A, Narayanan J and McHargue C J, *Appl.Phys.Lett.*, 54, 2455, (1989)

[47] Malshe A P, *J.Mater.Res.*, 4, 1238, (1989)

[48] Wagal S S, Juengeerman E M and Collins C B, *Appl.Phys.Lett.*, 53, 187, (1988)

[49] Varnin V P, Teremetskaya I G, Fedoseev D V and Deryaguin B V, *Sov.Phys.Tech.Phys.*, 29, 419, (1984)

[50] Ogman M and Duley W W, *J.Phys.Chem.*, 50, 1221, (1989)

[51] Chen X, Mazumdar J and Purohit A, *Appl.Phys.:A*, 52, 328, (1991)

[52] Angus J C and Hayman C C, *Science*, 241, 913, (1988)

[53] Martin J A, *Appl.Phys.Lett.*, 57, 1742, (1990)

[54] Cronberg H, *Appl.Phys.B:* 52, 155, (1991)

73

[55] Dreyfus R W, Kelly R and Walkup R E, *Nulc.Instrum.Methods:B*, 23, 557, (1987)

[56] Moorjani K, Bohandy J and Adrian F J, *Phys.Rev.B*, 36, 4036, (1987)

[57] Wayne A Weimer, *Appl.Phys.Lett.*, 52, 2171, (1988)

[58] Naito M and Marshall N F, *J.Mater.Res.*, 2, 713, (1987)

[59] Ying Q Y, Shaw D T and Kwok H S, *Appl.Phys. Lett.*, 53, 1762, (1988)

[60] Kwok L and Shi L, *Appl.Phys.Lett.*, 52, 1825, (1988)

[61] Weimer W A, *Appl.Phys.Lett.*, 52, 2171, (1988)

[62] Auciello O, Krauss A R and Gruen D M, *Appl.Phys.Lett.*, 53, 72, (1988)

[63] Inam A, Hedge M S, Chang C C and Wu X D *Appl.Phys.lett.*, 53, 908, (1988)

[64] Ivanov Z and Brorsson G, *Appl.Phys.lett.*, 55, 2123, (1989)

[65] Girault C, *Appl.Phys.lett.*, 56, 1472, (1990)

[66] Friichtenicht J F, *Rev.Sci.Instrum.*, 45, 51, (1974)

[67] Tang S P, Utterback N G and Friichtenicht J F, *J.Chem.Phys.*, 54, 3833, (1976)

[68] Utterback N G and Tang S P, *Phys.Fluids.*, 19, 900, (1976)

[69] Lynds L and Wu X D, *J.Elect.Spect.& Rel.Phenom.*, 29, 147, (1983)

[70] Dreyfus R W, Kelley R and Walkup R E, *Appl.Phys.lett.*, 49, 1478, (1986)

[71] Schwarz H and Tourtellotte J, *J.Vac.Sci.Tech.*, 6, 373, (1969)

[72] Lynds L, Peterson G G and Weinberg B R, *Appl.Phys.lett.*, 52, 320, (1988)

[73] Misra D S, Lourenco A and Palmer S B, *Bull.Mat.Sci.*, 14, 517, (1991)

CHAPTER III

EXPERIMENTAL SET UP FOR LASER PLASMA STUDIES

ABSTRACT

This chapter deals with the general experimental methods followed in the study of laser produced plasma. Details of the experimental set up used for the measurement of spectroscopic as well as time resolved analysis are discussed separately. The details of various subsystems like plasma chamber, spectrograph, monochromator, microdensitometer, boxcar averager and storage oscilloscope used for the above measurements are presented.

T_g. It is this averaging process that is responsible for the enhancement of the S/N ratio provided by the boxcar averager. If now, the sampling interval T_g is slowly scanned across the complex waveform, the entire waveform will appear at the output of the low pass filter provided, $T_g \gg 1/f_h$, where, f_h is the highest harmonic of significance in the waveform being measured and all the peaks of the frequency response up to f_h are of equal height. The complex waveform will then be faithfully reproduced if the scanning is done sufficiently slowly.

Here, $T_{eff} = CR/r$ (3.2)
Where, $r = T_g / T$ (3.3)

T = time between successive openings of the gate. The bandwidth of each peak in the frequency response is $1/\pi T_{eff}$ ie, $r/\pi CR$. By fixing the delay and the gate width so that only the voltage from the part of the signal pulse alone is measured, it is possible to temporally separate out the PMT signal due to the emission of the particular species from other unwanted signal components contained in the signal pulse, thus improving the S/N ratio of the detection. Since the PMT signal has a definite time delay with respect to the laser pulse, short detection times thus allows for better discrimination between the signal due to the species and the PMT noise. The typical PMT signal, the time delay and the gate width of the box-car are shown in figure (3.10).

3.3.4. TIME DELAY MEASUREMENTS OF SPECIFIC SPECTRAL LINES

In order to study the time resolution characteristics of the particular species in the plasma produced by the laser ablation method, the characteristic lines were selected using a monochromator and the PMT output was fed to a fast storage oscilloscope.

The storage oscilloscope(100 MHz, Tektronix model 466) was used to monitor the PMT signal and the laser pulse. Using this, the

pulse shapes can be stored and photographed. The oscilloscope is also required while setting the gate width and delay of the gated integrator. The signals from the PMT, the energy meter and the gate signals from the box-car averager are all monitored on the oscilloscope, which is triggered by the trigger pulse from the laser.

The oscilloscope trace of the PMT response of the emission from different species in the plasma shows a noticeable time delay between the incident laser pulse on the target and the onset of emission from a particular species. All time delays are measured with respect to this laser trigger pulse which coincides with the incident laser pulse. A comparison of plasma production delay times in the case of UV lasers and also lasers in the visible and IR wavelength region shows that the delay times are substantially shorter in the case of UV lasers. The decrease in delay in the plasma production was due to better absorption of the UV light and greater energy of photons [11]. The delay times for the plasma production depends on the power density of the laser beam on the surface of the target, type of the substrate material and on the nature and the pressure of the surrounding gas. The longest time delay is obtained in the case of insulators. The time delay in the plasma production was found to decrease as the ambient pressure is increased (10^{-2} Torr to 10 Torr) or when the power density of the laser light is increased. For the various gases used to fill the plasma chamber, shortest time delay obtained in the case of helium. The leading edge of the emission pulse from the resulting plasma corresponds to the width of the laser pulse, after this stage we observed a non-exponential decay of emission intensity.

The decay time of emission of the species can be defined as the time at which the species decay into (1/e) of the maximum intensity of emission.

REFERENCES

[1] Pearse R W B and Gaydon A G, *"The identification of Molecular Spectra"*, (Chapman and Hall, London, 1965)

[2] William F M, Charles H and Bourdon F S, *"Tables of Spectral line Intensities, Pt.I & II"*, (US National Bureau of Standards, 1975)

[3] Quanta Ray Model DCR - 11 Nd:YAG laser instruction Mannual

[4] Huddlestone R H and Leonard S L, *"Plasma diagnostic Techniques"*, (Academic press, New York, 1965)

[5] Candler C, *"Practical spectroscopy"*, (Hilger and Watts Ltd., Great Britain, 1949)

[6] Ahrens L H and Taylon S R, *"Spectrochemical analysis"*, (Pergamon press, London Paris, 1961)

[7] Wu X D, Dutta B and Hedge M S, *Appl.Phys.Lett.*, 52, 179, (1989)

[8] Jarrel -Ash , Instruction Mannual; Engneering Publ.No. 82-00/1M-RW 7 (1971)

[9] Photo multiplier tubes, conastruction and operating characteristics, Hamamatsu, Japan

[10] Stanford Research Systems Boxcar avrager insruction mannual

[11] Panchenko A N and Tarasenko V F, *Sov.J.Plasma Phys.*, 14, 451, (1988)

CHAPTER IV

LASER INDUCED PLASMA FROM POLYMER SAMPLE

ABSTRACT

This chapter deals with the spatial and temporal analysis of laser induced plasma from a polymer sample (polytetrafluoroethylene). Results of some measurements done on laser etching of Teflon are also presented. Detailed study of the spatially resolved emission spectra shows distinctly different characteristics for emission from different parts of the plasma plume. From the relative intensities of molecular bands in the plasma, the vibrational temperatures of the molecules present in the plasma are calculated. From the time resolved studies of the different species in the different regions of the plasma, the time delay as well as decay time of emissions are obtained. In the last section the spatial distribution of the ionic species and the spatial variation of the electron temperature in the plasma, studied using Langmuir probe technique are described.

4.1. INTRODUCTION

The interaction of high power laser pulses with organic materials has been investigated extensively over the past two decades. Most of these investigations have clearly demonstrated the potential use of this processes in technology and medicine. The ablation of polymeric materials and biological tissues by ultraviolet laser irradiation has direct applications in micro fabrications and in micro surgery respectively as it provides a means for precise removal of material with high spatial resolution [1]. There has also been recent interest in the use of polymers for optical materials and in the laser machining of polymers *via* ablative photo decomposition [2].

When pulsed IR laser radiation falls on the surface of an organic substance, the material on the surface layers is spontaneously etched away to a depth of several microns. The principal feature of this phenomenon in the interactions of IR or visible pulses were the control that can be obtained by controlling the number of pulses and fluence of the beam. Such controlled etching has important applications in photo-lithography [3]. The photo etching rate has been reported to be depend on the laser fluence, molecular structure of the polymer and the absorption coefficient. Depending on the type of the polymers the absorption coefficient can vary by several orders of magnitude.

It has been suggested that 'ablative photodecomposition' occurs as a result of direct bond scission by the multiphoton processes induced by UV laser photons [4,5], whereas material absorbing visible and IR radiation is heated and vapourized [6]. The removal of material by such thermal processes leaves the substantial part of the laser energy to remain as heat which can cause some thermal damage to the rest of the material. It is possible that the photodissociation processes responsible for creating emission in the plume are different from those needed for the subsequent breaking of the polymeric bonds which cause the ablation, although it is much more likely that direct bond

scission by UV photons is also responsible for the breaking of relatively weak polymeric bonds. The rapid rupturing of these bonds causes sudden increase in pressure at the ablation site which then leads to highly energetic fragments in the plume. The resultant energetic molecular fragments then rapidly ablate from the irradiation sites [7]. It is shown that laser pulses from IR lasers can produce fast heating accompanied by surface damage [8]. Under such excitation, photochemistry is simplified and the ablation processes is best described as explosive thermal decomposition [9]. The use of IR lasers gives rise to multiphoton excitations over the vibrational levels of the ground electronic states which is then followed by thermal decomposition.

The IR radiation from a high power laser pulse usually generates intense plasma emission from the target surface. The nature and characteristics of the laser induced plasma (LIP) from a solid target depend on various parameters like the chemical composition of the target [10], wavelength of radiation [11], energy deposited on the target, pressure of the residual gas in the plasma chamber etc. The composition of the plasma will in general depend on its distance from the sample surface as a result of rapid expansion of the plasma from the target followed by lowering of the plasma temperature. The population of the various types of molecular, ionic and neutral species in the plasma will also depend on the spatial separation of the point of observation from the target.

In this chapter, results of some of the measurements done on laser etching of Teflon are presented in the first part of this thesis and the etch depth of the sample are measured. The variation in etch depth with number of pulses at different laser energies are obtained and are discussed. The results of investigation carried out on the spatial and temporal analysis of the laser induced plasma emission spectra from polytetrafluroethylene (PTFE) target obtained with 1.06 μm radiation from Q- switched Nd:YAG laser have been presented in detail. The plasma emission spectra in the extended region of

the plasma is dominated by C_2 and CN molecules. From the relative intensities of all these bands, the molecular vibrational temperatures of these two molecules are obtained and the variation of with respect to laser energy is also obtained. The analysis and the results are explained at different sections.

The interaction of the laser beam with polymer surface is an ablative photodecomposition which result in the etching. This ablative plasma decomposition is a function of wavelength, chemistry of the material which determines its absorbtivity and fluence of the laser beam at the polymer surface [12]. Srinivasan and co-workers suggested that with 193 nm radiation in polymers is essentially photochemical bond breaking, whereas at longer wavelengths thermal contribution may arise [13,14]. The surface morphology of the polymer after ablation produce a substantial temperature increase [15,16,17].

PTFE is a highly crystalline, orientable polymer which consists of CF_2 - CF_2 chains . The chemical structure of the polymer is shown in the figure (4.1). The absorption of laser radiation in PTFE is due to the strongly allowed electronic transitions involving conjugated C-C double bonds [18]. PTFE is weakly UV absorbing and its bond energy is very high so that intense short pulse can induce strong absorption [19,20]. The IR spectrum of PTFE is shown in the figure (4.2), which shows that it has moderately low absorption $\approx$ 10 % in the IR region [21].

PTFE film has a well established chemical and thermal stability, excellent toughness, low frictional coefficient, high electrical and thermal resistance, high melting point, high melt viscosity, which make the thin film of this sample suitable for wide variety of commercial applications such as optical waveguides, anti-reflection coatings, microelectronics, insulation tape and capacitive dielectrics. PTFE has extremely good electrical properties and its dielectric constant is low $\approx$ 2. The electrical applications of the polymers are wire and cable insulation, insulation for motors, generators, transformers, coils and capacitors and high frequency electronic uses. PTFE
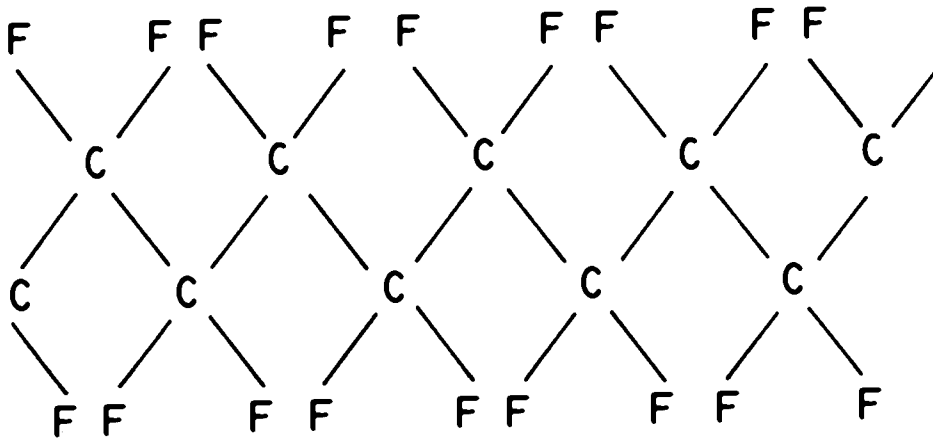
Fig.4.1.   Chemical structure of PTFE
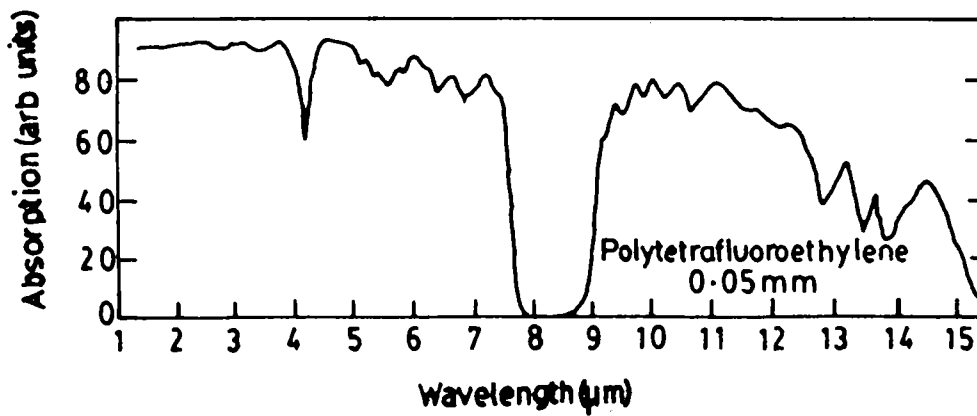
Fig.4.2.   Infrared spectrum of PTFE

films are also being used to protect the magnetic media in the computer data storage components like the floppy and hard disks.

Laser induced plasma spectroscopy (LIPS) has been successfully used in the present study to probe transient species such as C_2 and CN in the laser ablation process of polymers. Here the results of the spectroscopic as well as the time resolved analysis of laser induced plasma emission from PTFE (Polytetrafluroethylene) at various distance from the target surface are highlighted. In the photoablation of polymers, knowledge of the time evolution of ablation process is of considerable significance since it may, in conjunction with theoretical models [22], help to resolve uncertainties in the interaction mechanism and thus lead to improved understanding of this phenomenon which has important practical applications [23]. The time delays and decay times of the emission from different species in the three distinct regions of the plasma have been measured in the present study. The results throw much light on the complex recombination process at work in the laser induced plasma.

The band emission appear to be stronger in the partial vacuum conditions than in air, since the gas collision frequency is lower in the vacuum case so that the plume will extend to a greater distance than in air at 1 atmosphere pressure. The emission front of the substrate extends completely to fill the vacuum chamber. Thus the apparent increase in the intensity of emission for vacuum environment is due to an increase in the size of the plasma source [19].

4.2. CHEMICAL PHYSICS OF THE ABLATION PROCESSES : TIME PROFILE

A pictorial representation of the interaction of the laser pulse with a polymer surface is shown in the Figure (4.3). As shown in the figure (4.3a), the stream of photons from a single pulse falls on the polymer and is absorbed in a depth that is defined by Beer's law. This depth can be as little as a fraction

of micron for intense absorbers and to many tens of micron for a weakly absorbing polymers. The weak and strong absorption refer to a specific wavelengths so that same polymer can absorb weakly at one laser wavelength and strongly at another wavelength. Figure (4.3b) shows that within the absorption depth, there are numerous bond scissions. In figure (4.3c), the fragments are shown to be ejected from the surface, leaving the etch pit behind.

A knowledge of the timing of the ablation processes is fundamental to an understanding of the chemical physics of the phenomenon. Early studies were based on the spectroscopic investigation of the light emission that accompanies the impact of a UV laser light pulse on a polymer surface. Koren *et al* [24,25] timed the intensity of emission at various distance from the target surface and concluded that in the etching of polymers by 193 nm laser beam.the emission had a fast component that appeared simultaneously with the laser excitation, and a slower component that lasted 10-100 times longer than the laser pulse itself. In order to calibrate the velocity of UV laser ablation, Davis and co workers timed the peak intensity of emission of CH radicals at various distances from the target surface and placed the beginning of the emission signal at times of the order of width of the laser pulse [26]. These studies show that polymeric structure could begin to ablate on a time scale that is even shorter than the width of the a pulse from the laser beam.

4..3. MEASUREMENT OF ETCH DEPTH

When intense pulsed radiation falls on the surface of an organic polymer material (PTFE in this case), the material at the surface is spontaneously etched away to depth o.1 μm to several microns. The depth of etching can be controlled by controlling the number of pulses and the fluence of the laser and the lack of thermal damage to the substrate. The result is an etch pattern in the solid with geometry that is defined by the light beam [27]. The etch depth for multiple pulse was measured using a surface
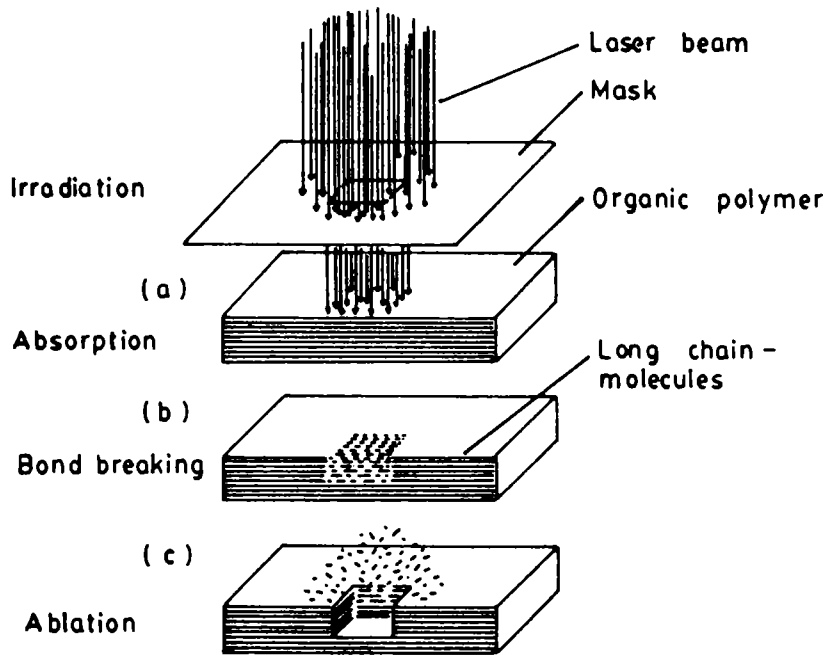
Fig.4.3. Schematic impact of laser pulse on polymer surface
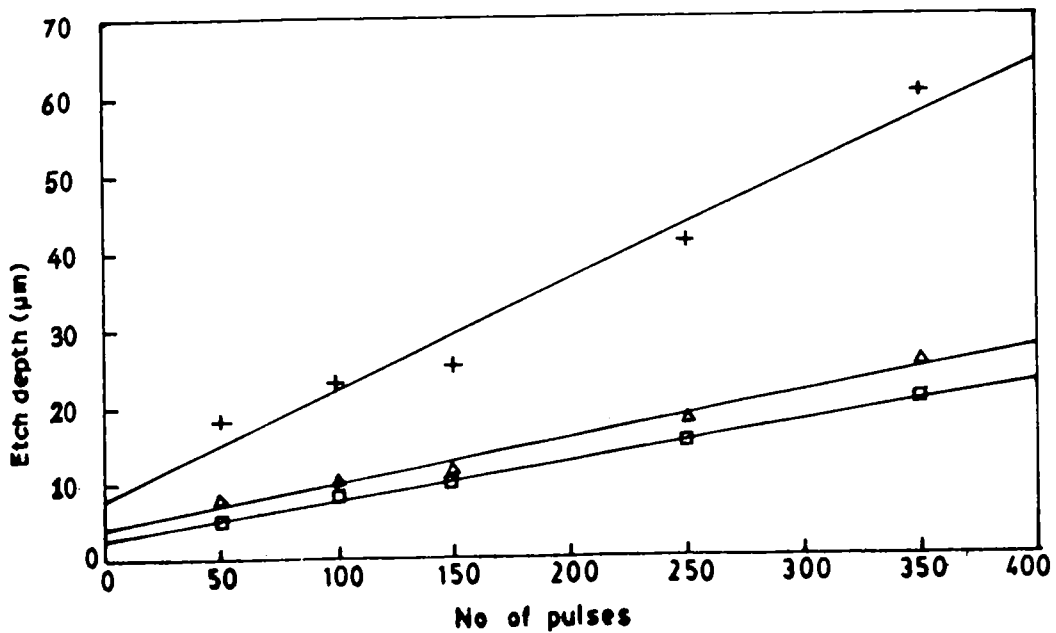
Fig.4.4. The variation of etch depth as a function of number of pulses at different laser fluences (+ - 12 J/cm², Δ - 7 J/cm², □ - 3 J/cm²)

profiler and the etch depth per pulse was calculated by dividing it with the number of pulses [28]. The energy per pulse reaching the target was measured using an on line energy meter in the path of the laser beam.

The etch depth per pulse depends on the absorption coefficient of the material. Depending on the type of the polymer, the absorption coefficient can vary several orders of magnitude [29].

At low fluences, increased absorbance results in an enhanced etch rate due to higher photon flux absorbed per unit volume. As the fluence is increased, additional broken bonds (photo chemical effect) per unit volume enhance the etch rate until a saturation fluence level is reached. At this point a smaller dependence of the etch rate with fluence is observed. This inflection point was observed to vary reciprocally with the absorption coefficient [30]. The self developing nature of the photoetching process of the polymers offers itself for use in microelectronic fabrication and device packaging.

The dependence of the ablation on the absorption is not simple. The laser power absorbed per unit volume of the polymer must be above threshold in order for ablation to occur. Thus the polymer must have a minimum absorption coefficient at a given laser power. When the absorption coefficient is above threshold, the penetration depth of the laser into the polymer is relatively large so that large volume of the material is ablated. But as the absorption coefficient increases, the penetration depth decreases, as radiation is absorbed near to the surface and less material is ablated so that a plot of amount of material ablated as function of absorption coefficient has a maximum for a given laser power and decreases for high absorption and low absorption. This result was observed experimentally in the study of dependence of etch depth for polymers with different optical absorption coefficients. At low laser power, polymers with both low and high absorption coefficients have small etch depths, while the polymers with intermediate absorption coefficients had the largest etch depth [31].

A relationship between the light absorption and single etch depth per pulse can be obtained by considering some assumptions. If the etching is viewed as a two step processes in which initial light absorption is followed by material ablation, then according to Beer-Lambert law,

$$\phi_x = \phi_{inc} \exp(-\alpha x) \qquad (4.1)$$

ϕ_x is the attenuated energy fluence at depth x into the material, ϕ_{inc} is the incident pulse fluence and α is the absorption coefficient at the given wavelength. In order to cause ablation, the material fluence threshold must be reached. When $\phi_x = \phi_{thresh}$, then ϕ_{inc} must be increased over ϕ_{thresh} by a factor of $\exp(\alpha x)$ so that single pulse etching occurs to the desired depth x.

$$\phi_{inc} = \phi_{thresh} \exp(\alpha x) \qquad (4.2)$$

The single pulse etch depth X is given by [32,33,34],

$$X = \alpha^{-1} \ln [\phi_{inc} / \phi_{thresh}] \qquad (4.3)$$

When the etching behaviour was studied in air, vacuum and in argon, it was found that using the identical conditions etch rates for air, vacuum and argon were same. The bright luminescence is seen to project outward from the polymer surface during the etching in air and argon which is missing in vacuum where only a surface luminescence is visible. This shows that luminescent plume is not important for etching [34].

In our experiments, the sample is taken in the form of a disk of ≈ 2 cm diameter with an energy density at the focal point ≈ 5 J/cm^2. When the laser pulse strike on the surface, a loud audible sound will be heard and depending upon the wavelength the material would have been etched away with a geometry that is defined by the light beam.

The etch depth per pulse does not settle down to a value until

after the first 5-10 pulses under certain conditions of wavelength and fluence. All irradiations were performed in air at ambient room temperature, so that a bright plume is ejected from the surface which is extended to a few mms. After the irradiation, the sample is cut through the etch hole and the length of the etch hole is measured using a microscope. Figure (4.4) shows the variation of the average value of the etch depth versus the number of pulses at different fluence of the laser (3 J/cm^2, 7 J/cm^2 and 12 J/cm^2). The depth etched was a linear function of the number of pulses, but note that there is a long extrapolation between the origin (zero pulses) and the first data point. At first few pulses, the uniformity does not exist because the first pulse sees a virgin material whereas each subsequent pulse sees a sample that has already been modified by in part by the preceding pulse. The slopes of the lines in the above figure gives an average value for the etch depth per pulse at that wavelength and fluence of that material. These values are reproducible within the uncertainties in the measurement of the fluence of the laser and the depth of etching. Considerable non-uniformity in the etch pit occurred at low fluence, which was due to non-uniform heating of the surface near the threshold for ablation and reflects the same inhomogeneity in the profile of the laser beam. Usually absorption of the polymer decreases with increasing wavelength. The threshold fluence tends to increase with increasing wavelength and the linear portion increases in slope. At higher wavelengths, the characteristics of the etching passes over from photoablation to the thermal ablation which is observed in the case of visible and IR laser wavelengths. Both the onset of etching and the flattening at high fluences become quite abrupt. If the polymer has no absorption at a particular wavelength, etching does not decrease to zero. But as the fluence is increased, etching does set in, but the two characteristics that are readily available in UV laser ablation are no longer to be observed. They are the control that can be exercised over the depth of etching in a reproducible manner and the lack of thermal

damage to the substrate.

4.4. SPATIAL AND TEMPORAL ANALYSIS OF LIP FROM TEFLON

(a). SPECTRAL FEATURES

When the target surface is illuminated in air at atmospheric pressures, a white zone appeared next to the target surface. But when the pressure of the surrounding air is decreased, the bright zone was found to be completely removed from the target surface. If the sample is kept in a vacuum chamber so that low pressure is maintained within the chamber then the bright zone is surrounded by a large well defined coloured hemispherical zone is observed. The colour of the hemispherical zone is the characteristics of the target material used. When the laser energy increases, the extension of the plasma was also found to increase. A typical photograph of the plasma generated from the polymer sample (PTFE) is shown in the figure (4.5).

The experimental set up for the spectroscopic analysis of the plasma is described in the chapter III. The plasma emission spectra from the three distinct regions *viz.*, the central (A), middle (B) and extended (C) regions of the plasma were recorded photographically using a Carl-Zeiss three prism spectrograph and appropriate optics for focussing [35]. The plasma emission spectra of PTFE from the three different regions are shown in figures (4.6(a), 4.6(b) and 4.6(c)) along with mercury spectrum for wavelength calibration. The wavelengths of the emissions of the different atomic, ionic and molecular species in the plasma were estimated using the Hartmann's formula in the standard manner. The observed wavelengths are compared with standard spectral data sources [36,37] for identification of the various species found in the plasma plume.

As can be seen from the spectra, (fig.4.6(a),4.6(b) and 4.6(c)) corresponding to the three regions, the recorded results show distinctly different characteristics. The emission lines due to
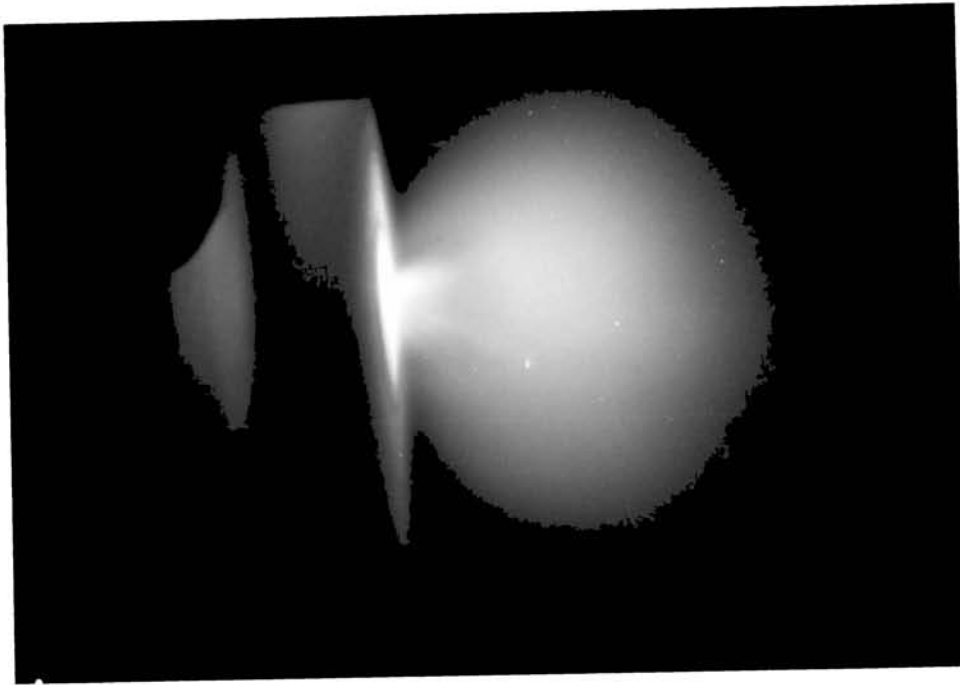
Fig.4.5. Photograph of the laser induced plasma emission from PTFE at a laser energy density of $\approx$ 12 J/cm^2 showing the studied regions of the plasma.
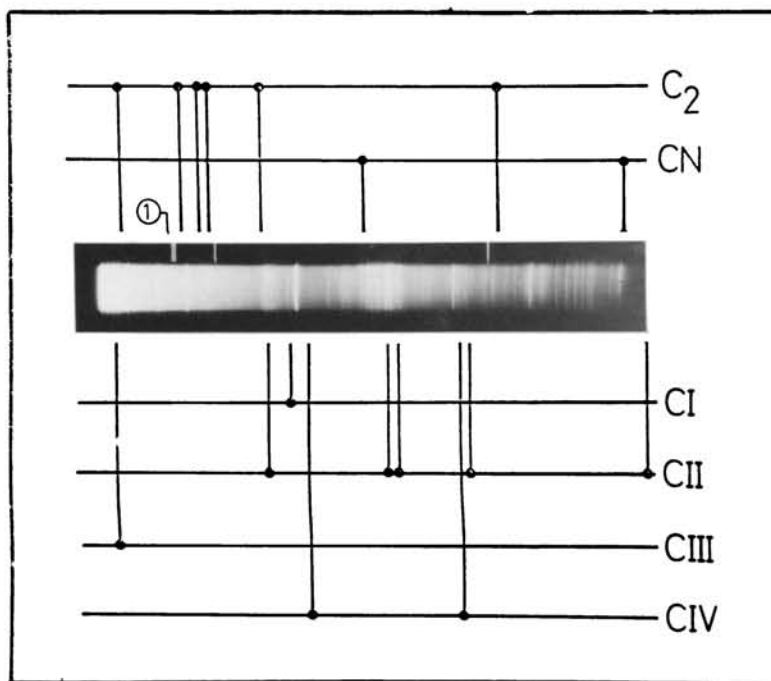
Fig.4.6. The emission spectrum from the centre region (A) of the laser induced plasma from PTFE. (Laser energy density $\approx$ 12 J/cm^2) 1 - Mercury reference λ = 579.0 nm

C_2

CN

①

(B)

CI

CII

CIII

CIV

C_2 Swan bands

Region C

0,0
1,1
2,2

1,0
2,1
3,2
4,3

2,0
3,1
4,2

0,1
1,2
2,3
3,4
4,5
5,6

CN

4,5
3,4
2,3
1,2
0,1
①

(C)

CI

CII

CIII

CIV
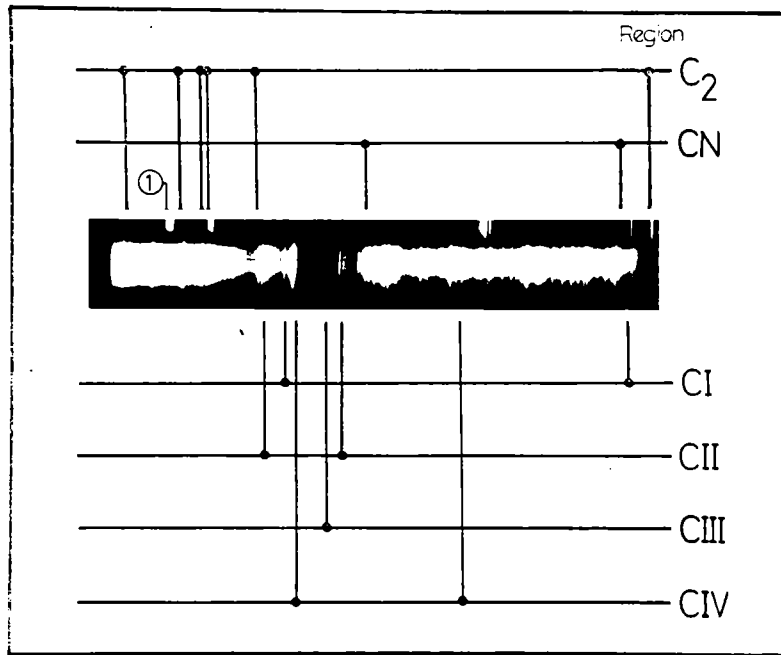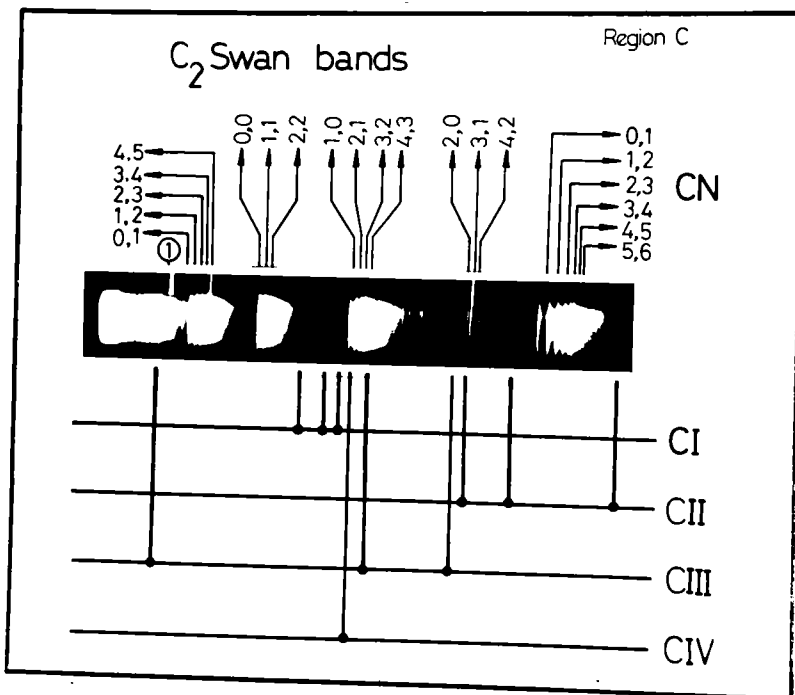
Fig.4.6.   The emission spectrum from the mid (B) and extended (C) regions of the laser induced plasma from PTFE. (Laser energy density $\approx$ 4 J/cm^2)
1 - Mercury reference λ = 579.0 nm

higher ionization states of carbon (CI, CII, CIII and CIV) are clearly seen in the core and mid regions of the plasma (fig.4.6(a) and 4.6(b)). Molecular bands corresponding to the $A^3\Pi_g$ — $X^3\Pi_u$ transitions of C_2 (Swan Bands) [36] in the wavelength range from 500 to 590 nm, are predominant in the spectrum of the extended region. Presence of the characteristic $B^2\Sigma$ — $A^2\Sigma^+$ bands of CN molecule is seen in the violet region of the spectrum. The presence of strong violet bands (CN) is probably due to the the creation of this species by photochemically induced reaction of the ablated species with the surrounding air. Even in normal vacuum conditions the background concentration of the air is sufficient to make these bands appear stronger in this case because of the high intensity of the plasma source.

(b). TIME RESOLVED ANALYSIS

In the time resolved analysis, a part of the plasma plume was focussed on to the slit of a monochromator (McPherson, 0.2 meter) coupled to a photomultiplier tube (PMT), (Hamamatsu R446, 3 nsec rise time) and a storage oscilloscope/Boxcar averager. In order to study the time evolution of a particular species produced by laser ablation, the characteristic lines were selected using the monochromator, and the PMT output terminated at 50 ohms resistance, was fed to a 100 MHz storage oscilloscope (Tektronix Model 466) [38]. The experimental details for the time resolved analysis is given in the chapter III.

Typical oscilloscope (CRO) traces of the PMT response to the emission from the C_2 species in the three different regions (A, B and C) of the plasma plume are shown in figure ((4.7(a), 4.7(b) and 4.7(c)) respectively. The amplitudes of the pulse shapes were monitored by a Gated integrator and Boxcar averager (Stanford Research Systems Model SR250).

From the above mentioned figures, which is the CRO trace
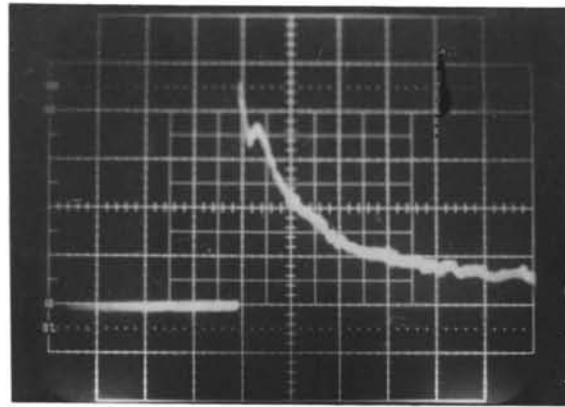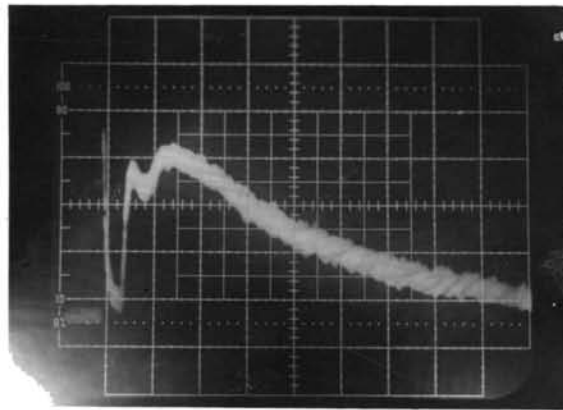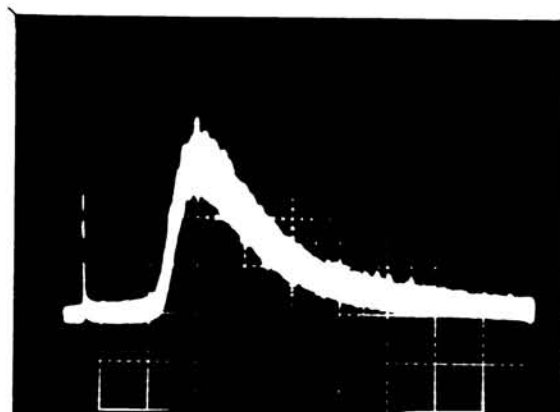
Fig.4.7. Typical oscilloscope trace of the PMT response to the plasma emission from the C_2 species (at λ = 562.1 nm) from the different regions of the plasma. (A) Central region, (B) Mid region, (C) extended region (1 μsec, 0·1 V)

shows a sharp, 'prompt' emission and a delayed emission peaking
after a few micro seconds [39,40]. The 'prompt' emission could
easily result from the ablated species ejected from the target
surface. On the other hand, the delayed emission is most likely
to be due to electronic and/or molecular collisional excitations
[39]. From the measured value of the time delay exhibited by the
PMT signal trace of the emission (figure.(4.7.c)), the velocity of
the species is obtained and the corresponding energy calculated is
found to be $\approx$ 6 eV. Since the energy of the ablated species is
much greater than 1 eV, in all possibility, the delayed emission
is predominantly due to the collisional excitation rather than
from evapourated species. From the above figures, it is obvious
that there is a notable time delay between the incidence of laser
pulse (all time delay measurements are taken with respect to the
'prompt' emission) on the target and the onset of emission from a
particular species in the three different regions of the plasma.
This is due to the fact that in the core of the plasma (A), the
plasma temperature is maximum and most of the species consists of
ionized atoms which results in the smaller time delay (of the
order of nanoseconds) of emission. In the region B of the
plasma, where, apart from ionized species, both neutral and
certain amount of molecular species are present due to
recombination and other allied processes, which results in a
comparatively larger time delay of emission (of the order of
microseconds) as compared to that of the core region of the
plasma. The emission is still further delayed in the region C of
the plasma where molecular bands predominate. It must be noted
that the overall optical emission begins only after about 0.5
μsecs following the start of the laser pulse. Figures (4.8(a),
4.8(b) and 4.8(c)) show the variation of the radiation emission
time delays of certain identified species in the three different
plasma regions with laser energy.

From the time delays observed, it is seen that in all the three
different regions of the plasma, the molecular band (C_2 and CN)
emissions have got much larger time delays as compared to emission
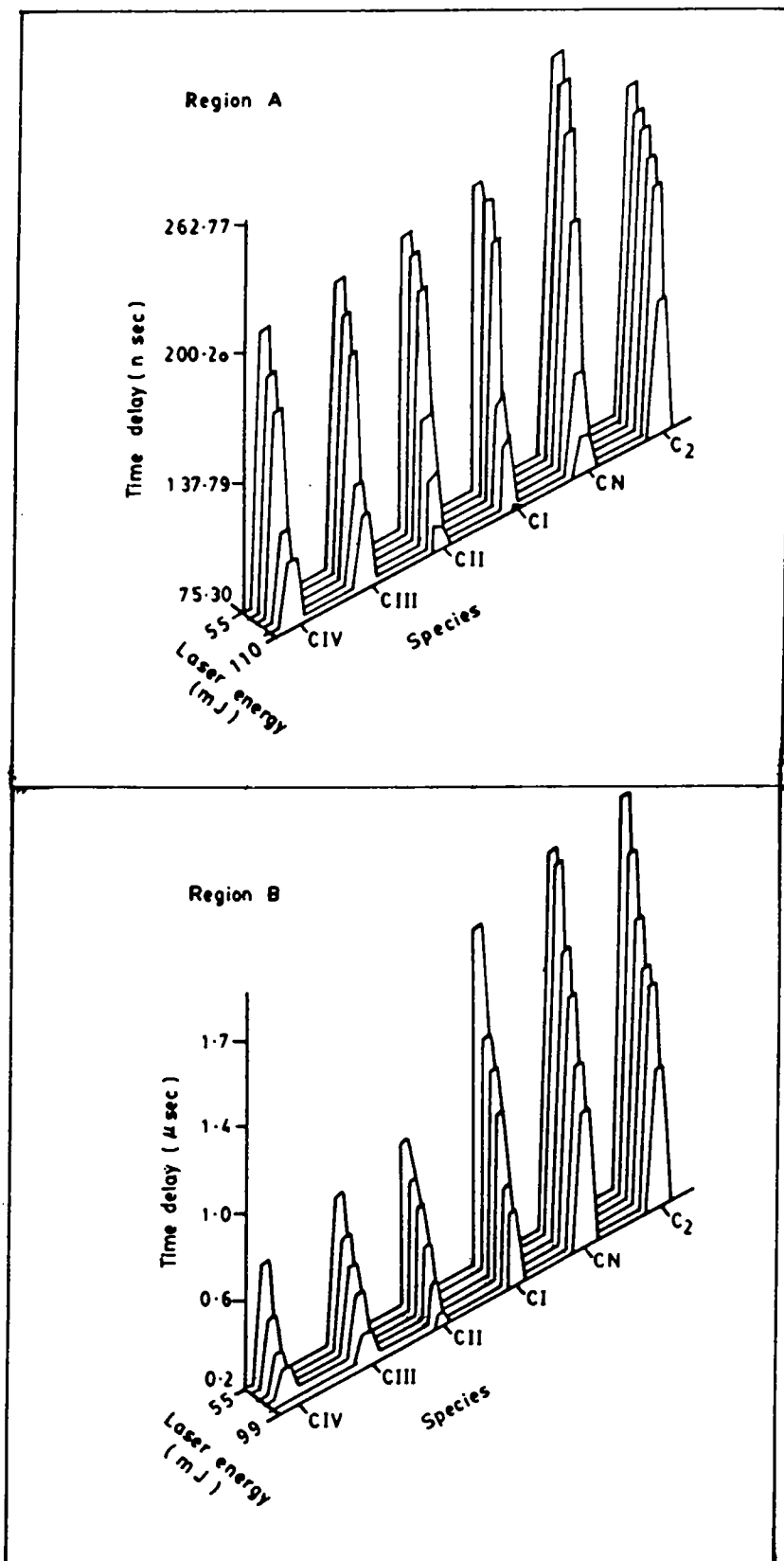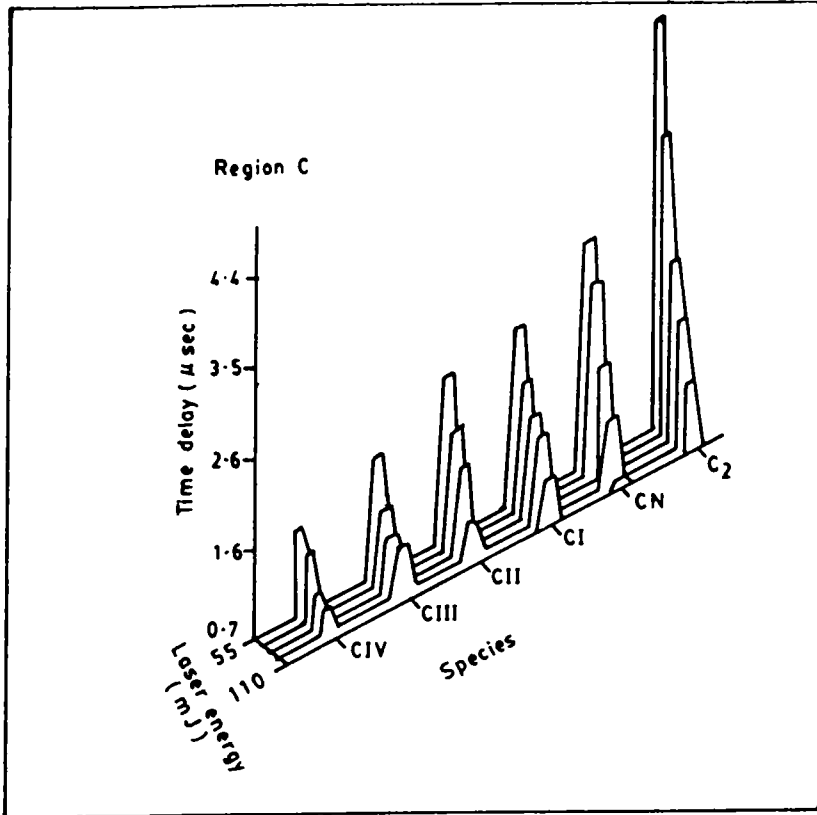
Fig.4.8. Variation of the time delays of emission of the different species with laser energy for regions (A and B) of the plasma.

Fig.4.8. Variation of the time delays of emission of the different species with laser energy for region (C) of the plasma.
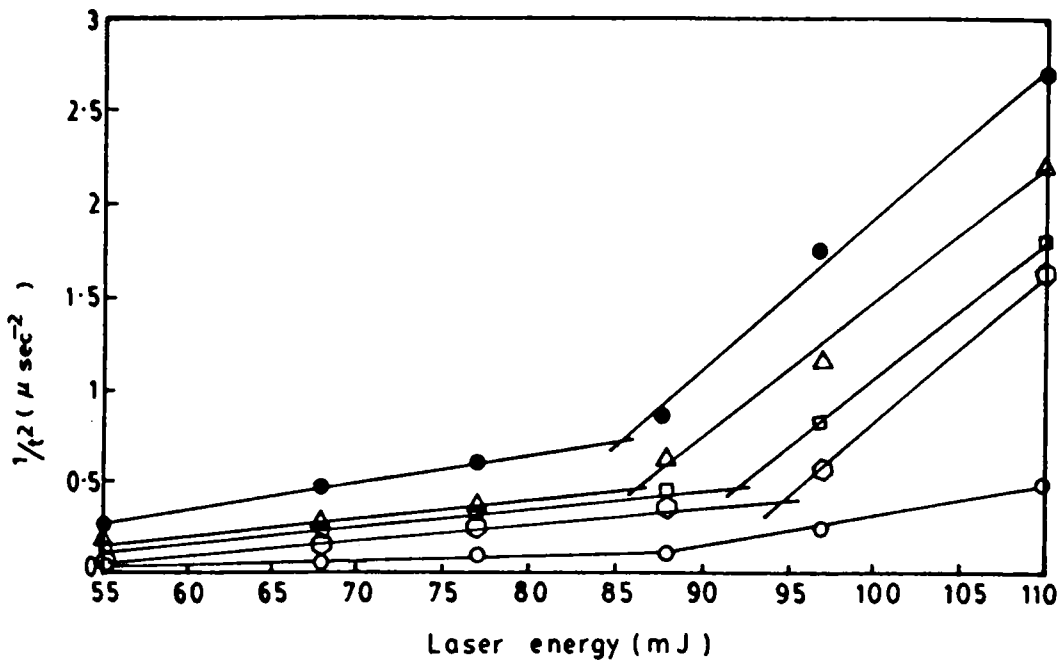
Fig.4.9. Variation of $1/t^2$ with laser energy of different species in the region C of the plasma.
(● - CIII, △ - CII, □ - CI, ○- CN and o - C_2)

from ionic/neutral species. From such time delays it is also observed that the spectral lines of higher ionized species are first to appear and these are followed in turn by those of successively lower states of ionization [41]. In general, there is a decrease in time delay as the laser energy increases. There are many reasons for the occurrence of time delay for emission from any species. Prominent among them are, (1) time-of-flight of the species (2) thermal processes leading to generation of plasma from the target (3) recombination and/or dissociation of the species. As a consequence of the non-linear effect mentioned earlier, the enhancement of the effective power density of the laser beam in the plasma will cause a corresponding increase in the velocity of the species, thereby decreasing the delay of emission. This can result in the sudden change of slope at the threshold as seen in figure.(4.9). Variation of the time-of-flight of the different species from the LIP from a plexiglass target using 30 psec, 1.06 μm wavelength Nd:YAG laser pulses was reported by Rohr *et al* [42]. If the time-of-flight alone were responsible, we expect the time delay to be proportional to $M^{1/2}$ (M is the mass of the species) which is not found to be the case with the present results. For example, the various ions of carbon have different time delays, which should have been same if the time delay was proportional to $M^{1/2}$. If we assume that the plasma temperature is proportional to laser energy E, then one would expect that E be proportional to $1/t^2$, Where t is the time delay of emission for a particular species. This is not in accordance with the observation as seen in figure (4.9), which shows the variation of $1/t^2$ with laser energy for different species in the extended region of the plasma. Variations of t with laser energy for other species in different regions of the plasma are not much different from what is shown in figure (4.9). This also supports the conclusion that the time-of-flight is not the major cause of the emission delay.

The variation of decay time of the emission from different species with laser energy in the three regions are shown in

102

figures [4.10(a), 4.10(b) and 4.10(c)] .   It is also seen that the molecular bands have got larger decay time as compared to ionic species.   As the laser energy increases, the thermal diffusion processes remaining unchanged, the plasma generation becomes more rapid and we expect a decrease in decay time of emission.   Also, the increased laser energy will produce much larger densities for various species thereby decreasing the mean free path and increasing the collision rate.   All these complex processes will give rise to the variation of time delay as well as decay time with laser energy.   An increased collision rate can also account for the decrease in decay time of emission with laser energy as observed in the present case.   Such decreases in decay time and of the delay of emission with plasma temperature are found to occur as we go towards the centre or core region of the plasma.

4.5. VIBRATIONAL TEMPERATURE MEASUREMENTS OF C_2 AND CN MOLECULES

The relative intensities of the vibrational bands were obtained using a microdensitometer (Carl-Zeiss).   The intensity distribution in a band can be used for determining the vibrational temperature of the plasma emission source [43].   The method of calculation used for the measurement of vibrational temperature is given in the chapter I.

The vibrational distributions in the excited states of C_2 molecule are shown in figure (4.11).   Similar distributions were observed in the case of CN bands also in all different regions of the plasma.   The inverse distribution observed for vibrational distributions less than 2 in the case of C_2 molecule is in accordance with Franck-Condon principle.   Similar distributions have been observed in certain other molecules also [44,45].

The variations of vibrational temperature with laser energy corresponding to the C_2 Swan bands and CN molecules in the mid region (B) of the plasma emission are shown in figure (4.12). The vibrational temperature was found to vary from 1.75 x 10^4 K to 5.6 x 10^4 K corresponding C_2 molecules and from 1.455 x 10^4 K to
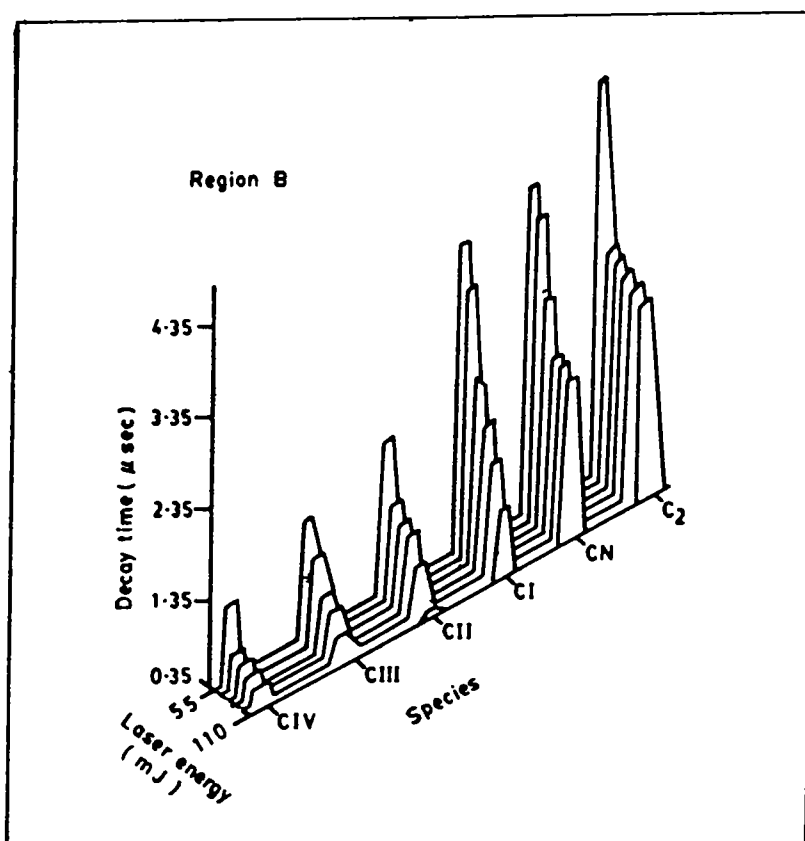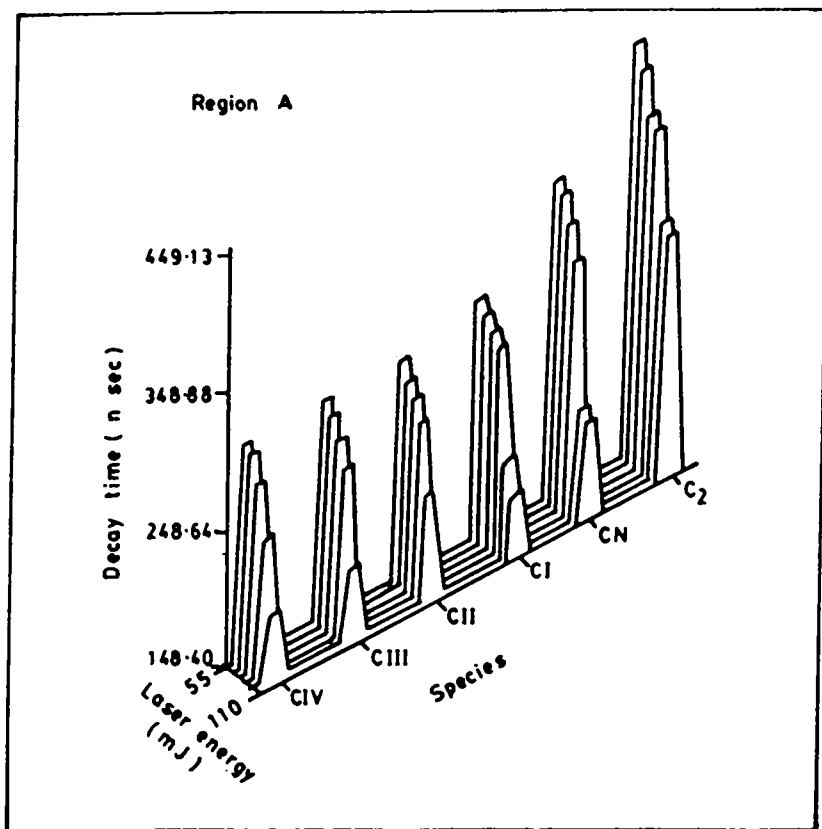
Fig.4.10. Variation of the decay times of emission of the different species with laser energy for regions (A and B) of the plasma.
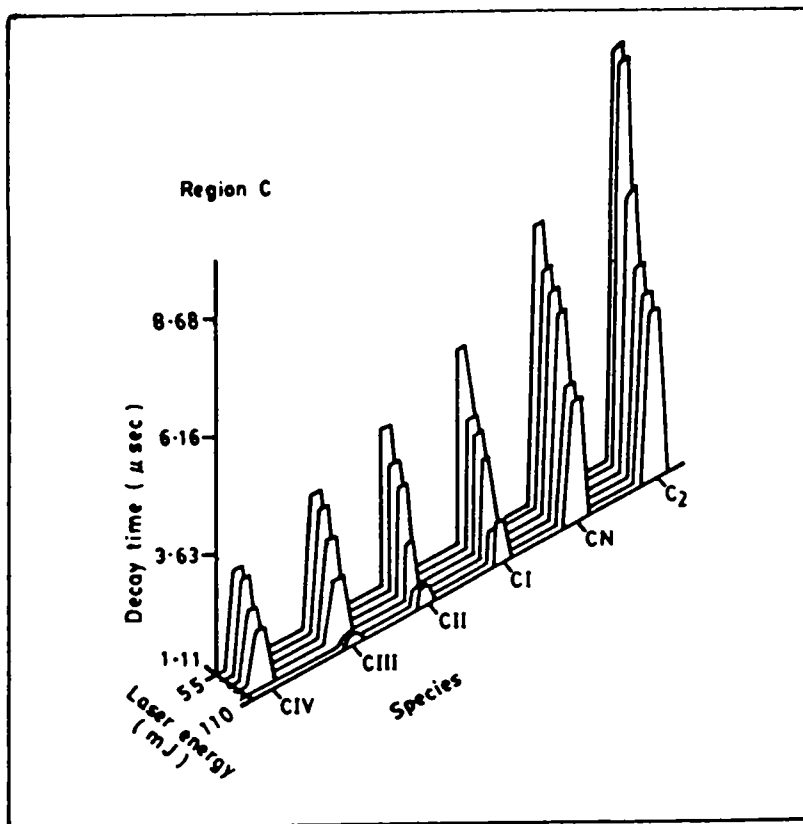
Fig.4.10. Variation of the decay times of emission of the different species with laser energy for region (C) of the plasma.
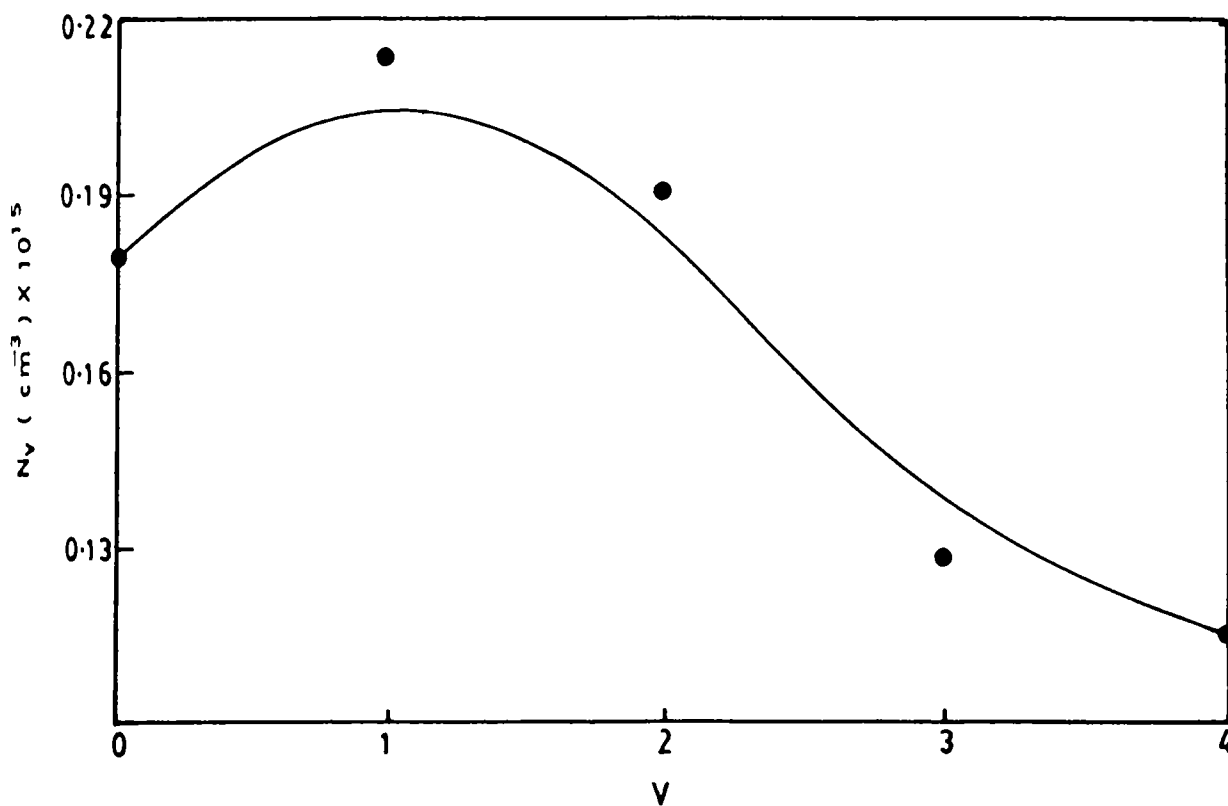
Fig.4.11. The vibrational distribution in the C_2 Swan bands (562.1 nm) in the region C of the plasma. (Laser energy of $\approx$ 68 mJ)

4.6×10^4 K for CN molecules in the mid region as the laser energy is varied from 55 mJ to 98 mJ. This variation of vibrational temperature with laser energy is essentially due to the fact that as the incident beam power increases, comparatively larger number of molecules are excited into the higher vibrational states. Similarly the variation of vibrational temperature for the C_2 Swan bands and CN molecules in the extended region (C) of the plasma emission with laser energy is shown in figure (4.13). Here, the vibrational temperature was found to vary from 5.33 x 10^3 K to 2.252×10^4 K for C_2 molecules and from 5.23×10^3 K to 2.326×10^4 K for CN molecules in the extended region as the laser energy is varied from 55 mJ to 98 mJ. In this region, which is comparatively cooler, the recombination processes dominates and this could also contribute to an increase in the vibrational temperature of the molecules as the laser energy is increased. The knee appearing in figure (4.13). is evidently due to a threshold-like phenomenon resulting from the possible non-linear interactions like self-focussing of the laser beam within the plasma medium. The Debye length, which is the characteristic screening length of the plasma is given by [46,47],

$$\lambda_D = \left[\frac{k_B T_o}{8\pi N_o e^2} \right]^{1/2} \qquad (5.4)$$

where, k_B is the Boltzmann's constant, T_o the equilibrium plasma temperature ($\approx 10^5$ K), N the equilibrium concentration ($\approx 10^{12}/cm^3$), and e the electron charge.

It is known that the self-focussing phenomena of laser beams in plasma will be predominant if the Debye length is less than the beam diameter [48,49]. In our case, $\lambda_D \approx 3~\mu m$ which is much less than the beam diameter (≈ 1 mm). Such self-focussing of the laser beam in the plasma leads to an enhanced effective power density resulting in more intense emission. The threshold for this non-linear effect for region C is clearly seen in figure (4.13) and it occurs at ≈ 70 mJ. It is interesting to note that such a threshold-like phenomenon is not explicitly evident in the
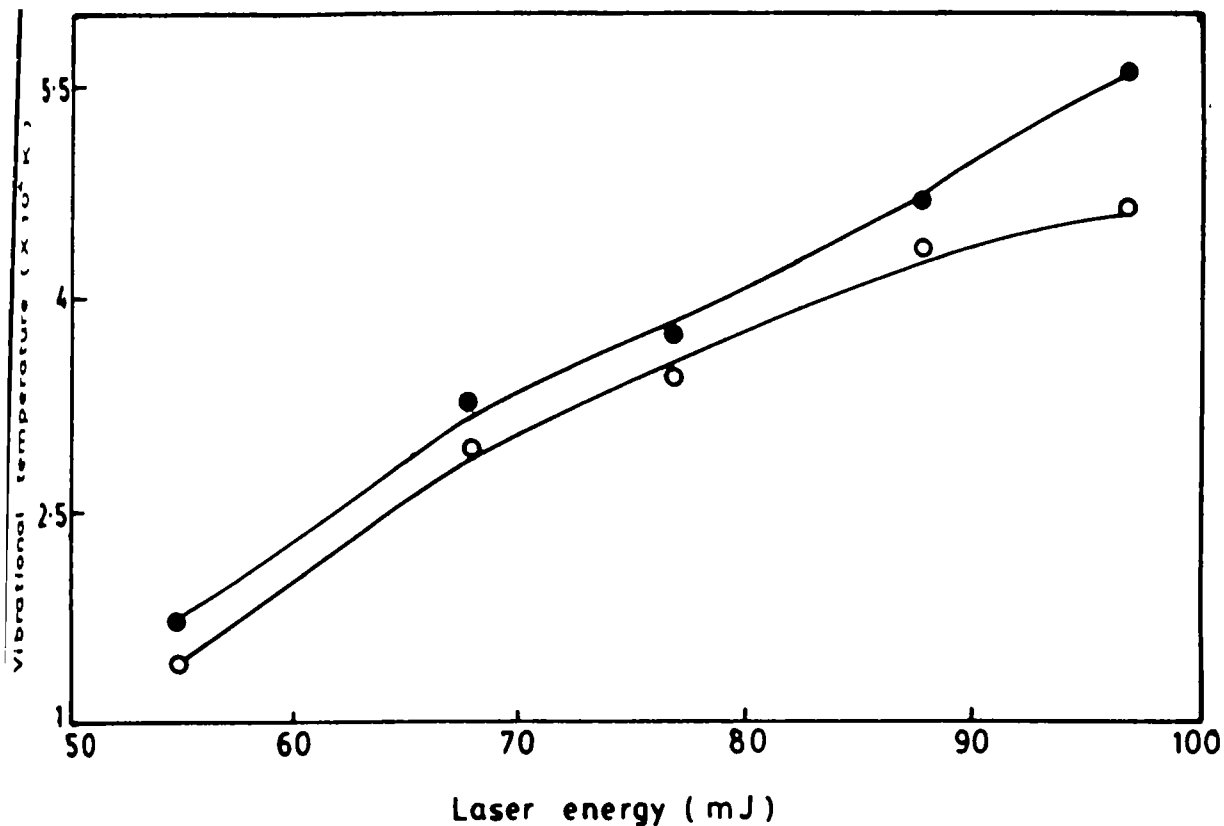
Fig.4.12. The variation of the vibrational temperature of the C_2
Swan bands and CN bands in the B region of the plasma
emission with laser energy. ($\bullet$ - C_2 and o - CN)
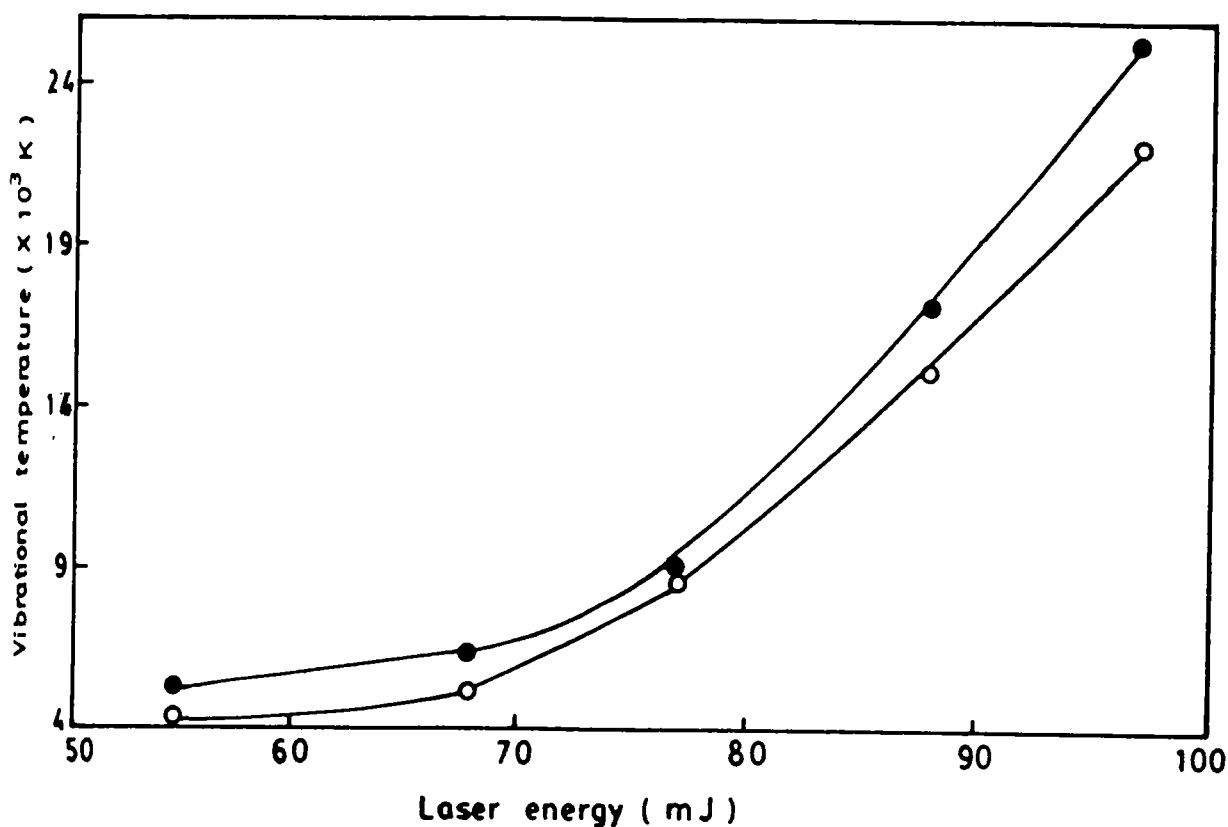
Fig.4.13. The variation of the vibrational temperature of the C_2
Swan bands and CN bands in the C region of the plasma
emission with laser energy. ($\bullet$ - C_2 and o - CN)

region B (figure (4.12)). Apparently, this is due to the fact that greater laser energy density due to self-focussing and a larger plasma density and temperature lead to a much lower value for this threshold in region B < 55 mJ which is near the saturation region [50,51].

4.6. LANGMUIR PROBE STUDIES

The electron temperature at different distance from the target surface was obtained from the volt-amphere characteristics of the Langmuir probe. Experimental details about the measurement of Langmuir probe is given in the chapter III and the calculation used for obtaining the plasma temperature is described in the chapter I (equation no.1.61). Here the probe consists of a series of thin copper rods kept at different distance from the target and each can be biased with a dc voltage so that electron (plasma) temperature at various distance from the target surface can be studied. The variation of electron temperature with distance from the target surface is shown in the figure (4.14).   It was found that plasma (electron temperature) temperature decreases as the distance from the target surface is increased.   This shows that in the region close to the target surface the density of the ionic species are so high which result in the large value of the temperature and as the distance from the target surface increases, the density of the ionic species decreases which result in a lower value of the plasma temperature.

4.7. CONCLUSIONS

From the studies on laser etching of polymer (PTFE), the etch depth was calculated and their variation with number of pulses were also obtained.   It is observed that the etch depth was to be a linear function of the number of pulses.

The results of the spatial and temporal analysis of laser induced plasma from a typical polymer sample of PTFE lead to
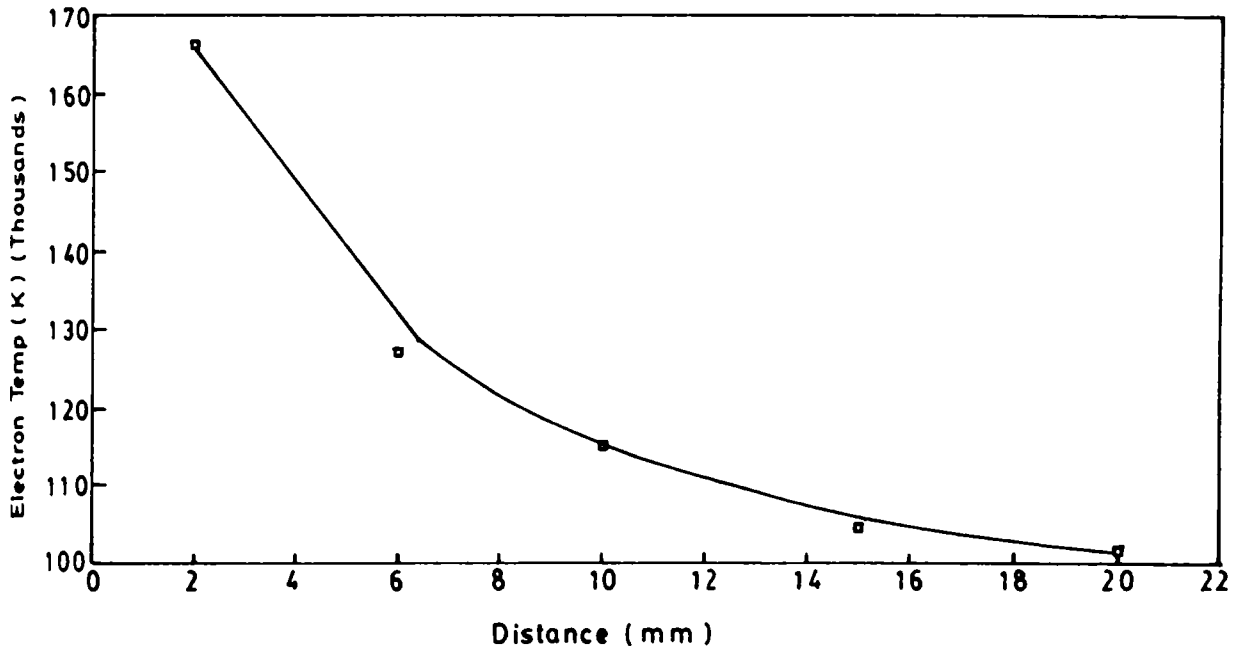
Fig.4.14. The variation of plasma temperature as function of distance from the target surface, Laser energy ≈ 80 mJ.

several interesting conclusions related to the structure and composition of the plasma. Detailed study of the emission spectra clearly indicate the existence of molecular species like C_2 and CN in addition to higher ionized states of carbon. The time resolved studies of the spectral emission also throw much light in revealing some of the complex interaction processes occurring in the plasma. From the time delays observed, in the case of higher laser energies, it can be safely concluded that the molecular bands are mainly formed when the plasma temperature begins to fall. This lends support to the view that the molecular species may not be originating from the target material at higher laser powers, but are formed as a result of recombination processes as the hot plasma cools down *ie*, the molecular species are formed in the expanding plasma due to collisions of the atomic and ionic species expelled from the target surface. Also, the non-linear interactions between the laser and the plasma gives rise to phenomena like self-focussing which exhibit threshold-like characteristics.

The spatial variation of electron temperature were calculated by the Langmuir probe technique and it is observed that the plasma temperature decreases with distance from the target. Thus the spatial composition of the ionic species in the plasma can be studied by the Langmuir probe technique. The production of large number of ions in the plasma plume is essential for the thin film deposition. Langmuir probes can thus become useful tools for monitoring laser deposition of thin film of various materials.

REFERENCES

[1] Gorodetsky G, Kazyaka T G, Melcher   R L and Srinivasan R,
     Appl.Phys.Lett., 46, 828, (1985)

[2] Kim H, Postlewaite J C,   Zyung   T   and   Dlott   D   D,
     J.Appl.Phys., 64, 2955, (1988)

[3] Srinivasan R and Braren B., , *Chem.Rev.*, 89, 1303,(1989)

[4] Srinivasan R and Mayne-Banton V, *Appl. Phys. Lett.*, 41, 576,
     (1982)

[5] Srinivasan R, *J. Vac.Sci.Tech.*, B1, 923, (1983)

[6] Bloembergen N, *"Laser solid interaction and laser processing"*,
     (AIP, New York, 1979)

[7] Davis G , Gower M C, and Fotakis C, *Appl.Phys.A*, 36, 27, (1985)

[8] Zyung T, Kim H, Postlewaite J C and Dlott D D, *Appl.Phys.Lett.*,
     55, 1, (1989)

[9] Kim, H, Postlewaite, J C , Zyung, T, and Dlott, D D,
     Appl.Phys.Lett., 54, 2274, (1989)

[10] William R C and Brenna, J T, *J. Chem. Phys.*, 92, 2269, (1990)

[11] Ageev V P, Akhasakhalyan A D, Gaponov S V, Gorbunov A A,
     Konov V I and Luchin V I, *Sov.Phys.Tech.Phys.*, 33, 562,
     (1988)

[12] Srinivasan R, *Appl.Phys.Lett.*, 58, 2895, (1991)

[13] Letokhov V S, *Nature*, 316, 325, (1985)

[14] Deutsch T F and Geis M W, *J.Appl.Phys.*, 54, 7201, (1983)

[15] Andrew J A, Dyer P E and Key D, *Appl.Phys.Lett.*, 43, 717,
     (1983)

[16] Koren G and Yeh J T C, *Appl.Phys.Lett.*, 44, 1112, (1984)

[17] Wayne a weimer , *Appl.Physlett.*, 52, 2173, (1988)

[18] Brannon J H, Shell D and Kay E, *Appl.Phys.A*, 52, 160, (1991)

[19] Kuper S and Stuke M, *Appl.Phys.Lett.*, 54, 4, (1989)

[20] Srinivasan R, Sutcliffce S and Braren B, *Appl.Phys.Lett.*, 51,
     1285, (1987)

[21] Billmeyer F W, *"Text book of Polymer Sciences"*, (New York,
     London 1962)

[22] Garrison B J and Srinivasan R, *J.Appl.Phys.*, 57, 2909, (1985)

[23] Dyer P E and Srinivasan R, *Appl.Phys.Lett.*, 48, 445, (1986)

[24] Koren G and. Yeh J T C, *Appl.Phys.Lett.*, 44, 220, (1984)

[25] Koren G and. Yeh J T C, *J.Appl.Phys.*, 56, 212, (1984)

[26] Davis G M and Gower M C, *Appl.Phys.A.*, 36, 27, (1985)

[27] Srinivasn R and Leigh W J, *J.Am.Chem.Soc.*, 104, 6784, (1982)

[28] Neifeld R A, Croft M and Shaheen S A., *J.Appl.Phys.*, 69, 1107, (1991)

[29] Philip H R, *Appl.Phys.Lett.*, 48, 192, (1986)

[30] Cole H S, Liu Y S and Philip H R, *Appl.Phys.Lett.*, 48, 76, (1986)

[31] Creasy W R and Brenna J T, *J.Chem.Phys.*, 92, 2269, (1990)

[32] Deutsch T F and Geis M W, *J.Appl.Phys.*, 54, 7201, (1983)

[33] Jellinck H H G and Srinivasan R, *J.Phys.Chem.*, 88, 3048, (1984)

[34] Srinivasan R and Braren B, *J.Polym.Sci.*, 22, 2601, (1984)

[35] Padmaja G, A V R Kumar, P Radhakrishnan, V P N Nampoori and C P G Vallabhan, *Pramana-J.of Phys.*, 32, L693, (1989)

[36] Pearse R W B, Gaydon A G, *"The identification of Molecular spectra"*, (London : Chapman & Hall Ltd.,), (1965)

[37] William F M, Charles H Corliss and Bourdon F S, *'Tables of spectral line intensities, Part I & II,'* (U.S. National Bureau of Standards), (1975)

[38] Padmaja G, A V R Kumar, P Radhakrishnan, V P N Nampoori and C P G Vallabhan, *J.Phys:D,* 22, 1558, (1989)

[39] Wu X D, Dutta B and Hegde M S, *Appl.Phys.Lett.*, 54, 2, 179, (1989)

[40] Koren G, Gupta A and Baseman R J, 1989, *Appl.Phys.Lett.*, 54, 19, (1990)

[41] Boland B C, Irons F E, and Whirter M C, *J.Phy : B,* 1, 1180, (1968)

[42] Rohr K, Dinger R and Weber H, *Laser & Part.Beams,* 7, 157, (1989)

[43] Herzberg G, *Molecular spectra and molecular structure I. Spectra of Diatomic molecules',* 1950, 2nd edition (Van Nostrand-Reinhold, New York), (1950)

[44] MacDonald M A, David S J and Coombe, R D, *J.Chem.Phys.,* 84, 5513, (1986)

[45] Stephen R L, Charles W B and Alistair P R, *J.Chem.Phys.,* 92, 3000, (1990)

[46] Sodha M S, Ghatak A K and Tripathi V K, *"Self Focusing of Laser Beams in Dielectrics, Plasmas and Semiconductors",* (Tata McGraw-Hill, New Delhi, 1974)

[47] Shkarofsky I P, Johnston T W, and Bachynski M P, *"The Particle Kinetics of Plasmas",* (Addison-Wesly Publishing Co.,1966)

[48] Ginzburg V L, *"The Propagation of Electromagnetic Waves in Plasmas"* (Pergamon Press), (1961)

[49] Dinger R, Rohr K and Weber H, *Laser & Part.Beams,* 5, 691, (1987)

[50] Balmer J E and Donaldson T P, *Phys.Rev.Lett.,* 39, 1084, (1977)

[51] Pearlmann J S, Thomas J J, and Max C E, *Phys.Rev.Lett.,* 38, 1397, (1977)

3.1. INTRODUCTION

Laser ablation of the solid surface is one of the methods to produce a clean plasma of the material. Detailed study of the spatial and temporal characteristics of the emission of the laser produced plasma plume from the sample provides information about the composition and lifetime of the ablated materials since the plasma is produced due to the ablation of the target alone. Basically, the laser induced plasma can be produced even in air provided the energy density of the incident beam is large enough. However, at atmospheric pressures, the plasma is compressed and is confined to the sample surface. Thus it is necessary to use a vacuum chamber to produce elongated plasma. Based on the composition, physically, LIP emission can be divided into three broad spatial regions viz., (1) the central or the core region of the plasma emission close to the surface, where the temperature is maximum and most of the species consists of ionized atoms, (2) the mid region where apart from ionized species, both neutral and a certain amount of molecular species are present and (3) the extended region in which the plasma temperature is comparatively lower and larger number densities of molecular species occur.

In this chapter a comprehensive account of experimental technique for the spectroscopic as well as time resolved analysis of the LIP and of the various subsystems needed for the experiments are given. These experimental details are divided into two sections. In the first section the experimental set up for the spatially resolved spectroscopic recording of the plasma is given. The description of the various sub-systems like excitation source, plasma chamber, detection and other set up for the recording the plasma spectrum, such as spectrograph and microdensitometer is given. In the second section, the experimental set up for the time resolved measurements and various sub-systems like monochromator coupled PMT, boxcar averager, oscilloscope and related instruments for these studies are described.

3.2. EXPERIMENTAL SET UP FOR SPATIAL VARIATION STUDIES OF THE LIP SPECTRUM

Plasma was generated by pulsed laser ablation of the solid sample. Samples of metals (Aluminium and Copper), polymers (PTFE), Graphite and high T_c superconductors ($YBa_2Cu_3O_7$ and $GdBa_2Cu_3O_7$) were studied using LIP technique. The sample is taken in the form of cylindrical disc (2.5 cm diameter and 5 mm thickness) and placed in a partially evacuated chamber (Pressure $\approx$ 200 mTorr) provided with quartz windows. The laser beam was focussed to a diameter of $\approx$ 1 mm (energy density $\approx$ 19 J/cm^2) on to the target, which is rotated about its axis by an externally controlled d.c. motor to avoid non-uniform pitting of the target surface. The bright plasma emission was observed through a side window at right angle with respect to the plasma expansion direction. The plasma emission spectrum from the three distinct regions ie, central, middle and extended regions, (region A, B, and C respectively) of the plasma were recorded photographically using a Carl-Ziess three prism spectrograph with appropriate focussing optics along with the mercury spectrum as a standard. The schematic diagram of the experimental arrangement for recording the plasma emission spectrum is given in figure (3.1). Figure (3.2) shows the typical plasma plume from a teflon target clearly indicating the three regions of measurements. The wavelength of emissions of the different atomic, ionic and molecular species in the plasma were measured from the recorded spectra using standard spectral data sources [1,2]. By using spectroscopic analysis of the plasma, it is possible to identify the constituents and different states of ionization of the same. Further by focussing the different regions of the plasma, the spatial composition of the plasma and ionization state at different regions of the plasma can be studied.
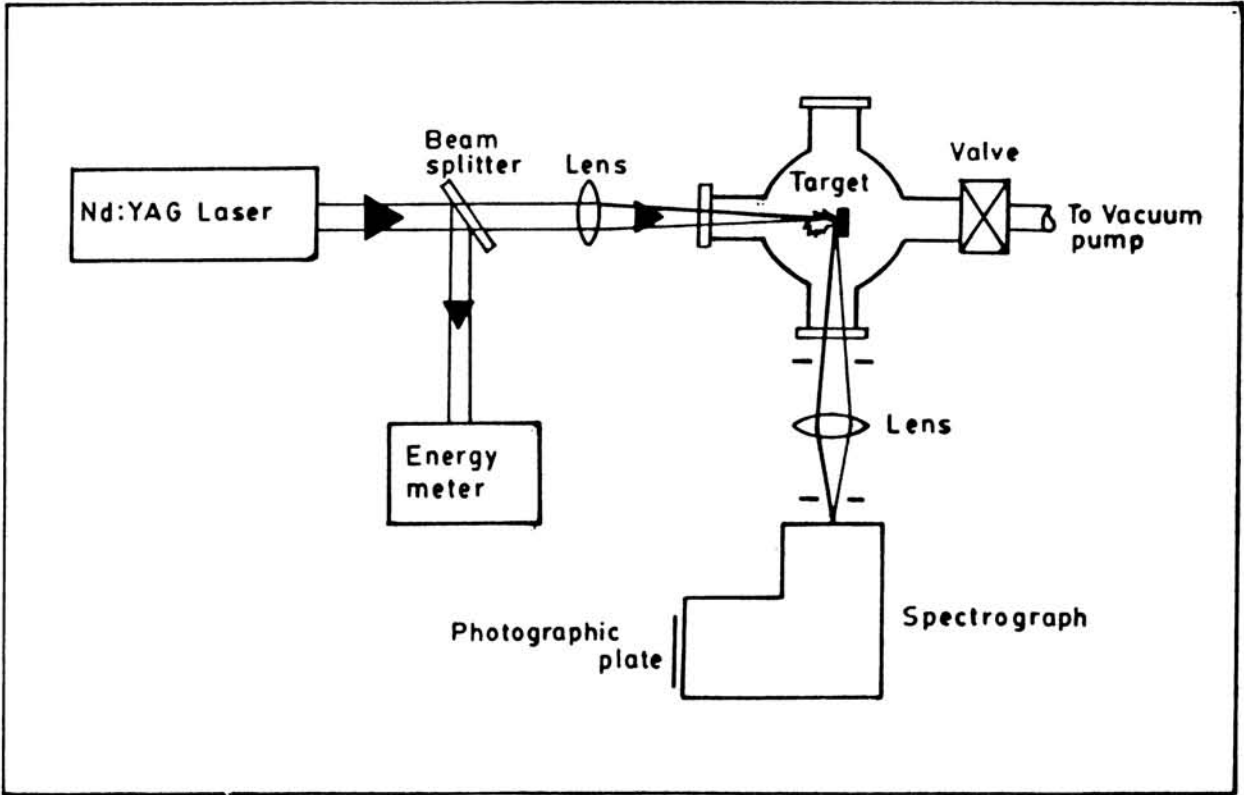
Fig.3.1. Schematic diagram of the experimental set up for spectroscopic analysis of laser produced plasma
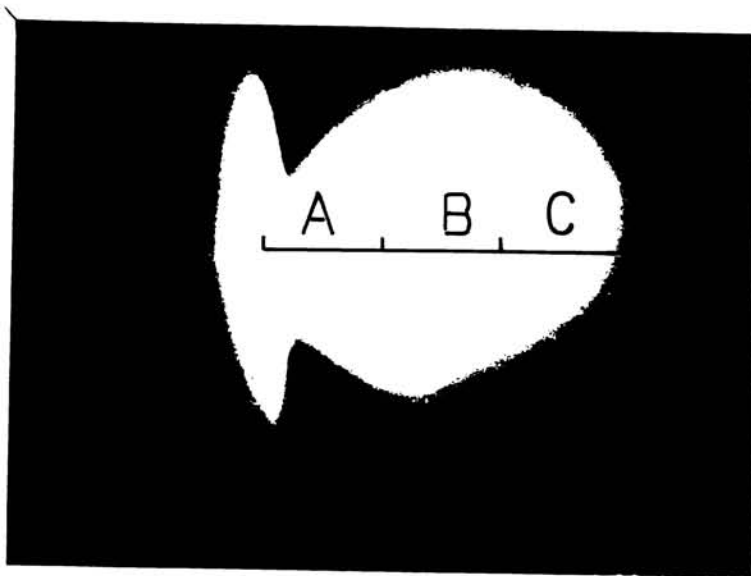
Fig.3.2. Typical photograph of the plasma plume from the surface of the teflon target indicating the three distinct regions in the plasma

3.2.1. THE Nd: YAG LASER

The pulsed laser used here for the plasma studies is a electro-optically Q - switched Nd:YAG laser having a fundamental output of 1.06 μm (Quanta Ray DCR 11). The diffraction coupled resonator delivers a 'doughnut' shaped beam profile at energies of the order of 275 mJ at $\approx$ 10 nsec pulse width with a power stability of $\pm$ 4 % [3]. The laser is capable of pulsing at a rate of 1-16 pulses/sec. It has a second harmonic generator (KDP crystal) which can be placed in the path of the fundamental beam to provide the second harmonic output at 532 nm at less than 10 nsec pulse width with a conversion efficiency of $\approx$ 50 %. Figure (3.3) shows the schematic of the Nd:YAG laser. Higher order harmonics at 355 nm and 266 nm can be obtained by introducing the appropriate crystals in the beam path. The laser beam has a typical line width of < 1 cm^{-1} with 220 MHz spacing between the longitudinal modes and a beam divergence of < 0.5 mrad. The laser provides trigger outputs to synchronize the oscilloscope, energy meter, boxcar averager etc.

3.2.2. PLASMA CHAMBER

The plasma chamber is essentially a vacuum chamber, suitably designed and fabricated using a cylindrical steel tube of $\approx$ 25 cm diameter and is provided with eight 'O' ring sealed window attachments of $\approx$ 4 cm in diameter. Quartz flats are used as windows where the laser beam enters the chamber and the window corresponding to the spectrograph. Glass flats are used in the other windows, which are used as observation ports. A few window openings are converted to vacuum feed-throughs to provide the electrical connections to the d.c. motor, substrate heater, the Langmuir probe and the thermocouple inside the chamber. The chamber is sealed on the top with a heavy stainless steel disk with an 'O' ring. The whole chamber is placed on a bottom disk, which in turn is directly coupled to the rotary vacuum system.

Pulsed Nd:YAG Laser

1060 nm

532 nm

Flash lamps

Laser rod

Mirror   Q-Switch

Mirror

Polarizer

SHG

|7mm|

2mm

Beam Profile

Energy

Distance

Fig.3.3. The schematic of the Nd:YAG laser

Window

Ion probe

Window

Laser

Sample motor

Valve

To vacuum pump

Window
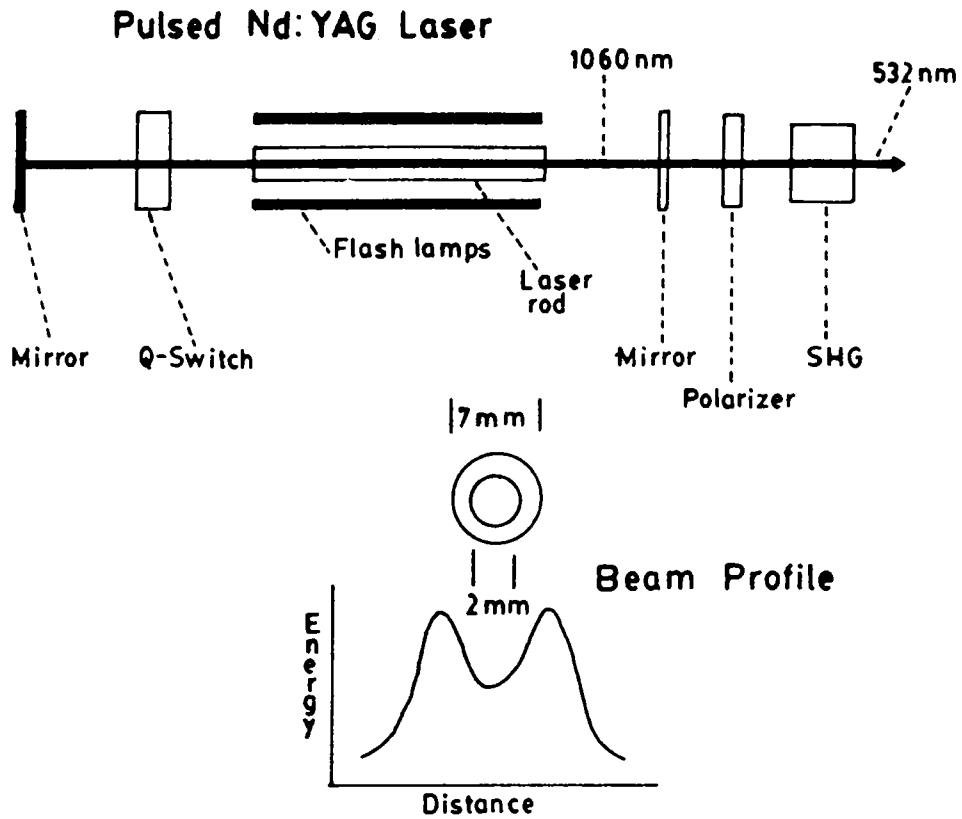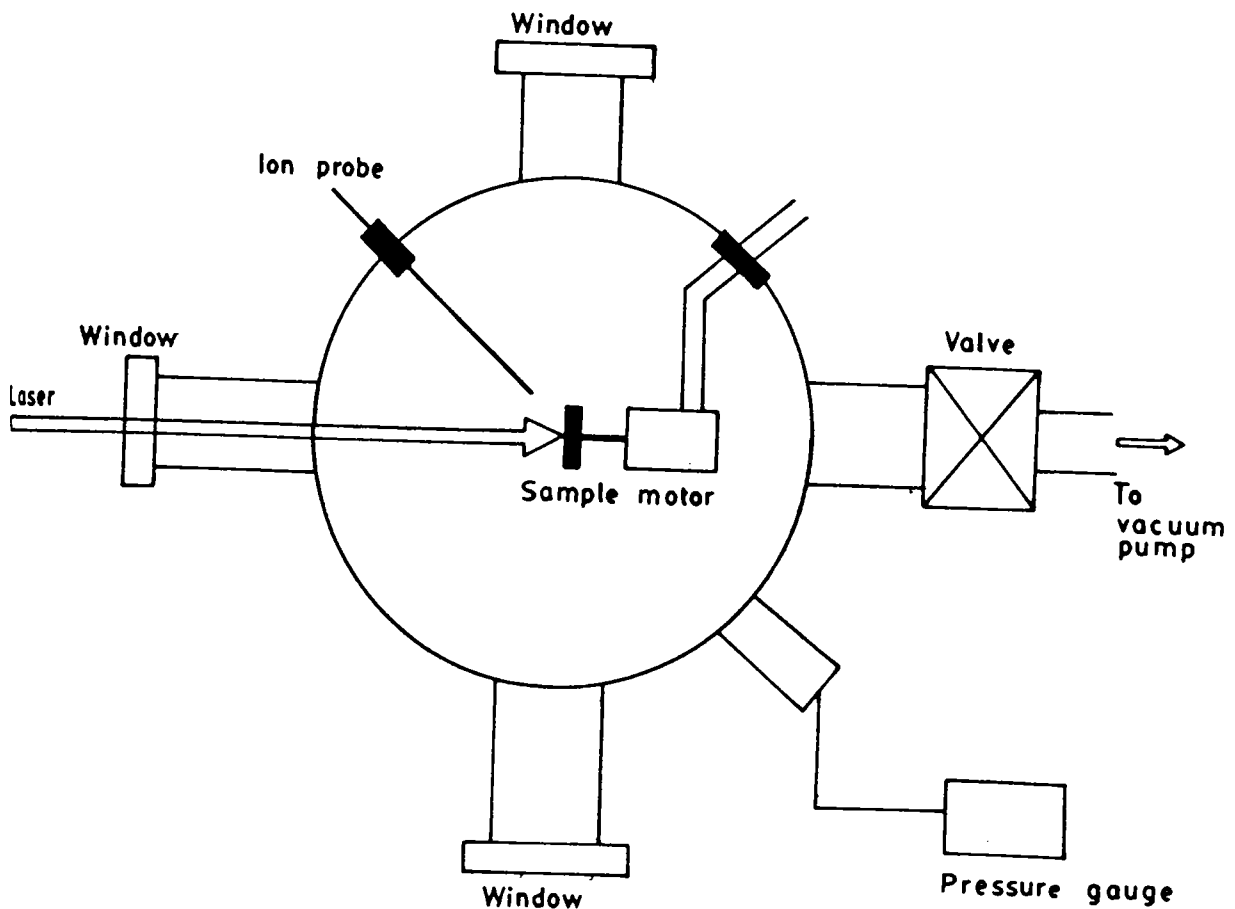
Pressure gauge

Fig.3.4. The schematic figure of the plasma chamber

The chamber pressure is monitored by a high pressure Pirani gauge (VT-DHP-11) capable of pressure measurements from atmosphere to 10^{-3} mbar with good resolution in the high pressure regions. This gauge is provided with relay control outputs to control solenoid valves for precise gas filling.

The schematic figure of the plasma chamber is shown in the figure (3.4). The pressure inside the chamber was fixed at $\approx$ 200 mTorr. The sample holder is fixed on to a d.c. motor and is mounted on the holder. The angle of the sample with respect to the incident laser can be varied to suit the specific kind of application. For emission studies, the sample is mounted so that the surface is at right angles to the laser beam and for plasma assisted deposition studies, the sample surface is at 45° to the laser beam. The sample is rotated about the axis of the target at a constant speed so that fresh area of the surface will always be exposed to successive laser shots, resulting in a uniform plasma emission intensity. The bright plasma emission was observed through a side window to which the focussing optics and the prism spectrograph are aligned.

3.2.3. THE PRISM SPECTROGRAPH

The plasma emission spectrum covering large wavelength range will give some preliminary information on the time and spatial dependence of the spectrum. These functions can be obtained by a spectrograph with photographic recording. For spatial resolution, the particular region of the plasma is imaged on to the entrance slit of the spectrograph which is then provided with the coordinate at right angles to the wavelength axis $ie.$, along the slit direction corresponding to the one of the coordinate of the emitting volume element of the source. The same instrument can be used for time resolution by masking the window of the plasma cell, except for a narrow slit at right angles to the entrance slit of the spectrograph and sweeping image of the first slit across the entrance slit with a rotating mirror (However we

have not adopted this method in the present study). Either quartz or glass prism spectrograph would be suitable for this purpose depending on the desired wavelength range.

For the determination of the emitted species by its characteristics spectral lines, a wavelength accuracy of about ≈ 1 A$^\circ$ is usually sufficient. The measurement of spectral lines and continuum intensities can also be done with an instrument at moderate dispersion. The plasma emission from the core of the plasma has an intense background emission which usually masks out the emission lines, thus necessitating short exposure times. The plasma emission in the middle and the extended regions have a relatively weaker background emission and the emission characteristics of the species are more vivid. At shorter wavelengths, since the light gathering efficiency of the spectrograph falls off sharply, a much larger exposure time is required [4].

In our measurements, a Carl-Zeiss three prism glass spectrograph is used for the photographic recording in the wavelength range from 400 nm to 600 nm of the plasma emission spectrum. This spectrograph has a resolution of ≈ 0.02 nm which is adequate for these studies. Method of spectrograph illumination is shown in the figure (3.5).

Different regions of the plasma are photographed by using appropriate optics and suitable masks in front of the entrance slit of the spectrograph. A cylindrical lens is used finally to produce a line image of the plasma region of interest on the entrance slit. The entrance slit width and the angle of dispersion of the spectrograph are then adjusted to obtain the optimum spectral resolution. The spectrum is recorded on the photographic film (typically 9x6 cms 100/400ASA panchromatic) placed in the film holder. In order to measure the wavelength of the spectra obtained, a mercury standard spectrum is photographed simultaneously with the plasma spectrum. The spectrum covers the wavelength range from violet to red. The plasma emission spectrum at moderate resolution can be obtained by this
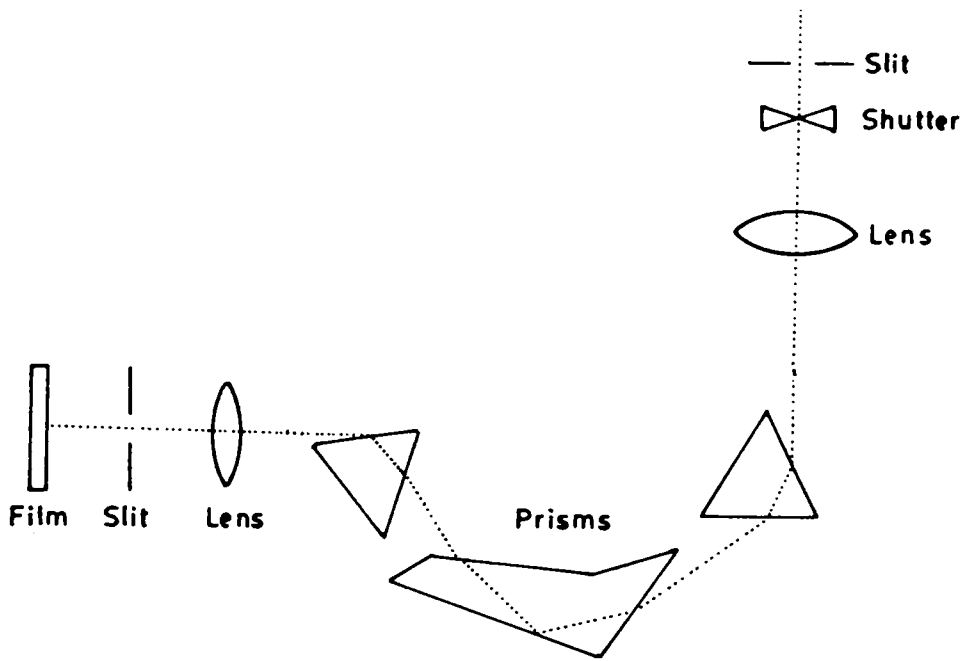
Fig.3.5. The light transmitted in a carl - zeiss 3-prism spectrograph
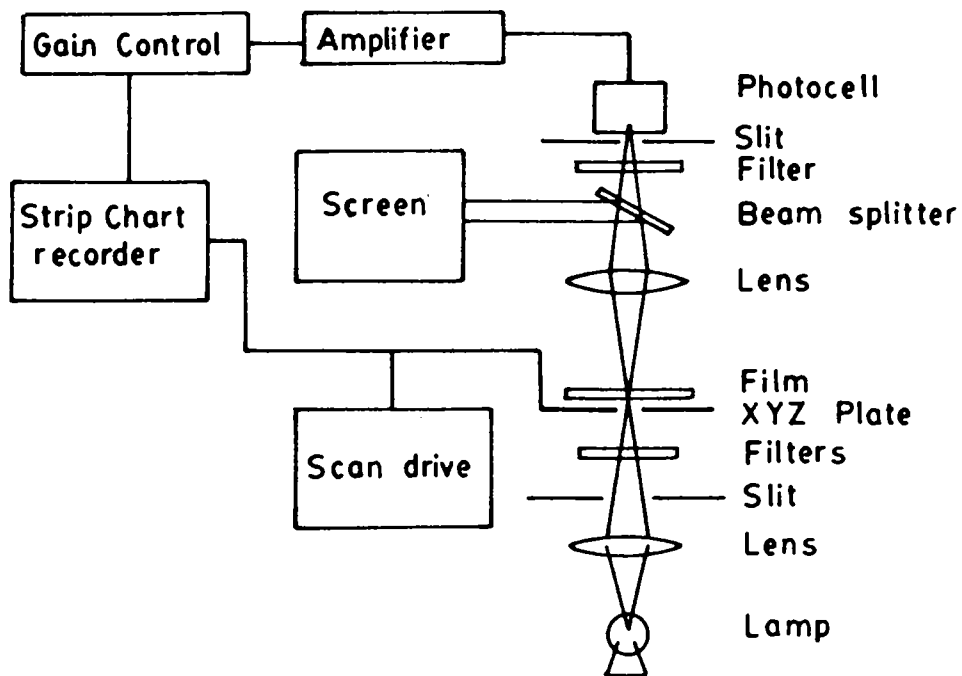
Fig.3.6. The optical system of a typical microdensitometer

instrument. The design requirements of the spectrograph using photomultiplier tube as detectors are different from those of an instrument designed to use photographic film. The density of the photographic film approximately proportional to the log of the exposure per unit area, while the signal from PMT is proportional to the total flux falling on the photocathode. The advantage of using photographic recording of the plasma emission spectrum compared to other techniques is that, in photography simultaneous recording of the spectrum in a wide wavelength range is possible (similar to optical multichannel analyzer recording) thus reducing the recording time.

For the spectroscopic observation of the plasma in certain regions, which are comparatively weaker in intensity, we have to use a high speed film which has a larger grain size. Optimum film contrast and sensitivity can be obtained by properly adjusting the exposure and the developing times.

3.2.4. MICRODENSITOMETER

The density of silver deposited at any portion of the photographic emulsion is most readily measured with a densitometer, a photometric device designed to determine the reduction in the intensity of light when sent through a restricted area of the emulsion. When the area is small in the case of spectrum lines, the instrument may be called a microdensitomerter [5]. Since the plasma emission spectrum is recorded photographically, the relative intensities of all these spectral lines can be recorded using the microdensitometer. This instrument is used for measuring the photographic response to the exposure of the film to light accurately. Here the beam of intensity I_o is passed through the spectral line on the film which is to be measured. The transmitted light of intensity I then activates a photocell whose current response is recorded by a galvanometer swing or deflection d or as the movement of a pen recorded across a scale which has 50 or 100 divisions [6].

The density of the silver produced per unit area in a developed image is closely proportional to the ratio log (I_o/I), which is of fundamental significance and commonly employed as a measure of photographic response. The linear relationship between the intensity of the light incident on the microdensitometer photocell and the galvanometer deflection can be written as,

$$D = \log \frac{I_o}{I} = \log \frac{d_o - d'}{d - d'} \qquad (3.1)$$

where d_o is the galvanometer deflection for I_o (equivalent to a light transmitted by a perfectly clear area on the photographic film, that is the area which has received no light exposure) and d' is the deflection when no light enters the photocell.

If the different area of the photographic film are exposed to different known relative intensities, such relationship is known as calibration curve. The calibration curve can also drawn by plotting the percentage of transmission (T) versus log intensity.

$$T = I/I_o \text{ and consequently } D = 1/T$$

In a clear glass, deflection of 100 divisions is equalent to 100 % transmission, each deflection for an area is a measure of percentage of transmission. If then, log d versus log I is plotted the characteristic curve is obtained. Fundamental features of a densitometer are a source of light that provides a beam to measure the plate, provision for ensuring that this beam pass through only that part of the emulsion which is to be measured and a device to compare the intensity of beam of light after passing through the exposed emulsion to that of the same beam passed through an unexposed area of emulsion. In a direct reading densitometer the deflection is a function of the density of the photographic film.

The microdensitometer used in our measurements is a Carl-Zeiss system having automated scanning and recording facilities. The

optical system of a typical microdensitometer is shown in figure (3.6). Two beams may be supplied one with which to inspect the plate to help in locating the exact spot to be measured and a second to carry out the measurements. Using this instrument, the percentage of transmission T of the spectral lines in the photographic films were measured. The response of the film was obtained by focussing a small part of the He-Ne laser beam of known energy for various time duration of exposures and the corresponding calibration curve is obtained. Using this calibration curve, the relative intensity of the spectral lines were calculated.

3.3. EXPERIMENTAL SET UP FOR THE TEMPORAL MEASUREMENTS IN THE LIP

The time resolved measurements of the plasma evolution processes in the laser induced plasma from different solid materials were studied using spectroscopic and ion probe techniques.

As described in the previous experimental set up for spectroscopic studies, same pulsed laser radiation was used. The sample was mounted in a vacuum chamber so that the target can be irradiated at normal incidence and the ejection from the surface can be viewed at right angles. The laser beam was focussed on to the target using a quartz lens. A part of the plasma plume at about 1.5 cm away from the target surface was focussed on to the slit of the monochromator (Jarrel - Ash, 0.5 m) coupled to PMT and a CRO/ Boxcar averager. Since we have used a 0.5 m monochromator for the wavelength separation ($\Delta\lambda < 1$ A^o)., the line selection is much more accurate than the work of Wu et.al.[7]. Since we had already recorded the spectra photographically using a spectrograph and the various atomic and molecular species were identified, in order to study the time evolution of the species produced by the laser irradiation, the characteristics lines could be easily selected using a monochromator. The PMT output was fed to a 100 MHz storage

oscilloscope (Tektronix Model 466) with a 50 ohm termination. The schematic diagram for the measurement of time resolved analysis of the plasma produced by the laser ablation technique is given in the figure (3.7). The time resolved studies of the plasma give vital information regarding the time taken for a particular state of a constituent to evolve after the plasma is formed. Thus this measurement is important for obtaining knowledge of complicated ablation and transport processes occurring in the plasma produced by the laser ablation technique.

In the ion probe technique, a variable bias voltage was applied between the probe and the body of the vacuum chamber. The electrons in the plasma were collected by the probe (3 cm length and 1.6 mm diameter) kept at the about 1.5 cm away from the target surface ((figure (3.7)). The voltage pulse developed was measured across a 50 ohm load resistance on a 100 MHZ storage oscilloscope. By using this technique the electron temperature and velocity of positive ions as well as electrons were obtained. The method of calculation used for obtaining above parameters are given in the chapter I.

3.3.1. MONOCHROMATOR

For the wavelength selection of plasma emission, a medium resolution scanning instrument was needed. This purpose was served by 0.5 m scanning monochromator (Jarrell-Ash Model 82-025). Since we have used this monochromator for wavelength selection, the line selection is more accurate. This spectrograph is provided with a smooth scanning motion in ' eight speeds ranging from 2 nm/min to 50 nm/min. It gave 1.6 nm/min dispersion in the first order with maximum resolution of 0.02 nm. It covered a spectral range of 400 to 900 nm using a reflection grating with 1800 groves/mm blazed at 500 nm and is driven by a reversible motor [8].

The apparatus consists of an inlet slit S_1 and exist slit S_2. The light enters through S_1 and falls on a concave mirror having
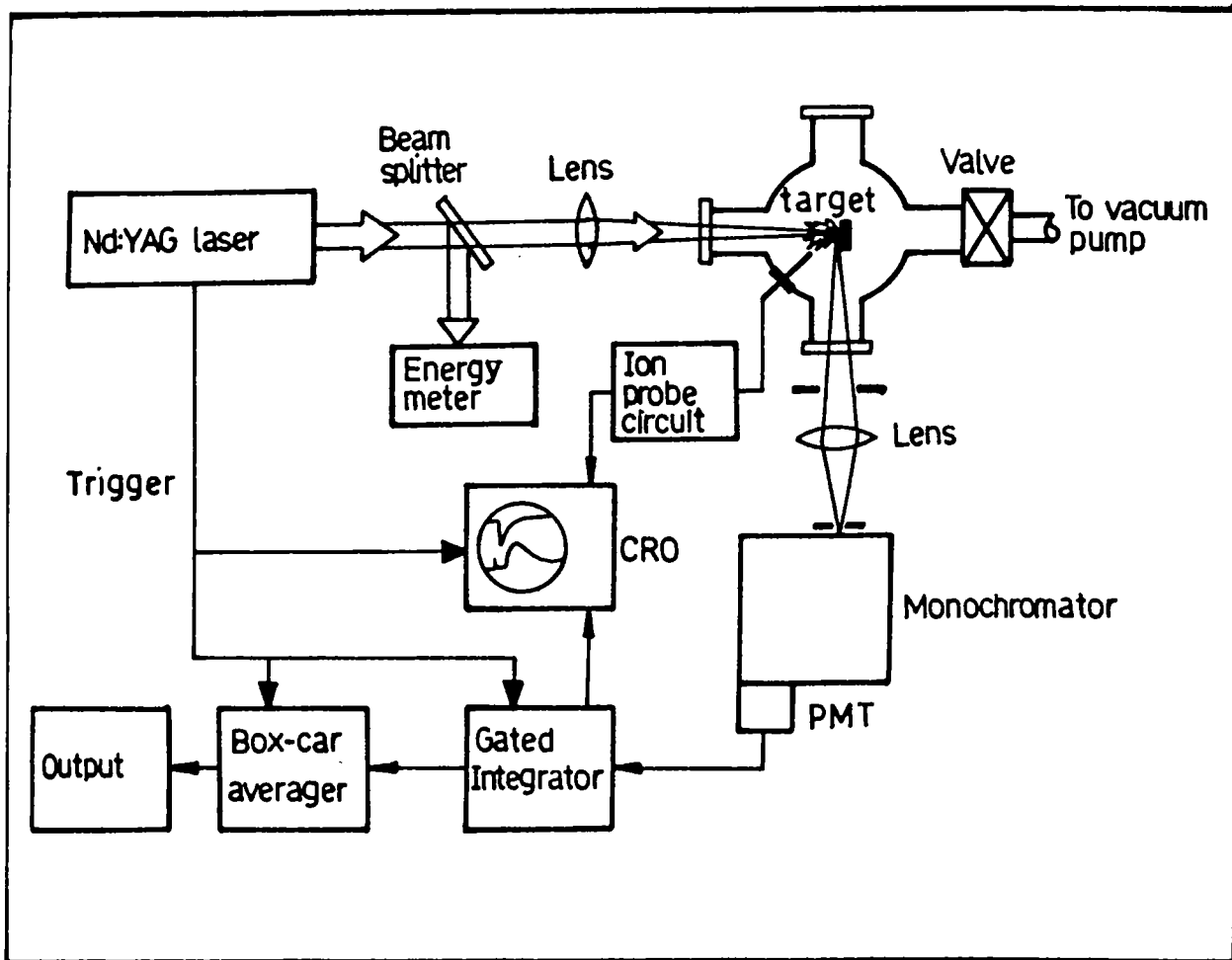
Fig.3.7. Schematic diagram of the experimental set up for the time resolved analysis of laser produced plasma
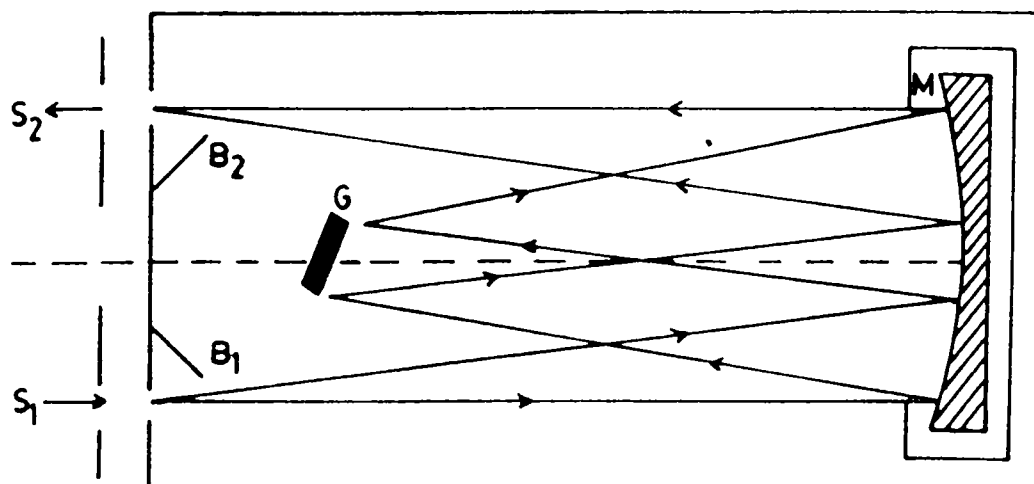
Fig.3.8. Light reflection in a monochromator

150 mm diameter and 0.5 m focal length, gets collimated and reflected to fall on the grating, where it undergoes dispersion and is again reflected back into the mirror and comes out through the exit slit S_2. The light reflection in a monochromator is shown in the figure (3.8). The wavelength of monochromatic light emerging at the exit slit is changed by simply rotating the grating about its centre (through Ebort mounting).

3.3.2. PHOTOMULTIPLIER TUBE (PMT)

The PMT is a photosensitive device consisting of a photo emissive cathode (photocathode) followed by focussing electrodes, an electron multiplier (dynodes) and an electron collector (anode) in a vacuum tube as shown in the figure (3.9). When light hits the photocathode, the photoelectrons emitted into the vacuum are directed by the focussing electrodes towards the electron multiplier where, electrons are multiplied by the process of secondary emission by successive dynodes maintained at increasing voltages (figure (3.9)). The multiplied electrons are collected by the anode as an output signal. Due to the process of secondary -emission multiplication, PMTs are uniquely sensitive among the photosensitive devices currently used to detect radiant energy in the UV, VIS and NIR regions. They also have a fast time response and low noise [9]

The output from the monochromator was detected by an EMI photomultiplier tube (Model 9683-KQB) with S-20 cathode. This tube was directly mounted at the exit slit of the monochromator. The PMT was operated at $\approx$ 1.3 kV dc. Since the output gain of the PMT highly depends on the voltage, any variation in the applied voltage causes a noticeable change in its gain. Hence a highly stabilized power supply (Thorn EMI PM28B) was used to operate the PMT, which maintained a constant output voltage across the terminals in spite of the variation of the load as well as line voltage. The tube was also provided with a good RF shielding. This PMT has got a fairly constant quantum efficiency
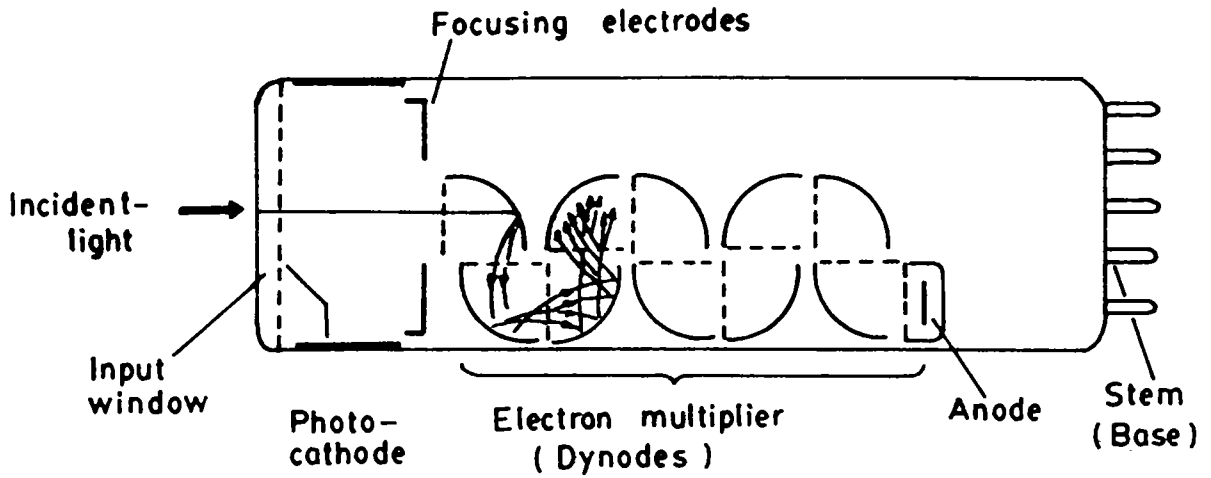
Fig.3.9. Cross section of head-on Type PMT
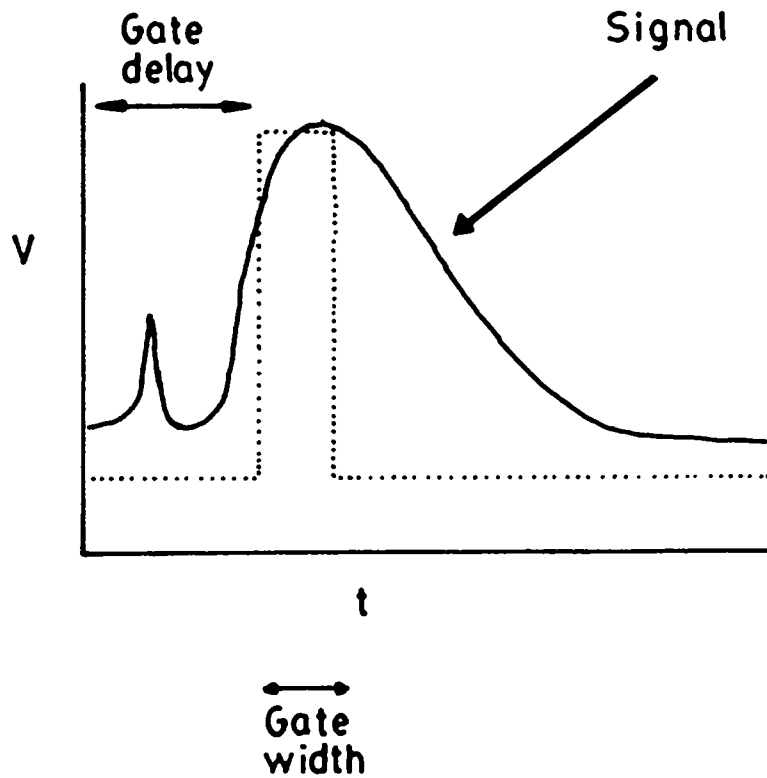
Fig.3.10. Typical PMT signal, Time delay and gate width of the of
the boxcar averager

in the spectral region 350-800 nm where all the present measurements were carried out. Before doing the experiment, the PMT was given sufficient cooling so that the dark current of the tube is reduced to minimum value.

3.3.3. USE OF GATED INTEGRATOR AND BOXCAR INTEGRATION TECHNIQUE

The amplitudes of the pulse shapes of different species in the plasma were identified by a gated integrator and a boxcar averager (Standford research systems Model SR250).

In some cases, it might be essential to recover a part or the whole of an output signal pulse so that the signal can be analyzed. To recover such a signal buried in noise, some form of averaging process is required and for that, some kind of multi -point averager or a Fourier transform analyzer is necessary. Signals of such transient nature, triggered by repetitive pulses from the excitation source can be analyzed in this fashion. This is achieved by the boxcar integrator, which essentially is an instrument used to recover complex repetitive signals hidden in noise [10]. It has a frequency response which is ideal for the recovery of such waveforms, consisting in the case of a waveform which repeats at regular intervals of a series of peaks at every Fourier component of the waveform plus a response extending from zero up to the cut off frequency $1/2\pi T_{eff}$ (where T_{eff} is the effective time constant) of the equivalent low pass filter used in the Boxcar integrator. The response is zero at all other frequencies. The bandwidth of every peak in the same can be set by the C-R filter. The usual practical boxcar has a C-R low pass filter which is connected to the voltage waveform to be measured for a short interval T_g once during each cycle of the complex waveform cycle. Since the time constant τ_r of the low pass filter is chosen to be >> T_g, it requires many repetitions of the sampling time T_g for the voltage on the capacitor of the C-R filter to approach the final value ie, the average value of the complex waveform (at specific point) plus noise during the time

86

CHAPTER V

FEATURES OF LASER INDUCED PLASMA FROM GRAPHITE

ABSTRACT

This chapter concerns with studies on the spatial variation of spectroscopic and time resolved analysis of plasma generated from the graphite surface using Nd:YAG laser pulse. The plasma emission spectrum in the centre region is found to be dominated by higher ionized states of carbon lines (up to CV), whereas the spectrum in the outer region is dominated by the molecular bands of C_2 and CN. From the time delays of different species in the plasma, the expansion velocities of the various species are calculated and their variation with respect to laser energy is also obtained. From the relative intensities of molecular bands, the vibrational temperature of the above molecules are calculated for different values of laser energies.

5.1. INTRODUCTION

In the last few years there has been growing interest in data concerning the composition and temperature of the laser ablation plasma of graphite [1-5]. Here the emission spectrum shows C_2 and CN molecules. From the above studies it is seen that CN molecules produced by using excimer laser lasers are due to photo-chemical ablation processes where as CN molecules produced by NIR (Nd:YAG) laser are due to thermal processes. The spatial and temporal evolution of vibrational temperature of CN molecules have studied by Hatem *et.al.*[6].

The C_2 radical has been found important in astrophysics and flame spectroscopy was studied by many workers [7,8,9]. The exact mechanism responsible for the swan band emission are difficult to determine and evidently vary with the wavelength and the gas medium surrounding the target. These mechanism are multiphoton in nature for wavelengths greater than 266 nm in acetylene, ethylene *etc.* and may be single photon in the complex mixtures of gases in the reaction zones of some flames. Regardless of the mechanism involved, swan band emission is a likely result at any time when intense laser pulses of almost at any wavelength are focussed on to the carbon containing gases eventhough the sample may not contain any nascent C_2 and the laser wavelength is not resonant with any single or multi photon resonances of C_2 [9]. Because the emission spans much of the visible region of the spectrum, it can interfere with fluorescence detection of many atomic and molecular species and can adversely affect a wide range of laser induced diagnostic technique [9].

Nagel and Co-workers [10] in 1985 first reported the use of laser ablation source of carbon ions to produce diamond like films at high rates of growth $\approx$ 0.3 μm/h. Pulsed laser ablation of high purity graphite is considered one of the effective methods for deposition of diamond-like carbon (DLC) thin films. Large area films (10 cm^2) of optical quality and uniformity were grown in vacuum by several authors [11 -14] and in gas mixtures containing

111

hydrogen [15,16]. In all cases laser plasma forms above the surface of the graphite. The physical properties of the plume such as temperature and species concentration directly affect the properties of the film. Carbides of transition metals are a very important class of ceramic material regarding their properties with respect to hardness and chemical inertness. Thin film deposition for applications in optics and microelectronics are extensively reviewed [17]. Development of a systematic procedure for these technological applications may be based on the information obtained from this method of synthesis. Studies have shown that carbide cluster ions can be produced by simply irradiating a graphite or mixtures of Group IV elements with graphite by a laser source [18]. This processes may of particular interest when applied to transition metals. Carbides may be formed by direct metal and graphite combination [19] or by the reduction of metal oxides at high temperatures in the presence of carbon under the action of laser beam [20]. The laser ablation was performed in order to understand the chemical reactivity of the neutral and charged particles produced in the plasma under the action of laser beams [21]. The high proportions of ions to neutrals in the plasma produced by laser ablation are responsible for uniform quality of the diamond like carbon films.

Laser ablation is a convenient method for producing C_{60} molecules. When the graphite surface is vapourized by a pulsed laser in a high density He atmosphere, producing remarkably stable carbon cluster consisting of 60 carbon atoms [22]. Since this C_{60} molecule is stable in macroscopic and condensed phases, this would provide a topologically noval aromatic nucleus for new branches of organic and inorganic chemistry. The studies of the mechanisms for electron creation and acceleration in a laser - induced plasma from a graphite surface is useful because here the laser induced emission of clusters is believed to be a thermal process [1]. Electronic excitation and ionization should therefore be due to processes in the plasma and not in the bulk. The inverse bremsstrahlung is the primary mechanism for the

acceleration of the electrons which is consistent with the theory of Phipps *et al.* [23]. Subsequent processes involve electron impact ionization/dissociation and emission of UV photons via bremsstrahlung. This latter mechanism leads to photo excitation, photo-ionization and photo-fragmentation [24]. In the case of laser ablation of graphite, the vapour plume is likely in thermodynamical equilibrium with the melting graphite surface. The occurrence of atomic, ionic and molecular carbon in the plume was found to depend on laser intensity. C_2 emission from the plasma was often reported by Chen *et.al* [25] the mechanism of which is due to plasma excitation and recombination processes .

The intensity of emission of carbon lines tends to fade as the laser etches into the graphite target because it creates large interaction area and reduces the effective laser power intensity. With an estimated maximum spot size of ≈ 1 mm, the laser intensity of 7×10^8 W/cm^2 can be regarded as the approximately the threshold intensity for excitation of atomic emission [2].

In this chapter the spectral as well as time resolved analysis of plasma produced at various distance from the graphite target surface is described. From these studies the information about plasma composition and vibrational temperature of various molecules such as C_2 and CN molecule in the carbon plasma were obtained and their variations with laser energy were also studied. The plasma emission spectrum near to the surface of the target shows the presence of highly ionized states of carbon atoms (up to CV line). From the time resolved studies, the expansion velocity of different species in the plasma were also obtained and their variation with respect to laser energy at different distance from the target were evaluated.

5.2. SPECTRAL CHARACTERISTICS OF SPATIALLY RESOLVED PLASMA FROM GRAPHITE

The plasma emission from graphite is given in figure (5.1). The plasma emission spectra at three regions of the plasma from
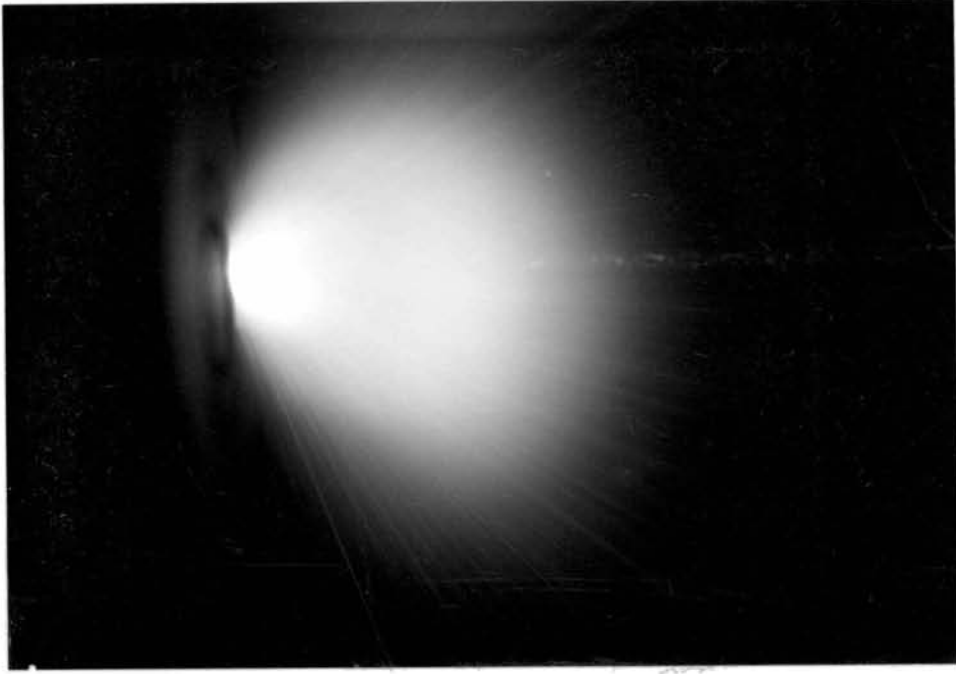
Fig.5.1. Plasma emission from graphite surface at a laser energy density of ≈ 12 J/cm^2 showing the studied regions of the spectra
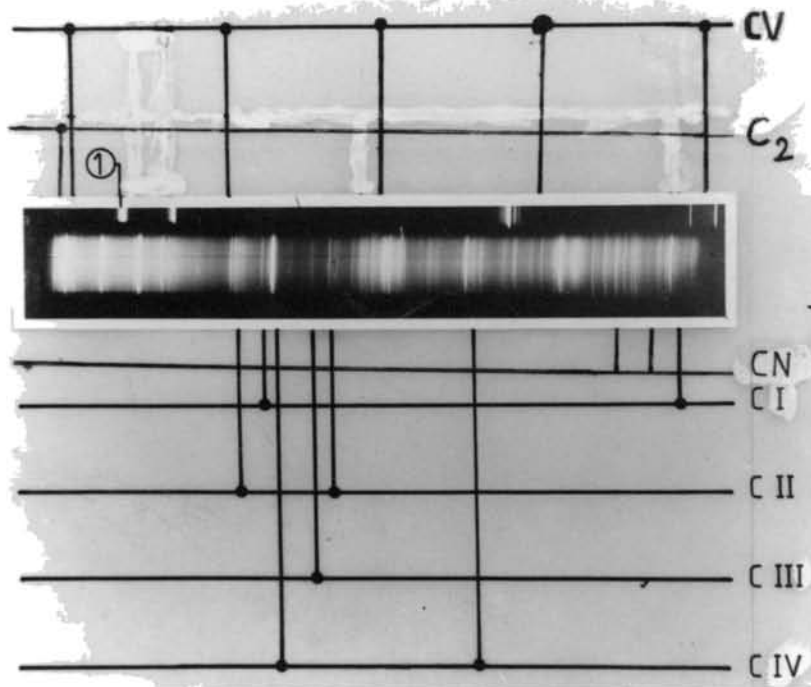
Fig.5.2. The emission spectrum from the central core (A) of the laser produced plasma from graphite (Laser energy density ≈ 12 J/cm^2)

(B)

(C)
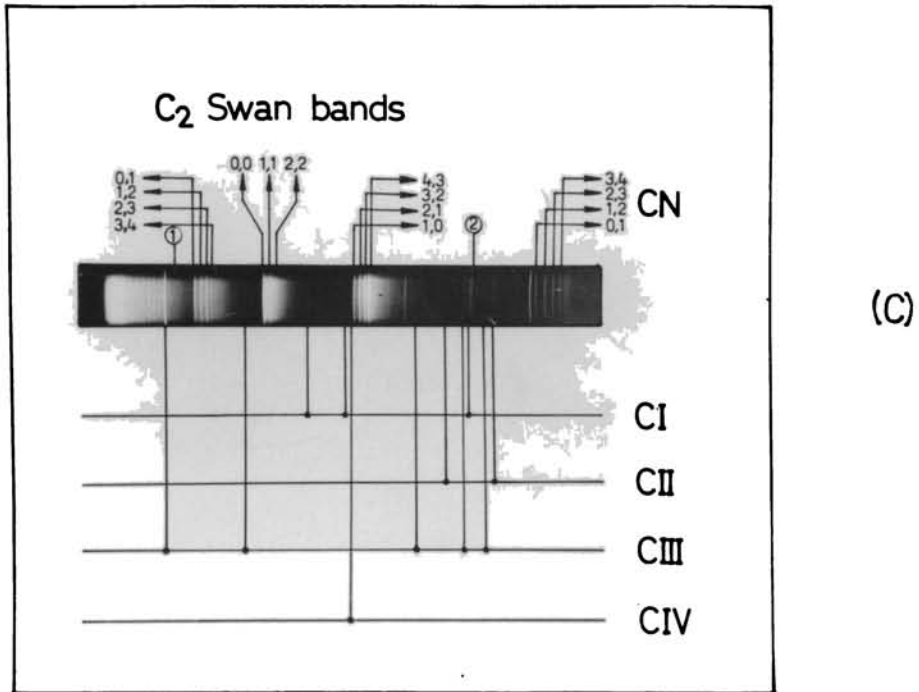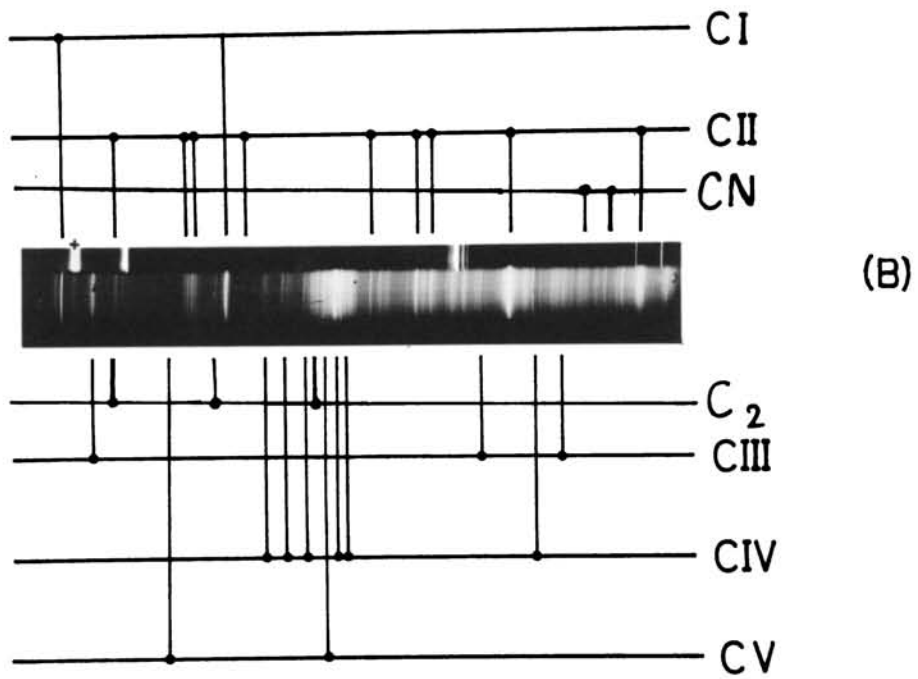
Fig.5.2. The emission spectrum from the mid (B) and extended (C) regions of the laser produced plasma from graphite (Laser energy density ≈ 12 J/cm^2)

the target surface such as (a) Central core, (b) mid region and (c) extended region are shown in figure (5.2(a), 5.2(b) and 5.2(c)) along with Hg spectrum for calibration of wavelength of different species.

As in the case of Teflon, the recorded plasma emission spectra from the graphite corresponding to the three regions, show distinctly different characteristics. The emission lines due to higher ionization states of carbon (CI, CII, CIII, CIV and CV) are clearly seen in the core and mid regions of the plasma. The continuum emission intensity in the plasma emission is greatest in the region close to the target and decreases within a few millimeters from the target surface, this continuum is that resulting from the free - bound transitions on to the ground electronic state of carbon atoms (excited). The molecular bands corresponding to transitions $(A^3\Pi_g - X^3\Pi_u)$ of C_2 in the wavelength range 500-590 nm dominate in the emission spectrum of the plasma in the extended (C) region. The CN band emission $(B^2\Sigma^+ - X^2\Sigma^+)$ in the ultraviolet region indicates a secondary reaction of the excited carbon with the residual nitrogen present in the partial vacuum of the plasma chamber.

Here the spatial resolution was better than 0.2 mm in the direction along the laser (plasma expansion) axis, and it was controlled by a slit in the light path to the monochromator and by the grazing incidence transfer mirror and entrance slit of the monochromator. The line spectra at various distances from the target could be recorded at high resolution. In the region close to the target surface, density in the plasma core is so high that, much of the broadened line emission cannot be separated from the background. Further away from the target, in the case of the excited atomic carbon, the lines become narrower and weaker with increasing separation from the target [26]. The broadening of such isolated lines close to the target surface can be attributed to electron - ion collisions [26].

5.3. TIME RESOLVED ANALYSIS OF LIP FROM GRAPHITE

The experimental arrangement for the time resolved analysis of the LIP emission from graphite is described in chapter III. The plasma chamber including the lens can be mounted on a slide so that plasma portions at any distance from the target surface can be focussed on to the field of view of the monochromator. A stop positioned on the entrance slit which could be varied, made it possible for the monochromator to select any point in the plasma at right angles to the plasma expansion axis [27].

The time delays and decay time of the radiation emission of the identified species at the extended regions (region C) of the plasma plume with laser energy are given in the Table (5.1). From the time delays observed, it is seen that in all three regions of the plasma, the molecular band (C2 and CN) emissions have much larger time delays as compared to ionic/neutral species. Generally there is a decrease in time delay as the laser energy increases. The variation of the time delay and decay time of emission of various species with laser energy in the mid region and the central core (region A) of the plasma are given in the Table (5.2 and 5.3) respectively. The observed time delays and decay time of the species in the mid region are less than that of the value obtained in the extended region. But in the case of central core of the plasma, the time delay and decay time for all species are very much less than (nsec) those for the extended as well as mid region (μsec). In all three regions of the plasma both the above parameters for all species decrease with the increase in laser energy. As in the case of the time delays, the molecular bands have a larger decay time compared to the ionized species. As the laser energy increases, the decay time of the emission of the species was found to decrease. Typical oscilloscope recordings of all the observed excited carbon lines in the extended region of the plasma from the target at the laser energy ~ 70 mJ is shown in figure (5.3) in order to compare the time delays of these excited carbon lines. The zero on the time
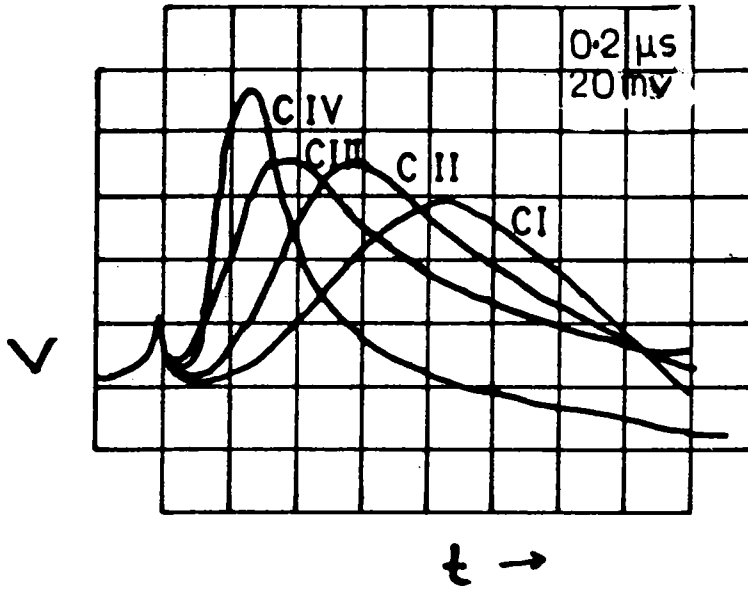
Fig.5.3. The CRO trace of the PMT responses for the comparison of the time delays of the observed excited carbon line emissions
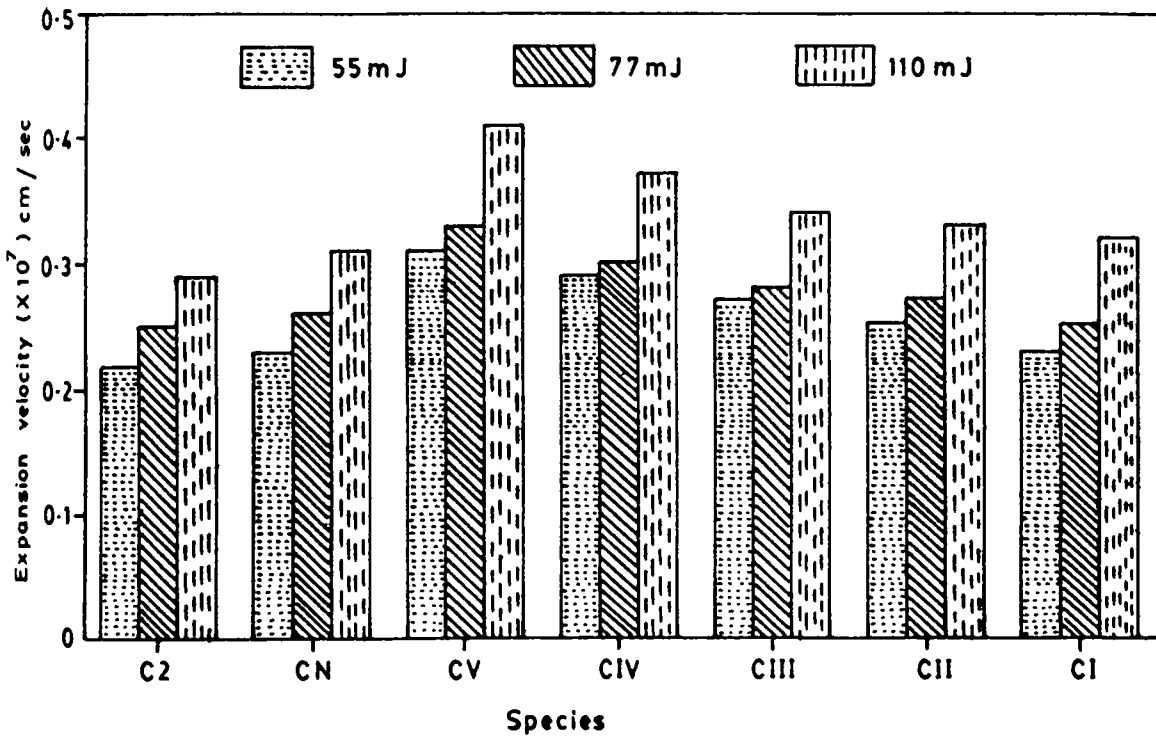
Fig.5.4. Variation of plasma expansion velocity of the different species in the carbon plasma in the extended region (C) of the plasma with laser energy

Table (5.1) The variation of time delay and decay time of emission of the various species with laser energy in the region (C) of the plasma

	C_2 Swan band λ = 516.5 nm		CN band λ = 421.6 nm	
Laser Energy (mJ)	Time delay (μsec)	Decay time (μsec)	Time delay (μsec)	Decay time (μsec)
55	0.95	1.23	0.89	1.12
68	0.91	1.16	0.82	1.09
77	0.81	1.08	0.78	0.98
88	0.78	1.02	0.73	0.93
97	0.72	0.96	0.70	0.87
110	0.68	0.91	0.64	0.81

CV line λ = 494 nm		CIV line λ = 580.1 nm		CIII line λ = 538.3 nm	
Time delay (μsec)	Decay time (μsec)	Time delay (μsec)	Decay time (μsec)	Time delay (μsec)	Decay time (μsec)
0.70	0.81	0.75	0.88	0.79	0.99
0.66	0.79	0.69	0.82	0.73	0.96
0.61	0.74	0.65	0.77	0.71	0.90
0.59	0.70	0.61	0.73	0.67	0.85
0.53	0.67	0.57	0.69	0.61	0.78
0.49	0.62	0.54	0.66	0.58	0.72

CII line λ = 426.7 nm		CI line λ = 595 nm	
Time delay (μsec)	Decay time (μsec)	Time delay (μsec)	Decay time (μsec)
0.82	1.02	0.89	1.09
0.78	0.99	0.83	1.01
0.75	0.93	0.80	0.97
0.71	0.88	0.77	0.91
0.65	0.81	0.69	0.85
0.61	0.75	0.63	0.79

Table (5.2) The variation of time delay and decay time of emission of the various species with laser energy in the region (B) of the plasma

	C_2 Swan band λ = 516.5 nm		CN band λ = 421.6 nm	
Laser Energy (mJ)	Time delay (μsec)	Decay time (μsec)	Time delay (μsec)	Decay time (μsec)
55	0.92	1.19	0.84	1.1
68	0.89	1.15	0.82	1.04
77	0.84	1.12	0.78	0.94
88	0.81	1.10	0.72	0.91
97	0.78	1.08	0.67	0.85
110	0.75	1.07	0.65	0.78

CV line λ = 494 nm		CIV line λ = 580.1 nm		CIII line λ = 538.3 nm	
Time delay (μsec)	Decay time (μsec)	Time delay (μsec)	Decay time (μsec)	Time delay (μsec)	Decay time (μsec)
0.45	0.78	0.53	0.85	0.68	0.95
0.41	0.75	0.51	0.8	0.64	0.93
0.39	0.73	0.47	0.74	0.61	0.87
0.34	0.67	0.44	0.71	0.52	0.83
0.31	0.64	0.40	0.66	0.48	0.74
0.30	0.61	0.38	0.64	0.46	0.70

CII line λ = 426.7 nm		CI line λ = 595 nm	
Time delay (μsec)	Decay time (μsec)	Time delay (μsec)	Decay time (μsec)
0.75	0.99	0.82	1.06
0.70	0.96	0.80	0.98
0.67	0.92	0.76	0.94
0.62	0.86	. 0.68	0.88
0.56	0.80	0.61	0.82
0.51	0.73	0.58	0.76

117

Table (5.3). The variation of time delay and decay time of emission of the various species with laser energy in the region (A) of the plasma

	C_2 Swan band λ = 516.5 nm		CN band λ = 421.6 nm	
Laser Energy (mJ)	Time delay (nsec)	Decay time (nsec)	Time delay (nsec)	Decay time (nsec)
55	37.778	45.556	33.33	41.556
68	35.556	43.292	32.22	41.273
77	33.33	40.326	31.667	40.89
88	29.44	39.884	30.556	38.99
97	26.22	33.333	26.444	35.07
110	21.28	32.798	25.82	33.48

CV line λ = 494 nm		CIV line λ = 580.1 nm		CIII line λ = 538.3 nm	
Time delay (nsec)	Decay time (nsec)	Time delay (nsec)	Decay time (nsec)	Time delay (nsec)	Decay time (nsec)
18.38	29.98	21.04	31.14	21.64	31.44
17.48	27.85	18.62	30.34	19.33	30.87
15.32	25.32	16.53	28.19	17.34	28.87
9.76	21.09	10.16	23.86	11.13	26.13
7.23	19.87	8.92	21.58	9.34	23.12
4.91	16.23	5.99	21.00	6.09	21.63

CII line λ =426.7 nm		CI line λ = 595 nm	
Time delay (nsec)	Decay time (nsec)	Time delay (nsec)	Decay time (nsec)
23.33	35.83	23.89	37.09
21.01	32.13	21.289	36.13
20.09	31.18	20.89	30.55
18.72	30.05	19.63	30.13
17.85	24.81	18.39	26.64
16.61	23.17	17.79	25.78

axis is the time of arrival of the laser pulse at the target surface. From the above figures, it is observed that the spectral lines of more highly ionized species are first to appear and are followed in turn by ions of successively lower stages of ionization. Since the time delays of all identified species were recorded at three regions (A,B and C) from the target surface, the expansion velocity of each species were calculated and their variation with laser energy were also obtained. Comparing the plasma expansion velocity of all species at different regions of the plasma, it was observed that the velocity decreases as the distance from the target surface increases ie, the velocity decreases with the expansion of the plasma. Figure (5.4) shows the expansion velocity of different species in the carbon plasma at a laser energy $\approx$ 55 mJ. Variations of the expansion velocities of different species with laser energy in the three regions of the plasma are given in the Table 5.4(a), 5.4(b) and 5.4(c) respectively. From these tables it is seen that the ionic species have large value for the expansion velocity compared to that of the molecular species and the expansion velocity of the species in the plasma increases with laser fluence.

Comparing the time delays obtained for different species at different regions in the plasma from Teflon as well as graphite material, it is observed that smaller time delays were obtained in the case of graphite plasma which were due to the low threshold for the plasma formation at the graphite surface compared to that of Teflon sample [28]. As a result expansion velocities for all species in the graphite plasma have larger values compared to those in the Teflon plasma.

5.4 CALCULATION OF VIBRATIONAL TEMPERATURE OF C_2 AND CN MOLECULES IN A SPATIALLY RESOLVED PLASMA

As described previously, the emission band in the extended region of the plasma emission spectrum is dominated by the molecular bands of C_2 and CN species. The molecular band emission

Table (5.4). The variation of expansion velocity of the different
species in the graphite plasma at different regions
from the target surface with laser energy

(a) Extended region (C): 2 cms

Species	Expansion velocity $(x\ 10^7 \text{cm/sec})$					
	Laser energy					
	55 (nJ)	68 (nJ)	77 (nJ)	88 (nJ)	97 (nJ)	110 (nJ)
C_2	0.21	0.22	0.25	0.26	0.28	0.29
CN	0.22	0.24	0.26	0.27	0.29	0.31
CV	0.28	0.3	0.33	0.34	0.38	0.41
CIV	0.27	0.29	0.3	0.33	0.35	0.37
CIII	0.25	0.27	0.28	0.3	0.33	0.34
CII	0.24	0.26	0.27	0.28	0.31	0.33
CI	0.22	0.24	0.25	0.26	0.29	0.32

(b) Mid region (B) : 1 cms

Species	Expansion velocity (x 10^7 cm/sec)					
	Laser energy					
	55 (mJ)	68 (mJ)	77 (mJ)	88 (mJ)	97 (mJ)	110 (mJ)
C_2 band	0.22	0.23	0.26	0.27	0.30	0.32
CN band	0.23	0.25	0.27	0.29	0.31	0.34
CV Line	0.31	0.33	0.36	0.38	0.43	0.49
CIV Line	0.29	0.31	0.34	0.36	0.39	0.43
CIII Line	0.27	0.29	0.30	0.33	0.36	0.38
CII Line	0.25	0.27	0.29	0.30	0.32	0.39
CI Line	0.23	0.25	0.26	0.27	0.31	0.33

(c) Central region (A) : 0.66 cms

Species	Expansion velocity (x 10^7 cm/sec)					
	Laser energy					
	55 (mJ)	68 (mJ)	77 (mJ)	88 (mJ)	97 (mJ)	110 (mJ)
C_2	1.73	1.83	1.96	2.21	2.5	3.06
CN	1.96	2.02	2.1	2.13	2.46	2.53
CV	3.54	3.73	4.25	6.6	9.01	9.4
CIV	3.09	3.5	3.94	6.4	7.30	8.17
CIII	3.01	3.37	3.76	5.86	6.9	8.06
CII	2.79	3.1	3.25	3.5	3.7	3.9
CI	2.73	3.06	3.12	3.32	3.50	3.60

intensities can be used to calculate molecular vibrational temperatures (T_{vib}). The details for calculation of vibrational temperature is given in the Chapter I. At moderate resolution, the electronic transitions of diatomic molecules often possess band structures due to the excitation of many vibrational levels [29]. When we observe the plasma emission spectra in the extended and mid regions of the plasma, a predominance of the C_2 and CN emission have been found.

The intensity profile of spectrum obtained in the photographic film in the extended and mid regions of the plasma produced from the graphite target were obtained using a microdensitometer, and the optical density in the photographic plate was converted into intensity from the knowledge of calibration constants and each spectrum is normalized with respect to the maximum intensity which finally gives the relative intensities of the bands. All the C_2 bands have been recorded, which include $\Delta v = -1$, 0, and +1 in the wavelength region from 468.4 nm to 563.5 nm, where $\Delta v = (v'-v'')$ is the difference of the vibrational quantum numbers between the upper (v') and lower (v'') states of transition. Figure (5.5) shows the C_2 swan bands of $(v'v'') = (0,1)$ up to (4,5) ($\Delta v = -1$). These bands are degraded towards the violet, which is the characteristics of the C_2 swan bands. C_2 bands with $\Delta v = 0$ with $(v'v'') = (0,0)$ up to (2,2) were observed in the spectrum (Figure 5.5). The bands with $\Delta v = +1$ with $(v'v'') = (1,0)$ up to (4,3) can also be seen in the spectrum (Figure 5.5). There is no evidence of atomic or ionic emission in this region. The violet regions of the spectrum ((Figure (5.6)) shows the presence of CN violet bands with $\Delta v = -1$ in the wavelength region from 415.8 nm to 421.6 nm, which contain bands from (0,1) to (5,6). Since the spectra are recorded with only a moderate resolution using a spectrograph, the rotational structures are not resolved. The CN molecules resulting from the secondary reaction of excited carbons with the residual air in the plasma chamber give very intense bands in the UV region. Most of these set of bands are used to calculate molecular vibrational temperature of C_2 and CN

122

Wavelength (nm)
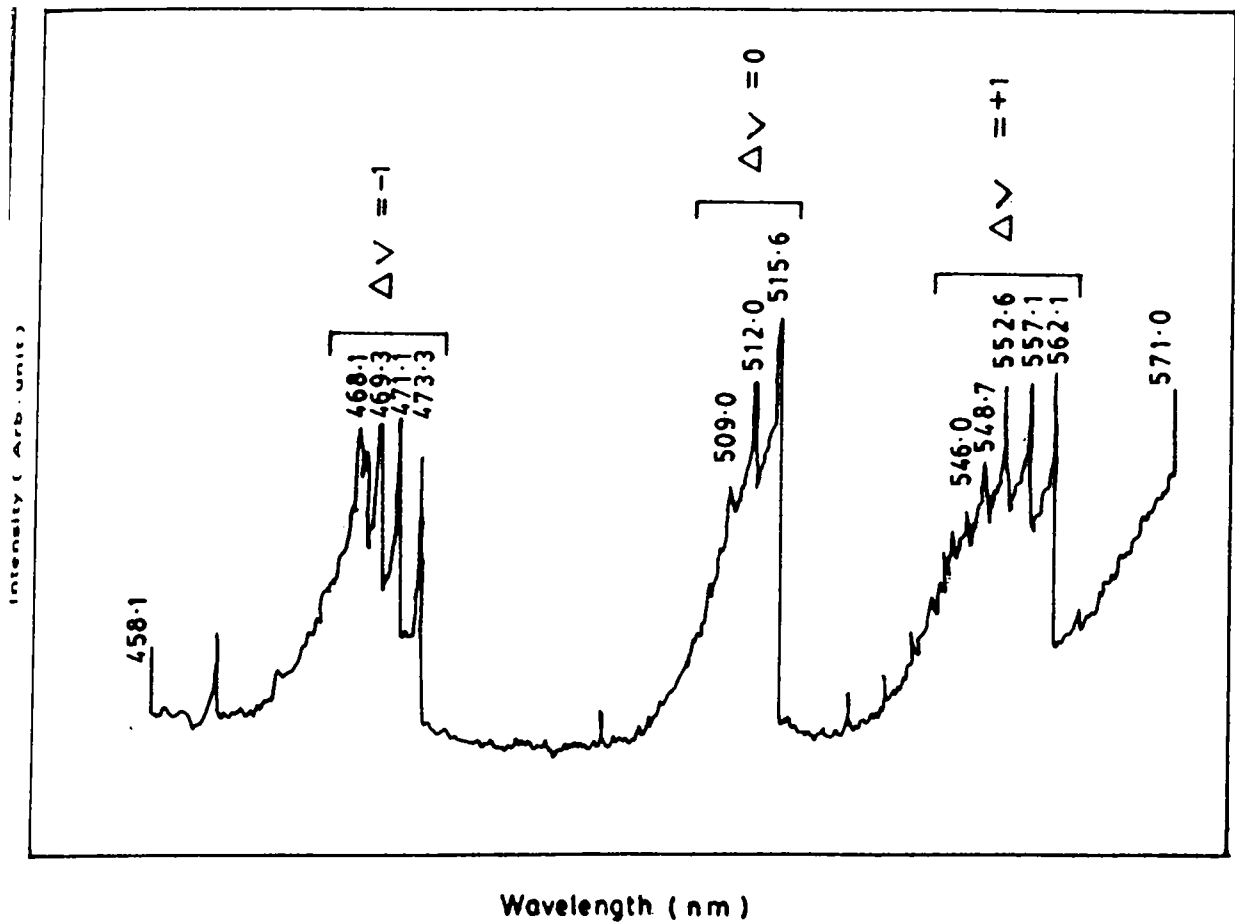
Fig.5.5. C$_2$ Swan bands with Δv = -1 , 0 and +1

Wavelength (nm)
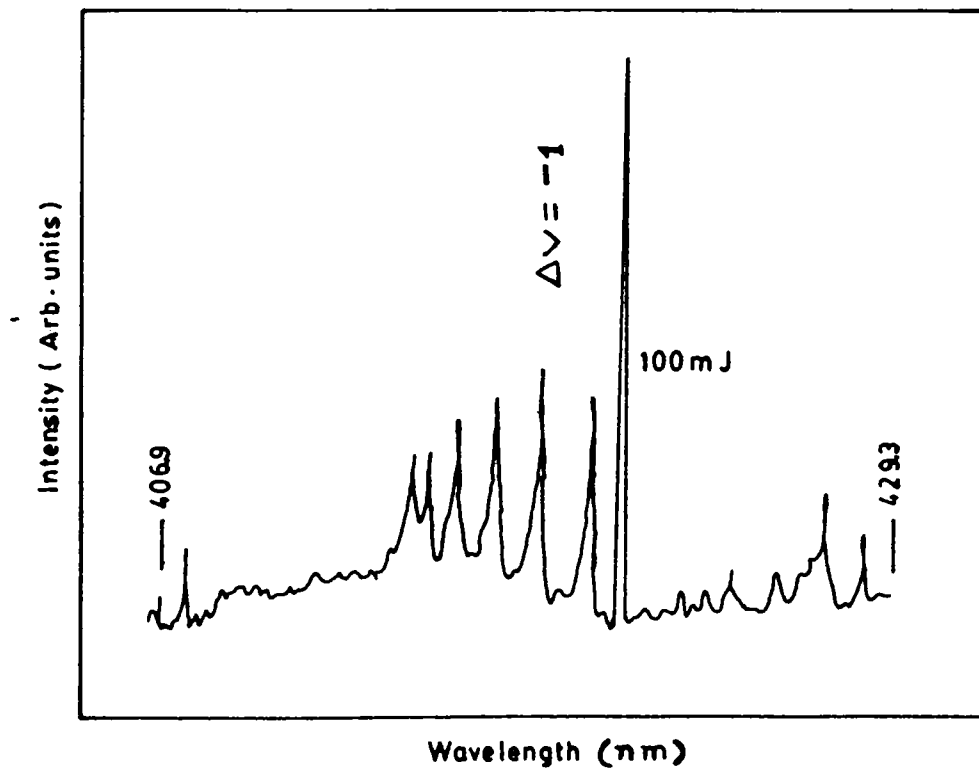
Fig.5.6 CN violet bands with Δv = -1

molecules. Vibrational temperature of C_2 radicals were calculated from the emission intensities of the above set of bands, which are corrected for the photographic film response which is predetermined using a standard lamp.

A comparison among the excited state levels of C_2, CN, CI, CII, CIII and CIV etc. and the ionization potential of carbon seems to explain the requirement of the higher laser energy needed to generate ionized carbon line emission [30]. Upper states of the C_2 swan bands ($A^3\Pi g$) and CN violet bands ($B^2\Sigma^+$) are at 20,000 - 30,000 cm^{-1} and 27,000 - 37,000 cm^{-1} respectively [24], while those for carbon and C^+ (for visible transition) are greater than 80,000 cm^{-1} and 130,000 cm^{-1} respectively. The ionization energy of carbon is 90,878 cm^{-1}. The 1060 nm laser photons corresponds to 9,434 cm^{-1}. So unlike in the case of Chen et al. (1991) direct photoexcitation of C_2 is not readily available here for higher electronic states followed by the collisional relaxation to the $A^3\Pi g$ level. But the C_2 molecules in the plasma are mainly formed due to the recombination occurring in the same when the plasma cools down. At the same time, the excitation and ionization of carbon would have to be through multiphoton absorption that require higher laser intensity. An indirect mechanism is the absorption of photons by residual electrons through inverse bremsstrahlung [31,32]. Upon collision the energetic electrons excite or ionize the other species in the plume. Recombination processes due to slow electrons also take place [16]. In all cases, the C^+ creation and CI, CII etc. emission occur at higher incident laser energies.

An estimation of C_2 as well as CN concentration was made from the band intensity. The vibrational distribution in the excited states of CN molecules in the extended region (C) are shown in the Figure (5.7). Similar distribution were observed in the case of C_2 Swan bands also in the region (B) and (C) of the plasma and this is according to Frank - Condon principle.

When Log Σ ($\lambda^4 I_{v' \cdot v''}$) is plotted against vibrational term values $G(v')$ of the upper electronic state, the slope of this straight
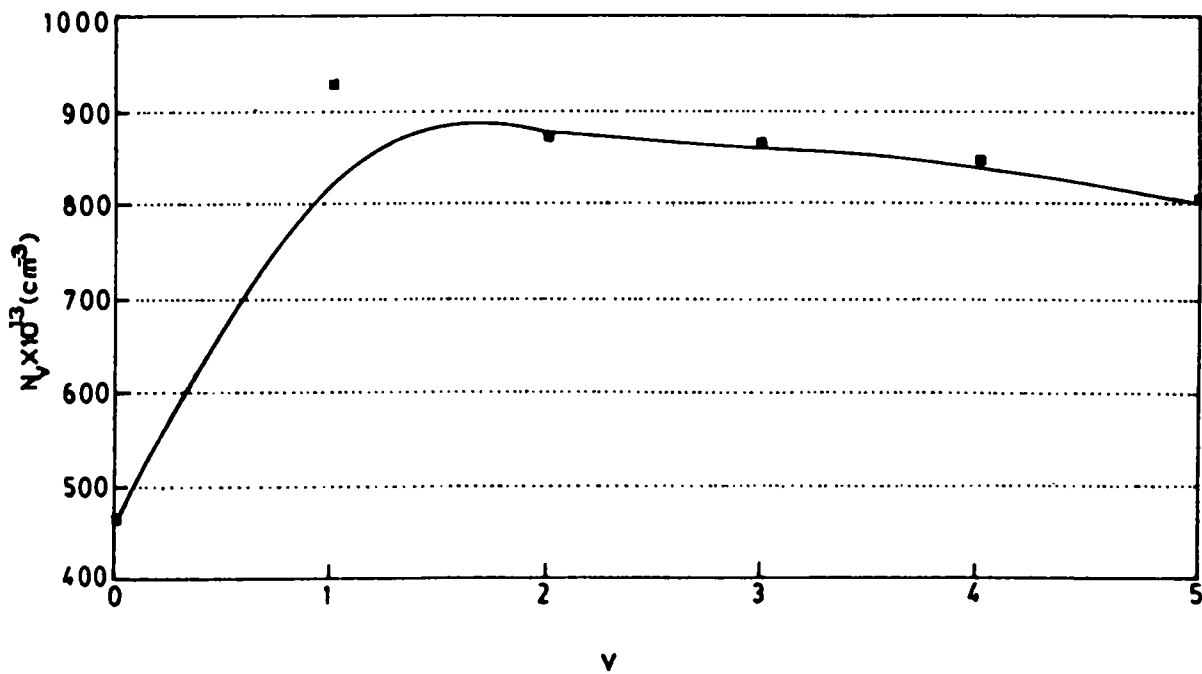
Fig.5.7. The vibrational distribution of CN band in the region (C) of the plasma
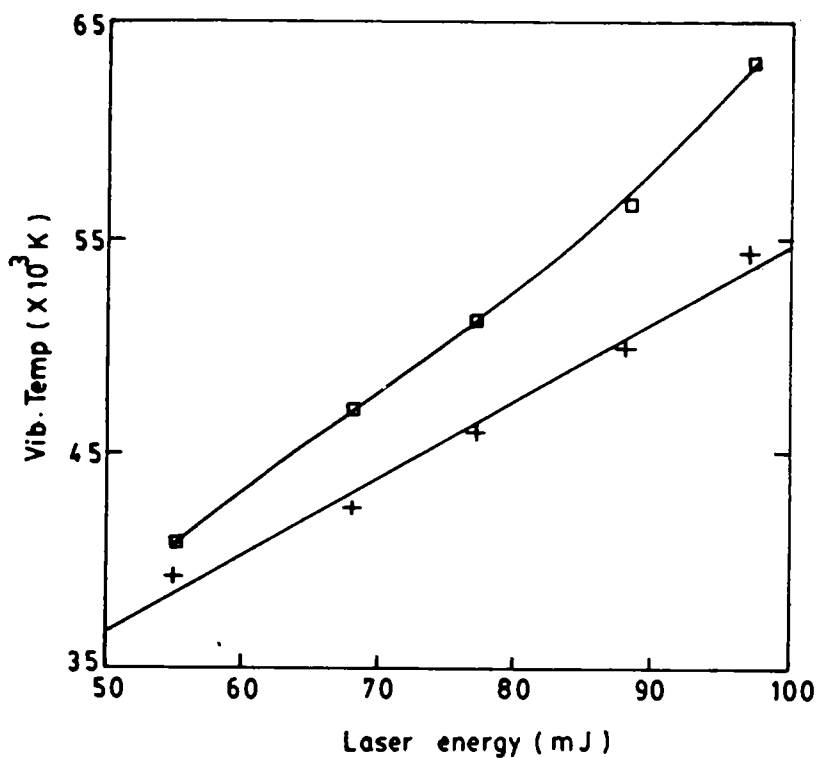
Fig.5.8. The variation of vibrational temperature of C_2 and CN molecules with laser energy in the mid region (B) of the plasma. ($\square$ - C_2 molecule and + - CN molecule)
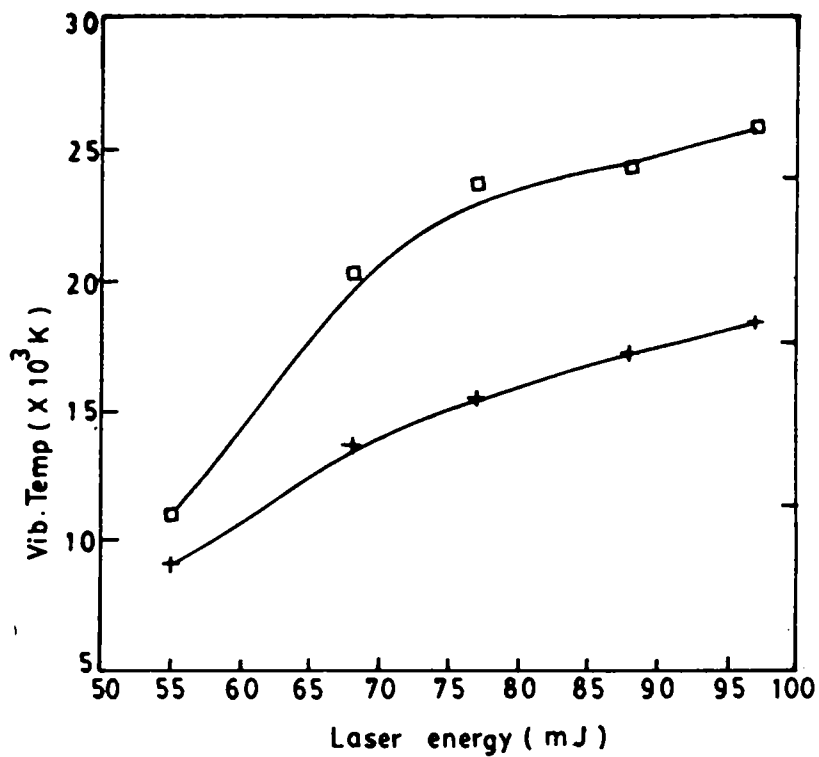
Fig.5.9. The variation of vibrational temperature of C_2 and CN
molecules with laser energy in the extended region (C) of
the plasma. (□ - C_2 molecule and + - CN molecule)

line curve give the value of the vibrational temperature. The variation of vibrational temperature corresponding to the C_2 swan bands and CN molecules in the mid region (B) of the plasma emission with laser energy is shown in the figure (5.8). The vibrational temperature was found to vary from 4.081×10^4 K to 6.289×10^4 K for C_2 molecules and from 3.928×10^4 K to 5.628×10^4 K for CN bands in the mid region (B) of the graphite plasma as the laser energy is varied from 55 mJ to 98 mJ. This curve shows a linear variation of T_{vib} with laser energy, which supports the view that molecular excitation to higher energy levels occurs as we increase the laser energy. The variation of T_{vib} with laser energy in the extended region of the plasma is shown in the figure (5.9). In this case, the vibrational temperature was found to vary from 7.426×10^3 K to 2.772×10^4 K for C_2 molecules and from 6.116×10^3 K to 2.592×10^4 K for CN bands in the extended region (C) of the graphite plasma as the laser energy is varied from 55 mJ to 98 mJ. In the extended region of the plasma where the temperature is lower compared to that of the mid region, the recombination processes dominate which results in the drastic variation of vibrational temperature with laser energy. From the above figures it is clearly seen that a saturation of the T_{vib} occurs at higher laser energy in the extended region of the plasma. Compared to Teflon target, graphite has a lower work function so that threshold like phenomena as in the case of Teflon will appear at a much lower laser energy (< 55 mJ) and after this threshold region, when the laser energy is further increased, the saturation phenomena will appear. But in the case of mid region, where the plasma temperature is higher and as the laser energy increases more molecules are excited to the higher vibrational levels, which result in the linear increase in the vibrational temperature.

5.5. CONCLUSIONS

In the case of laser induced plasma from graphite target, the plasma emission spectrum in the centre and mid region is found to be dominated by higher ionized states of carbon lines (up to CV), where the spectrum in the outer region is dominated by the molecular bands of C_2 and CN. Thus the spatially resolved plasma emission spectrum shows distinctly different characteristics.

From the time resolved studies, the time delays of different species in the plasma are obtained and the expansion velocities of the various species are calculated. Their variation with respect to laser energy is also obtained. From this it is seen that the ionic species have large value for expansion velocity compared to that of molecular species. The time resolved studies of the spectral emission of different species in the plasma throw much light on the complex interaction processes occurring in the plasma. From the time delays, we can conclude that molecular species may not be originating from the target material at higher laser energies, but are formed as a result of recombination processes as the hot plasma expands and cools ie, the molecular bands are formed due to collisions of atomic and ionic species.

It was also found that the values obtained for vibrational temperature for C_2 and CN molecules are in good agreement with each other, but these are much higher than the graphite melting point of about ≈ 4000 K. The laser interaction with the plasma plume is considered to be responsible for this. An estimation of concentration of these species also has been made in this study.

REFERENCES

[1] Dreyfus R W, Kelly R and Walkup R E, *Nucl.Instrum. Methods B*, 23, 557, (1987)

[2] Chen X and Mazunder J, *Appl.Phys.Lett.*, 57, 2178, (1990)

[3] Koren G and Yeh J T C, *J.Appl.Phys.*, 56, 2120, (1984)

[4] Brake M L and Meachum J, *IEEE Trans.Plasma*, 15, 73, (1987)

[5] Deshmukh S and Rothe E W, *J.Appl.Phys.*, 66, 1370, (1984)

[6] Haten G, Colon C and Campos J, *Spectro.Chem.Acta.*, 49a, 509, (1993)

[7] Herzberg G, *Spectra of diatomic molecules*, 2nd edition (Van Nostrand Reinhold, New York), (1950)

[8] Gaydon A G, *"The Spectroscopy of flames "*, (Chapman and Hall, London, 1974)

[9] Goldsmith J E M and Kearsley D T B, *Appl.Phys.B*, 50, 371, (1990)

[10. Nagel D J and Williams R T, *"Etching of electronic materials"*, (Mater.Res.Symp.Proc., 1985)

[11] Demers R T and Harris D G, *Proc.SPIE*, 1146, 48, (1990)

[12] Krishnaswamy A, Rengan J and Narayan C, *Appl.Phys.Lett.*, 54, 2455, (1989)

[13] Rithschild M, Amone C and Enrich D J, *J.Vac.Sci.Technol. B*, 4, 310, (1986)

[14] Wagal S S, Juengerman E M and Collins C B, *Appl.Phys.Lett.*, 53, 187, (1988)

[15] Varnin V P Fedoseev D V and Deryaguin B V, *Sov.Phys.Chem.*, 29, 419, (1984)

[16] Ogmen M and Duley W W, *J.Phys.Chem.Solids.*, 50, 1221, (1989)

[17] High temperature chemistry of inorganic materials (The chemical society, Burlington House, London, 1977)

[18] Consalvo D, *Int.J.Mass Spectrom.Ion Processes*, 91, 319, (1989)

[19] Pelino M, *"High Temt.High Pressures.*, 20, 413, (1988)

[20] Becker S and Dietze H J, *Int.J.Mass Spectrom.*, 82, 287, (1988)

[21] Teghil R, *Appl.Surface Science*, 46, 220, (1990)

[22] Kroto H W, *Nature*, 318, 162, (1985)

[23] Phipps,Turner T P, Harrison R F and King T R, *J.Appl.Phys.*, 64, 1083. (1988)

[24] Cronberg H, Nielsen H B and Matthias E, *Appl.Phys :B*, 52, 155, (1991)

[25] Chen X, Mazumder J and Purohit A, *Appl.Phys.A*, 52, 328, (1991)

[26] Huang Y W, Wang J S, Moreno J C and Grien H R, *Phys.Rev.Lett.*, 65, 1757, (1990)

[27] Boland B C, Irons F E and McWhirter R W P, *J.Phys.:B*, 1, 1180, (1968)

[28] Sell J A and Heffelfinger D M, *Appl.Phys.Lett.*, 55, 2345, (1989)

[29] Jeunchomme M and Schwenker R P J, *J. Chem.Phys.*, 42, 2406, (1965)

[30] Rockstroh T J and Mazumder J, *J.Appl.Phys.*, 61, 917, (1987)

[31] Chen X and Mazumder J, *J.Appl.Phys.*, 66, 5756, (1989)

[32] Green J M, Silvfast W T and Wood O R, *J.Appl.Phys.*, 66, 2753, (1989)

CHAPTER VI

CHARACTERISTICS of LASER INDUCED PLASMA FROM
HIGH T_c SUPERCONDUCTORS

ABSTRACT

This chapter deals with the results on the spectral as well as the time resolved analysis of plasma emission from two high T_c superconductors, viz. $YBa_2Cu_3O_7$ and $GdBa_2Cu_3O_7$. From the time resolved analysis, the time delay and decay constants of the all the identified species present in the plasma are measured and several interesting results were obtained. Using the ion probe technique plasma temperature and velocities of the positive ions as well as electrons are also calculated.

6.1. INTRODUCTION

The discovery of superconducting ceramic materials by Bednorz and Muller [1] in 1986 is a notable milestone in the history of science. Most of these rare earth based oxide ceramics are superconducting above liquid nitrogen temperature and that are expected to have tremendous applications in various devices and systems. For many of the device applications, it is necessary to fabricate these materials in thin film form. Recently it has been demonstrated that laser ablation is a viable technique for producing thin films of high T_c ceramic materials [2,3,4].

The laser ablation of high T_c target is accompanied by the formation of brilliant elongated plasma located over the target surface and extending outward up to about ≈ 2 cm from it [5]. It was found by earlier workers that the major luminescent species in the plume of laser ablated high T_c materials are arising from neutral, ionized atoms and diatomic species. Analysis of the optical emission spectrum from the plasma plume has been used to identify vapourized and ejected species from the target [6,7,8]. Identification of these species is important in understanding the complicated ablation, transport and deposition processes. Studies on laser-induced plasma emission provides [9] information on various species ejected from the target and the same could be used as a signal source for processes monitoring or studying the mechanism involved in the formation of thin films.

An excimer laser with very high photon energy may causes an internal electronic excitation and atomic bond breaking. It was observed earlier that YBaCuO has got smaller absorption coefficient for the IR radiation compared to that for the excimer laser [10] so that more thermal effects can be expected rather than electronic excitation and atomic bond breaking effects which happen in the case of excimer laser radiation. Fragments emitted from the surface by the irradiation of the IR laser beam are probably clusters or droplets near the threshold energy for the sputtering.

The spectral emission intensity variation was studied by Puell et.al [11] and was found to decrease only slowly with increasing distance from the target surface up to $\approx$ 1 mm, but beyond this it fell rapidly. As the radiative life times [11] of the states monitored are short ($\leq$ 10 nsec), these observations rule out excited atoms and ion being formed slowly at the surface and suggests that excitation is maintained within the first 1 mm or so of the target by collisions and electron recombination. This is equivalent to a model where the plasma plume undergoes one dimensional expansion for a spot diameter of $\approx$ 1 mm and three dimensional expansion beyond this [12]. The density falls much rapidly under certain conditions and excitations. Relatively high temperature appears to accompany ablation, resulting in high velocity of emission ($\approx$ 10^4 m/sec) and the corresponding particle energy ($\approx$ 25 - 50 eV). The extend of ionization in the plume is low ($<$ 4%) for low fluences so that neutral rather than ionized species will predominate in the deposition processes under this conditions [13]. The ionized species are predominant at higher laser intensity. Several studies indicate that the onset of ablation occurs during the early portion of the laser pulse and afterwards, interaction between the later portion of the pulse and the material ablated from the target will occur [14-17].

It is observed by several authors [18,19] that the emission in the plasma results from the free-free electronic and free-free bound recombinations which produce continuum emission and bound-bound transitions which produce line emission.

The time resolved emission peaks of all identified species were measured by Girault et.al. [20] with the help of PMT coupled to a monochromator and fast oscilloscope. The signal consists of an initial sharp peak which is due to scattered light from the ablating laser pulse followed by emission from the intense plasma created at the target surface. The broad delayed peak corresponds to the emission from the fragments in the plume [20]. Since the temporal variation of the emission is closely related to the ablated fragment distribution, the average expansion

velocity of the fragments can be calculated from the measured time delay .

When the spectroscopic and time resolved measurements are taken by Wu *et.al.* in oxygen atmosphere, it was observed that the emission intensities of all detected lines and bands are enhanced compared to that in vacuum [21]. The ejection velocities of the ablated species are sensitive to oxygen pressure in the chamber. The velocity of the ionic species are very sensitive to oxygen pressure. It is observed that velocity of neutral and ionic species remain constant from vacuum to oxygen pressures up to $\approx$ 10^{-2} mbar and decreases rapidly beyond this, whereas velocity of the diatomic species seem to decrease regularly with the oxygen pressures.

In order to understand the detailed aspects of laser beam interaction with the target material and recombination processes following the laser ablation, the time resolved studies of the spectral emission from the plasma offer the most convenient approach. The time resolved studies of plasma can give vital information regarding the the time taken for a particular state of a constituent to evolve after the plasma is produced and different state of ionization of the same. Time resolved studies of LIP yield a greater amount of information regarding the complex ablation and transport processes [22]. The dynamic measurements of Wu *et al* [21,22] are limited due to the line selection using optical filters ($\Delta\lambda \approx 100$ A$^{\circ}$) which make it clearly impossible to study unambiguously the the time evolution of the line and band emissions from the individual species.

In this chapter the results on spectroscopic as well as time resolved analysis of the evolution processes in the laser induced plasma from high T_c superconductors like YBa$_2$Cu$_3$O$_7$ (T_c = 90 K) and GdBa$_2$Cu$_3$O$_7$ (T_c = 93 K) are given along with ion probe techniques. These studies provide information on ablated species, expansion velocities and their extent of ionization in the plasma plume. From the ion probe measurements, important plasma parameters such as electron temperature and velocity of positive ions as well as

electrons were obtained.

Most of the spectroscopic studies do not clearly reveal the existence of CuO and Cu^+ [4,3,8]. Geyer and Weimer observed the presence of YO in the plasma generated from the Y-Ba-CuO target. Weimer and Wu [23] established the presence of oxides of Ba and Cu in the excimer laser produced plasma from the Y-Ba-CuO target. However the present study shows clearly the excistance of GdO, YO, BaO, CuO and Cu^+ along with the neutral atoms and ions in the laser produced plasma from YBaCuO and GdBaCuO targets. In earlier studies, oxides and ions might have escaped detection due to the fast decay of emission from these species as a result of recombination and plasma cooling.

6.2. SPECTRAL ANALYSIS OF LIP FROM Gd-Ba-CuO AND Y-Ba-CuO HIGH T_c SAMPLES

The observation of the presence of diatomic oxides in the plasma produced from high T_c samples by the pulsed laser ablation with 1.06 μm radiation from Nd:YAG laser is presented below.

Typical plasma emission from high T_c material is shown in the figure (6.1). The experimental arrangement used for the spectroscopic studies is described in the chapter III. Here we used laser pulses having energy $\approx$ 150 mJ, which was focussed on the sample with a laser spot size of (1 mm). The energy density at the target was estimated to be $\approx$ 19 J/cm^2. The target of high purity high T_c material pressed and sinterd cylindrical pellet was used [23]. The plasma emission spectra for Y-Ba-CuO and Gd-Ba-CuO samples in the region λ = 400 nm to 600 nm are given in the figures (6.2a and 6.2b) respectively. Emission wavelengths observed were compared with literature values and they are given in the Table (6.1) [24].

Spectrum consists of a continuum emission that centered in the visible region and several emission lines. The continuum background is plasma emission from sample surface and the spectral lines are emission from sublimented ions/atoms [25]. These

132
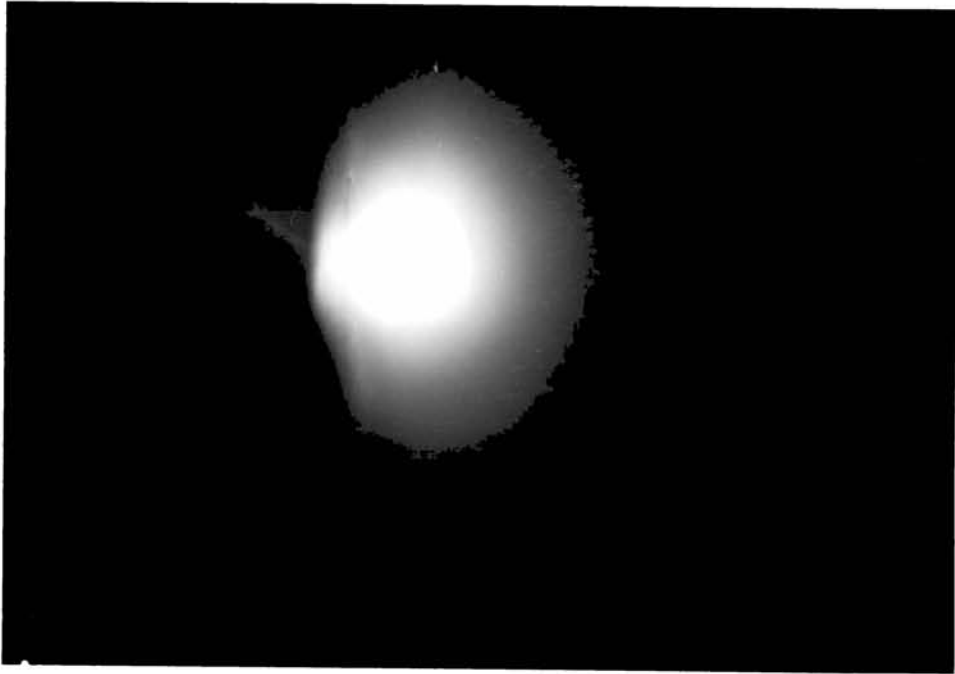
Fig.6.1. Typical plasma emission from high T_c Superconductor
(Laser energy density ≈ 12 J/cm^2)
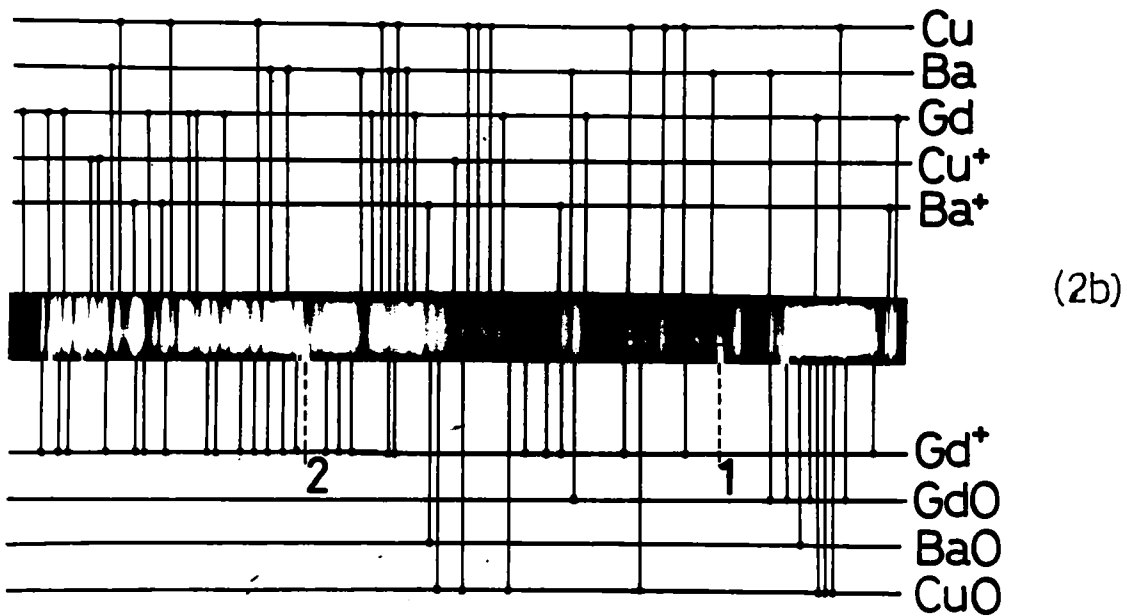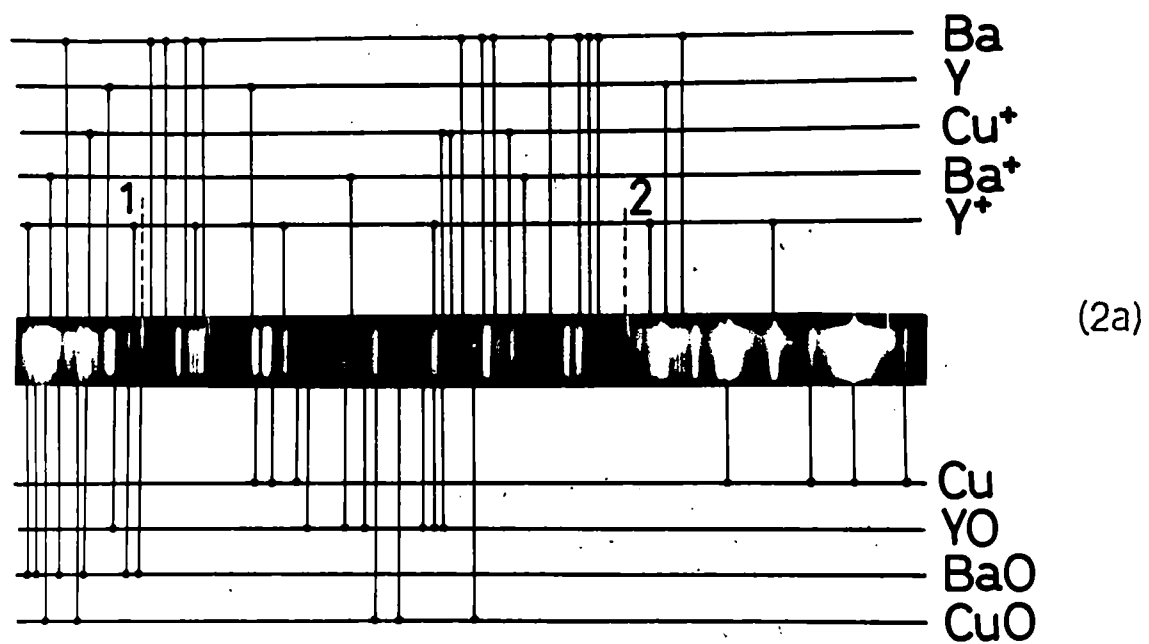
Fig.6.2. 2(a) Plasma emission spectra of $YBa_2Cu_3O_7$ ($T_c \approx 90$ K)

2(b) Plasma emission spectra of $GdBa_2Cu_3O_7$ ($T_c \approx 90$ K)

(Laser energy density ≈ 19 J/cm^2)

plasma emission spectra show prominent lines due to Y^+, Ba^+, Cu and Gd^+, Ba^+ and Cu in the case of the two targets respectively. The emission spectra thus reveal the presence of rare earth ions and Ba^+ in the plasma. Lines due to Cu^+ do exist in the plasma though they are comparatively weak due to higher ionization energy of copper (Cu $\simeq$ 7.726 eV, Ba $\simeq$ 5.211 eV, Y $\simeq$ 6.378 eV, and Gd $\simeq$ 6.16 eV). It should be mentioned that the recorded spectra clearly show the bands due to diatomic oxides YO and GdO in addition to the bands of BaO and CuO. The bands are easily identified due to the better resolution possible with a prism spectrograph in comparison with a multichannel analyzer [1]. The existence of gas phase oxides are encouraging since it reduces the possibility of deposition of oxygen deficient films.

Presence of ions in the plasma is very significant since it will enhance the possibility of the formation of metal oxides within the plasma. Spectra also show the intense lines due to the presence of excited neutral atoms produced by the unionized species indicating that plasma is not fully ionized. As seen from the spectra, lines due to Gd and Y species can be easily identified by looking for the lines which are not common to Gd and Y based samples. Ions are mainly produced by thermionic emission and atom-electron collision.

6.3. TIME RESOLVED ANALYSIS

(a). Gd-Ba-CuO SAMPLES

For the time resolved studies a part of the plasma plume at about 1.5 cm away from the target surface was focussed on to the slit of the monochromator (Jarrel - Ash, 0.5 m) coupled to a PMT and a CRO/Box car averager. The experimental set up for the time resolved studies are given in the chapter III. Since a 0.5m monochromator has used for wavelength separation ($\Delta\lambda$ < 1 A°), the line selection is more accurate than the work of Wu et al. (1989).

The pulse shape of the selected emission line of all the species in the plasma could be recorded [26] using a storage oscilloscope (100 MHz).

A typical CRO trace of the PMT response due to the line (λ= 455.5 nm) emission of copper ions is shown in the figure (6.3). The response in this case has a time delay of 0.14 μsec with respect to the laser pulse. This figure shows clearly two features, one a strong prompt emission and the other a slow emission peaking after few microseconds. The overall optical emission starts after a 7 nsec time delay after the start of the laser pulse indicating that the time required for significant evapouration of the species from the surface. The prompt emission is due to the laser excitation of the evapourated species, whereas the slow emission is most likely due to the electronic collisional excitations and is sensitive to oxygen pressure, particularly for oxide species [16]. This time delay was found to vary for different species. The time delays measured for emission from different atomic, ionic and molecular species are displayed in the figure (6.4). The most significant feature of the result is that emissions from oxides has got greater time delay as compared to that from ionic and atomic species. This evidently is due to the fact that the initial plasma temperature is so high that formation of oxides is not possible. As the plasma cools down, recombination processes may give rise to the formation of more oxides. A closer observation of the pulse shape shows a non - exponential decay of the emission. This becomes clearer from the Log I-Log t curve.

A Log-Log plot of the time dependence of the plasma intensities of all species reveals an initial period of slow decay followed by a comparatively faster decay. Figure (6.5) shows the such typical plots of plasma emission lines of Cu, Cu^+ and CuO. The temporal decay of emission due to plasma cooling can be expressed as a power law,

$$I(t) = H(t_1 - t)t^{-b_1} + H(t - t_1)t^{-b_2} \qquad (6.1)$$
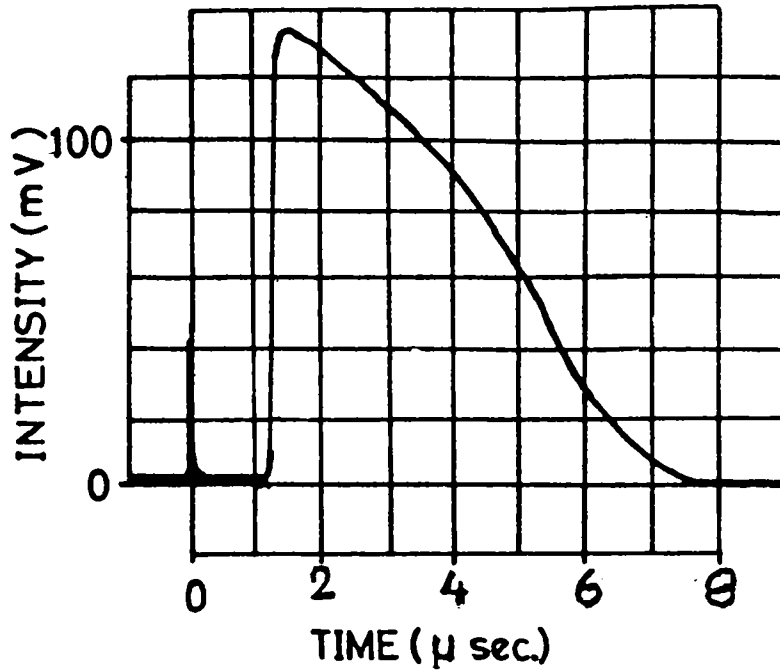
Fig.6.3. CRO trace of the PMT response due to the emission line
(λ = 455.5 nm) of copper ions
(Laser energy density ≈ 12 J/cm²)
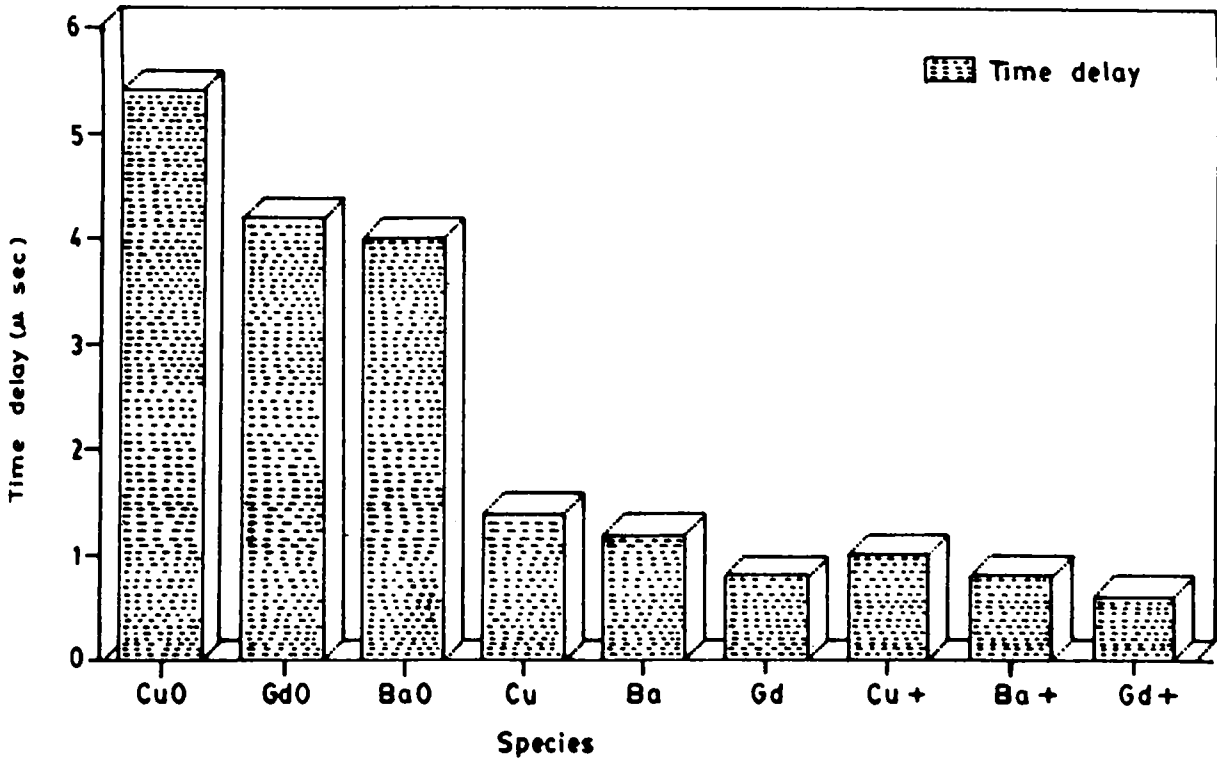
Fig.6.4. Time evolution of the spectral emission corresponding to
various species (Laser fluence = 12 J/cm²)
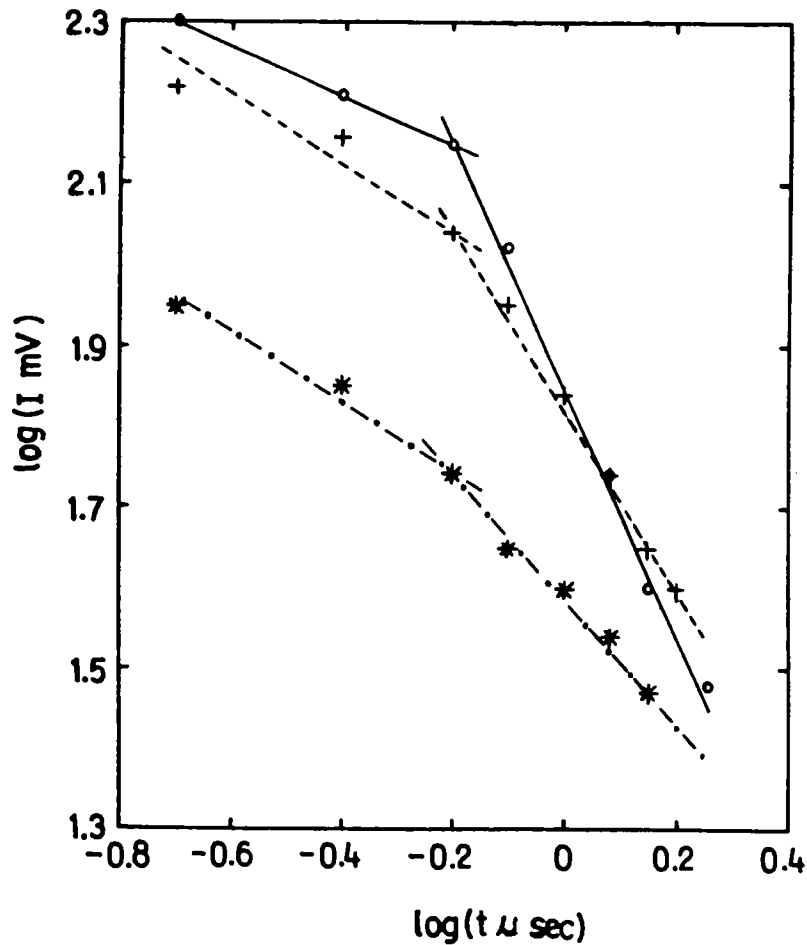
Fig.6.5. Plot of Log I aganist Log t for the plasma emission
intensities of [o — Cu (λ= 612.7 nm), + — Cu$^+$
(λ= 455.5 nm) and $\ast$ — CuO (λ = 616.3 nm)]
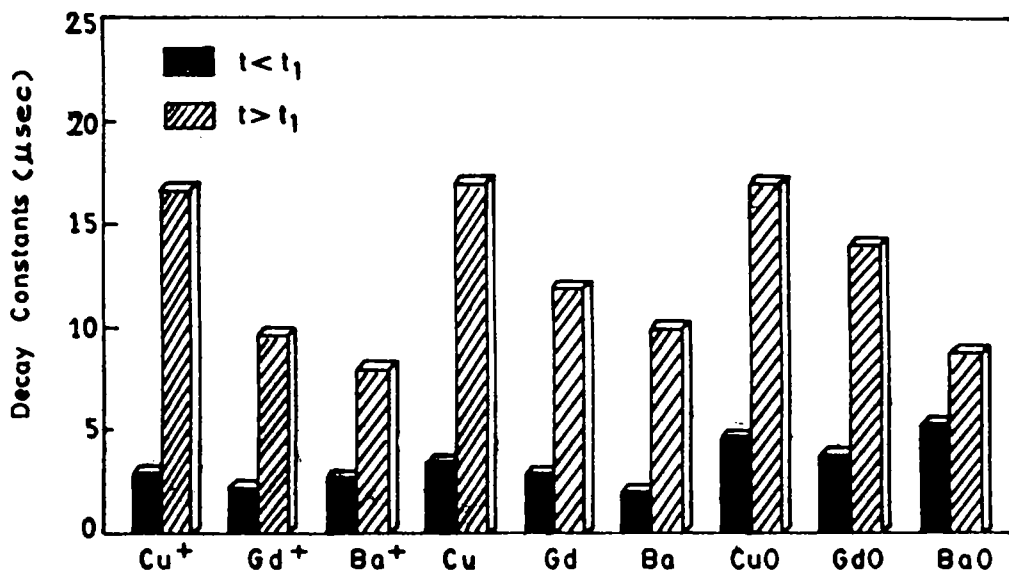
Fig 6.6. Decay constants corresponding to the spectral emission
from various species (Laser energy density $\approx$ 12 J/cm^2)

Where $H(\tau)$ is the Heaviside function.   So that $H(\tau) = 1$ for τ $>> o$ and o for $\tau < o$ and b_1 and b_2 are the decay constant in the hot and cold phase of the plasma.   For $t < t_1$, it is observed that b_1 < 1 for all species, while $b_2 > 1$ except for BaO and Ba.   Decay constants b_1 and b_2 observed for the spectral emission from various species in the plasma is shown in the figure (6.6).   Due to collisional excitations and recombinations, initially plasma is in a highly non-equilibrium state and   for $t > t_1$,   it   tends   to thermal equilibrium with a   faster   cooling   rate.   A   careful examination of the analysis of these   magnitudes   will   give   some valuable information required for   plasma diagnostics.   The   two time periods in a Log t-Log I curve represent   the   hot   and   cold phases of the plasma.   It is worth noting that in the hot plasma

$$|b_1| \; GdO < |b_1| \; CuO < |b_1| \; BaO \qquad\qquad (6.2)$$

and in the cold plasma,

$$|b_2| CuO > |b_2| GdO > |b_2| \; BaO \qquad\qquad (6.3)$$

which shows that emission from   CuO   molecules   dies   down   rather quickly.

(b). Y-Ba-CuO SAMPLES : TIME RESOLVED STUDIES

The time resolved studies of this material also have   different time delays for all the different species emitted from the target. Here the   time delays   of   each   species   with   respect   to   laser fluence was measured.   Comparing emission from different   species , the oxide species were found to have larger time delays.   As noted above, this could be due   to   the   reason   that   oxides   are mainly formed due to recombination, when the   plasma   cools   down. Table (6.2)   shows   the   variation   of   time   delays   of   all   the identified species with respect to laser fluence.   Similarly   the variation of decay time of all the species with respect   to   laser energy is also shown in the   table   (6.2).   Here   also   it   is

Table (6.2) The variation of time delay (TD) and decay time (DT) of different species in the Y-Ba-CuO high T_c material with laser energy

Laser Energy	55 mJ		65 mJ		75 mJ		88 mJ		99 mJ	
Spec -ies	TD (μsec)	DT	TD (μsec)	DT	TD (μsec)	DT	TD (μsec)	DT	TD (μsec)	DT
CuO	0.59	2.7	0.54	2.3	0.51	1.9	0.48	1.6	0.44	1.4
BaO	0.48	1.9	0.45	1.5	0.41	1.2	0.39	1.0	0.36	0.98
YO	0.51	2.4	0.49	2.1	0.45	1.9	0.43	1.7	0.40	1.4
Cu	0.18	1.7	0.16	1.5	0.13	1.2	0.1	1.0	0.09	0.97
Ba	0.15	1.01	0.13	1.0	0.11	0.98	0.1	0.92	0.08	0.88
Y	0.08	1.16	0.06	1.1	0.03	0.99	0.01	0.96	0.009	0.93
Cu^+	0.07	1.09	0.05	1.05	0.03	1.02	0.01	1.0	0.009	0.98
Ba^+	0.05	1.0	0.02	0.96	0.009	0.92	0.008	0.89	0.007	0.87
Y^+	0.04	0.92	0.02	0.9	0.01	0.86	0.01	0.82	0.009	0.8

Table (6.3) Time evolution of the Langmuir probe pulse for various probe voltages at two values of laser fluence (Gd-Ba-CuO sample)

Probe Voltage (Volt)	Decay Constants			
	Laser energy 25 J/cm^2		Laser energy 19 J/cm^2	
	S_1	S_2	S_1	S_2
20	0.84	1.67	0.82	1.93
22.5	0.94	1.44	0.40	1.38
25	0.53	1.31	0.13	0.80
27.5	0.17	1.15	---	----

observed that the oxide species will have larger decay time as compared to that of the ionic or neutral species. As the laser energy increases, plasma generation becomes more rapid and due to the generation of high density of the species, the probability of collision will increase and correspondingly the mean free path decreases. All these complex processes result in the decrease in the time delay of all the species present in the plasma with laser fluence. This will also result in the decrease in the decay time of emission of all identified species with laser fluence. Also it was observed that the ionic species decay faster than that of the atomic species.

6.4. LANGMUIR PROBE STUDIES

In the ion probe technique a variable bias voltage (0 to 30 Volt) was applied between the probe and the body of the plasma chamber. The typical probe circuit used for the analysis is shown in the chapter I. The experimental arrangement used for the probe studies are given in the chapter III. The electrons in the plasma were collected by the probe (3 cm length and 1.6 mm diameter) kept at about 1.5 cm away from the target surface. The voltage pulse developed was measured across a 50 ohm load resistance on a storage oscilloscope. The probe current was studied as a function of probe voltage and from the I-V characteristics thus obtained, plasma temperature and velocity were evaluated. The oscilloscope trace of the time resolved probe signal is shown in the figure (6.7), which consists of a sharp initial photoelectric component attributable to UV excitation from the plume and after a considerable delay the broad signal corresponding to to the arrival of ions at the collector [12,6]. Figure (6.8) shows the time evolution characteristics of the plasma recorded using a Langmuir probe at a laser energy density of $\approx$ 19 J/cm^2. From the slope of the I-V plot, the plasma temperature is calculated using the equation given in the chapter I (equation no. 1.62).
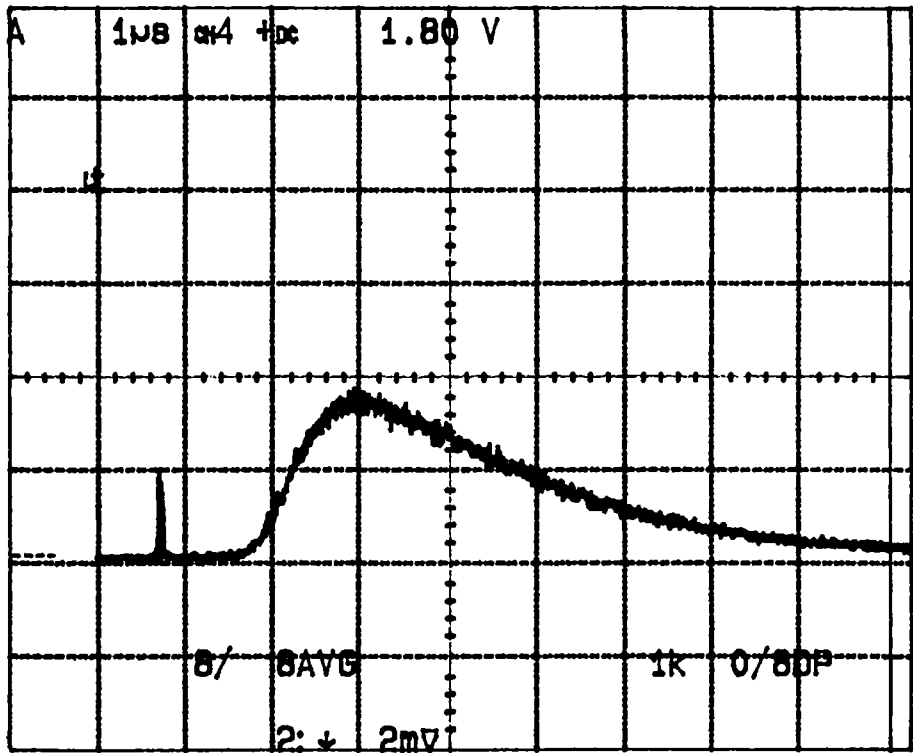
Fig.6.7. Oscilloscope trace of the time resolved probe signal
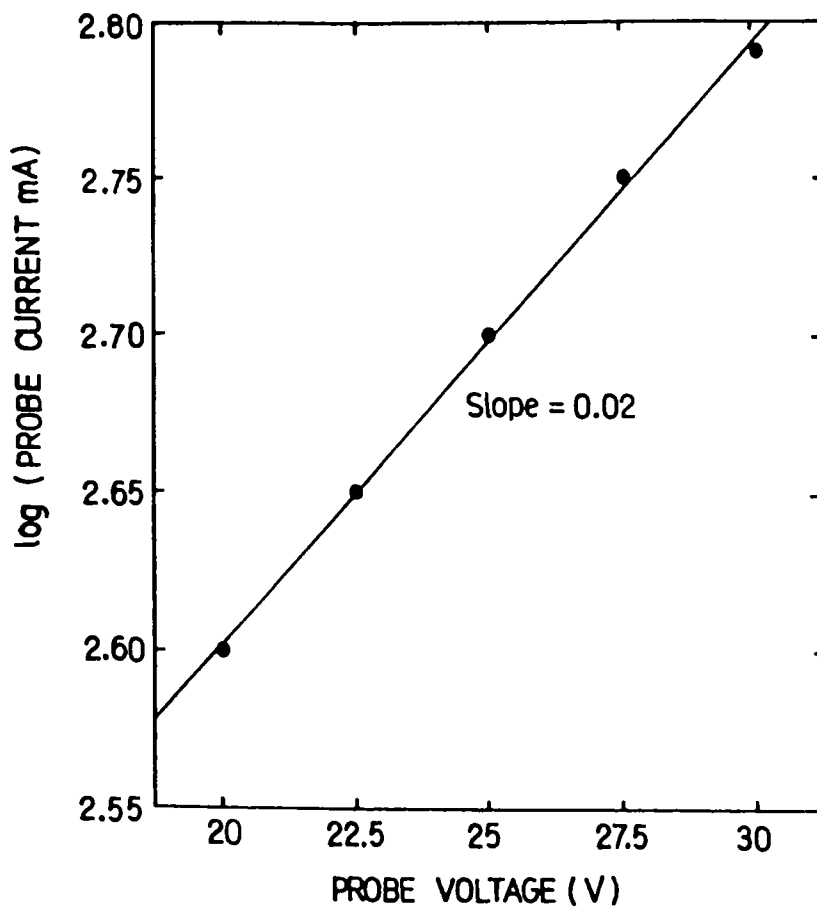
Fig.6.8. The time evolution characteristics of the plasma recorded using Langmuir -probe signal at a laser energy density of $\approx$ 19 J/cm^2, Slope $\approx$ 0.02.

The slope of the I-V curve S $\approx$ 0.02. for which, the temperature of the plasma was calculated to be $\approx$ 5.8 x 10^5 °K. The plasma (electron as well as positive ions) velocity is described in the chapter I (equation no. 1.62). From that, the velocity of the electrons in the plasma was calculated to be $\approx$ 4.5 x 10^8 cm/sec. The velocities of the positive ions in the plasma were calculated to be $\approx$ 1.06 x 10^6 cm/sec (for an average value of positive ion mass in the plasma).

However, the observed values of the particle velocities proved that the time delay of emission from various atomic and molecular species are not due to the time of flight phenomenon as suggested by Dyer *et.al.* [12] while the plasma expansion velocities can bring about a small delay, the major part observed delays does seem to arise from the recombination processes. The Log I-Log t plot of the laser produced plasma from high T_c Gd-Ba-CuO sample at various probe voltages (laser energy density $\approx$ 25 J/cm^2) are described in the figure (6.9). The Log-Log plot of the temporal decay of the ion probe current has two slopes S_1 and S_2, so that as in the case of plasma intensity variations. The probe current I(t) can be written as,

$$I(t) = H(t_1 - t) \, t^{-S_1} + H \, (t - t_1) \, t^{-S_2} \qquad (6.4)$$

Time evolution of the Langmuir probe pulse for various probe voltages and two values of the laser energy are described in the table (6.3). This table shows that decay constant in this case depends on the probe voltage. The electrons produced during laser ablation can develop as a sheath around the probe which cause initial slow decay of pulse. The decay becomes faster when the probe potential break the plasma sheath.
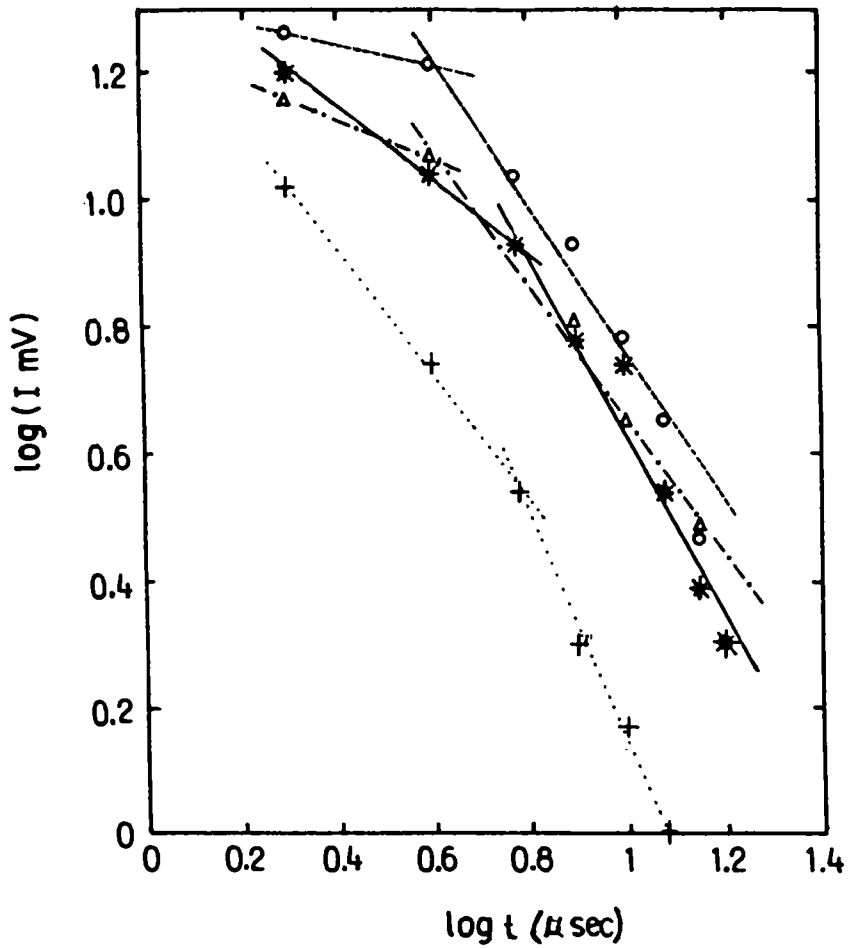
Fig.6.9. Plot of Log I aganist Log t of the laser produced plasma
from high T_c GdBa$_2$Cu$_3$O$_7$ plasma at various probe
voltages. Laser energy $\approx$ 25 J/cm^2 (o — 27.5 volt,
❋ — 25 volt, + — 22.5 volt and Δ — 20.00 volt)

5. CONCLUSIONS

The plasma emission spectrum of high T_c superconductors clearly shows the presence of diatomic oxides species along with the lines of neutral atoms and ions. Existence of oxides and ions in the plasma is important to obtain good quality superconducting thin films.

From the time resolved studies of plasma emission from high T_c samples the time delay as well as decay time of all species present in the plasma were measured. it has been observed that there is a fairly large time delay for the onset of emission from oxide species in comparison with those from atoms and ions of constituent elements present in the plasma. Faster decay occurs for emission from oxides and ions compared with that from neutral atoms. From the time delays observed it is evident that the oxide species are formed when the plasma temperature begins to fall. Under this condition, the presence of continued excitation processes are required for the emission from oxide species. These aspects also support to the view that oxide species may not be originating from the target material as such but are formed as a result of ion-oxygen recombination processes as the hot plasma cools down. The oxygen deficiency which is a crucial parameter for the superconductivity in high T_c ceramics, can thus be controlled by adjusting the partial pressures of oxygen in the plasma chamber during the process of thin film deposition using laser ablation technique.

Using the Langmuir probe technique, plasma parameters such as plasma temperature and velocity of positive as well as electrons in the plasma were evaluated. Here it is also observed that decay constant of the ion probe current depend on the probe voltage. Some control over the stochiometry and composition of the film obtained can therefore be

effected by creating an electric field near the substrate during the laser plasma deposition of high T_c materials. So the external electric field can affect the recombination rates and thus the composition of the high T_c thin films deposited on a substrate can be controlled to some extent, when the laser ablation method is used for this purpose.

Dyer *et al* [12] mentioned that time lags attributed for the various species in the plasma are due to time of flight so that velocity should have $(M)^{-1/2}$ dependence (M- mass of the ablated species)). But the time delay observed here does not support this view. Ofcourse, the plasma expansion velocity may also contribute to the time delays in certain cases (very small delays) but the major part of the observed time delays does seem to arise from the recombination processes. Results of initial measurements of plasma velocity using Langmuir probe gives values of $\approx 10^4$ m/sec for the positive ion velocities which lends support to the above conclusion.

REFERENCES

[1] Bednorz J G and Muller K A, *J.Phys.:B*, 64, 189, (1986)

[2] Dikkjamp K, Vekadesan T and Wu X D, *Appl.Phys.Lett.*, 51, 619, (1987)

[3] Moorjani K, Bohandy J, Adrian F J and Kim B F, *Phys.Rev.:B*, 36, 4036, (1987)

[4] Lynds L, Weinberger B R and Peterson G G, *Appl.Phys.Lett.*, 52, 320, (1988)

[5] Wayne a Weimer, *Appl.Phys.Lett.*, 52, 179,) (1988)

[6] Kwok H S, Shi L and Wang X W, *Appl.Phys. Lett.*, 52, 1825, (1988)

[7] Auciello O, Sito O E and Biunno N, *Appl.Phys.Lett.*, 53, 72, (1988)

[8] Geyer T J and Weimer W A, *Appl.Phys.Lett.*, 54, 469, (1989)

[9] Bozovic D, *Phys.Rev.Lett.*, 59, 2219, (1987)

[10] Corliss C H and Boznanw W R, *"Experimental tansition probabities for spectral lines in 70 elements"*, (NBS Monograph,53, 1962)

[11] Puell H and Naturfor Z, *Appl.Phys.lett.*, 25, 1807, (1970)

[12] Dyer P E, Key P H and Issa A, *Appl.Phys.Lett.*, 53, 534, (1988)

[13] Koren G and Yeh J T C, *J.Appl.Phys.*, 56, 2120, (1984)

[14] Gorodetsky G, Kazyaka T G, Melcher R L and Srinivasan R, *Appl.Phys.Lett.*, 46, 828, (1985)

[15] Feldman D and Holly S, *Appl.Phys.B*, 44, 81, (1987)

[16] Shinn G B, *J.Vac.Sci.Technol.*, 4, 1273, (1986)

[17] Hughes T P, *"Plasmas and laser light"*, (Wiley, New York, 1975), P.26

[18] Ready J F, *"Effects of high power laser radiation"*, (Academic, New York, 1971)

[19] Koren G, Gupta a and Baseman R J, *Appl.Phys.Lett.*, 54, 1920, (1989)

[20] Girault C, *Appl.Phys.Lett.*, 54, 2035, (1989)

[21] Wu X D, Inam Y and Venkatesan T, *Appl.Phys.Lett.*, 52, 179, (1988)

[22] Weimer and Wu X D, *Appl.Phys.Lett.*, 53, 1825, (1988)

[23] Harris D C and Hewston T A, *J.Soli. State.Chem.*, 69, 182, (1987)

[24] Zaidel A N, Prokofev V K and Raiskii S M, *"Tables of spectrum lines"*, (Berlin :Pergamon press, 1961)

[25] Yoo K M, Alfanoo R R and Guo X, *Appl.Phys.Lett.*, 54, 1278, (1989)

[26] Padmaja G, A V R Kumar, P Radhakrishnan, V P N Nampoori and C P G Vallabhan, *J.phys.D:Appl.Phys.*,22, 1558, (1989)

CHAPTER VII

SPECTRAL CHARACTERISTICS OF LASER INDUCED PLASMA FROM METAL TARGETS

ABSTRACT

Studies on spatially resolved plasma emission from two metal targets (Aluminium and Copper) obtained by the laser irradiation using pulsed Nd:YAG laser are presented. Using Langmuir probe techniques, various plasma parameters like plasma temperature, plasma density, frequency and velocity of ions in the plasma are calculated and are discussed in this chapter.

144

7.1. INTRODUCTION

The interaction of high intensity pulsed lasers with metals results in the formation of plasma and the observed optical emission from laser induced plasma is useful in characterizing both the laser target interaction [1] and the resulting plasma [2].

Light is absorbed in metals by internal photoelectric effect, raising the electron to higher energy states in the conduction band so that the mean free time between the collisions for electrons is $\approx 10^{-14}$ to 10^{-13} sec [3,4]. Thus for the times of the order of $\approx 10^{-9}$ to 10^{-8} sec, which is the usual laser pulse duration, the electrons have made many collisions among themselves and with lattice phonons. The energy absorbed by the one electron will be distributed and converted into the heat energy within the volume in which the light is absorbed. On exposing the metal surface to laser radiation, the metal surface will be vapourized resulting in the formation of plasma.

Studies of atomic and molecular ionization near metal surfaces have primarily considered the case in which the atoms/molecules are located in the ground electronic state [5]. In such cases ionization probability is close to unity when the metal work function exceeds the particle ionization potential whereas for the reverse relationship, ionization probability drops off sharply. In the latter case, the ionization efficiency can be increased significantly by exciting the particles to electron levels at which ionization energy is less than the work function [6].

When the laser radiation is incident on the Aluminum sample at room temperature most of the incident energy is reflected. The remaining is absorbed in a skin depth δ through inverse bremsstrahlung, through the excitation of conduction electrons in intraband transitions. This absorption of laser energy results in the rise of temperature of the sample surface. The thermal coupling coefficient A $\simeq$ Ea/Ei (where Ea is the

absorbed and Ei is the incident laser energy), which depends on the plasma properties like temperature, the speed of discharge propagation etc [7]. Usually when a dense plasma is already formed near the irradiated surface, its properties and subsequent evoluation are fully determined by the laser intensity I and geometry of the irradiation and do not depend on the surface characteristics. When the target surface is involved in an initiation of gas breakdown, it influences the threshold intensity I_{th} which is required for the plasma formation. It was shown that [8] in the initial stage of gas breakdown near the metal surfaces, defects near metal surface are overheated by the laser irradiation, evapourate and serve as a microplasma sites.

The laser induced plasma generation of Copper is described by an intense emission centered in the green region of the visible spectrum [9]. The dynamics of the plasma formation is controlled by the dynamics of the desorption processes and accompanying changes in the optical and electromagnetic properties of the surface [10]. The generation and identification of the Copper species by laser induced ablation from a clean Copper surface are of interest in the context of the process occurring in the laser induced thermal desorption (LITD), which is emerging as a new and versatile tool in area of surface sciences [11].

Plasma has been characterized in terms of their appearances, their spectra, their electron temperature and density profiles [12]. The appearance and spectral characteristics of LIP from metal targets are position dependent. The region just above the sample surface (region A, primary plasma) has a strong continuous emission whereas, the surrounding region (region B and C, secondary plasma) will have a strong line spectrum characteristic of the sample with negligible background signal [13,14]. The concentration of a particular species is proportional to the area under its emission curve. Continuum emission is produced by both free-free bremsstralung (elecron collision with atoms) and the electron - ion recombination.

The knowledge of the plasma information is of importance as it

may modify both energy coupling and also the energy and the nature of the ablated species thus influencing the deposited film in the use of laser plasma deposition processes.

The spatial and temporal resolution of optical emission spectra of Aluminium plasma produced by the flash lamp pumped dye laser was studied by Knutdson et.al.[2]. Relative emission intensities provide electron temperatures as a function of time, distance from the target surface and the incident laser intensity and they obtained the electron temperature $\approx$ 6 eV

In this chapter spatial variation of spectroscopic analysis of the plasma emission from Aluminium and Copper targets are reported. From the relative intensities of AlO bands population distribution in various vibrational levels and vibrational temperature of AlO molecules are calculated. Using Langmuir probe technique in the Aluminium plasma various plasma parameters like electron temperature and velocities of positive as well as negative ions obtained are also given here.

7.2. SPECTRAL CHARACTERISTICS OF METAL PLASMAS

The experimental arrangement for the spectroscopic analysis of the spatial variation of the plasma emission from the metal targets (Aluminium and Copper) was described in detail in chapter III. Typical plasma emission from Aluminium and Copper targets are shown in the figure (7.1) and figure (7.2) respectively.

The plasma emission spectra from Aluminium and Copper target in the region (A) and region (C) of the plasma are shown the figure $[7.3(a), 7.3(b)]$ and Figure $[7.4(a), 7.4(b)]$ respectively along with mercury spectrum for the wavelength calibration.

In the case of the plasma emission spectrum of Aluminium target it is observed that the spectrum in the extended region (C) is dominated by the intense molecular bands of AlO with $\Delta v = +2$, $+1$, 0, -1 and -2 due to the transition from $B^2\Sigma \longrightarrow X^2\Sigma$ ground state in the wavelength region from 447.0 nm to 542.43 nm. The spectrum of first positive system of nitrogen molecule due to
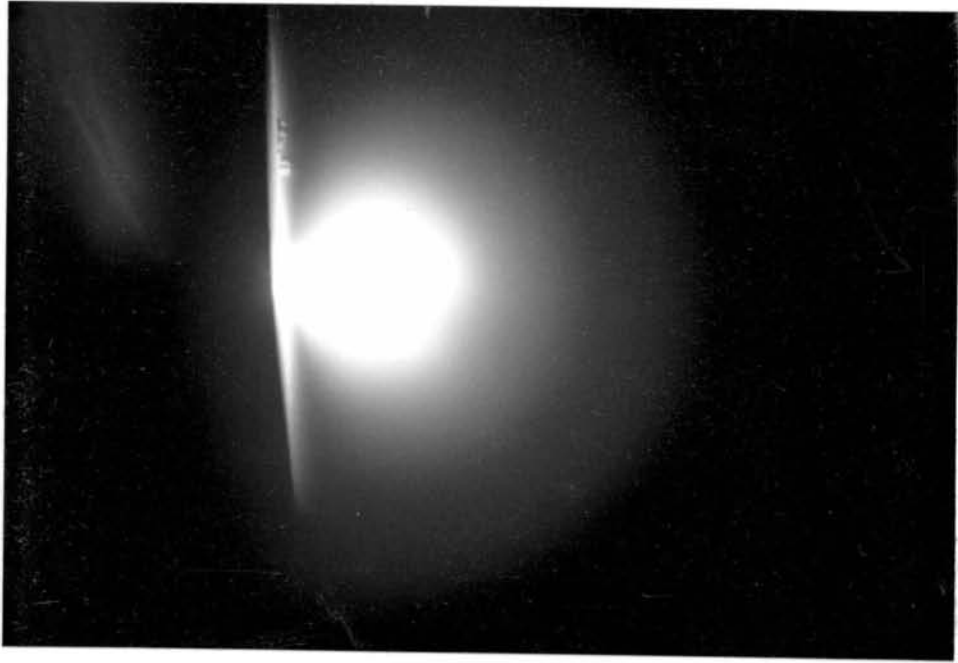
Figure 7.1. Typical plasma emission from an Aluminium target
(laser fluence ≈ 12 J/cm^2)
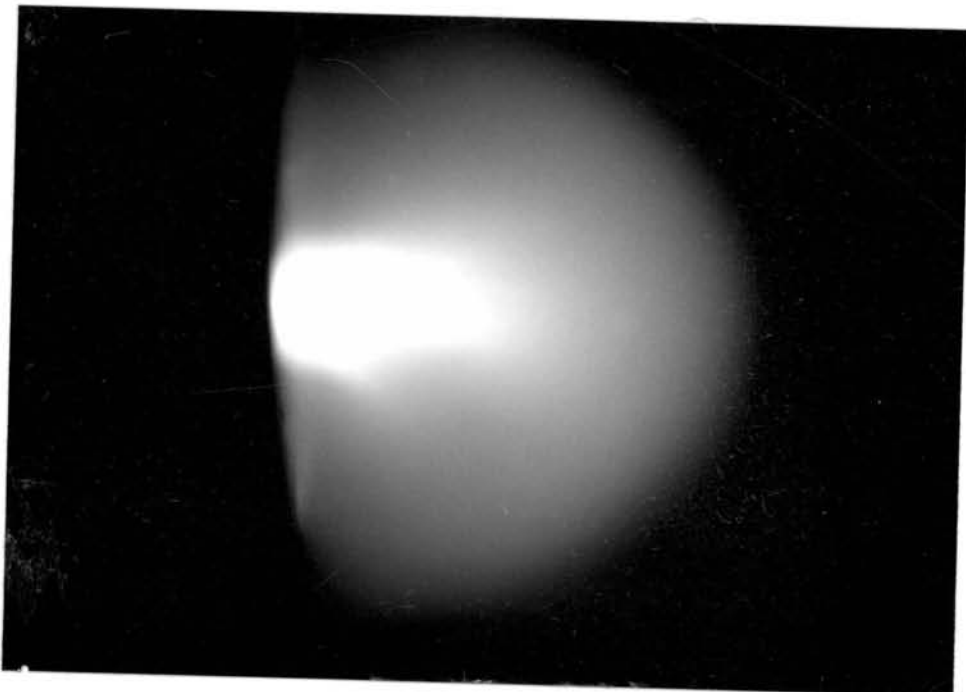
Figure.7.2 Typical plasma emission from a Copper target
(laser fluence ≈ 12 J/cm^2)

Ist Positive IInd positive N$_2$

(7,4) (8,5) $\Delta\nu=-2$ $\Delta\nu=-1$ $\Delta\nu=0$ $\Delta\nu=+1$ $\Delta\nu=+2$ (0,4) (1,5) (4,8) AlO

Al

Al$^+$

Al^{2+}
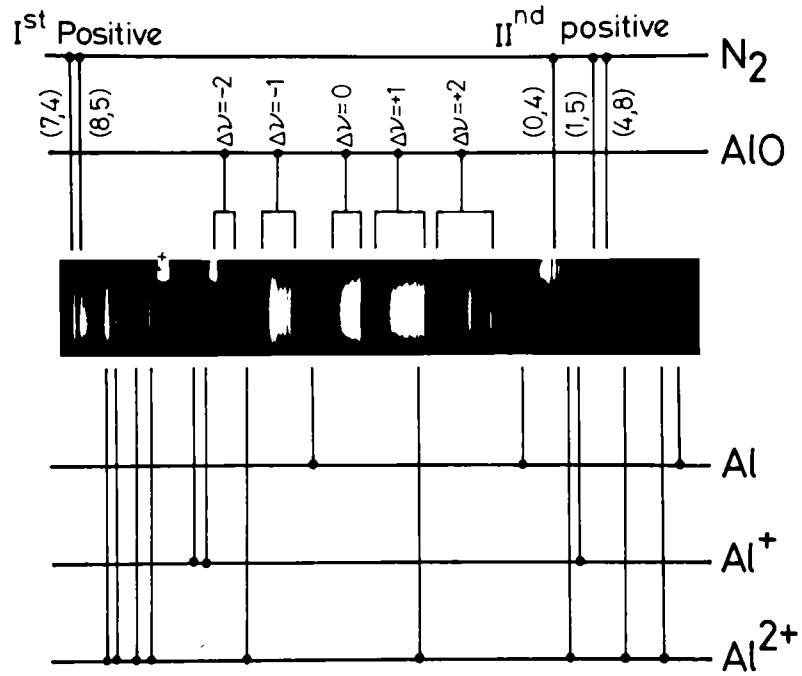
Fig.7.3(a)   Plasma emission spectrum from the extended region (C) of the Aluminium plasma (laser fluence $\approx$ 12 J/cm^2)

AlO

Al

Al I

Al II
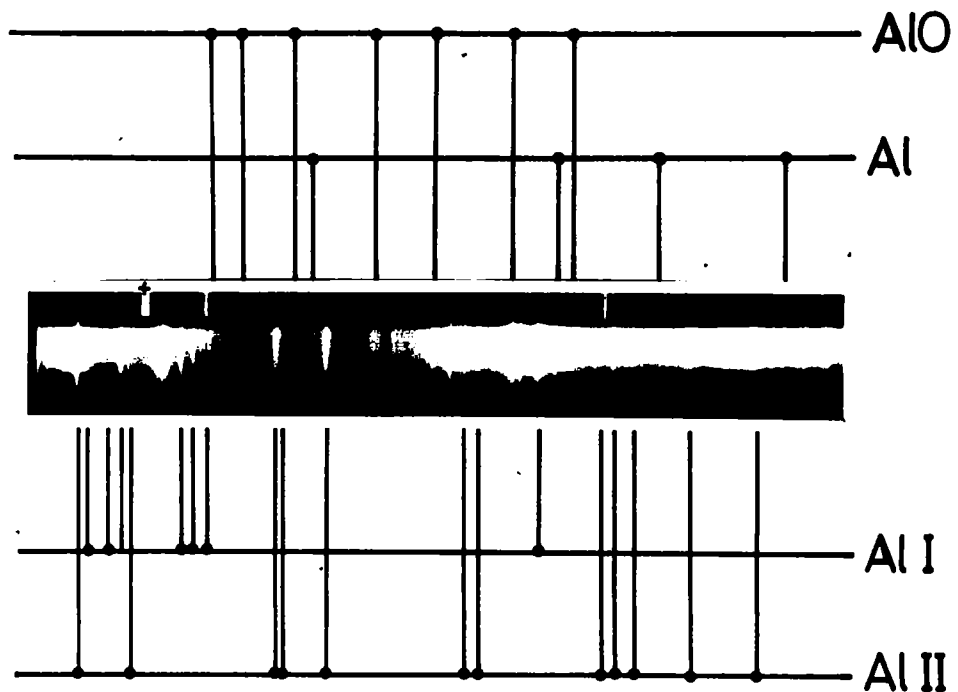
Fig.7.3(b)   Plasma emission spectrum from the central region (A) of the Aluminium plasma (laser fluence $\approx$ 12 J/cm^2)
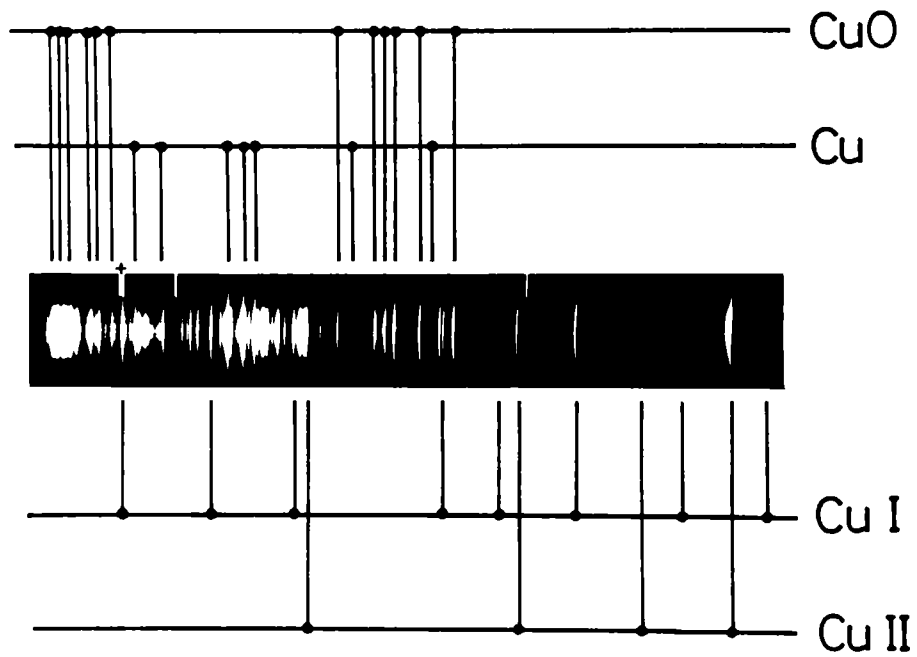
Fig.7.4(a)   Plasma emission spectrum from the extended region (C)
              of the Copper plasma (laser fluence ≈ 12 J/cm²)
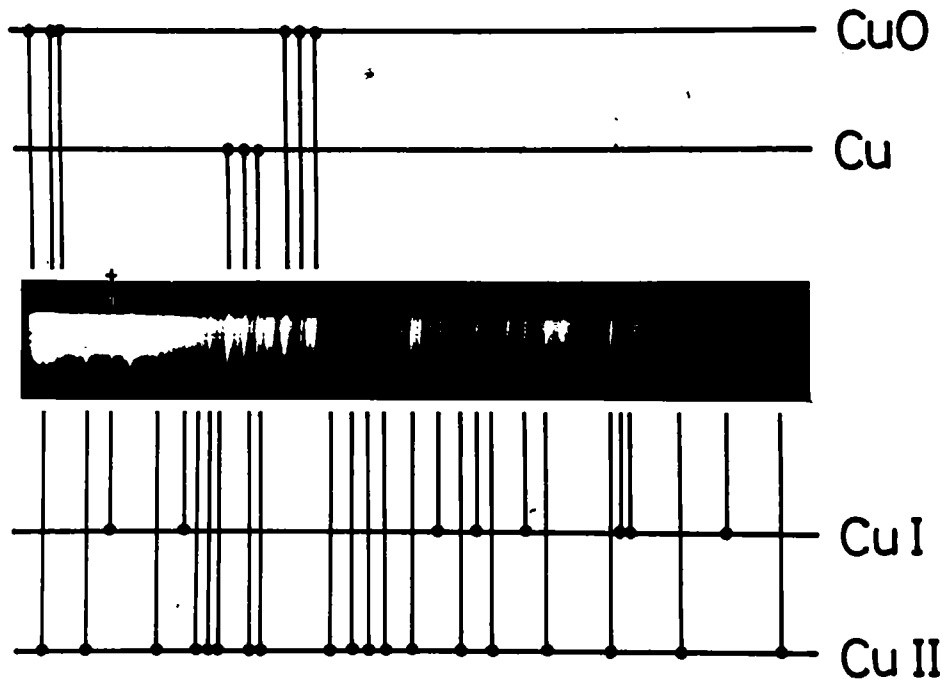
Fig.7.4(b)   Plasma emission spectrum from the central region
              (A) of the Copper plasma (laser fluence ≈ 12 J/cm²)

transitions from $B^3\pi$ --> $A^3\Sigma$, (degraded to violet) with two bands (7,4) and (8,5) in the wavelength region 654.48 nm and 646.85 nm and IInd positive due to transitions from $C^3\pi$ --> $B^3\pi$, (degraded to shorter wavelength) with two bands (1,5) and (4,8) in the wavelength region 426.9 nm to 409.4 nm were also observed. The existence of bands due to the nitrogen molecule was due to the breakdown of residual air in the partially evacuated plasma chamber by the high intensity laser pulse. But the plasma emission spectrum in the center region of the plasma was dominated by the Al^{2+} and Al^+ along with neutral aluminum atoms. In the case of Copper plasma, the plasma emission spectrum in the central region consists of continuous background with ionic (Cu^+ and Cu^{++}) and neutral lines superimposed on it, whereas the spectrum in the extended region consists of well defined neutral and ionic lines without any background continuum. Generally the lines due to ionic species are less intense and broadened as compared to those due to the neutral atoms. The laser induced plasma generation of Copper is accompanied by an intense visible emission centered in the green region of the visible spectrum. The bands obtained in this region were very weak including the small group of band heads. The intense band systems of CuO exist in the red region of the spectrum, which was beyond the detection range (400 nm - 600 nm).

Thus one notices absence of prominent band system in case of the plasma emission spectrum from Copper target. But some weak band heads due to CuO are however seen in the emission spectrum in the outer region (region (C)) of the Copper plasma, whereas ionic lines are dominant in the region (A) of the same. But in the case of Aluminium plasma intense AlO bands are present in the visible region. In both cases, the ionic lines in the spectrum are generally found very weak and broadened compared to that of neutral lines. This spatial variation in the plasma emission spectrum is essentially due to the fact that in the core region (A) of the plasma, the plasma temperature is very high so that only ionic and neutral species are present whereas, in the

extended region of the plasma where the plasma temperature is comparatively lower, the recombination processes are predominant which result in the formation of molecular bands.

From the relative intensities of AlO bands, the vibrational temperature was calculated (the details of calculations used here are given in the chapter I). Figure (7.5) shows the population distribution of AlO molecules in various vibrational levels. The variation of vibrational temperature of AlO with laser energy is shown in the figure (7.6).

7.3. LANGMUIR PROBE CHARACTERISTICS OF THE ALUMINIUM PLASMA

The experimental arrangement of the Langmuir probe characteristics are given in the chapter III and the basic calculation used for obtaining the various parameters from this study is given in the chapter I. The probe consisting of a Copper wire of few mm diameter was introduced into the Aluminium plasma at a particular distance from the target so that both electrons and positive ions can be detected by suitably biasing the probe with positive as well as negative voltage. The corresponding probe characteristics were approximately measured. The probe characteristics for the Aluminium plasma is shown in the figure(7.7). The details about this type of characteristics was given in the chapter I. From the probe characteristics, the saturation current (I_i) was found to be ≈ 0.4 mA so that

$$I_i = 0.25 \, n_+ \, e \langle V_+ \rangle \, A, \qquad (7.1)$$

where A is the area of the probe
The plasma density was obtained as $n_e = n_+ = 3.6 \times 10^{10}/cm^3$
from these parameters the plasma frequency was obtained as,

$$\omega_{pl} = \left[\frac{4\pi n_e^2}{m_e} \right]^{1/2} = 10.6 \text{ GHz} \qquad (7.2)$$

149
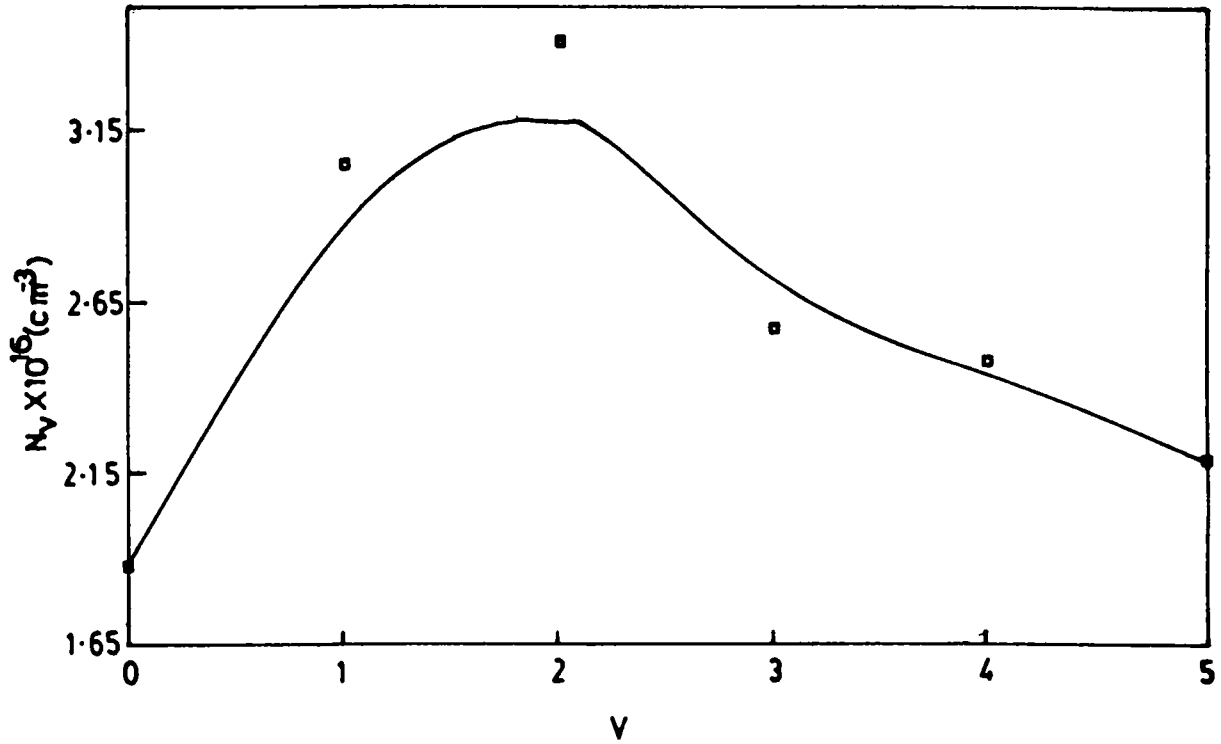
Fig.7.5.   The population distribution of   AlO   bands   at   various
            vibrational levels
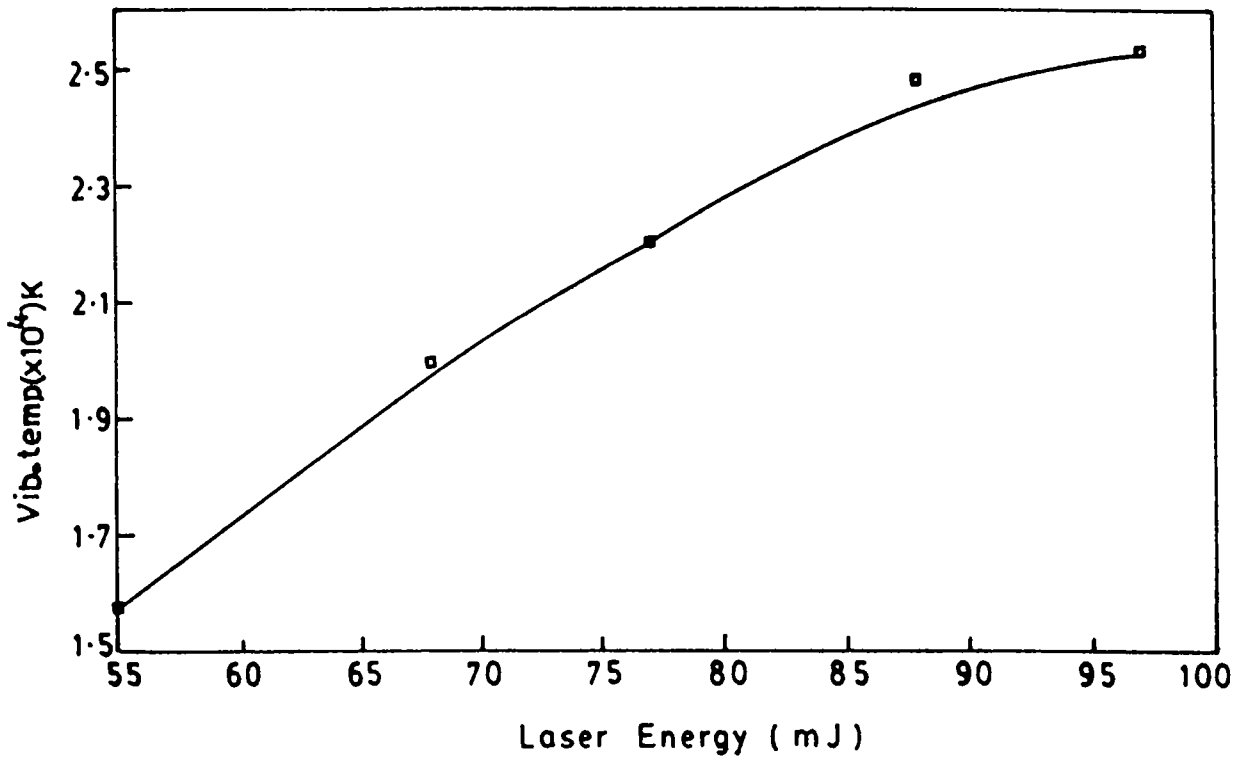
Fig.7.6.   The variation of vibrational temperature of   AlO   bands
            with laser energy
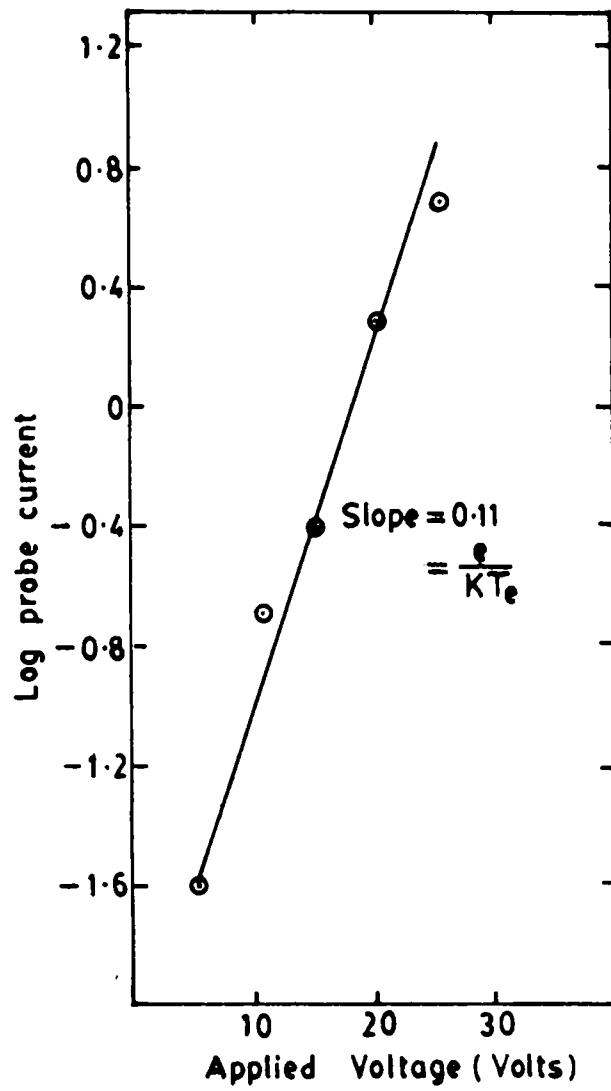
Fig 7.7. Characteristics of the langmuir probe in the Aluminium plasma
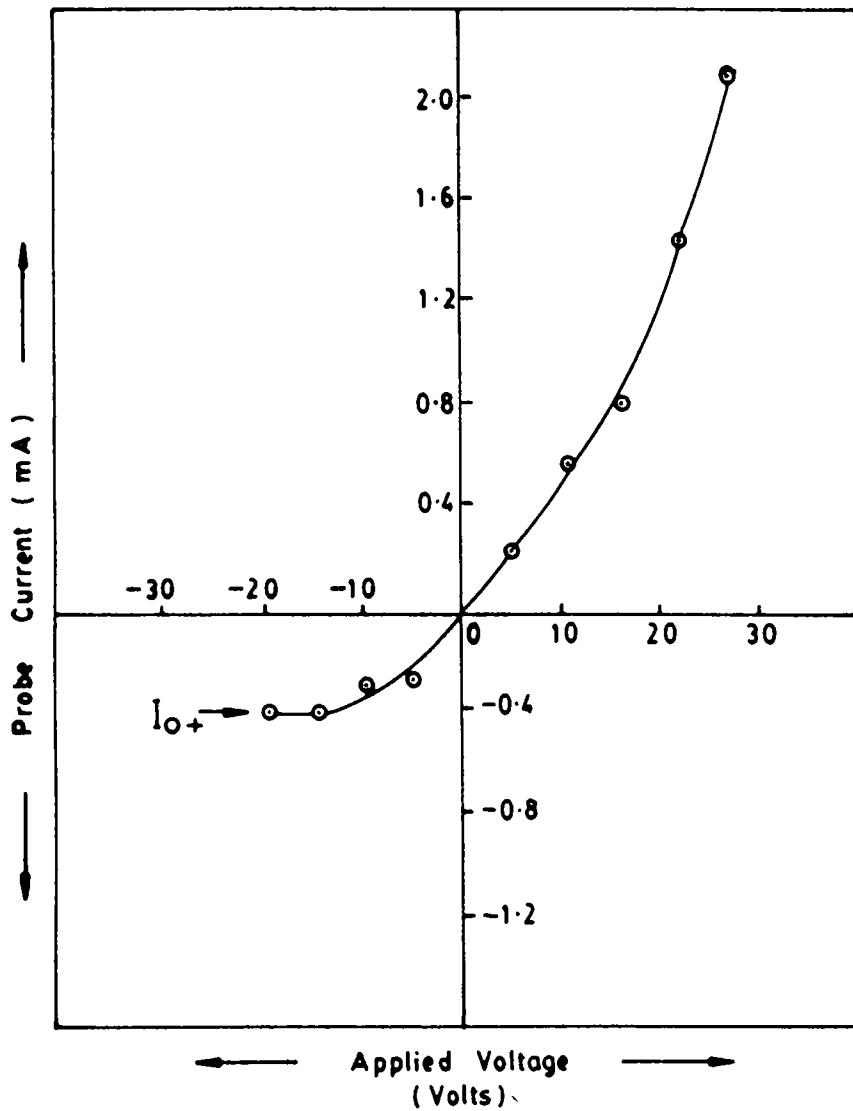
Fig .7.8. Probe voltage versus log probe current to obtain the electron temperature

when the probe voltage versus log (probe current) is plotted, a straight line is obtained and from the slope of this curve (figure (7.8) the electron temperature was obtained by using the equation (1.61) in the chapter I,

The electron temperature $T_e \approx 10.6 \times 10^4$ K ≈ 9.0 eV

From this velocity of electron as well as velocity of the positive ions were obtained.

Electron Velocity $\langle V_e \rangle = 2.2 \times 10^8$ cm/sec

Positive ion velocity $\langle V_+ \rangle = 9.9 \times 10^5$ cm/sec

Thus various plasma parameters were obtained by Langmuir probe method.

7.4. CONCLUSION

The spatially resolved plasma emission spectrum of Aluminium and Copper shows distinctly different characteristics. The plasma emission spectrum in the outer region of the Aluminium plasma was dominated by the molecular bands of AlO and centre region was dominated by Al^+, Al^{++} along with neutral Aluminium atoms. In the case of Copper plasma, the plasma emission spectrum in the central region consists of continuous background with ionic (Cu^+ and Cu^{++}) and neutral lines superimposed on it, whereas the spectrum in the extended region consists of well defined neutral and ionic lines without any background continuum. Generally the lines due to ionic species are less intense and broadened as compared to those due to the neutral atoms. Such variations in the characteristics of the plasma emission spectrum could result mainly from the variation in the plasma temperature at different distance from the target surface.

From the relative intensities of AlO bands, the population distributions of AlO molecules at different vibrational levels were obtained. The vibrational temperature of AlO bands was calculated and their variation with laser energy was also obtained.

From the Langmuir probe technique, it was found that this can be effectively used to diagnose high density plasmas generated by

the laser ablation. Both electron temperature and velocity of negative as well as positive ions were calculated. Since there exists fairly high electron density, it can be concluded that substantial optical absorption occurs in the plasma directly. Thus this technique will provide valuable insight to the laser produced metal vapours in terms of their plasma characteristics. It is also evident that the Langmuir probe method can provides information which is complementary to that obtained from spectroscopic measurements.

REFERENCES

[1] Allen M V "*Laser Beam interaction with metals Vol.II*" (Springer-Verlag, Berlin, 1987), p.228

[2] Knudtson J T, *J.Appl.Phys.*, 61, 4771, (1987)

[3] Dyer P E and Key P H, 55, 1630, (1989)

[4] Capjack C E, *Phys.Fluids*, 30, 515, (1987)

[5] Zandberg E V and Ionov N F, *Surface Ionization*, (Moscow 1969)

[6] Chaplik T and Teor Z H, *J.Appl.Phys.*, 44, 332, (1968)

[7] Marcus S, Lowder J E and Mooney D L, *J.QE.*, 11, 490, (1975)

[8] Walters C T, Pavlenko T and Inam Ya A, *J.Appl.Phys.*, 49, 2937, (1978)

[9] Hussla I and Viswanathan R, *Surf.Sci.*, 145, 492, (1984)

[10] Block J H, Jentsch T H and Drachsel W J, *Mass Spectrom.Ion Phys.*, 38, 195, (1981)

[11] Welder G and Ruhmann H, *Sur.Sci.*, 121, 464, (1982)

[12] Kenneth J G and George L P., *J.Vacuum.Sci.Tech.*, 44, 1349, (1990)

[13] Kagawa K and Yokoi S, *Spectro.Chim.Acta*, 37B, 789, (1982)

[14] Animosov V N, *Sov.Tech.Phys.Lett.*, 13, 337, (1987)

CHAPTER VIII

DEPOSITION OF METALLIC THIN FILMS BY LASER ABLATION TECHNIQUE

ABSTRACT

This chapter is divided into two sections. Section A describes an experimental set up for the preparation of thin films by laser ablation using pulsed Nd:YAG laser. As a preliminary study, copper metal films have been deposited by this technique. Their optical transmission characteristics with respect to different parameters such as laser energy, number of pulses, substrate temperature and the distance between the target and the substrate are studied. In order to obtain a better and more uniform film, a modified set up for the substrate heater is also discussed in this chapter. Section B presents advantages and some of the applications of laser deposition technique.

SECTION A

8.1. INTRODUCTION

(a) GENERAL INTRODUCTION

The use of intense laser beams to evapourate refractory materials for the preparation of thin films was described as early as 1965 [1]. While the interest in laser evapouration to produce thin film was continued [2], recent developments have seen the use of lasers for chemical vapour deposition, photodecomposition and electroplating. In addition, laser annealing has been used in the recrystallization of amorphous films produced by RF-sputtering. Ruby, CO_2 and Nd:YAG lasers have been used in the deposition of thin films by laser evapouration method. Generally the CO_2 laser is preferred for the evapouration of insulating and most semiconducting materials, while ruby or Nd:YAG lasers are preferred for evapourating metals. The composition of the resulting film has been shown to depend on the geometrical factors and pulse intensity [3,4,5].

As described in earlier chapters, ablation of sample using pulsed lasers produce brilliant elongated plasma extending outwards from the target. As the sample kept in the vacuum chamber is irradiated, the material is vapourized and ejected from the surface towards the substrate, which can be suitably heated and placed in the region of the plasma plume [6]. The gaseous species condense on a relatively cooler substrate to form thin films.

(b) METALLIC FILMS

The ablation of material from a metal target by high energy laser pulses and the deposition of the ablated material on to the substrate kept in close proximity to the target is a challenging alternate technique for patterning micro electronic

154

devices and lithography [7,8].   In   order   to   optimize   printing
method, it   is   essential to understand   laser   ablation   of metals.
Laser assisted evapouration is a thin   film   deposition   technique
that is   compatible   with   ultra   high   vacuum   environment   where
significant amount of energetic species are generated [9].   Ions
with hypothermal energies in the 100-1000 eV   range   are   produced
when high power (10^7-10^9 W/cm^2) pulsed lasers   are   used   for   the
evapouration.   The   interaction   of   the   laser   beam   with   the
evapouration   target   was   found   to   generate   a   plasma   in   the
evapourant stream containing ions with high kinetic energy.   The
thin films grown by this method were   found   to   have   bulk   index
values and optical properties that   were   environmentally   stable.
The   improved   structural   properties   were   attributed   to   the
existance of energetic particles (ionised   found   in   the   plasma)
[10], produced during the laser ablation of the target.

When metal films are irradiated in air by a powerful laser
beam, the corresponding oxides are obtained [11].   In the case of
Copper, it was found that the characteristic growth depends on the
initial Copper film thickness.   Each point on the film   sees   the
laser beam many times, each time with   different   absorbed   laser
beam power density,   oxide   thickness,   temperature   etc.   The
extended thin film of CuO can be synthesized by scanned laser beam
irradiation of Copper film in air.   The   optical   characteristics
of the resulting oxide films are dependent on the laser beam power
density and thickness of the initial Copper film.   The   substrate
temperature   has   dramatic   influence   on   the   microstructural
development of these films.   The   higher   substrate   temperature
induces   substantially   higher   nucleation   rate   and   causes   the
complete conversion of the film into the   crystalline   structure.
The increased temperature instead of enhancing the crystal growth,
leads to larger average grain size [10].

This chapter is divided into two sections (A & B).   In
section A, the laser ablation technique for preparing   thin   films
of metal (Copper)   on   glass   substrates   is   described.   A

preliminary report on the optical transmission properties in the wavelength region 350-1000 nm of the thin films of Copper produced using this laser ablation technique is given. The variations of the optical transmission of these thin films with parameters like laser energy (E), number of pulses (N), target-substrate distance (d), and substrate temperature (T) are also discussed. A modified set up for substrate heater for obtaining better uniform film is discussed in this chapter. The final section of this chapter describes the various advantages and some of the applications of laser produced plasma deposition technique.

The structural morphology of the films produced by the laser deposition (Copper and Aluminium) has been observed here using a metallographic microscope in the transmission /reflection mode. The morphology of these films were also studied as a function of the above parameters and are discussed in this chapter.

8.2. EXPERIMENTAL TECHNIQUE

The 1.06 μm laser radiation from a Q-switched Nd:YAG laser (Quanta Ray, DCR-11) having a 10 nsec pulse width at a repetition rate of 10 Hz was focussed to a diameter $\approx$ 1 mm (energy density $\approx$ 20 J/cm^2) using a convex lens on to the surface of the sample of Copper (diameter 2.5 cms and thickness 5 mm) kept inside a stainless steel vacuum chamber (Pressure $\approx$ 200 mTorr) provided with quartz windows. The target (Copper) is rotated so that pitting of the target surface by the laser beam will be uniform. During laser irradiation, the bright and elongated plasma plume is formed in the forward direction towards the substrate and it is slightly divergent [12]. The laser energy was monitored for each laser pulse using an on-line pulsed laser energy meter (Delta developments), triggered in synchronization with the laser pulse.

The substrate (glass slide) is mounted on the heater and is placed close to the target surface. The schematic diagram of the
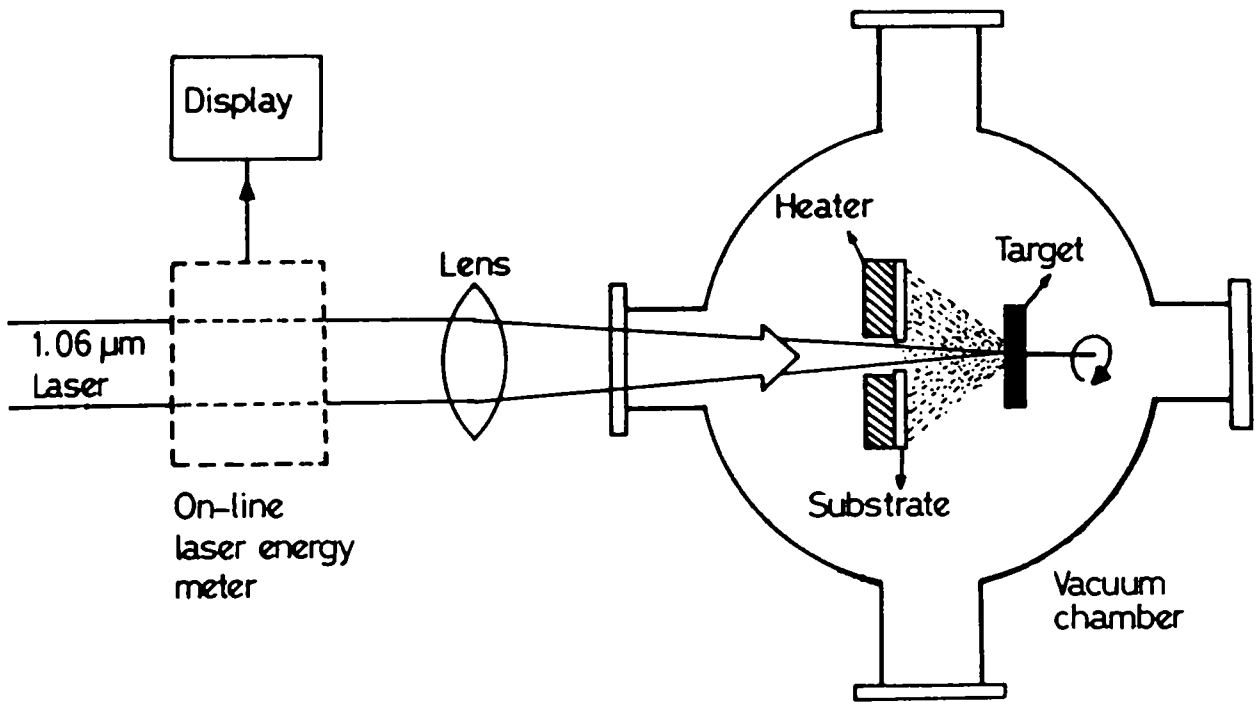
Figure 8.1a. Schematic diagram of the experimental set up for thin film deposition
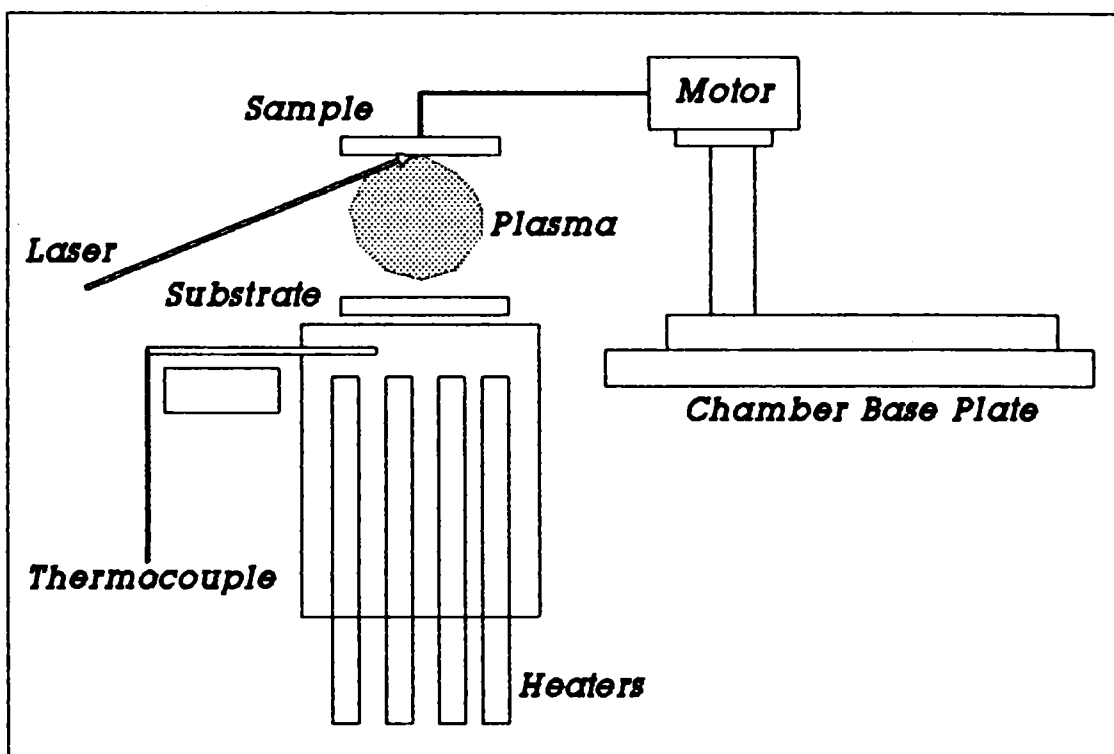
Figure 8.1b. Schematic diagram of the modified substrate holder for thin film deposition

experimental set up is shown in the figure (8.1a). The distance between the substrate and the target (d) can be varied up to a few centimeters. The optical transmission curve of these prepared Copper metal films were studied as a function of number of pulses (N), laser energy (E), substrate temperature (T) and also the distance between the target and the substrate (d).

The variation in the surface morphology of the films were studied by obtaining micrographs of these films prepared under various parameters.

The thin film prepared by the above set up may not be uniform so that a modified set up was used in which the target was positioned at 45 ^{o} with respect to the laser beam axis. The schematic of the modified set up for the substrate holder is shown in the figure (8.1 b) . The film obtained by the above set up was found to be more uniform compared to that of the earlier set up.

8.3 OPTICAL CHARACTERISTICS OF METAL FILMS

The optical transmission curve of these metal films were taken as a function of the above parameters using a UV-VIS-NIR spectrophotometer (Hitachi model U-3410). From the spectrophotometer data, it is seen that the percentage of transmission decreases towards the shorter wavelength region. Preliminary studies show that by controlling the substrate temperature, the cut-off wavelength of transmitted light can be shifted towards the blue-green region.

Figure (8.2) shows the variation of the percentage of transmission (%T) of the film as a function of substrate temperature at λ = 600 nm. From this graph it is observed that the % T decreases with substrate temperature, indicating that as the temperature increases, there is more adhesion resulting in the formation of a thicker film. The variation of the % T at λ = 600 nm with the distance d, between the target and the substrate is

157
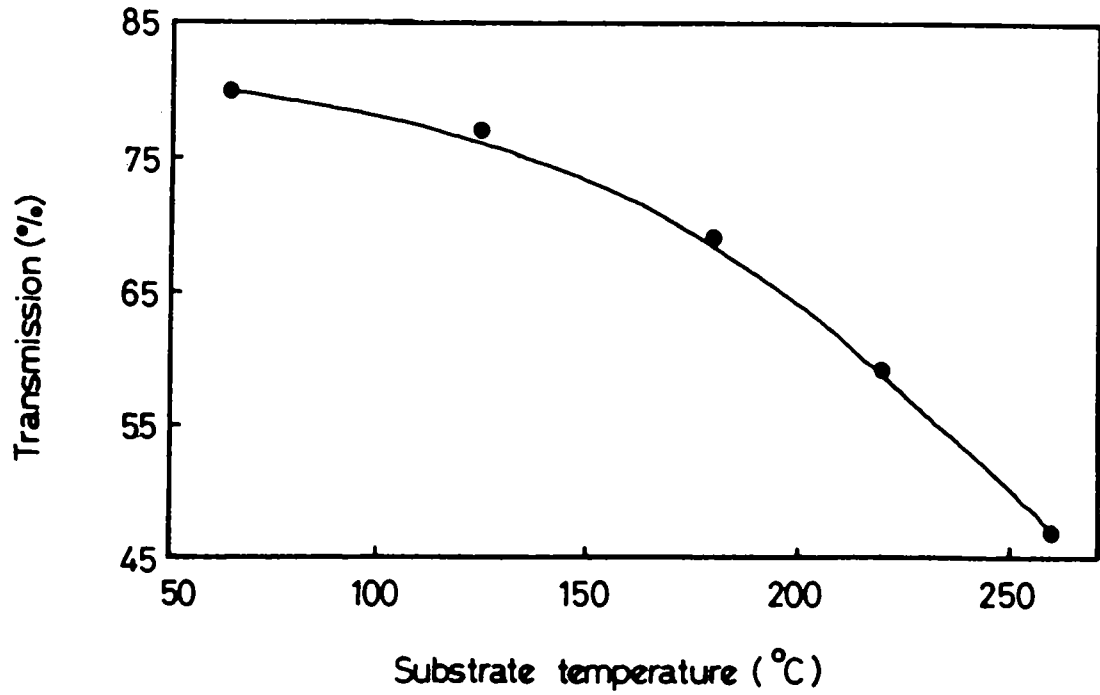
Figure 8.2.   The variation of the % T at λ = 600 nm with substrate temperature T.(d = 3 cms, E = 185 mJ, N = 18000 pulses)
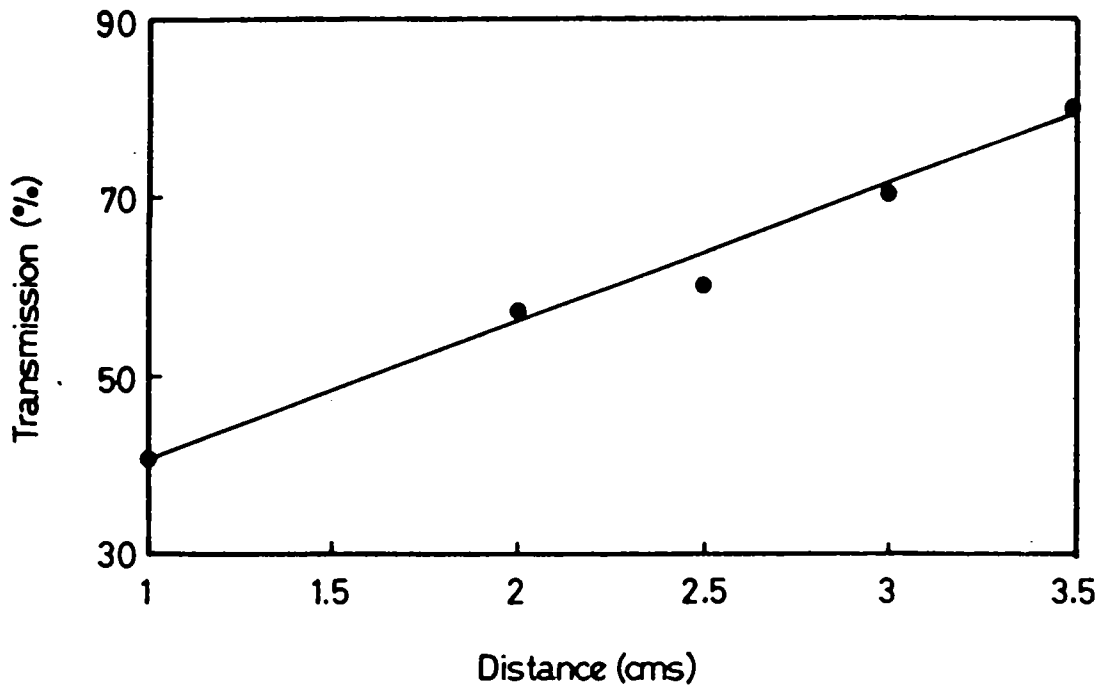
Figure 8.3.   The variation of the % T at λ = 600 nm with distance between the target and the substrate d. (T = 190°C, E = 185mJ, N = 18000 pulses)
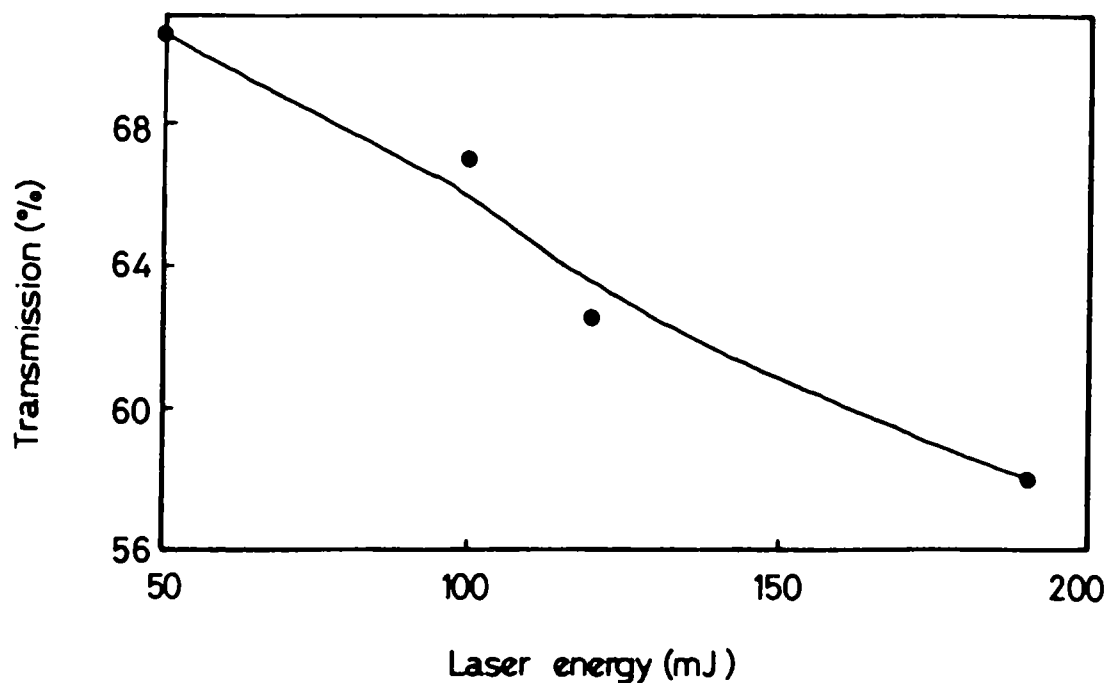
Figure 8.4.   The variation of the % T at λ = 600 nm with laser
              energy E (T = 190°C, d = 3cms, N= 18000 pulses)
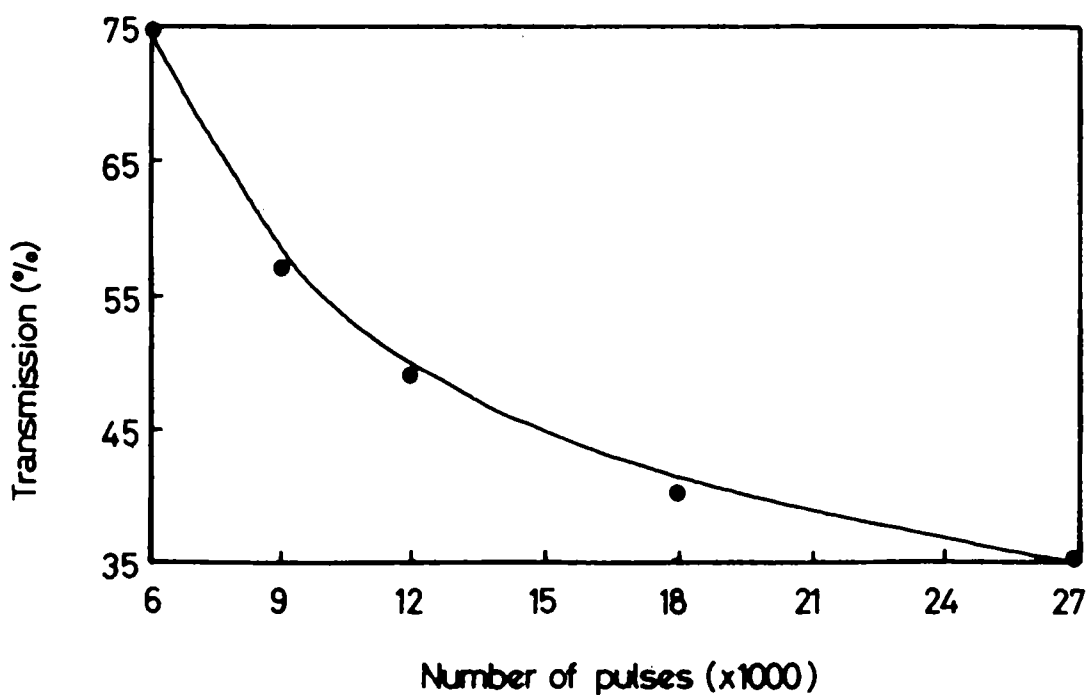
Figure 8.5.   The variation of the % T at λ = 600 nm with number of
              laser pulses N (T= 190°C, E = 185mJ, d = 3cms)

shown in the figure (8.3). As distance increases, the film formed is thinner and more uniform as compared to that formed when the substrate is placed close to the target. When the plasma expands, density decreases which results in the increase of the transmission of the film with increasing distance between the target and substrate. As the laser energy E is increased, the film again becomes more opaque and uniform (Fig.8.4) and thus %T also decreases as a result of the increased plasma density. Similar variations in the %T are observed when the number of laser pulses (N) is increased (Figure 8.5).

The morphology and the composition of the film were studied by taking the micrograph of the film surface using a metallographic microscope (Versamet-2) with a 20x magnification. Figure [8.6 (a) and 8.6 (b)] show the micrograph of the Copper films prepared at substrate temperatures of 68° C and 250° C respectively. Comparing the above two figures, it was observed that the cluster and island formation are more in the case of film produced at lower temperature resulting in a larger grain size. When the substrate temperature increases these clusters will have more energy so that they will orient themselves, correspondingly the grain size decreases resulting in a more uniform film. Similarly figure [8.7 (a) and 8.7 (b)] show the micrograph of the Aluminium films prepared at substrate temperatures of 68° C and 250° C. In this case also it was observed that the film was more uniform at higher substrate temperature.

8.4. CONCLUSIONS

These preliminary observations show that by optimizing the various deposition parameters that control the properties of the thin film obtained by laser ablation technique, it is possible to obtain thin film (metal) coatings of specific reflection/transmission properties. These results indicate that laser assisted evapouration can be an advantageous and convenient
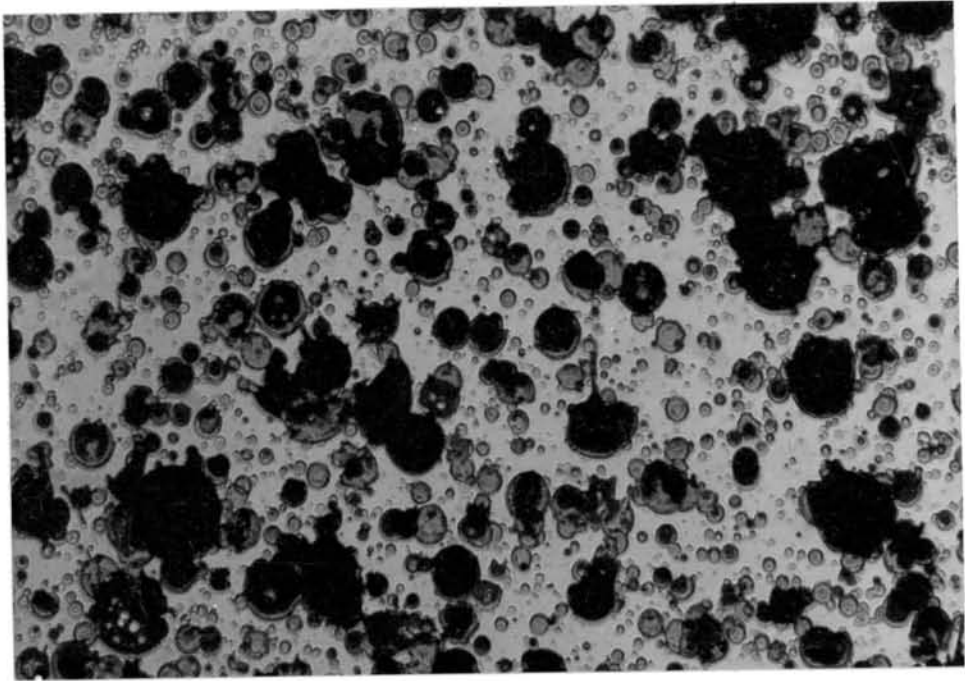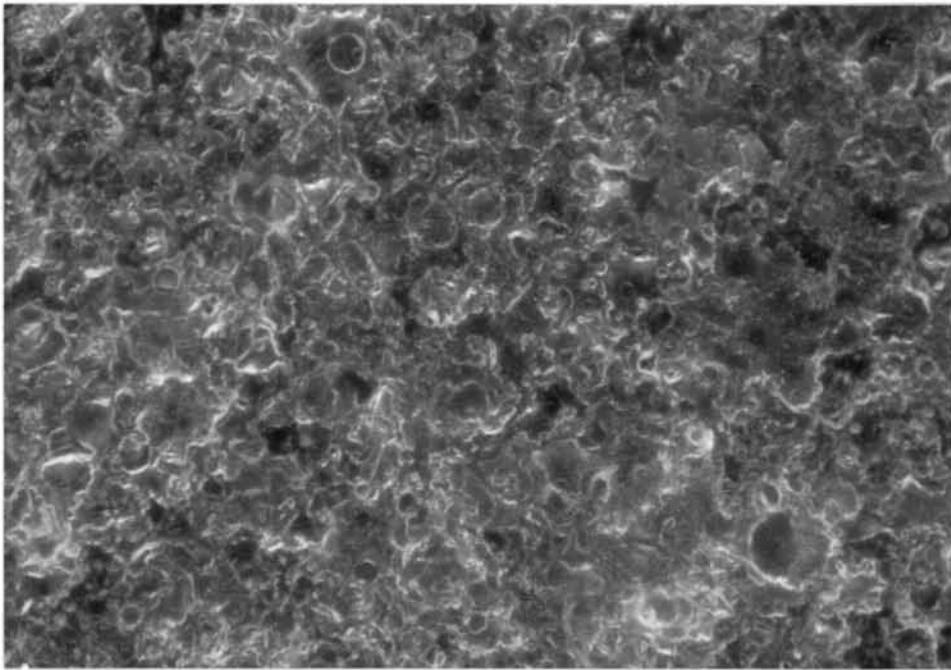
Figure 8.6. The transmission micrograph for Copper films deposited on glass with substrate temperatures of (a) 65° C and (b) 250° C
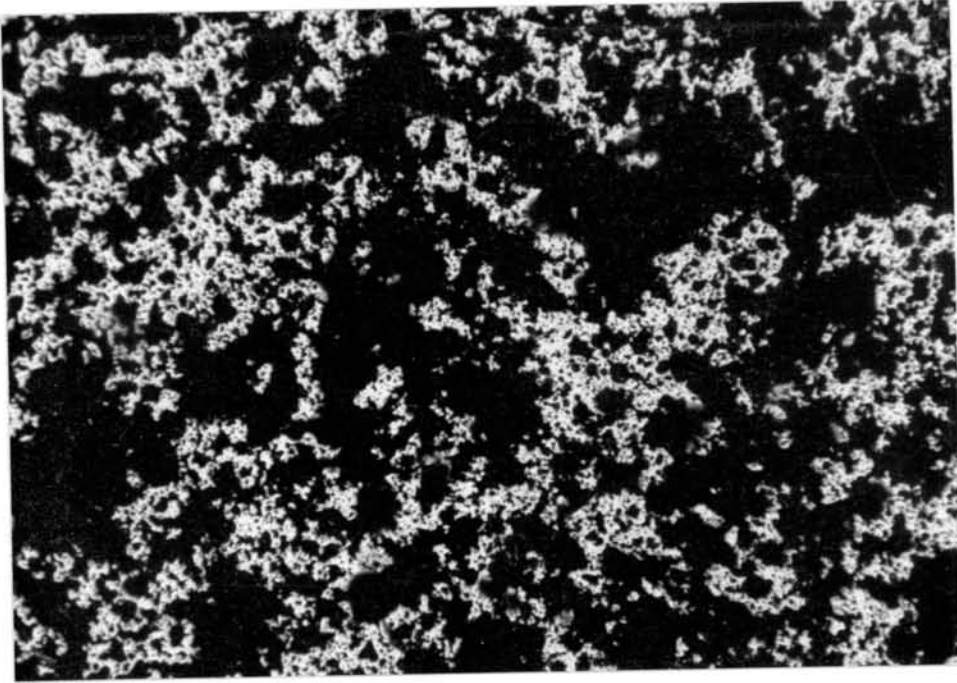
(a)
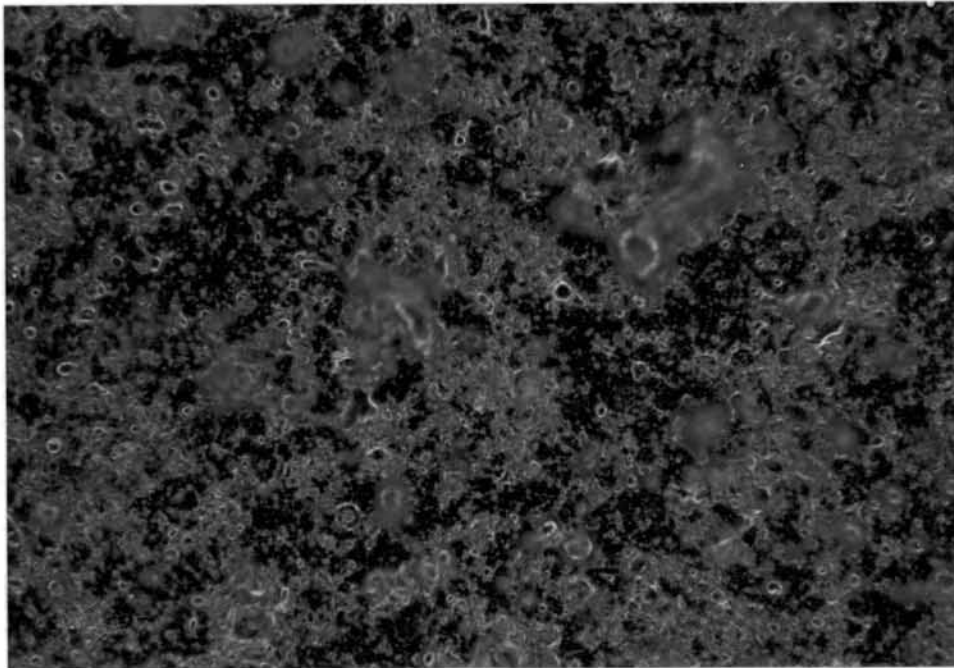
(b)

Figure 8.7. The transmission micrograph for Aluminium films deposited on glass with substrate temperatures of (a) 65° C and (b) 250° C

deposition techniques for producing optical films.   Thus   these
films can be used as optical filters so that by controlling the
deposition parameters optical filters of desired characteristics
can be obtained.

SECTION B

8.5. ADVANTAGES AND SOME APPLICATIONS OF LIP DEPOSITION TECHNIQUE

I. ADVANTAGES

Many novel thin   film   optical   devices   have   stringent
requirements on their optical performances and must survive in
severe environments.   This has driven the development of
processes for depositing reproducible, stable, hard and
stress-free films that are also invariant under various
environment conditions.   These desirable film properties are
associated with bulk like properties of the material at hand.
The thin films obtained by conventional physical vapour deposition
methods contain grain boundaries and various other structural
defects that are responsible for less than ideal characteristics
of thin film properties [13,14].   High temperature processes such
as chemical vapour deposition or post deposition annealing can
produce dense films with large grain size, but these processes can
also promote undesirable chemical reaction, diffusion or
segregation phenomena, which may destroy the composition profile
of the multi-component films.   Recently, several low temperature
($\approx$ < 300 K) and high vacuum techniques have produced dense high
optical quality films [15,16,17].   These techniques are based on
the bombardment of the growth surface with energetic particles
during deposition.   Pulsed laser assisted vapourization is one
such technique that offers a unique combination of many
advantageous features.

The specific advantages of laser assisted deposition are :
a. The production of ionized and excited species with high
    kinetic energies, which result in a crystalline growth of

159

the thin film.

b. Possibility of evapourating numerous compound congruently with negligible heating of the target [10]

c. Instantaneous control of the evapouration process

d. The number of independent controlling deposition parameters are found to be large

The advantages of laser sintering [18] as compared to electron beam and thermal annealing are reduced contamination, instaneous nature of the processes and pseudoequlibrium state.   Laser sintering also appears to have a phase stabilizing effect on materials whereas commercially available techniques are polymorphic.   The optical structural properties of the films appear to co-relate the starting material conditions.   Films deposited from the laser processed material were found to be optically more homogeneous than film deposited from the inprocessed material.   The film produced from a laser sintered material were found to have a stable single phase crystalline structure.   This results indicate that the structural variations in the film, which is one of the source of optical inhomogeneity can be reduced or eliminated by using stabilized starting material.

Laser ablation is a convenient method to produce diamond like carbon thin films (CVD).   The high proportions of ions to neutrals in the plasma produced by laser ablation [19]   are responsible for the uniform optical quality of the DLC films. DLC films which contain no hydrogen offer some unique advantages when used in IR applications [20].

Using laser ablation technique for high T_c films is a (1) a direct technique to produce very thin films with excellence superconducting properties (2).   This is the fastest and most reproducible method for the fabrication of high T_c thin films [21].

Evapouration techniques using thermal sources produce primarily neutral materials in gas phase and result in oxygen deficient

films [22]. It may be possible to enhance the formation of metal oxides within the plasma by producing ionic forms of the species during laser ablation. Transporting materials from the target to the substrates primarily as gas phase oxides may be the reason to eliminate the deposition of oxygen deficient films. Compared to other techniques, the formation of high T_c thin films can be prepared using a background oxygen ambient gas in the plasma chamber. The elimination of post-annealing process is important in growing multiple layers of different materials [23]. Laser deposition has been demonstrated to be a viable method for producing high quality superconducting thin films [24,25]. Pulsed laser ablation of the materials is relatively simple to implement and can transfer large amount of materials from the target to the substrate at large rates. The energy of the ejected species tend to appear in the transitional rather than the internal (electronic, vibrational, rotational) degrees of freedom [25-28]. Consequently, for many materials, large molecules can be transferred from the target to substrate without decomposition so that the stochiometry of the target can be preserved in the deposited film [29].

II. APPLICATIONS

The pulsed laser deposition is an effective technique for depositing multicomponent oxide glass films on various substrates. These films retain the composition and optical properties of the bulk glass. This method also have shown promise to allow the building of the integrated all optical elements [12].

Pulsed laser generated material plumes have wide range of applications in the thin film deposition and surface microanalysis and as fast atom beams, X-Ray sources or ion sources for beam lines and controlled fusion devices. The power densities of the laser vary between 10^7 to 10^{14} W/cm^2. In the laser ablation, relatively low laser fluxes (10^7- 10^8 W/cm^2) are used. So the

plasma plume is expected to consist of a much cooler plasma than in other methods. The particle mean kinetic energies were in the range 10-100 eV which causes high degree of ionization [30]. This kinetic energy affect the thin film properties in a significant manner.

For many applications, the ability to prepare different structures of the thin film of the material is important. Interest in diamond like carbon films is motivated by their unique combination of physical hardness, electrical strength, high thermal conductivity and optical transparency [31]. Studies have been accelerated by prospects of their commercial applications for optics and semiconductor technology [32].

Many microwave and microelectronics applications of the metal oxide based high T_c will require high critical current superconducting thin film. Laser deposition offers considerable promise for the fabrication of such films [33]. The rapid energy deposition possible with laser source results in temperature rise so rapid ($> 10^{11}$ K/sec) that congruent evapouration can occur without significant elemental fractionation.

Although high T_c thin films have often been prepared with post annealing at high temperatures, preparation of as-grown superconducting thin films by low temperature processes is needed for device application. As grown films are generally prepared by oxygen atmosphere or with its plasma activation so that stronger oxidizing gas is required for the formation of crystallized as grown film at lower temperatures [34]

Recently a variety of applications of high T_c films ranging from IR detectors to fast optically triggerd switches has emerged [35,36]. These applications depend on the the nature of optical interaction on these materials and how the superconducting electrical properties are thereby affected [37]. One can rightfully expect that laser deposition of thin films of all kind will play a major role in technology in the days to come.

•

162

REFERENCES

[1] Smith H M and Turner A F, *Appl.Opt.*, **4**, 147, (1965)

[2] Duley W W, *"CO₂ Lasers:Effects and Applications"*, (Academic Press, New York, 1976)

[3] Baldwin J M, *Appl.Spectrosc.*, **24**, 429, (1970)

[4] Baldwin J M, *J.Appl.Phys.*, **44**, 3362, (1973)

[5] Kliwer J K, *J.Appl.Phys.*, **44**, 490, (1973)

[6] Sankur H O, Denatale J, Gunning W and Nelson J G, *J.Vac.Sci.& Tech.*, **A5**, 2869, (1987)

[7] Bohandy J, Kim B F, and Adrian F J, *J.Appl.Phys.*, **60**, 1538, (1986)

[8] Adrian F J, Bohandy J, Kim B F, Jette A N and Thompson P, *J.Vac.Sci.& Tech.*, **B5**, 1490, (1987)

[9] Haluk O S and William G, *Appl.Opt.*, **28**, 2806, (1989)

[10] Sankur H, *J.Vac.Sci.Technol.:A*, **5**, 15, (1987)

[11] Bunkin F V, *Sov.Phys.*, **25**, 662, (1982)

[12] Vogale E M, Chase E W, Jackal J L and Wilkens B J, *Appl.Opt.*, **28**, 649, (1989)

[13] Macleod H A, *SPIE proceedings*, **21**, 325, (1982)

[14] Guenther K H, *SPIE Proc.*, **401**, 31, 91983)

[15] Martin P J, *J.Mat.Sci.*, **1**, 21, (1983)

[16] Sites J R, Gilstrap P and Rugkorakam R, *Opt.Engg.*, **22**, 447, (1983)

[17] Takaji T, *J.Cryst.Growth*, **45**, 318, (1978)

[18] Okutomi M, *Appl.Phys.Lett.*, **44**, 1132, (1984)

[19] Spencer E G and Schmidt P H, *Appl.Phys.Lett.*, **29**, 118, (1976)

[20] Davanloo F, *J.Appl.Phys.*, **67**, 2081, (1990)

[21] Frohlingsdorf J, Zander W and Stritzker T, *Solid State Commun.*, **67**, 965, (1988)

[22] Naito M, Hammond R H and Hahn M R, *J.Mat.Res.*, **2**, 713, (1987)

[23] Witanachchi S, *Appl.Phys.Lett.*, **53**, 234, (1988)

[24] Neifeld R A, Croft M and Shaheen S A, *Buul.Amer.Phys.*, **33**, 109, (1988)

[25] Friichtenicht J F, *Rev.Sci.intrum.*, **45**, 51, (1974)

[26] Tang S P, Utterback N G and Friichtenicht J F, *J.Chem.Phys.*, **64**, 3833, (1976)

[27] Utterback N G,Tang S P, and Friichtenicht J F, *Phys.Fluids.*, 19, 900, (1976)

[28] Dreyfus R W, Kelley R and Walkup R E, *Appl.Phys.Lett.*, 49, 1478, (1986)

[29] Schwarz H and Tourtellotte H A, *J.Vac.Sci.Technol.*, 6, 373, (1969)

[30] Inam A, Hegde M S, Vekatesan T and Wu X D, *Appl.Phys.lett.*, 53, 908, (1988)

[31] Angus J and Hayman C C, *Science*, 241, 913, (1988)

[32] Wagal S S, Juengerman E M and Collins C B, *Appl.Phys.Lett.*, 53, 187, (1988)

[33] Muenchausen R E, *Appl.Phys.Lett.*, 56, 578, (1990)

[34] Kanai M, *Appl.Phys.Lett.*, 54, 1802, (1989)

[35] Wantelet M and Kwok H S, *J.Phys:D*, 20, 1318, (1987)

[36] Leung M, *Appl.Phys.Lett.*, 51, 2046, (1987)

[37] Donaldson W R, *Appl.Phys.Lett.*, 54, 2470, (1989)

CHAPTER IX

GENERAL CONCLUSIONS

High power lasers are ideal tools for the production of plasma from various target materials. The previous chapters of this thesis describe such studies on laser induced plasma from a variety of targets including metals, ceramics and polymers. Discussions and important results from these studies were included in them. This chapter gives the general conclusions derived from the present studies.

The investigation made here are centered around the study of plasma characteristics from different solid targets mainly by spectroscopic technique. The optical emission from laser induced plasma (LIP) has been shown to be very useful in characterizing both the laser target interaction and the resulting plasma. The time resolved studies of the plasma gives some vital information regarding the evolutionary processes of a particular state of a constituent after the plasma is formed. Thus this measurement was found to be important in unravelling the complicated ablation and the transport processes occurring in the plasma produced by the laser ablation technique.

The spatially resolved plasma emission spectra obtained from all the materials studied here show distinctly different characteristics. It was observed that the spectrum in the outer region of the plasma is dominated by molecular bands (C_2 and CN molecules in the case of Teflon and graphite, AlO and CuO in the case of Aluminium and Copper targets), whereas the same in the inner region of the plasma is dominated by emission line due to highly ionised states of the constituent element. From the relative intensities of the above bands the vibrational temperature of these bands were calculated and their variation

with laser energy were investigated. The non-linear interaction between the laser and the plasma gives rise to phenomena like self -focussing, which exhibit threshold like characteristics and this is clearly observed in the variation of vibrational temperature with laser energy in the extended region of the plasma.

From the time resolved analysis of the different species in the plasma the variation of the time delay as well as decay time of emission at different regions of the plasma were obtained and several interesting conclusions related to the structural composition of the plasma could be drawn from these measurements. The time resolved analysis of the plasma emission throw much light on some of the complex interaction processes occurring in the plasma. From such measurements, it is seen that in all the three regions of the plasma, the molecular bands CC_2 and CN in the case of Teflon and graphite and the corresponding oxides in other targets) have got larger time delays as compared to that of the ionic/neutral species. From such time delays it is also observed that the spectral lines of higher ionized species are the first to appear and these are followed in turn by those of successively lower states of ionization. In general there is a decrease in time delay as laser energy increases. From the results obtained from the time delay of different species it was concluded that the time of flight is not the major cause of the emission delay in many cases as in molecular systems. Similarly from the decay time of emission of all species, it was seen that the molecular bands have got larger decay time as compared to ionic/neutral species. Also increased laser energy will produce much larger densities for the various species thereby decreasing the mean free path and increasing the collision rate. All these complex processes result in a decrease in the time delay as well as decay time of emission of various species in the plasma with laser energy. Such decrease in time delay as well as decay time with plasma temperature are found to occur as we go towards the central core of the plasma.

From the time delays observed in the case of higher laser

energies, it can be safely concluded that the molecular species are not originating from the target surface but are formed as a result of recombination processes as the plasma cools down, ie, the molecular species are formed in the expanding plasma due to the collisions of the atomic and ionic species expelled from the target surface.

The plasma characteristics were also studied by the Langmuir probe technique and from these different plasma parameters like plasma temperature, plasma density and the velocity of positive as well as negative ions were calculated. In the Langumuir probe studies of high T_c material, from the log t-log I plot of decay of emission of plasma intensity it was seen that nature of the decay of probe currents depends on the probe voltage. At low probe voltage electrons form a sheath around the probe which result in slow decay and this decay was found to be faster when the probe potential breaks the plasma sheath. Studies made with a Langmuir probe indicate that some control on the stochiometry of the film can therefore be effected by creating an electric field near the substrate during the laser plasma deposition of the high T_c materials. From the high electron density obtained here, it can be concluded that substantial optical absorption occurs in the plasma directly. So this technique will provide valuable insight into the laser induced metal vapours in terms of their plasma characteristics. The spatial composition of the ionic species in the plasma were also studied by the Langmuir probe technique. Studies made here indicate that monitoring of laser deposition of thin films can be done with such ion probes.

The final chapter of this thesis deals with the practicability of thin film deposition by laser ablation. Successful deposition of Copper and Aluminium on suitable substrates has been achieved by laser ablation technique and optimization of thin film characteristics has been carried out.

$G_{5}45_{o}$-